THE UNIVERSITY *of* EDINBURGH

The Structure and Development of Complex Plasmodesmata

Jessica J. Fitzgibbon

Thesis submitted to fill the requirements for the degree of
Doctor of Philosophy

The University of Edinburgh
2012

Declaration

I hereby declare that the work presented in this thesis is my own except where the contributions of other parties are clearly acknowledged, and that the text is of my own composition. This work has not previously been submitted for any other degree or professional qualification.

Acknowledgments and Thanks

This PhD thesis was produced thanks to my very good fortune to work with the people I did.

It was a privilege to be supervised by Karl Oparka, and I owe him many thanks for his enthusiasm, inspiration, support, and knack for gaining access to amazing microscopes. I was also very lucky to work with Karen Bell. To describe my gratitude for all the support she's given me over the last four years would probably embarrass her, so I'll just say: thanks, Karen.

I enjoyed being an appendage to the University of Edinburgh's Institute of Molecular Plant Sciences and I thank everyone else who was part of it, particularly Sophie Haupt for looking after us all, Patricia Watson for looking after our plants, Christine Faulkner for helping me get my project started, and all the other past and present Oparka Lab members for their support.

I also thank Silke Robatzek, Ji Zhou and Martina Beck of The Sainsbury Laboratory in Norwich for their enthusiastic collaboration on the high-throughput study. Their contributions to the project are described more fully in the appropriate chapters, but they deserve my thanks here also.

I am very grateful to the Biotechnology and Biological Sciences Research Council for funding my project and my attendance at the International Plasmodesmata Symposium in Sydney.

Of course, I need to thank Mum, Dad, Jed, and Nana (and possibly, by extension, St. Jude).

And, finally, I give a tip of my hat to all my friends and comrades. It was fun, wasn't it?

Abstract

This thesis presents an investigation into the development of plasmodesmata (PD), which are specialised pores in plant cell walls through which the cytosol and membranes of neighbouring cells are linked. Modification of PD from their initial single-tube (‘simple’) structures to branched (‘complex’) structures is an important part of tissue maturation as it allows cells to restrict the movement of syplasmically mobile molecules including hormones, RNAs and proteins. Conversion of PD from simple to complex is co-ordinated across large populations of cells to produce symplasmic domains, transport barriers, and preferential transport pathways. The development of PD is therefore intrinsic to the wider development and morphogenesis of cells, tissues, and organs.

The aim of this project was to investigate the development of PD from simple to complex, particularly during the predictable, large-scale conversion of PD structure that accompanies the leaf transition from sink state to source. To study this I used transgenic plants expressing a GFP-tagged viral protein which accumulates specifically in complex PD, while leaving simple PD unlabelled.

The project follows the development of complex PD from the early stages of leaf development to maturity using a range of microscopy techniques. Structured illumination microscopy was used to view labelled PD at super resolution, which gave new structural details about complex PD using a breakthrough technology. Conventional and high-throughput confocal and electron microscopy were used to localise PD within tissues in a broad survey of PD location in leaves to identify patterns of PD development. An imaging chamber was developed that allowed the development of complex PD to be viewed in real time and identified conditions that can trigger structural conversion of PD. Finally, a high-throughput microscopy study was performed to identify how hormones, sugar availability, environmental stresses, defence responses and inhibitors can affect PD development.

Abbreviations

2,4-D	2,4-Dichlorophenoxyacetic acid
3D-SIM	Three dimensional structured illumination microscopy
A. majus	*Antirrhinum majus*
A. thaliana	*Arabidopsis thaliana*
Ani	Anisocytic
ARF	AUXIN RESPONSE FACTOR
BA	6-Benzylaminopurine
BFA	Brefeldin A
CC	Companion cell
CW	Cell wall
CLSM	Confocal laser scanning microscopy
CMV	Cucumber mosaic virus
$DiOC_6$	3,3'-Dihexyloxacarbocyanine iodide
DT	Desmotubule
E-E	Wall interfaces between two leaf epidermal cells
E-M	Wall interfaces between a leaf epidermal cell and a mesophyll cell
EM	Electron microscopy
ER	Endoplasmic reticulum
FESEM	Field emission scanning electron microscopy
FRAP	Fluorescence recovery after photobleaching
GAT	GFP ARRESTED TRAFFICKING
GFP	Green fluorescent protein
h	Hour
IAA	Indole-3-acetic acid
ISE	INCREASED SIZE EXCLUSION LIMIT
KNOX	KNOTTED-LIKE HOMEOBOX
LD	Long day grown plants
LPI	Leaf plastochron index
M-M	Wall interfaces between two leaf mesophyll cells
Mann	Mannitol
MeJa	Methyl jasmonate
MP	Movement protein
MP17	Potato leafroll virus movement protein 17
MP30K	Tobacco mosaic virus movement protein 30K
mRFP	Monomeric red fluorescent protein
MT	Microtubule
N. tabacum	*Nicotiana tabacum*
NAA	1-Naphthaleneacetic acid
NCAP	Non cell autonomous protein
OMX	Optical microscope experimental (3D-SIM)
PD	Plasmodesma, plasmodesmata
PDCB	PLASMODESMATA CALLOSE BINDING
PDLP	PLASMODESMATA LOCALISED PROTEIN
PLRV	Potato leafroll virus
PHB	PHABULOSA
PHV	PHAVOLUTA

PI	Propidium iodide
PIN	PIN-FORMED
PLRV	Potato leaf roll virus
PPU	Pore plasmodesmata unit
PR	Pathogenesis response
PSF	Point spread function
PTGS	Post-transcriptional gene silencing
ROS	Reactive oxygen species
SA	Salicylic acid
SAR	Systemic acquired resistance
SAM	Shoot apical meristem
SD	Short day grown plants
SE	Sieve element
SEL	Size exclusion limit
SER	Sieve element reticulum
SIM	Structured illumination microscopy
SUC2	SUCROSE TRANSPORT PROTEIN
Sorb	Sorbitol
SP	Sieve Plate
TEM	Transmission electron microscopy
TMV	Tobacco mosaic virus
VIGS	Virus-induced gene silencing
WF	Widefield microscopy
WT	Wild type

Table of Contents

Introduction: Project background and aims

1.1 Plasmodesmal Structure and Function

1.1.1 Plasmodesmata: intercellular organelles

This thesis presents an investigation into the structure and development of plasmodesmata: plant-unique organelles that are fundamental to many aspects of plant biology. Plasmodesmata (singular: plasmodesma, abbreviated to **PD**) are specialised pores in plant cell walls through which the cytosol, endoplasmic reticulum and plasma membrane of adjacent plant cells are connected (Figure 1A). These structures allow neighbouring cells, which are otherwise held apart by cellulose cell walls, to exchange a wide range of solutes and macromolecules including ions, small molecules, RNAs and proteins (reviewed in Jackson, 2005) (Figure 1B). PD are therefore essential for a wide range of plant developmental and behavioural phenomena. These include nutrient uptake, many aspects of phloem function and loading, local and long-distance defence signalling, tropisms, and, as I shall discuss in more detail later, many aspects of plant development from cell differentiation to tissue patterning to organ morphogenesis (Roberts and Oparka, 2003). Plasmodesmata are important because they are one of the structures that make plants *plants.* As described above, they are intrinsic to many biological processes, even those that are carried out in the absence of PD in other organisms. They are also essential: mutations that affect PD are almost without exception embryo lethal, and all plant cells have functional PD for at least part of their lives.

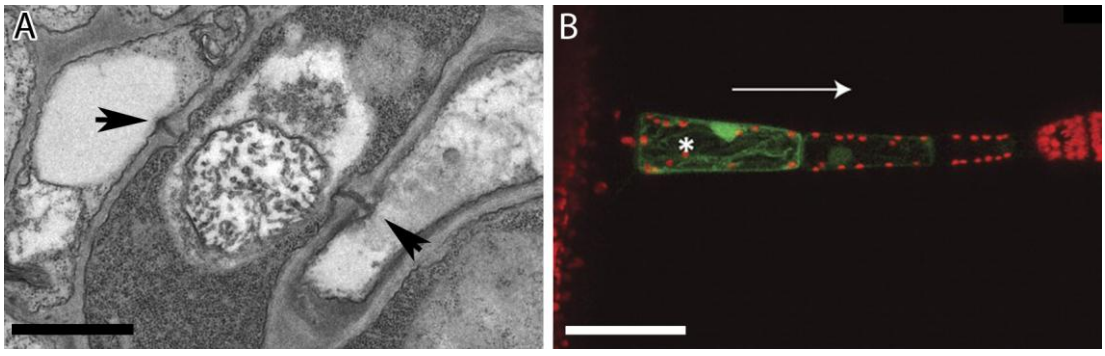

Figure 1: A: electron micrograph of plant tissue showing PD connecting neighbouring cells (arrows). B: PD-mediated symplasmic movement of PAGFP from the basal cell (*) to the tip cell of a trichome (B from Christensen et al, 2009). Scale bars: A = 1µm, B = 50µm.

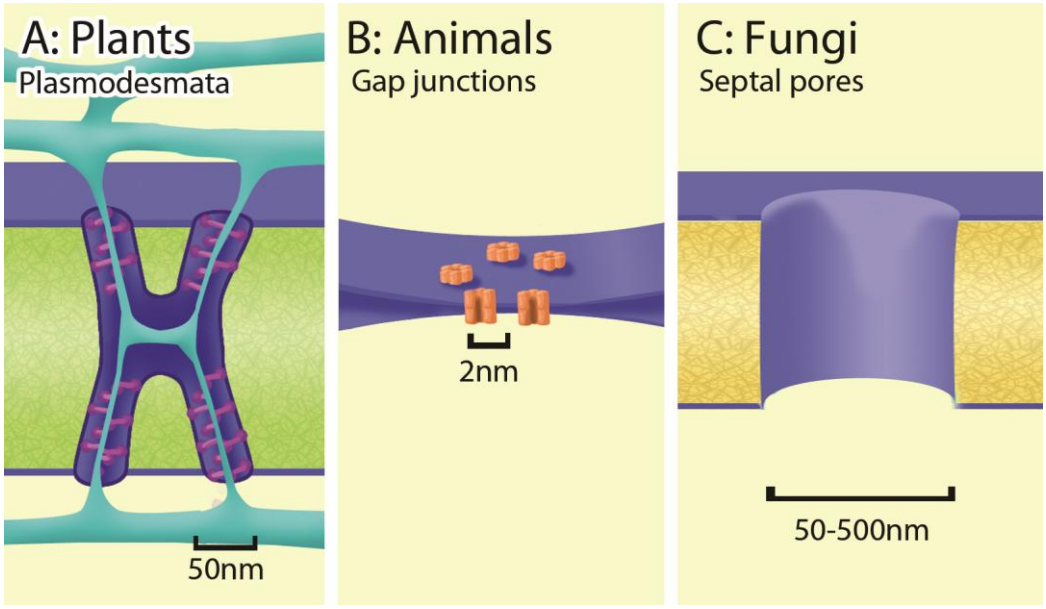

Figure 2: Cartoons of major cell-cell connections. (A) The PD of higher plants, incorporating cellular membranes and proteins, (B) the proteinaceous gap junctions found throughout the animal kingdom, and (C) the membrane-lined septal pores of fungi. Illustrations not to scale.

Most organisms require cell-cell connectivity, and structures broadly analogous to PD exist throughout nature (Figure 2). These include; the recently-discovered and still little-understood tunnelling nanotubules of animal cells (Rustom, 2009) that are membranous tubules of 50 nm width and varying lengths that are thought to allow passage of a broad range of cargo; the 2 nm-wide proteinaceous animal gap junctions (Figure 2B) which allow transfer of small molecules and ions and facilitate functions including rapid transfer of action potentials cell-to-cell (Simon and Goodenough, 1998); the simple septal pores of fungi (Figure 2C), which are literal holes-in-the-wall that allow almost all cellular constituents, including nuclei, to flow through cells; and the transient cell-cell connections of single-celled organisms, such as the various conjugation mechanisms of prokaryotes. However, the cell-cell communication situation in plants is unique due to the level of control that each cell has over its PD, which can be modified in number of ways to open, close, restrict and filter communication between cells. Due to their PD, plant cells exist as part of a larger supracellular network and yet, due to the level of fine control possible through PD, each cell may also be discrete. This allows for many of the unique features of plant biology.

This thesis is an investigation into plasmodesmal development, in particular the *complex PD* that allow finely tuned control of cell-cell connectivity necessary for cell function. This introduction will first describe PD and the present state of knowledge about their structure and biology, before moving on the focus on what we understand about plasmodesmal development in general, and the particular questions that this work aims to address.

1.1.2 Plasmodesmal structure

Although the basic structure of PD is widely agreed upon in the literature, many of the details of PD structure are unknown or unproven. Genetic studies of PD are difficult for two reasons; the first is that mutagenesis studies are hampered because mutations that affect PD are embryo lethal. The second is that PD are very sensitive to cellular conditions, and modification of PD is a typical plant response to a wide range of stresses, and so plasmodesmal phenotypes often result from genes which are not themselves plasmodesmal. Examples of these include *INCREASED SIZE EXCLUSION LIMIT 1,* a mitochondria-localised DEAD-box RNA helicase (Kobayashi et al., 2007) and *GFP ARRESTED TRAFFICKING* (*GAT1*) (Benitez-Alfonso et al., 2009), whose PD phenotypes are the result of increased cellular ROS levels. On the other hand, efforts to identify protein components have historically met with limited success due to the inaccessible location of PD and the difficulties in isolating them from the walls in which they are embedded (Maule, 2008). A putative PD proteome was recently published from membrane-enriched wall fractions (Fernandez-Calvino et al., 2011). However, 35% of the identified proteins are from other cytoplasmic compartments and are expected to represent contaminants or cargo, and so far this work has proved more useful for supporting the localisation of putative PD proteins identified through other means rather than the initial identification of PD proteins themselves. At present, therefore, most of the details of PD structure are in fact extrapolated from electron microscopy images (Figure 3, Figure 4).

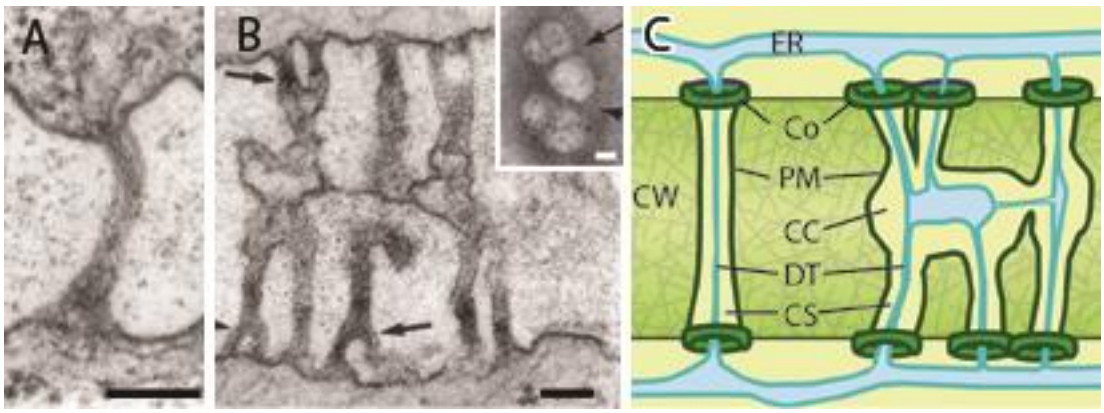

Figure 3: Simple and complex PD. A: EM images of longitudinal section through a PD, B: EM images of longitudinal and transverse (inset) sections through complex PD and a simplified cartoon interpretation of a simple (C left) and complex (C right) PD. CW = cell wall, ER = endoplasmic reticulum, Co = callose collar, PM = plasma membrane, CC = central cavity, DT = desmotubule, CS = cytoplasmic sleeve. Scale bars = 0.1 µm A and B from Ehlers and Kollmann, 2001, B inset from Faulkner *et al*, 2008.

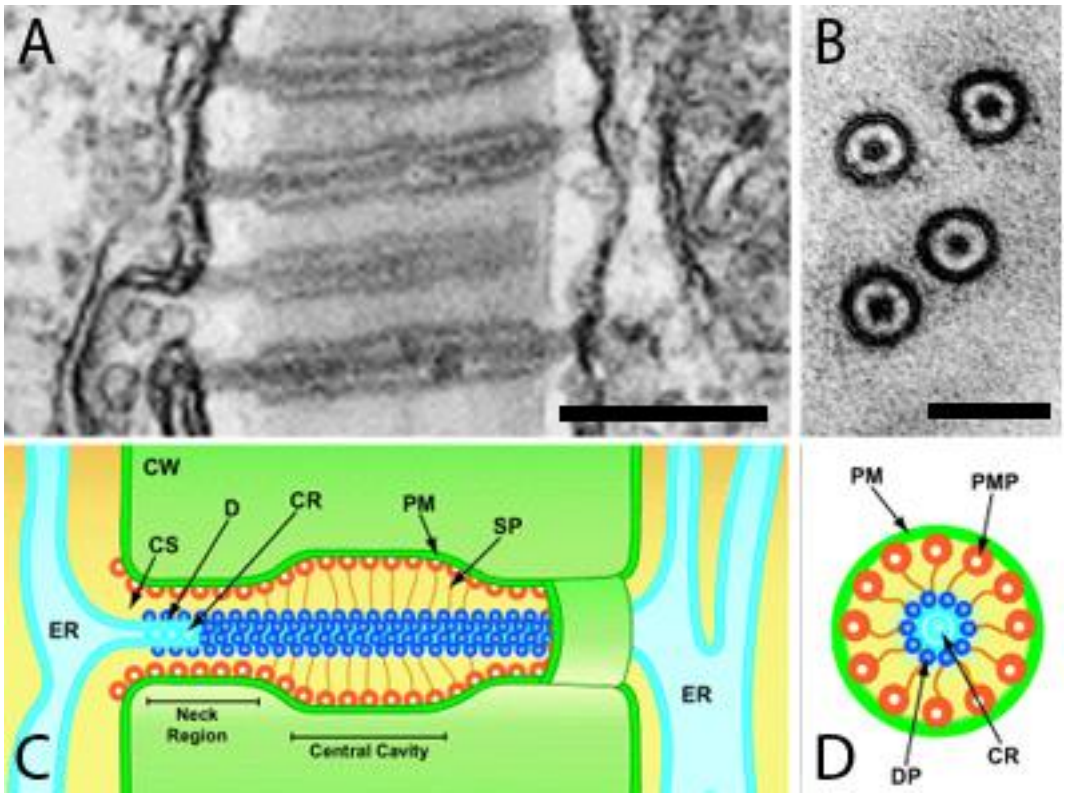

Figure 4: EM images of simple PD in longitudinal (A) and transverse (B) sections, and the corresponding model interpretations of these structures (C and D). CW = cell wall, CS = cytoplasmic space, D = desmotubule, CR = central rod, PM = plasma membrane, SP = spoke-like protein, ER = endoplasmic reticulum, PMP = plasma membrane protein, DP = desmotubule protein. Adapted from Roberts and Oparka, 2006. Scale bars A = 200 µm, B = 100 µm.

PD come in two main structural types (Figure 3): simple PD, which are single pores with a core and lining of membranes, and the complex PD that are the primary focus of this thesis, which have multiple branches connected in the middle lamella region of the wall by an expanded central cavity. Despite the fact that most PD in mature tissues are expected to be complex, most published models of PD ultrastructure focus exclusively on simple PD.

The major structural constituents of PD are well established (Figure 4). At the centre of the pore is the desmotubule, a membranous structure that traverses the PD and connects the ER of the cells on either side of the wall. Desmotubules have usually been imaged in a narrow configuration interpreted as a tightly furled tube of membrane, but have also been seen in an apparently dilated state displaying what appears to be an expanded central lumen (Ehlers and Kollmann, 2001). The electron-opaque centre of undilated desmotubules was initially interpreted as a proteinaceous 'central rod', and later as the appressed hydrophilic part of the inner ER membrane leaflet (Overall and Blackman, 1996; Robards and Lucas, 1990). More recent interest in PD membranes has again supported the idea of a proteinaceous central core, now as part of the scaffold of membrane-embedded proteins that allows the ER membrane to adopt the very highly curved desmotubule structure (Tilsner et al., 2011).

The outer edge of the PD is delineated with plasma membrane continuous with the membrane of the two interconnected cells. Between the plasma membrane and the desmotubule is a sleeve of cytoplasm. Many EM studies, both of lateral and transverse views of PD, have imaged particles within this sleeve. These have been interpreted in various ways, but most commonly as an arrangement of spoke-like and globular proteins which subdivide the cytoplasmic sleeve, either into smaller 2-6nm wide microchannels (references in (Overall and Blackman, 1996; Robards and Lucas, 1990) or form a sieve-like structure (Turgeon, 2006). These proteins are often thought to be related to the plant cytoskeleton, particularly actin, which has been localised along the entire length of PD (White et al., 1994). The exact localisation and arrangement of the actin is unknown but many published models depict actin in close contact with the desmotubule, often running along or wrapped around it, and

have suggested that the spokes within the cytoplasmic sleeve may be myosins that facilitate trafficking of molecules through PD (Maule, 2008; Overall and Blackman, 1996). The PD pore often appears to be constricted by 'necks' at either end, close to the interior of the cells, which have been speculated to be the site of regulation of PD aperture. Actin has been localised at these necks, and cytochalasin treatment has been shown to disrupt the constriction in this region (Simpson et al., 2009; White et al., 1994), suggesting that the cytoskeleton may play a role in PD aperture regulation as well as transport through PD. Studies have demonstrated the presence of extracellular particles and callose (β1→3 glucose) (Northcote et al., 1989; Simpson, et al., 2009) in the wall beneath the constriction (Badelt et al., 1994; Robards and Lucas, 1990) although there still remains the possibility that the necks are an artefact of fixation (Overall and Blackman, 1996). The idea that this structure acts as a valve or sphincter (see Badelt et al., 1994 for references) for general regulation of PD appears out of favour at the time of writing, but the appearance or absence of these structures has been correlated with plasmodesmal permeability (Erwee and Goodwin, 1985; Rinne and van der Schoot, 1998). The wall around the whole length of the PD may have a specialised constitution (Roy et al., 1997), and contain sphincters and spiralling particles, possibly proteinaceous (Badelt et al., 1994) which, again, may control aperture and trafficking. Around the opening at either end, external to the PD itself, is often a raised wall collar. Callose is also deposited at the collar region and may be involved in regulation of PD aperture (Simpson et al., 2009 and references therein).

The structure of the necks and branches of complex PD is expected to be similar or identical to those of simple PD, but how the structural constituents are arranged within the central cavity is unknown, and few interior details can be discerned from EM images. TEM studies show complex PD in section, and so will only show the branches that are on a single plane and therefore give a limited view of the overall 3D shape of the complex pore. Longitudinal sections show that complex PD can

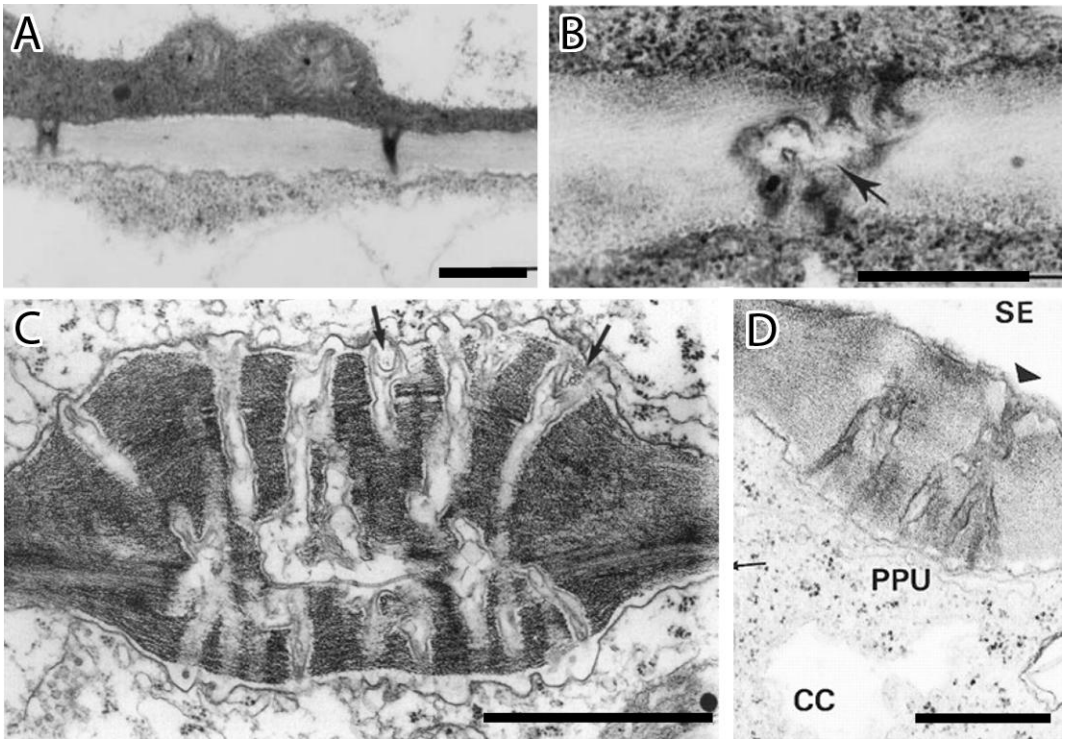

Figure 5: Various complex PD. A) X- (left) and Y-shaped (right) PD are complex PD with minimal additional branches. B) A typical symmetrical complex PD with an expanded central cavity (arrow). C) A large and highly branched complex PD in the specialised Strasburger cells of *Metasequoia glyptostoboides*. Arrows show additional levels of branching in the thickened wall. D) A pore-plasmodesmal unit (PPU): specialised asymmetrical PD found in the phloem. These PD have multiple branches leading from the supporting companion cell (CC) which fuse into a single pore (dart) leading to the sieve element (SE). A and B from Itaya *et al* (1998), C from Ehlers and Kollmann (2001), D from Kempers *et al* (1998). Scale bars A, B, D = 0.5 µm, C = 1 µm.

have as few as one or two extra branches, creating a Y-, X- or H-shaped profile (Figure 5A), or may have highly branched structures with more than six branches in a single plane on either side Figure 5B, C). Complex PD can also be asymmetrical, with multiple branches on one side of the cavity and few on the other. The specialised pore-plasmodesmal units (PPUs) found between the sieve elements and companion cells are always asymmetrical and facilitate trafficking from the supporting companion cell to the enucleate and dependent sieve element (Figure 5D) Transverse sections across the cavities of complex PD are relatively rare; and intriguingly suggest that many complex PD do not consist of branches joined in a single central cavity, but multiple expanded cavities that are linked by fine strands (Figure 3B) (Faulkner et al., 2008).

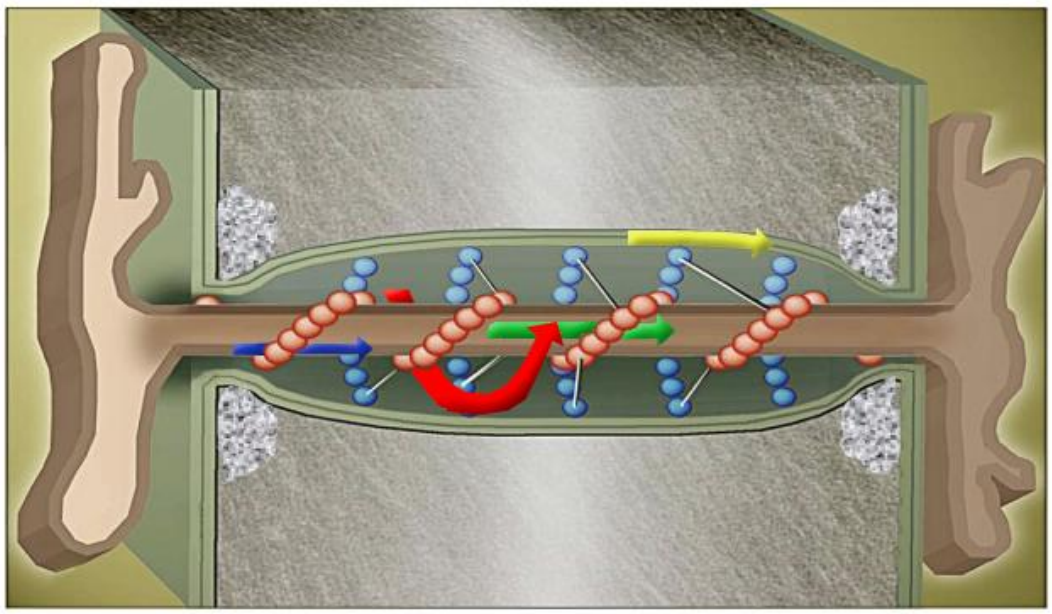

Figure 6: Four possible routes of movement through PDs: through or attached to the desmotubule membrane (blue arrow), through the cytoplasmic sleeve (red arrow) through the desmotubule lumen (green arrow) or through or attached to the plasma membrane (yellow arrow). Original PD illustration from Maule 2008.

1.1.3 Trafficking through plasmodesmata

The basic structure of the PD pore means that plants have both a symplasmic (cytoplasmic) and an endomembrane continuum connecting groups of cells. The structure described above prevents four obvious routes for the trafficking of molecules between cells: (i) attached to or within the plasma membrane, (ii) through the cytoplasmic sleeve, (iii) attached to or within the desmotubule membrane and (iv) through the lumen of the desmotubule (Figure 6). All of these seem possible routes of transport (for the desmotubule membrane see Grabski et al. (1993) and Martens et al. (2006); for the desmotubule lumen see Cantrill et al. (1999), although this is disputed by Crawford and Zambryski (2000); for the cytoplasmic sleeve see numerous studies reviewed in Roberts and Oparka (2003)) with the exception of the plasma membrane, whose flow appears restricted between cells (Grabski et al., 1993). Of these, the cytoplasmic sleeve seems to be the most likely conduit for small molecules (reviewed in Roberts & Oparka, 2003).

Movement is known to occur via two basic mechanisms: passive diffusion and selective trafficking (Figure 7). Passive diffusion, thought mainly to occur via the cytoplasmic sleeve, is the mechanism by which small molecules move cell-to-cell

non-specifically through PD. A wide range of molecules move in this way, mainly small molecules that are not trafficked or targeted to PD specifically but are not sequestered within organelles or anchored to cellular components (Crawford and Zambryski, 2000). However, some relatively large molecules, including proteins (e.g.: the transcription factors KNOTTED and LEAFY, and the flurophore GFP) are able to move through PD in this way. Various fluorescent tracer molecules (e.g. CFDA) are also able to move passively and, when introduced via microinjection or bombardment, produce a gradient in the cells surrounding the initially labelled cell (Figure 6 a and b) (Kobayashi et al., 2005). Although this type of movement is diffusive, it is regulated in the sense that the efficiency with which molecules are trafficked depends on their size, shape, subcellular localisation and their availability for trafficking (Crawford and Zambryski, 2000). It is worth noting that PD still act as a barrier to diffusive transport compared to movement through the cytoplasm of a cell, slowing the rate of movement by as much as 80 times to compared to general diffusion rates (Tucker et al., 1989).

Much of the work describing passive movement via PD was done in the 1980s, often using non-model plants with large trichomes or nectaries to facilitate the study. Early studies used microinjection, a process which can cause wounding and turgor-induced modulation of PD aperture (Oparka and Boevink, 2005). Later studies focused on particle bombardment (Crawford and Zambryski, 2000), or stable expression of probes in transgenic plant lines. These studies established that PD have a basal size exclusion limit (SEL) that defines the maximum size of molecules that may move passively. This is often given as 1kDa (Ding et al., 1993, and others) based on the size of the microchannels in the cytoplasmic sleeve. However, this value is somewhat misleading as the ability of molecules to traffic is more dependent on their shape, rather than their size (Terry and Robards, 1987), hence the ability of 27kDa GFP to move passively in many cell types due to its compact barrel shape (see Kobayashi, et al., 2005, for a review of several GFP studies). While the 1kDa baseline can be fairly accurate, the SEL can vary widely among PD, particularly within specialised cells (Waigmann and Zambryski, 1995), over the course of development (Kim et al., 2005), in different species (Itaya et al., 1998; Pina et al.,

2009), in different structural PD types (e.g.: PPUs, which can allow passive movement of molecules as large as 67kDa (Stadler et al., 2005)), and even over the lifespan of a single cell (Crawford and Zambryski, 2000). The most notable determinant of trafficking for the current study is PD structure; complex and simple PD display different trafficking properties, with complex PD showing more refined and restricted trafficking properties compared to simple PD.

PD SEL can also be transiently or permanently modified by a range of factors. Many stresses promote the deposition of callose externally at PD in the area around the neck regions to decrease PD SEL. Generally, callose has been thought to be primarily involved in wound responses and sealing of PD rather than in regulated modulation of the SEL (Overall and Blackman, 1996). A good example of this is seen in cotton fibre cells, where complete closure of the PD by callose allows the cell to drastically increase turgor and promote the rapid expansion of the fibre (reviewed in (Pfluger and Zambryski, 2001). However, several recent studies also suggest that callose deposition may be used for finer adjustments of aperture and SEL. (Guseman et al., 2010). Increases in cellular Ca^{2+} concentration (and other ions including Mg^{2+} and Sr^{2+}) are also known to decrease PD SEL, and calreticulin (a calcium sequestering protein) and centrin (a calcium-dependant contractile protein) have been localised to PD (reviewed in Aaziz et al., 2001). Ca^{2+} also induces callose deposition and inhibits cyclosis which may affect trafficking (Robards and Lucas, 1990). Increases in ATP concentration can result in an increase in cell-to-cell communication (Overall and Blackman, 1996). Turgor and osmotic stress cause strong effects on PD, with plasmolysed cells showing increased SELs that are unaffected by additional factors such as changes in ion concentration (Roberts and Oparka, 2003). Cytoskeletal elements are known to be localised to PD and, while inhibition of actin does not affect trafficking of molecules which move by diffusion, experiments using various depolymerising and stabilising drugs have illustrated that both actin and myosin may play a role in SEL control (Aaziz et al., 2001; Roberts and Oparka, 2003). Some authors argue for distinct PD states, such as ‘closed’, ‘open’ and ‘dilated’ (Crawford and Zambryski, 2000) in response to the functional needs of the cell, but the general consensus is that PD may modulate their SELs

between a completely closed state that prevents all transport and a dilated state that allows movement of very large macromolecules in a more controlled process.

Selective trafficking, in contrast to passive movement, is performed by molecules specifically targeted to PD (Figure 7). Many molecules trafficked in this way move in defined or directed patterns, for example the transcription factor KNOTTED can traffic from leaf mesophyll cells to the epidermal layer (but not *vice versa*), and SHORT ROOT can move one cell layer outwards from the stele. Selective trafficking also allows molecules much larger than the basal SEL of a PD to move cell-to-cell. This transient increase in SEL is termed 'gating', and may be performed by the (macro) molecule being transported or by a separate molecule. The ability of PD to traffic large molecules in defined patterns allows a wide range of developmentally important host non cell autonomous proteins (NCAPs) and RNAs to traffic throughout the tissue (see Oparka, 2004 for a review). Many viruses also move this way, and encode movement proteins (MPs) able to gate PD in order to facilitate transport of viral components and allow infections to spread cell-to-cell. In fact, most of the studies of NCAP trafficking have used viral MPs as models (see (Vogel et al., 2007; Waigmann and Zambryski, 1995) and (Ding et al., 1992) for some examples), and so many of the published models actually focus on transport of non-host molecules (Oparka, 2004). However these studies give important insights into host mechanisms of PD transport, especially as many viral MPs appear to be evolutionarily derived from plant proteins, e.g.: the 30K superfamily of MPs shares sequence homology with CmPP16 phloem proteins (Melcher, 2000).

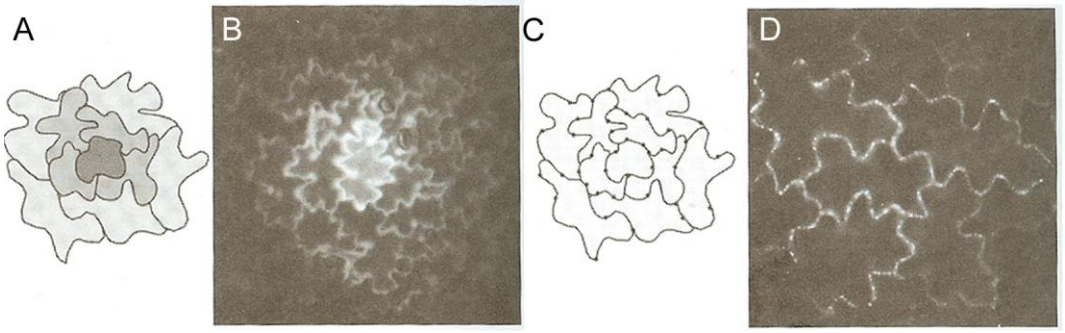

Figure 7: Movement patterns of fluorescent probes introduced to single cells via bombardment. A non-targeted probe moves diffusively, producing a gradient from the cell of production (A), as shown by free GFP (B). A selectively-moving probe is probe is rapidly trafficked from cell to cell so that the initial bombarded cell can not be distinguished (C) as shown by MP-GFP (D). Taken from Kobayashi et al, 2005.

The mechanisms by which molecules are targeted to PD for selective trafficking are unknown but are thought to be similar to (or indeed derived from) the intracellular transport pathways that deliver cargo to other organelles (reviewed in Kragler, 2005). No common sequence has been identified in selectively trafficked proteins that could target them to PD in a way analogous to the nuclear localisation signal and so it has been proposed that the PD targeting signal may be part of the wider three-dimensional structure of transported proteins (reviewed in Kragler, 2005). In support of this, the PD targeting of the plasmodesma callose binding (PDCB) family of PD-localised (but not trafficked) proteins is known to be dependent on the length of their transmembrane domain, although the mechanism for this is not understood (Simpson et al., 2009). Other components of the PD trafficking pathway have also been discovered. For example, NON CELL-AUTONOMOUS PATHWAY PROTEIN1 (NCAPP1) in *Nicotiana tabacum* is involved in trafficking both host proteins such as cmPP16 (an RNA-binding protein found in the phloem) and viral proteins including the TMV (tobacco mosaic virus) 30K MP (Lee et al., 2003). Members of the 70kDa heat shock protein family of chaperones (HSP70) have also been proposed to play a role in cytoskeleton-mediated trafficking of cargo to PD (reviewed in Kragler, 2005). It has also been shown that the microtubule network may play only a limited role in trafficking to PDs (Gillespie et al., 2002).

Selective movement is much more efficient than diffusion, both in terms of the numbers of cells that will allow a bombarded targeted probe (such as a movement protein linked to GFP) to traffic, and in the number of cells it will traffic to from a single initial bombarded cell (Crawford and Zambryski, 2000). Targeted proteins tend to have distinct subcellular localisations, e.g.: TMV MP is localised to PD, ER and microtubules. This is in contrast to the diffuse localisation of passive probes, such as bombarded rsGFP, which is seen in the cytoplasm and nucleus of cells (Figure 7A and B) (Crawford and Zambryski, 2000). In the case of bombarded fluorescent probes, those that move by selective trafficking will produce a more regular labelling pattern than the fluorescence gradient produced by probes that move via diffusion (Figure 7C and D) (Kobayashi, et al., 2005). Disruption of the actin network by cytochalasin has no effect on movement by diffusion (White et al.,

1994). Also movement of selectively trafficked proteins is less affected by factors such as tissue age and physiological state (Kobayashi et al., 2005).

1.2 Plasmodesmal Development

1.2.1 Insertion of plasmodesmata & increasing complexity

As well as being classed in terms of their architecture (simple and complex), PD can be categorised by how and when they form. **Primary** PD form at cytokinesis and develop from ER strands trapped within the phragmoplast of a dividing cell (Ehlers and Kollmann, 2001). **Secondary** PD develop *de novo* across existing cell walls and maintain the density of PD in an expanding cell, or to increase connectivity between mature cells (Figure 8). Despite their difference in origin, primary and secondary PD are indistinguishable once they have formed, and both types may be simple or complex. Some older literature used simple/primary and branched/secondary interchangeably; more recently there has been a push within the community to make clear the distinction between structurally and ontogenetically distinct classes of PD. That said, it is thought that most primary PD begin with a simple structure, which may later become complex. Insertion of primary PD is often described as 'random' and dependant on the chance arrangement of the ER during cytokinesis. It seems counter-intuitive that such a vital aspect of development is purely random and, indeed, this process does show some elements of control and patterning. For example the numbers of PD inserted into the cell plate is specifically reduced in certain cell wall types, perhaps related to the amount of expansion the wall in question is likely to undergo (Gunning, 1978). Gunning observed values ranging between 90 and 127 per μm^2 of shared wall in cell plates of different cell types. The mechanisms behind this are unknown. How entrapment of the ER within the wall leads to development of PD, with their characteristic and precisely arranged structure, is still a subject of research. In particular, the development of the desmotubule has been the subject of recent interest because, at 15-20nm in width, the desmotubule represents one of the most tightly constricted membranes found in nature. Reticulon proteins that induce membrane curvature are thought to be involved and these have been observed at the cell plate, suggesting that the machinery to construct PD is an integral part of the phragmoplast (Tilsner et al., 2011).

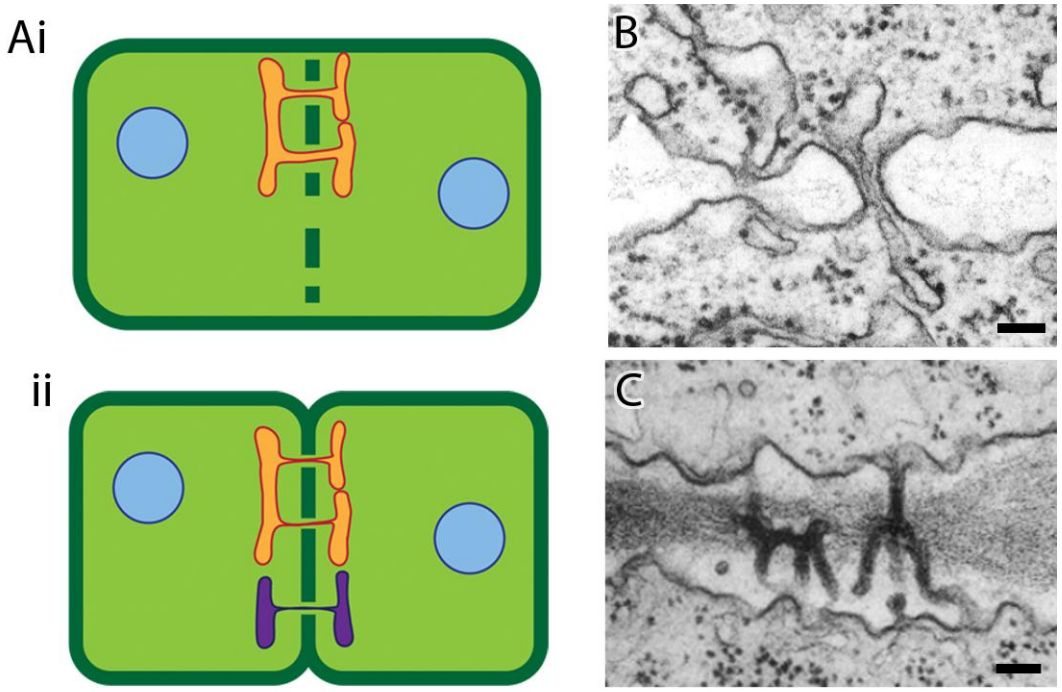

Figure 8: A: primary PD (orange) form from during cytokinesis, from ER strands trapped in the phragmoplast (i) while secondary PD (purple) are inserted across an existing cell wall (ii). B) Strands of ER trapped in the cell plate of dividing *Metasequoia glyptostroboides* cells, which could become primary PD. C) secondary PD at the interface of a graft union between *Vicia faba* and *Helianthus annus* are structurally indistinguishable from primary PD. B and C are taken from Ehlers and Kollmann (2001). Scale bars = 0.1 µm.

As cells mature, they alter their connectivity by the *de novo* insertion of secondary PD into cell walls after cytokinesis and by increasing the complexity of PD from simple to complex structures. Regulation of this connectivity is known to be influenced by stretching forces during wall extension (Faulkner et al., 2008), by reactive oxygen species (Kobayashi et al., 2007) and hormonally, e.g.: by cytokinins (Ormenese et al., 2006). Inhibition of secondary PD formation has been linked to early senescence (Ding et al., 1993). In many cases secondary PD are thought to help maintain the level of connectivity as cells expand, although some studies have found that the number of PD may vary as cells mature. In the trichome basal cell/epidermis interface in tobacco leaves the density of PD was observed to decrease from ~2.5 PD/µm^2 to 0.5 PD/µm^2 as cells expanded, even though new PD continued to be inserted (Faulkner et al., 2008). Early work by Gunning (1978) suggested that numbers of PD remain approximately constant in *Azolla* root cells as the cells

expand, leading to a decrease in PD density (at the time the existence of secondarily inserted PD had been proposed but not proven).

The actual mechanism by which PD are inserted *de novo* across the cell wall is unknown. Most models agree that it must involve a high degree of signaling between adjacent cells in order to co-ordinate the localised wall-thinning, membrane fusion and arrangement of the ER and other cellular components which will be incorporated into the PD (reviewed in Ehlers and Kollmann, 2001). In walls where primary PD are already in place, this may be controlled via symplasmic communication, however secondary PD are observed across graft unions and chimera boundaries that have no primary PD (Figure 8C) (Ehlers and Kollmann, 2001).

Many studies do, however, support the idea that existing PD may play a role in the insertion of new PD, and this may be related to the methods by which PD increase in complexity from simple, single-pored structures to complex, multi-branched structures. Until recently, one of the most widespread ideas for increasing plasmodesmal complexity was that simple PD could fuse together. This was mainly inferred from H-shaped PD profiles that were interpreted as intermediate stages of adjacent PD fusing together (e.g.: Ding et al., 1993), despite the fact that this would cause a decrease in the total number of PD which is not observed in most cell types (Faulkner et al, 2008). The alternative idea, that these profiles may show fission of a single multi-branched PD into two discrete PD had been proposed in 1960 (Krull, 1960, cited in Faulkner et al., 2008) but was not widely accepted (Robards and Lucas, 1990). A related idea is that the existing primary PD could act as nucleation sites or templates for the *de novo* insertion of new, adjacent secondary PD. Both of these latter models are supported by the fact that the PD in mature walls are often clustered together in pectin-rich wall depressions called pit fields. Several ideas have been proposed to explain this; for example, the factors needed to initiate and form a new pore may be localised to pit fields. Equally, the microdomain in the wall

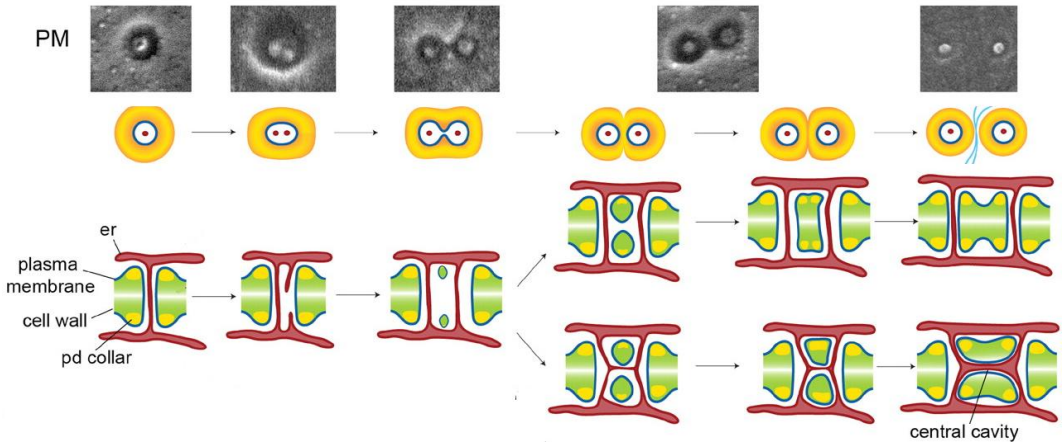

Figure 9: the 'twinning model' of complex/secondary PD formation, inferred from fission profiles of PD necks (top). In this model, existing PD may insert additional branches which may remain attached to form a complex PD, or separate and migrate apart to form a new secondary PD. Taken from Faulkner et al, 2008.

surrounding PD, and the pectin-rich nature of pit fields themselves may facilitate new PD formation. Branches of the wider ER network that feed into desmotubules may become entrapped in the wall during wall thickening which may develop into PD branches via a similar mechanism to that which forms primary PD (Ehlers and Kollmann, 2001).

This model received strong support in work by Faulkner et al. (2008) that studied the non-diving trichome basal cell-epidermal cell interface in *N. tabacum* leaves. They observed an age-related trend in PD distribution, with PD being found in progressively larger aggregations in older or more expanded wall areas. In the youngest and least expanded areas of wall PD necks were often observed singly or as closely paired 'twins' (Figure 9). In older extended areas of wall PD were seen progressively as triplets, quadruplets and subsequently larger aggregations, eventually forming pit fields. In these pit fields, which contained as many as twelve discretely labelled necks, the constituent PD could often still be observed grouped into pairs with touching wall collars. That this phenomenon was due to progressive insertion using existing PD as nucleation sites was supported by a computational model that predicted PD aggregations that matched those observed *in vivo*. This phenomenon was coupled not just with age but the rate of expansion. PD aggregations and MP-labelling showed that new necks and central cavities were initiated first at the outermost edges of the interface where the rate of expansion is

highest. This study also provided face-on images of PD in various states of twinning – some with what appeared to be two desmotubules within a single pore and others showing discrete pores with overlapping wall collars (Figure 9). PD twins in the tobacco trichome-epidermis interface are often seen to form parallel to the orientation of cellulose microfibrils in the underlying wall, suggesting the twinning process occurs in the direction of wall expansion. In the radially expanding trichome-epidermal wall interface this results in 'circular' pit fields. In other interfaces, such as the roots of *Azolla*, PD may form longitudinal files (Gunning, 1978).

A detailed EM study of the cambial zone in tomato (*Lycopersicon esculentum*) stems by Ehlers and van Bel, 2010, illustrates that the development of PD as cells mature from meristematic cambial cells, which contain a majority of simple PD, to mature phloem/xylem parenchyma cells, which contain a majority of complex PD, occurs in a manner consistent with the twinning model and is possibly facilitated by ROS-mediated wall loosening.

1.2.2 Developmental modulation of plasmodesmata

Many cell types undergo changes in the number, structure and location of PD as they differentiate and mature, with the general trend being to decrease and restrict the connectivity with surrounding cells. The majority of PD in undifferentiated and young cells will be simple, primary PD with high SELs. These allow for extensive communication and trafficking of a wide range of molecules, including macromolecules, hormones, nucleic acids and nutrients (Ormenese et al., 2000; also reviewed in Roberts and Oparka, 2003). During their development, cell types in many tissues show a switch from the majority of PD being simple to the majority being complex, and so transport in mature cells may be limited to selectively trafficked molecules and small (often <1kDa) diffusible molecules (see Kobayashi et al., 2005). Examples of this phenomenon are observed and described in a range of tissues (reviewed in Roberts, 2005), but one of the most striking is seen in leaves. A decrease in PD connectivity is an important part of leaf maturation, as the sink-source transition (the process by which a maturing leaf switches from a net carbon-importer to a net carbon-exporter) is accompanied by a large-scale conversion of simple PD to branched PD morphotypes, with the proportion of simple PD

decreasing from ~90% to ~20% (Oparka et al., 1999; Roberts et al., 2001), decreasing the connectivity between cells. Studies using bombarded 2xGFP (size: 54kDa) have shown that between 30-46% of sink leaf cells, but only 2-9% of source leaf cells, are able to traffic this probe (cited in Kobayashi et al., 2005). This phenomenon has led leaf tissue being adopted as the model tissue used for the majority of studies, and the particulars of the process of PD conversion in leaves will be discussed in greater detail in this thesis.

As well as a general conversion of PD from simple to complex forms, PD restriction is co-ordinated to show large-scale organisation and co-ordination. Groups of cells with low connectivity are positioned to form 'barriers' to the movement of molecules above a certain size, dividing tissues into functional domains (sometimes called 'symplasmic *fields*' where the SEL reduction is dynamic or transient (Rinne and van der Schoot, 1998). These barriers often occur between tissue layers or between organs (Kobayashi et al., 2005). In some cases, structural differences in PD at barriers can be seen, but in other cases the PD at the boundaries appeared identical to those in other tissues with high SELs. An early study by Erwee, and Goodwin (1985) using fluorescent tracers showed that the symplasmic continuum is divided into functional units. A range of differently-sized dyes were injected into different cell types throughout the plant and showed differential movement, revealing that SEL varied from >675 to <376kDa in different cells. They showed that PD are not merely heterogeneous with respect to SEL across a tissue, but actually show a large-scale organisation with respect to functional aperture. Numerous other examples of this phenomenon have since been discovered, with one of the most striking occurring during embryogenesis. The developing early heart-stage embryo is thought to consist of a single symplasmic domain with dilated PD, allowing free diffusion of relatively large probes such as 10kDa dextran (Kim et al., 2005). The SEL is then down-regulated at the mid-torpedo stage, roughly at the time the embryo disconnects from maternal tissue, with symplasmic barriers of complex PD developing between the tissues that will become the cotyledons, hypocotyl and root (Figure 10) (Kim et al., 2005). This also occurs in mature roots, where preferential movement between cells

of different types correlates with different abundances of complex PD in their connecting walls (Tirlapur and Konig, 1999).

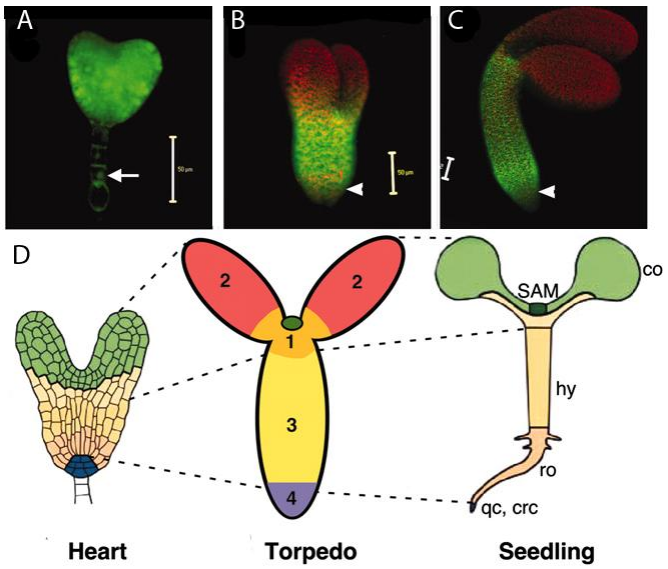

Figure 10: Example of symplastic domains in the developing embryo. 2xGFP expressed in the meristem specific STM promoter is able to move freely in early heart stage embryos (A), but is restricted to the hypocotyls in late heart- (B) and torpedo-stage (C) embryos. D: Diagrammatic representation of the symplasmic domains of an Arabidopsis torpedo-stage embryo (1:SAM, 2:cotyledons, 3:hypocotyl, 4:root) and how these correspond to the anatomy of heart-stage embryos (left) and a seedling (right). SAM = shoot apical meristem, co=cotyledon, hy=hypocotyl, ro=root, qc=quiescent centre, crc=central root cap. Scale bars = 50 µm. Adapted from Kim et al, (2005).

In other more specialised cell and tissues, symplastic isolation may be used for specific developmental programmes (reviewed in Pfluger and Zambryski, 2001). The increase in PD density observed in the SAM of *Sinapsis alba* after floral induction is transient, presumably due to cell expansion (Ormenese et al., 2000), while the loss of connectivity seen in birch (*Betula pubescence*) buds is reversible under certain conditions (Rinne and van der Schoot, 1998). Many cell types also experience a decrease in PD density that cannot be accounted for by dilution of primary PDs due to cell wall expansion. Age-related decreases in PD density are seen in both xylem and phloem cells (Gunning, 1978; also reviewed in Roberts, 2005), and PD can also be lost by insertion of transverse walls and cell separation (Gunning, 1978; Roberts et al., 2001). The most extreme form of PD loss is probably seen in stomatal guard cells where the cell occludes its PD as it differentiates, to become completely symplastically isolated at maturity (Willmer and Sexton, 1979).

As plant cell fate is more dependent on cell position than lineage (Kidner et al., 2000), a cell's eventual fate is very much dependent on the information it receives from the cells around it and, as much of that information will come through the PD, this down regulation of connectivity resulting from conversion of PD from simple to complex, is significant. A young cell with predominantly simple, high-SEL PD will receive a large amount of relatively unfiltered developmental information. Conversion of these PD to complex forms restricts this flow of information as the cell matures. Grouping of cells into domains between which communication and transfer of informational molecules is controlled further allows cells that are very close physically to receive different sets of information and signalling molecules, and thereby be in significantly different 'positions'. Hence, reduction of PD communication is often a pre-requisite for development (Kobayashi et al., 2005). This is underscored by the wide range of developmentally important molecules that are known to traffic through PD. Developmental signals trafficked through PD include transcription factors and proteins (either selectively trafficked, such as SHORT ROOT, or diffusively moving, such as LEAFY) , mRNAs (for example, *MOUSE EARS*; *KNOTTED*), and miRNAs that target transcription factors, such as those targeting *PHABULOSA* in leaves (reviewed in Jackson, 2005; Kobayashi et al., 2005).

What controls the conversion of PD from simple to complex is not understood. Several mutant studies suggest that conversion of PD structure can be induced in response to cellular redox states. The *INCREASED SIZE EXCLUSION LIMIT* genes were discovered via mutational screens looking for increased symplasmic transport of dyes during embryogenesis. ISE1 is a mitochondria-localised DEAD-box RNA helicase which, if knocked down by virus induced gene silencing (VIGS) in leaf tissues, increases the proportion of complex PD in epidermal-mesophyll interfaces from 7% to 20% (Burch-Smith and Zambryski, 2010). ISE2 is an RNA helicase that localises to cytoplasmic bodies thought to be related to stress granules. *ise1* mutants *ise2* mutants have increased embryonic symplasmic communication allowing the movement of probes after the mid-torpedo stage, and also conversion of up to 15% of embryonic PD to complex forms (Kobayashi et al., 2007). *GFP ARRESTED*

TRAFFICKING1 (*GAT1*) encodes a plastid thioredoxin m3, and mutants show an increase of complex PD close to the root meristem from ~0% complex to ~9% (Benitez-Alfonso et al., 2009). The PD phenotype of all these mutants is the result of altered redox state in the cells caused by ROS production from mitochondria or plastids and can be replicated by direct manipulation of redox states (Benitez-Alfonso et al., 2009; Stonebloom et al., 2012). However, whether redox state influences development of PD structure under normal growth conditions, or whether these results represent a stress response remains to be investigated. It is also unclear whether alteration of PD structure is a direct or downstream response to changing redox states.

1.2.3 The importance of PD to wider plant development

While we still understand relatively little about the development of PD themselves, the importance of PD to wider plant development is indisputable, as the presence of PD have been shown to be fundamental to everything from the development of physical shape and size, to the patterning of tissues into specialised layers, to the differentiation of individual cells.

For much of scientific history, two contrasting theories about plant development have been proposed. These are; the **cellular theory**, which purports that shape, development and morphogenesis are determined at the level of cells, their intrinsic identity and their local interactions; and the **organismal theory,** which proposes that development is determined by the organism as a protoplasmic whole. Evidence has long been in favour of the organismal theory (reviewed by Kaplan and Hagemann, 1991), as summed up by de Bary in 1879: "it is the plant that makes the cells, not the cells that make the plant" (discussed in Hamant and Traas, 2010). However, it is most likely that both of these theories are too simplistic, and the reality is somewhere in between. To allow for co-ordinated and tailored development, development is likely to be controlled both from the bottom-up (through the cells and their local interactions determined by genetics, mechanics and signalling), and from the top-down through feedback determined at the supracellular level from a combination of the local interactions (Hamant and Traas, 2010). For both of these elements

symplasmic signalling via PD is key, and I will briefly discuss some of the more prominent examples in leaves, which is the tissue studied in this thesis.

All leaves begin as dome-shaped outgrowths on the SAM, but develop a wide variety of forms; from strips to ovals to hearts, from deeply lobed to serrated to smooth, from simple structures to complex forms with multiple leaflets. The presence of the cell wall means that the cells cannot migrate or be removed by apoptosis, and therefore development of shape is determined almost entirely by two parameters: cell expansion and cell division (reviewed by Fleming, 2003), and it is thought that symplasmic communication plays a large role in this in order to co-ordinate the growth across the leaf. This is especially illustrated by the compensation mechanisms that ensure the size and shape of leaves are maintained, which mean that organisation at the cellular level can have little effect on overall organ morphogenesis. There are many examples showing that cell division rates and cell expansion rates are co-ordinated so that changes in one cause inverse changes in the other, thereby producing normally proportioned leaves. For example, the *ton* mutant in *A. thaliana* has leaves that are normally-proportioned despite containing many more cells, as the increased rate of cell division is compensated for by decreased cell expansion (reviewed in Marcotrigiano, 2001). In contrast, while the larger cells of polyploid plants generally results in increased organ size, plants that have diploid/polyploid mosaic tissues have WT-sized leaves, as cell division rates are reduced in the polyploid sectors to compensate for increased cell size (reviewed in Day and Lawrence, 2000). Overall organ shape is also maintained in mutants affecting cell shape; e.g.: the *Z. mays* mutant *tangled1* has normally-shaped (although small) leaves, despite having irregularly-shaped cells resulting from mispositioning of the cell plate during cytokinesis (reviewed in Day and Lawrence, 2000). Leaf shape can also be maintained despite environmentally induced decreases in size in the case of Bonsai trees, which are WT plants induced to grow in minimised forms (reviewed in Marcotrigiano, 2001). Although the signalling components that facilitate these growth compensation phenomena are not yet identified, symplasmic movement is expected to be a major element in their activity.

1.2.4 Mobile signals in leaf development

Leaf development is controlled by the interactions of hormones, transcription factors, small RNAs and lipid factors (Fleming, 2003). Layers of regulation are involved in determining leaf development, and the location of factors, and their ability to move symplastically or remain restricted, is an integral part of this. How organs co-ordinate cell division and cell expansion to form determinate organs of set sizes is a subject of much debate.

There is evidence that some patterns rely on gradients of symplastically moving signals, thereby suggesting a clear role for PD. An example of this relates to KLUH, a cytochrome P450 monooxygenase that regulates organ size. *kluh* organs grow at the normal rate but cease growth earlier in a manner suggestive of a cell-number feedback mechanism, resulting in smaller organs with fewer cells. *KLUH* itself is cell autonomous and its expression is restricted to groups of cells at the base or edges of organs, but it generates a mobile signal (as yet unidentified) that promotes growth. The suggested model is that as the organ expands, this mobile signal becomes more dilute, and once the organ reaches a certain size, the signal level falls below a growth-promoting threshold (Anastasiou et al., 2007). Gradients of signals are also expected to play roles in the ability of plants can 'measure' dimensions or axis lengths of leaves, as demonstrated in work by Tsuge (1996) that described two genes: ANGUSTIFOLIA (AN) and ROTUNDIFOLIA3 (ROT3). *an* has narrow leaves, resulting from decreased cell number and decreased cell elongation along the width of the leaf, and increased cell number along the length. Conversely, *rot3* mutants have short, wide leaves resulting from increased cell number across the width of the leaves, and show decreased elongation across the length of the leaf. Additionally, in the development of floral organs, which are themselves modified leaves, developmental factors have been shown to move symplastically through PD. These include *DEFICIENS* and *GLOBOSA,* two floral homeotic MADS box proteins which specify petal and stamen fate in *Antirrhinum majus* (Perbal et al., 1996).

The idea that RNAs could move through PD was first indicated by the ability of numerous viral genomes, including TMV, to move cell-to-cell as unencapsidated viral nucleoprotein complexes using many elements of the host plant machinery

(reviewed in Lucas et al., 1994). Until relatively recently, there were few known examples of endogenous symplastically moving RNAs in plant development, but work on small RNAs has provided several intriguing examples which give insight into how symplastic movement of sRNAs may work to produce highly complex layers of regulation that control patterning events. One example is *AUXIN RESPONSE FACTOR 3* (*ARF3*). *ARF3* is expressed throughout leaf primordia and is a nuclear localised transcriptional repressor involved in promoting abaxial cell fate. This location-specific activity of a broadly expressed gene is reliant on layers of post translational gene silencing) (PTGS). MIR390 is transcribed in a restricted area beneath the SAM and is processed to produce the *miRNA390* miRNA, which moves symplastically to accumulate throughout developing leaf primordia. *miRNA390* does not target *ARF3* itself, but triggers processing of the *TAS3* transcript through several steps to produce trans-acting siRNAs (ta-siRNAs) which target and degrade *ARF3* transcripts. However, the ARGONAUTE7 and TAS3A machinery necessary to produce these ta-siRNAs are restricted to the adaxial cells of the developing leaf. Hence, while *miRNA390* is found throughout the leaf, these ARF-targeting ta-siRNAs are only produced in the adaxial cells, but are also non-cell autonomous and form a gradient over the adaxial-abaxial axis. This gradient of ta-siRNAs promotes an inverse gradient of *ARF3* accumulation, with the strongest accumulation of the protein observed in the abaxial cells, where it promotes correct patterning (Chitwood et al., 2009).

There is still a great deal to be learnt about the roles of symplasmically moving signals in development but it is clear that the development of PD underlies many aspects of wider plant development. Therefore, understanding the patterns of complex PD development, both spatially and temporally, and which factors trigger and co-ordinate them, will allow deeper understanding of many plant developmental phenomena.

1.2.5 This project

As discussed above, although PD are a fundamental feature of plant development and plant cell biology in general, the small size, inaccessibility and exquisite sensitivity of these structures means that there are still many aspects of PD form and function yet to be understood. Complex PD in particular are not well understood, with only very recent work beginning to indicate their method of production and relationship to simple PD (Faulkner et al., 2008), their particular roles during development (Roberts and Oparka, 2003), and the mechanism underlying their co-ordination (Benitez-Alfonso et al., 2009; Burch-Smith and Zambryski, 2010).

This project aims to answer several related questions about the development of PD by asking them in a new way facilitated by a combination of new technologies and PD resources that have the potential to increase the scale and scope of PD research. As well as providing answers, this project also aims to develop techniques for studying PD that can be used for future research and lead to further widening of our knowledge about these fundamental plant organelles (Figure 11).

1.2.6 Aim 1: Investigate the suitability of available fluorescent markers for studies of PD development, and investigate the structure of PD using super resolution microscopy techniques.

Until now, electron microscopy has provided the lion's share of information on PD structure. However, despite the powerful resolution of EM techniques, we still have only basic understanding of PD structure due to a combination of limitations. EM techniques are restrictive in the positions and orientations that PD can be viewed, generally giving 2D images that section PD by chance and with the possibility of structural artefacts caused by harsh fixation protocols. Additionally, labelling and identifying structures in EM images is difficult as we have so little information about the protein components of PD, and hence many of the structures that have appeared in EM images for decades, such as the spoke-like proteins, remain unidentified (Bell and Oparka, 2011). Recently, however, new 'super-resolution' microscopy techniques have become available which circumvent the traditional limitations of light microscopy techniques, giving the potential for entirely new views of PD

structure. In addition, there are a number of putative PD-related and PD-localised proteins which, when linked to fluorescent tags, may provide useful probes for imaging PD structure via fluorescence microscopy, particularly viral movement proteins which specifically accumulate in the cavities of complex PD. For use in this project, I aim to assess the suitability of these for quantifying PD.

In Chapter 3, I will discuss these super resolution techniques and potential fluorescent markers for labelling PD in more detail and then present an investigation into PD structure using a combination of microscopy techniques, including the recently developed *Structured Illumination Microscopy*.

1.2.7 Aim 2: Survey the development of complex plasmodesmata in leaves

While we know that there is a general trend to reduce PD connectivity during development, often by conversion of simple PD to complex forms, imaging this process has so far been limited. Again, this restriction is largely because electron microscopy has been the only reliable way of determining the architecture of PDs. As before, while the resolution of electron microscopy images is excellent, the techniques have limitations for performing a detailed survey of PD development. With TEM, specific interfaces have to be sectioned longitudinally, capturing only a tiny slice of the information available. This, coupled with the laborious processing required, means that most studies using TEM use very small sample sizes. Field emission scanning electron microscopy (FESEM) methods allow us to image the surface of the wall, and so can give a great deal of information about the PD necks. However, only certain interfaces can be reliably imaged by FESEM, and no information about how the necks are connected beneath the wall is available, meaning it is impossible to study the distribution of PD structural types by this method.

The advent of markers for specifically labelling simple and complex PD offers the potential to survey PD structure and distribution using light microscopy techniques. Coupling traditional light-microscopy studies with new high-throughput microscopy

techniques should facilitate wide-ranging surveys of PD development that are broad in scope, significant in sample size and highly detailed.

Chapter 4 summarises the current state of knowledge of PD development in leaves with a brief literature review, and presents a survey of the development of complex PD in leaves using a combination of traditional and high-throughput microscopy.

1.2.8 Aim 3: Study complex PD development in real time.

The predominance of electron microscopy for studying PD development has a further limitation in understanding PD development in that these techniques require fixed samples. This precludes the possibility for dynamic studies which would allow us to follow PD development in real time. Instead, most of the temporal information we have about PD development is reconstructed from individual EM 'snapshots' of PD in tissues at different stages of development. This is problematic as PD development has been shown to be very variable. As above, however, the use of light microscopy methods and fluorescent markers opens the possibility for real-time studies of PD development in living tissues, allowing us to answer questions about the rates and ontogeny of complex PD.

Chapter 5 introduces the concepts of real-time imaging with a brief literature survey of current methods, with particular focus on the use of imaging chambers, and presents the first images of PD development in real-time. Additionally, this chapter investigates the particular uses of detached leaves for studying PD development.

1.2.9 Aim 4: Investigate the factors which control and co-ordinate the development of complex PD.

As discussed above, PD development shows large-scale organisation, both temporally and spatially, and it is expected that PD development is controlled by a wide range of cellular factors. So far, most of the information we have about the factors that control PD development come from EM analysis of mutants with altered PD formation, such as the *ise* mutants, described above.

Again, light microscopy, particularly high-throughput confocal microscopy opens the possibility of investigating the effects of various stresses and treatments on PD development more directly.

Chapter 4 discusses the potential of high-throughput confocal technology and software for studying PD development and presents an investigation into the patterns of PD development performed using high-throughput microscopy, while Chapter 6 presents a screen of a range of treatments for their effects on complex PD development.

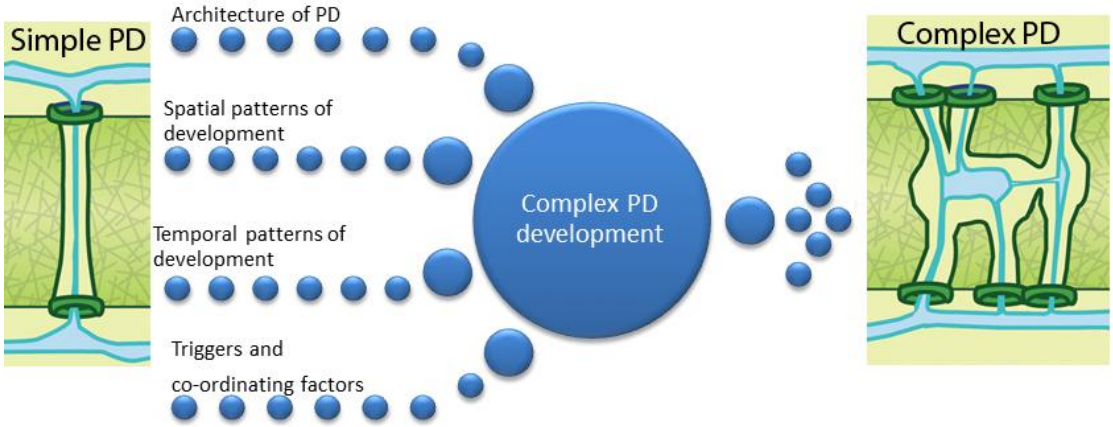

Figure 11: diagrammatic representation of my aims investigating the development of complex PD.

2 Chapter 2: Materials and Methods

2.1.1 Plant growth conditions

For *A. thaliana* grown on soil, seeds were stratified for at least two days at 4˚C, before sowing on compost. Plants were kept in controlled climate growth chambers (21˚C, 50% humidity) illuminated for 8h a day (short day conditions, SD) or 16h a day (long day conditions, LD) and bottom watered twice a week.

For *A. thaliana* grown on plates, seeds were surface sterilised by washing with 70% ethanol for 2 minutes, followed by washing with bleach for 10 minutes, before being thoroughly rinsed with sterile distilled water. Seeds were sown on prepared petri dishes of solid Murashige and Skoog medium (4.9 g/l MS salts, 3 g/l sucrose, 10 g/l Difco Agar. pH 5.8) using a pipette and sealed with Parafilm (Pechiney). Plates were vernalised for two days at 4˚C and then placed under a light bench on angled racks.

Nicotiana tabacum cv Xanthi plants and *Nicotiana tabacum* cv Samsun nn were grown from seed in a heated glasshouse and bottom watered daily. They were used for experiments between 30 and 55 days old.

2.1.2 Application of dyes

Unless otherwise noted, dyes were applied by immersing tissues for 5-15 minutes, and then rinsing with water. Where noted, infiltration was assisted by use of a vacuum infiltration chamber.

Aniline blue (Sigma-Aldrich) was used to stain callose. A working stock of 0.6 mM was made in PBS, and diluted to a working concentration of 0.25 mg/ml in dH_2O.

Calcofluor white (Sigma-Aldrich) was used to stain cell walls. A170 µg/ml stock was made in EtOH and diluted x10-100 in dH_2O for use.

$DiOC_6$ (Invitrogen Molecular Probes) was used to stain membrane structures. A stock solution of 5 mg/ml was used at a working concentration of 2 µg/ml.

Hexyl rhodamine B (Invitrogen Molecular Probes) was used to stain the sieve element reticulum. A stock was made at 2.5 mg/ml in DMSO, and used at a working concentration of 0.1 µg/ml.

Propidium iodide (Invitrogen Molecular Probes) was used to stain cell walls of living cells and to identify dead and damaged cells, where it also stains the nucleus. Stock solutions were made of 1-50 mg/ml depending on the application, and used at working concentrations of 50-100 μg/ml.

2.1.3 Widefield microscopy

Whole leaves, mounted on slides either with coverslips or with double-sided adhesive tape were imaged using a Leica DM 2500 Epifluoresence microscope with a x10 objective and a 480/40 filter to image GFP. Images were taken using *Leica Application Suite* software.

2.1.4 Confocal microscopy

Tissues were mounted on standard slides with coverslips and imaged using a Leica SP2 microscope using x5 or x20 dry objectives, x40 or x63 water immersion objectives, x63 water dipping objective or a x100 oil dipping objective. Images were taken using the *Leica Confocal Suite* software, which was also used to perform sequential scanning, lambda scanning and FRAP (see later for detailed method), and to perform limited aspects of image processing including production of projections from stacks. The following laser lines were used: 405nm, 488nm, 561nm and 663nm.

More advanced image processing was performed with *ImageJ* software.

2.1.5 FESEM imaging

Source leaves (8-15mm) were detached using a razor and mounted adaxial side down on a plate spread with colloidal graphite (Agar scientific G303). Leaves were then snap frozen in liquid nitrogen and transferred into a Gatan Alto 2500 cryopreparation chamber under low vacuum. The lower epidermis was then fractured by scraping a scalpel blade along the surface, before being coated with 60:40 gold:palladium alloy under an argon atmosphere. Samples were then imaged using a Hitachi 4700 II cold field-emission scanning electron microscope (Hitachi High Technologies). A modified method was used to produce clearer views of epidermal mesophyll connections. Leaves were mounted abaxial side down as above, and a square of steel mesh attached to the top surface with colloidal graphite. Leaves were frozen and treated as before, and the mesh peeled off to remove upper tissue layers of the leaf.

2.1.6 TEM

For TEM, tissue was fixed in 3% glutaraldehyde in 0.1 M sodium cacodylate (pH 7.3) for 3 hours and then washed for 3 x 20minutes in 0.1 M Sodium cacodylate on a rocker. The tissue was postfixed in 1% osmium tetroxide in 0.1 M sodium cacodylate buffer for 1 hour and then washed for 3x15 minutes in 0.1 M sodium cacodylate on a rocker. The tissue was then dehydrated in an ethanol series: 50% EtOH for 15 minutes, 70% EtOH for 15 minutes, 90% EtOH for 15 minutes, 100% EtOH for 3 x 15 minutes.

The tissue was then infiltrated in Agar100 epoxy resin (Agar Scientific, UK). Tissue was first immersed in a 1:1 mix of Agar 100 mix without accelerator (24 g Agar 100 epoxy resin, with 16 g DDSA hardener and 8 g MNA hardener) and propylene oxide for 1 hour on a rocker, then a 2:1 mixture of Agar 100 mix without accelerator and propylene oxide overnight, then in Agar 100 mix without accelerator alone for 2 x 1 hour, and then in Agar 100 with accelerator (24 g Agar 100 epoxy resin, with 16 g DDSA hardener, 8 g MNA hardener, 1.5 g BDMA accelerator) 1x 1 hour. The tissue in Agar 100 was then put into gelatin capsules, and baked in an oven at 58ºC for 48h.

Embedded tissues were then sectioned with a microtome, and imaged using a Philips BioTwin transmission electron microscope.

2.1.7 Fixation of tissue for SIM imaging

The abaxial epidermal layer was removed from mature *A. thaliana* or *N. tabacum* leaves with forceps and immediately fixed in PME buffer (50mM PIPES, 2 mM EGTA, 2 mM $MgSO_4$, pH6.8) with 4% paraformaldehyde and 0.25% gluteraldehyde for 1h. The tissue samples were then washed with PME. Peels were then mounted in Citifluor with slides and coverslips sealed with nail varnish.

2.1.8 Immunofluorescence

For immunofluorescence epidermal peels were taken and fixed as above. Alternatively, fresh tissue was embedded in 3% phytoagar (Duchefa Biochemie) and 15-50µm slices were taken using a vibroslice tissue cutter (model HA752, Campden Instruments) in PBS buffer. After peeling or sectioning, tissue was immediately fixed in PME buffer with 4% paraformaldehyde and 0.25% gluteraldehyde for 1h. The

tissue samples were then washed with PME and the walls digested with 2% Driselase (Sigma-Aldrich), 1% BSA and 5mM EDTA in PBS buffer for 15mins at 37˚C. The tissue samples were rinsed in PME with 10% glycerol and 0.2% Triton X-100 (Fisher Chemical), and then washed in PME. Non-specific antibody sites were blocked with PBS containing 3% BSA and 50 mM glycine for 20mins, before the peels were incubated overnight at 37˚C with the primary anticallose antibody (mouse) diluted to 1:100 with PBS with 1% BSA and 0.02% Tween-20. Peels were then rinsed with PBS containing 3% BSA and 50 mM glycine and were then incubated for 3h at 37˚C with the secondary anti-mouse Alexa 594 antibody diluted in PBS with 1% BSA and 0.02% Tween-20. Finally the peels were rinsed in PBS. The peels were mounted in Citifluor (Citifluor Ltd., UK).

2.1.9 Fluorescence recovery after photobleaching

FRAP was performed as described in Fitzgibbon et al. (2010), from which this method section is reproduced. Large petiole pieces were immersed in PBS and cut into fine longitudinal sections with a scalpel. Sections from MP-GFP plants were incubated in 0.25 mg/ml aniline blue solution while sections from wild-type tobacco (Samsun nn) plants were incubated in a 0.25 mg/ml aniline blue/ 2µg/ml $DiOC_6$ solution for 10 min. Sections were then immersed in clean PBS and washed for 5 min with agitation before being mounted on slides with coverslips.

FRAP was performed using the Leica Confocal Suite FRAP Wizard. Five pre-bleach images were collected with a 488 nm laser at 20% intensity (x63 water objective, unidirectional scan, zoom x3, resolution 512x512), and then a 10 μm^2 region was specifically bleached using ten scans with the 488 nm laser at 100% intensity. Postbleach images were then collected using the same settings as the prebleach images for approximately fifteen minutes in total. Scans were taken every second for the first 30s, then every 10s for the next 150s, and then every minute for the subsequent 12min. The background fluorescence was subtracted from all values, and each series was corrected for bleaching during the postbleach acquisition phase using an area of fluorescence outside of the cell containing the region of interest for reference. Fluorescence readings were then normalised to percentage values of the pre-bleach fluorescence and the normalised measurements averaged.

2.1.10 Structured illumination

SIM imaging was performed as described in Fitzgibbon et al. (2010) from which this method section is reproduced. The protocol applied was based on that described by Schermelleh et al. (2008). Images were acquired using a UPlanSApochromat 100x 1.4NA oil immersion objective lens (Olympus) and back-illuminated Cascade II 512x512 EMCCD camera (Photometrics) on the OMX version 2 system (Applied Precision) equipped with 405, 488 and 593 solid state lasers. Samples were illuminated by a coherent scrambled laser light source that had passed through a diffraction grating to generate the structured illumination by interference of light orders in the image plane to create a 3D sinusoidal pattern, with lateral stripes approximately 0.2 μm apart. The pattern was shifted laterally through 5 phases and through 3 angular rotations of 60' for each Z-section, separated by 0.125 μm. Exposure times were typically between 50-250 ms and the power of each laser was adjusted to achieve optimal intensities of between 2000 and 4000 counts in a raw image of 16-bit dynamic range, at the lowest possible laser power to minimise photo-bleaching. Where required, the cameras were run in EMCCD mode and gain was applied. Each frame acquisition was separated by a 300 ms pause.

Raw images were processed and reconstructed to reveal structures with greater resolution (Gustaffson et al., 2008). The channels were then aligned in x, y and rotationally using predetermined shifts as measured using a target lens and 100 nm Tetraspeck fluorescent microspheres (Invitrogen) in the Softworx alignment tool (Applied Precision).

2.1.11 Maintenance of detached leaves

Dishes were prepared by stapling together stacks of 8 filter papers (Whatman), and cutting parallel slits through the thickness of the stack using a clean razor. The paper stacks were then placed inside Petri dishes and soaked with water or 0.5%, 1%, 3%, 6%, 12% solutions of sucrose. Leaves were detached from soil grown plants using a clean razor and stood with petioles in the slits in the filter paper stacks. Dishes were sealed with Parafilm, and placed horizontally on a light bench.

Alternatively, leaves were detached using a clean razor and floated in Petri dishes filled with media as above.

2.1.12 Maintenance of detached leaves in an imaging chamber

For observation in chambers leaves were detached and mounted in a drop of sterile water in a 'chamber' formed by a standard no 1 coverslip and a section of breathable membrane (Lumox Folie 25 μm film, In Vitro Systems and Services) separated by a circle of double-sided adhesive (SecureSeal Adhesive Sheet, Grace Bio-labs) and mounted in a custom-made plastic frame (University of Edinburgh Darwin Building Workshop) with tape. In certain experiments water was replaced with a 1% solution of sucrose in distilled water. Chambers were maintained horizontally on a light bench.

2.1.13 Leaf removal experiments

Mature *pAtSUC2: GFP A. thaliana* plants at the 15-16 leaf stage were selected. All leaves but the youngest visible three were removed using tweezers. Plants were then imaged immediately (0 h) or returned to the growth chamber and imaged on the widefield microscope at 12 h or 24 h after leaf removal.

2.1.14 Growth and imaging of *A. thaliana* for the treatment survey

MP17-GFP or *pAtSUC2::GFP* seeds were sown on x0.5 strength Murashige and Skoog medium (0.215% MS salts, 0.6% Sucrose, 1% Phytoagar, pH 5.8) and vernalised at 4ºC for 2 days. Plates were then placed upright under a light bench and grown for 5 days, at which point the seedlings were established and the first true leaves had emerged. At this point, seedlings were transferred using fine forceps to 0.5 MS plates containing appropriate treatments and grown for a further five days.

A variation of this growth procedure was used for treatment with flg22 to avoid prolonged exposure of seedlings to the peptide. Seedlings were grown on solid 0.5 MS plates as above for 5 days. Before transfer, however, seedling roots were soaked in flg22 in liquid MS and incubated for 30 minutes. Roots were then rinsed with dH_2O and seedlings transferred to fresh 0.5 MS plates.

Treatment stocks were made and used as followed. Where solutions were filter sterilised, Millex syringe driven filters (Millipore, USA) were used.

1-Naphthaleneacetic acid (NAA): a 1mM stock was made by dissolving solid 1-NAA (Sigma-Aldrich), in 2 ml of hot EtOH, and made up to volume with hot dH_2O, and filter sterilised. The stock solution was diluted to working concentrations in melted 0.5 MS.

2,4-D: a 1mM stock was made by dissolving solid 2,4-D (Sigma-Aldrich), in 2 ml of hot EtOH, and made up to volume with hot dH_2O, and filter sterilised. The stock solution was diluted to working concentrations in melted 0.5 MS.

Benzylaminopurine (BA): a 400 μM stock solution was made by dissolving BA powder (Fisher Bioscience) in dH_2O and filter sterilising. The stock solution was diluted to working concentrations in melted 0.5 MS.

Befreldin A (BFA): a 50 mM stock solution was made by dissolving BFA powder (Invitrogen) in DMSO. The stock solution was diluted to working concentrations in melted 0.5 MS medium.

NaCl: a 1 M stock solution was made by dissolving NaCl (Fisher Bioscience) in dH_2O. The stock solution was diluted to working concentrations in melted 0.5 MS medium.

Sucrose: 0.5MS was melted, and sucrose (Fisher Bioscience) to the working concentration was added. The medium was then autoclaved again.

Glucose: 0.5MS was melted, and glucose (Fisher Bioscience) to the working concentration was added. The medium was then autoclaved again.

Sorbitol: 0.5MS was melted, and sorbitol (Fisher Bioscience) to the working concentration was added. The medium was then autoclaved again.

Mannitol: 0.5MS was melted, and mannitol (Fisher Bioscience) to the working concentration was added. The medium was then autoclaved again.

Hydrogen Peroxide: H_2O_2 was supplied as a 3% stock solution (Sigma-Aldrich). It was diluted to working concentrations in melted 0.5 MS medium.

Methyl Jasmonate: a 0.1 M stock was made by diluting a 95% stock (Sigma-Aldrich) with water. This was then filter sterilised, and diluted to working concentrations in diluted MS medium.

Salicyclic Acid: a 0.1 M stock was prepared by dissolving salicylic acid (Sigma-Aldrich) in dH_2O. This was filter sterilised, and diluted to working concentrations in diluted MS medium.

Flg22: A 1 mM stock was made by diluting powdered Flg22 (AnaSpec Inc, Canada) in water. This was diluted with liquid 0.5 MS (0.215% MS salts, 0.6% Sucrose. pH 5.8).

2.1.15 Imaging of plants in the treatment survey

Digital images of the plates were taken using a scanner (EPSON) and the root length measured using ImageJ software. The seedlings were weighed in batches of 4-5 and the 2nd youngest leaf (third leaf chronologically) was removed and scored along the midrib with a clean razor to aid dye penetration and reduce curvature. Leaves were then immersed in 100 mg/ml propidium iodide for ten minutes, rinsed in water, and mounted on standard slides with coverslips.

Leaves were imaged using a Leica SP2 with a x63 water immersion lens. GFP was imaged using a 488nm laser; PI was imaged using a 561nm laser. An area approximately halfway up the leaf was imaged. Mounted leaves were scanned and measured using ImageJ software. Estimates of cell area and cell periphery were taken from maximum projections of the propidium iodide stain, which were averaged to consistent weights and thicknesses using the *Threshold*, *Smooth*, *Skeletonize* and *Find Edges* tools, and measured using the *Analyze Particles* tool to produce a map of the cells with perimeter and circumference measurements. From these outlines, groups of 15 touching cells which had been fully imaged were selected and MP17-labelled PD in epidermal-epidermal cell interfaces were counted by eye using the 'multiple points' tool through all images of the original image stack.

2.1.16 Opera treatment experiments

For the Opera experiments, plants were grown as for the treatment survey as above, but were maintained on treatment media for six days before imaging.

For imaging, leaves were detached using surgical scissors and propidium iodide was infiltrated under vacuum for ten minutes. Leaves were mounted on a custom-built rubber stamp using silica gel and pressed into 96-well glass-bottomed plates (Griener).

Plates were imaged using a spinning disc automated Opera microscope system (PerkinElmer, Germany) as in Salomon et al., 2010. GFP was excited at 488 nm and PI at 561 nm and imaged using a 20x water immersion objective. In a single run, three image stacks of 27 images 1 μm apart were taken per well, and each plate was run three times to produce 9 stacks per well. Each plate was run three times, to take a total of 9, 27-image stacks in a grid around the centre of the imaging well.

The resulting stacks were analysed using custom scripts for Acapella software (PerkinElmer) written by Ji Zhou at The Sainsbury laboratory, Norwich.

2.1.17 Opera development experiment

For the development experiment, the youngest six leaves were removed from SD soil-grown plants using surgical scissors. Leaves of approximately 3 mm length or less were mounted whole, while a cork-borer was used to cut sections from the lamina of larger leaves which were mounted on stamps as above.

3 Chapter 3: Imaging Plasmodesmata

3.1 Introduction

3.1.1 Imaging and identifying PD using fluorescent markers

As discussed in Chapter 1, the overall aim of this project was to investigate the development of complex plasmodesmata. In order to follow and understand the development of PD it was necessary to image and identify them and, therefore, to label them.

There are two major classes of proteins that can be used to label PD: endogenous plant proteins and viral movement proteins (MPs). In general, endogenous plant proteins that localise to PD target PD of all kinds; simple and complex, primary and secondary; and so are useful for looking at the entire population of PD in a tissue. In contrast, several classes of viral movement proteins have been found to specifically accumulate in the central cavities of complex PD while leaving simple PD unlabelled, providing a useful means to distinguish simple and complex PD. Unfortunately, no labels currently exist that allow primary and secondary PD to be distinguished, and currently these classes of PD cannot be identified by any means other than precise recording of their ontogeny.

3.1.2 Labelling all PD with endogenous plant proteins

Few PD-related proteins have been identified due to the difficulties in analysing PD using standard genetic or proteomic processes, as discussed in Chapter 1. Recently, however, promising candidates for specific PD markers have been identified by Andrew Maule and colleagues through their proteomics work on PD-enriched cell wall fractions (Bayer et al., 2006; Fernandez-Calvino et al., 2011). This work led to the identification of two families of PD-related proteins: the plasmodesmata localised protein (PDLP) family and the plasmodesmata callose binding (PDCB) family (Figure 12A and B).

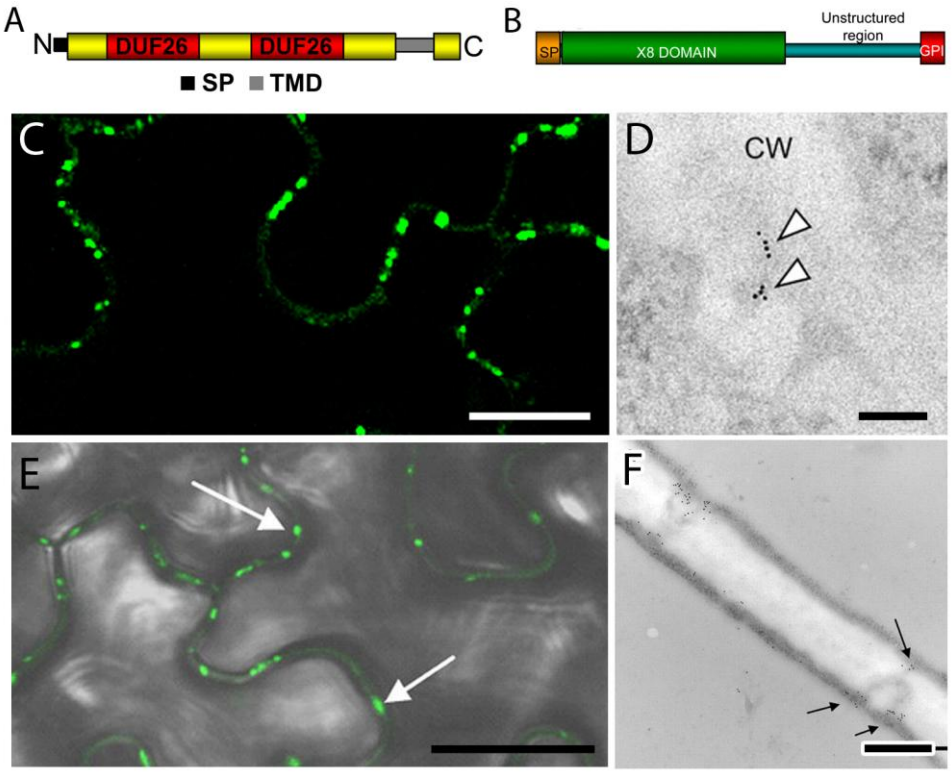

Figure 12: Proteins for labelling PD. A) Domain structure of PDLP1, SP = signal peptide, TMD = transmembrane domain. B) Domain structure of PDCB1. C) 35S::PDLP1a-GFP localises to punctate spots in the epidermal cell walls. D) Immunogold labelling of PDLP5-GFP with an antibody to GFP reveals that it localises to the middle region of PD (darts). E) Fluorescence image of 35S::ProYFP-PDCB1 localises to punctate spots in cell walls (arrows). F) Immunogold labelling of PDCB1 with PDCB1 antiserum shows it localises to PD necks (arrows). A and C from Thomas et al. (2008), B, E and F from Simpson et al. (2009), D from Lee et al. (2011), Scale bars: C and E = 10 µm, D = 100 nm , F = 500 nm.

The identification of PDLP1 led to discovery of an eight-gene family encoding 30-35 kDa type 1 membrane proteins. All of the PDLP genes localise to PD (Figure 12C and D) and all have a similar conserved structure: an extracellular N-terminal signal sequence, two extracellular DUF26 domains (function unknown), a trans-membrane domain and an intracellular C-terminal tail (Figure 12A) (Lee et al., 2011; Thomas et al., 2008). The transmembrane domain has been shown to be responsible for targeting this protein to PD (Thomas et al., 2008), and detailed studies of PDLP5 have shown that it localises to the plasma membrane at the central part of PD (Lee et al., 2011). Initially the function of these genes was unknown, although a role in PD gating was suggested by reduced trafficking in overexpression lines and increased trafficking in several PDLP double knock out lines (Thomas et al., 2008). However, recent work suggests that PDLP5 promotes callose deposition at PD and that its expression is promoted in a positive feedback loop by salicylic acid, the major long-

distance plant defence signal. This strongly suggests that PDLP5 forms a link between defence responses and restriction of PD SEL. Whether the other PDLP genes are also involved in defence response remains to be determined, although it is notable that 35S::PDLP1 lines do not exhibit the same spontaneous tissue death observed in 35S::PDLP5 lines. PDLP1 is therefore a good potential candidate for a general PD marker that could accurately label all PD for localisation by fluorescence microscopy.

Other candidates for specific PD tags found by the Maule group are the PDCB family of proteins which localise to the apoplastic face of the membrane around PD, binding via a covalent GPI-anchor (Simpson et al., 2009). The association with PD was confirmed by immunolocalisation, and a fluorescently tagged version was shown to mark wall punctae (Figure 12E and F). These proteins bind callose via their X8 domain but appear to have no catalytic activity. Expression of PDCB 1, 2 and 3 is strongest in the shoot apex and weaker in vegetative tissues, but so far the precise functions of these genes remains unknown. As with the PDLP family, overexpression may cause restriction of flux through PD that, due to the callose binding nature of PDCB proteins, is expected to be mediated by callose deposition at the PD pores. Despite this, overexpression lines show few phenotypes making these proteins potential candidates for use as fluorescent tags for labelling PD.

3.1.3 Labelling of complex PD with viral movement proteins

Many plant viruses encode viral MPs to facilitate their cell-to-cell trafficking through PD. Immunolocalisation has shown that MPs of certain strains accumulate specifically within PD central cavities of complex plasmodesmata, both alone and when fused to fluorescent proteins to facilitate imaging by fluorescence microscopy. The two viral MPs most widely used in studies related to PD are potato leafroll virus (PLRV) MP17 in *Arabidopsis* and tobacco mosaic virus (TMV) MP30K in *Nicotiana* species.

PLRV, a luteovirus, is aphid-transmitted and remains restricted to phloem tissues during wildtype infections (Schmitz et al., 1997) and its 17K movement protein is thought to play multiple roles to allow cell-cell spread of the virus. Its mechanisms

are yet to be fully identified, but it is known to have an N-terminal amphiphatic α-helix thought to function in oligomerisation, and a C-terminal single-stranded nucleic acid binding domain (Tacke et al., 1991). The MP targets PD using the actin cytoskeleton and the host secretory pathway machinery (Vogel et al., 2007), and it has been shown to specifically localise to complex PD when expressed in *A. thaliana* (Kronberg et al., 2007) and *N. tabacum* (Hofius et al., 2001) and a GFP-tagged versions retains strong localisation to PD (Vogel et al., 2007) (Figure 13A-C). MP17 appears to be very suitable as a label for studying PD, although studies have shown that MP17 may potentially modify carbohydrate partitioning (Hofius et al., 2001). This can cause some growth inhibition in overexpression lines but the effect is minimal in the young leaves which are the basis for this study, as proteasome-mediated degradation prevents the protein from building up to excessive levels (Vogel et al, 2007). Some researchers have questioned the PD specificity of MP17 after observing aggregations of MP17-GFP in root tissues (Burch-Smith et al., 2011). However we have never observed such aggregations in our lines at any stage of root development, and instead see specific PD labelling throughout tissues.

TMV is a tobamovirus and, as its 30K MP was the first viral MP identified, it has provided a great deal of insight to both virologists and plant scientists studying PD. Immunolocalisation studies have shown that 30K localises to complex PD, leaving simple PD unlabelled (Figure 13E-G)(Ding et al., 1992) and targets PD in both wild type infections (Tomenius et al., 1987) and in transgenic overexpression lines alone (Atkins et al., 1991) or fused to GFP (Lee et al., 2011). Accumulated virus material is sometimes visible in EM sections as filamentous material within the PD cavities, and this material is absent from simple PD (Ding et al., 1992). As well as transiently gating the PD pore, the 30K MP is thought to be directly involved in shuttling the virus from cell-to-cell via a single stranded RNA binding domain, an association with microtubules, and a tubule forming property (reviewed in Okada, 1999). TMV MP has been used in many studies of PD, including those identifying developmental shifts in PD architecture (Roberts et al., 2001).

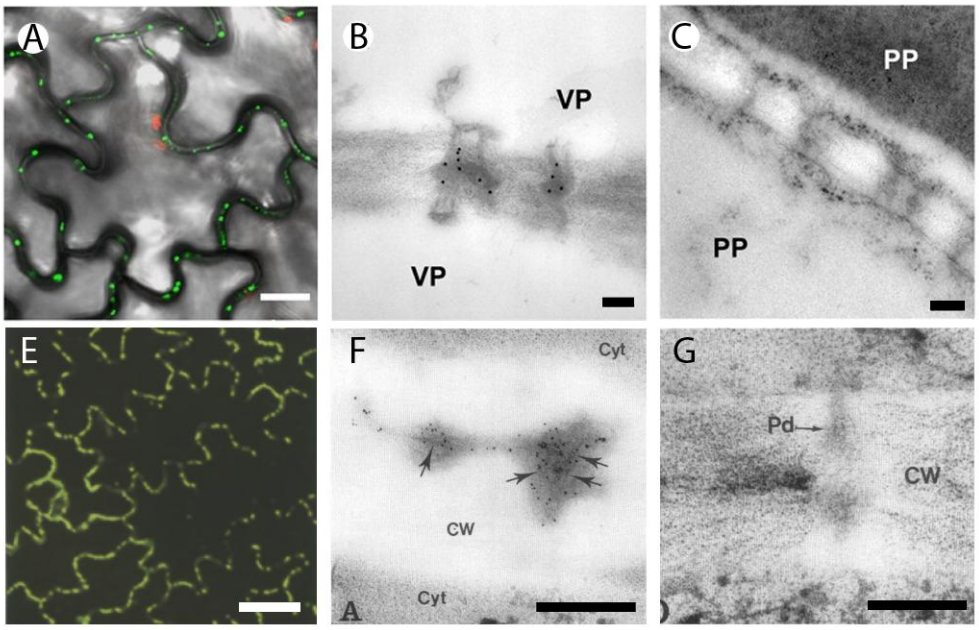

Figure 13: PD labelling by PLRV MP17 (top) and TMV 30K (bottom). A) 35S::MP17-GFP labels fluorescent spots in the wall of mature leaf epidermal cells. B) MP labelling of complex PD while, in the same study, simple PD (C) are unlabelled. E) 35S::30K-GFP labels punctate spots in epidermal cells. F) Immunogold labelling for 30K shows that it is present in cavities of complex PD (F, arrows) and, in the same study, absent from simple PD (G). VP = vascular parenchyma, PP = palisade parenchyma, CW = cell wall, Cyt = cytosol. Scale bars: A = 10 µm, B and C = 15 nm, E = 50 µm, F and G = 100 nm. A-C from Kronberg et al. (2007), E from Roberts et al. (2001), F and G from Ding et al. (1992).

3.1.4 Imaging the structure of PD

For the purposes of this investigation, it was not necessary to see the precise structure of every PD so long as the labels used to mark them were specific, and that markers for all PD or complex PD alone accurately reflect PD structure. There are two main options for imaging PD ultrastructure, each with its strengths and restrictions: electron microscopy techniques and super-resolution light microscopy techniques.

Electron microscopy (EM) has been used to study PD since the advent of the technology in the 1950s. The high spatial resolution of EM techniques, which can approach the molecular level, has produced the most informative views of PD ultrastructure so far (reviewed in Bell and Oparka, 2011). However, this high resolution comes with many restrictions. EM requires fixed samples, which precludes live-cell imaging and can induce tissue shrinkage and other artefacts. Also, unlike confocal laser scanning (CLSM) and other light microscopy techniques where tissues can be routinely imaged in three dimensions by optical sectioning, EM techniques such as transmission EM (TEM) and field emission scanning EM

(FESEM) generally only allow visualisation in a single plane. Techniques for 3D reconstruction of tissues exist, e.g.: serial block face scanning electron microscopy, but this requires either extremely technically challenging manual work or equipment for automated processing that is not yet widely available (Denk and Horstmann, 2004). Finally, but perhaps most significantly, while EM can give high-resolution images of structures, identification of those structures can be extremely difficult. This is why the identity and function of the 'spoke-like' and 'globular' proteins in the cytoplasmic sleeve, and spiralling particles in the wall around the PD channel, still remain to be identified (Maule, 2008).

Conventional light microscopy has traditionally been of little use for imaging PD structure as the resolution is limited by the diffraction of light. This means that a single point viewed through an objective appears as a point spread function (PSF) of 200 nm laterally and 500 nm axially (Figure 14A) (Fernandez-Suarez and Ting, 2008; Hell et al., 2004). This restriction also applies to CLSM systems where the detected light is focused through a pinhole to reduce the amount of out-of-focus light. With an average diameter of 100 nm (including the collar), the PSF comfortably accommodates a PD so while CLSM can be used to locate PD, the structural information available is extremely limited. This means that so far, the revolution in microscopy caused by the discovery of GFP has had little impact on our understanding of PD structure.

In recent years, a range of 'super-resolution' microscopy techniques have been developed that surpass the resolution limit of conventional fluorescence microscopy (Figure 14B). Although there is now a large range of super-resolution techniques, most of these are variations of two main core concepts that were developed more-or-less simultaneously: single molecule imaging, and mechanisms to circumvent the PSF (Galbraith and Galbraith, 2011). Although the first super-resolution images were generated in 1992, by a technique called near-field scanning optical microscopy super-resolution imaging in biological research is still becoming established (see Fernandez-Suarez and Ting, 2008) with off-the-shelf microscopes only just becoming available.

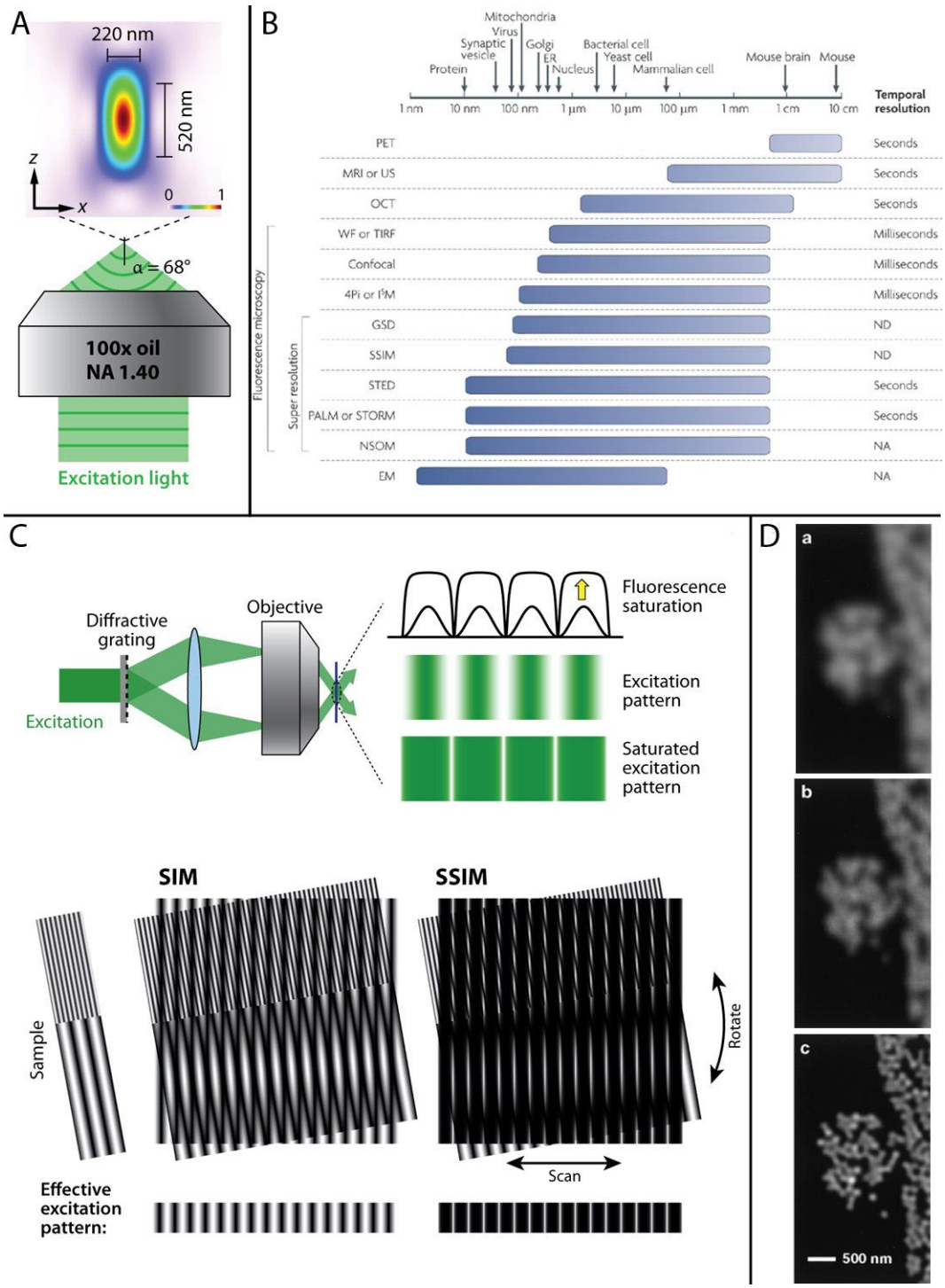

Figure 14: A: diagram illustrating the concept of a point spread function (PSF). Diffraction of light means that a focal point viewed through a microscope objective (grey box) appears as a blurred spot, limiting the spatial resolution. NA = numerical aperture of the lens. B) comparison of the spatial and temporal resolution of a range of common microscopy techniques, shown against the average sizes of a selection of biological subjects. C) Diagrammatic illustration of structured illumination microscopy (SIM). The excitation light is passed through a grid that gives it a sub-resolution 'structured' pattern (top). As the patterned light interacts with the sample it generates Moiré fringes (bottom) from which high-resolution data can be inferred. D: Comparison of (a) conventional widefield microscopy (b) CLSM and (c) SIM of 121 nm diameter fluorescent beads. A and C from Huang et al. (2009), B from Fernández-Suárez & Ting (2008), D from Gustafsson (2000).

One super resolution technique that is in the process of gaining widespread use is Structured Illumination Microscopy (SIM). This technique works by passing the illumination light through a fine, rotating grid that gives the light a sub-resolution pattern of stripes (i.e.: makes it 'structured'). Interactions between this sub-resolution striped pattern and sub-resolution details of the sample generate Moiré fringes that are large enough to be resolved by the microscope (Figure 14C). The known striped pattern can then be subtracted from the Moiré fringe pattern to reconstruct sub-resolution details in the sample (Gustafsson, 2000). In practice this decreases the resolution limit of the microscope to ~100 nm in xy and ~200 nm in z (Figure 14D). Additionally, SIM can work with conventional fluorophores and dyes and, unlike other super resolution techniques, can image tissues that have cell walls and autofluorescent structures (Fernandez-Suarez and Ting, 2008). Therefore, SIM offers the potential to look at PD in an entirely new way.

3.2 Aims

The availability of conventional light microscopy, EM techniques and super-resolution light microscopy, plus a suite of potential candidates for fluorescent PD tags, opened exciting possibilities for the study of PD structure and development. The work in this chapter was the foundation for future experiments that almost exclusively used confocal microscopy, and so aimed to establish as much information as possible about the fine structure of PD in leaves and the specificity of available markers for understanding development. The overall aims were:

- To ascertain the suitability of available PD markers for studying PD, both structurally and developmentally. These were MP17, MP30K, PDLP1, and PDCB1.

- To provide detailed, high-resolution images of PD in the tissues of interest using TEM, FESEM and SIM to provide a reference for future work reliant on lower resolution techniques.

- To use new super-resolution techniques to image the details of PD structure.

3.3 Results

3.3.1 CLSM imaging of complex PD in leaves using MP17-GFP

As the major aim of this project was to study the development of complex PD using *A. thaliana* as the model species, I expected that a 35S::MP17-GFP *A. thaliana* line would be one of the most valuable tools available. It was already well established through immunolocalisation studies that MP17-GFP specifically labels complex PD in *A. thaliana.* However, I wished to do additional experiments to confirm this. I therefore performed a study of the MP17-GFP accumulation pattern in leaves using CLSM. This would produce a map of complex PD location that could then be correlated with EM studies of PD location and architecture to help confirm the specificity of the marker. For CLSM imaging, mature leaves were either mounted whole, abaxial side up, or in thin cross sections made using a vibroslice (Campden Instruments). Leaves were incubated with propidium iodide (PI), which stains the walls of living cells and the cytoplasm and nucleus of dead cells, to allow the arrangement of PD within and between different tissue layers to be seen.

In the anticlinal walls between neighbouring epidermal cells (E-E interfaces), MP17-GFP labelling shows that PD appear around the entire circumference of all cells (Figure 15A and B), and may appear at any depth within the wall (Figure 15E and F). Although the MP17-GFP labelling shows some loose clustering, as shown by longitudinal views in which the punctae sometimes appear in groups with unlabelled regions between, the transverse view shows that they do not seem to form typical pit fields (Figure 15F).

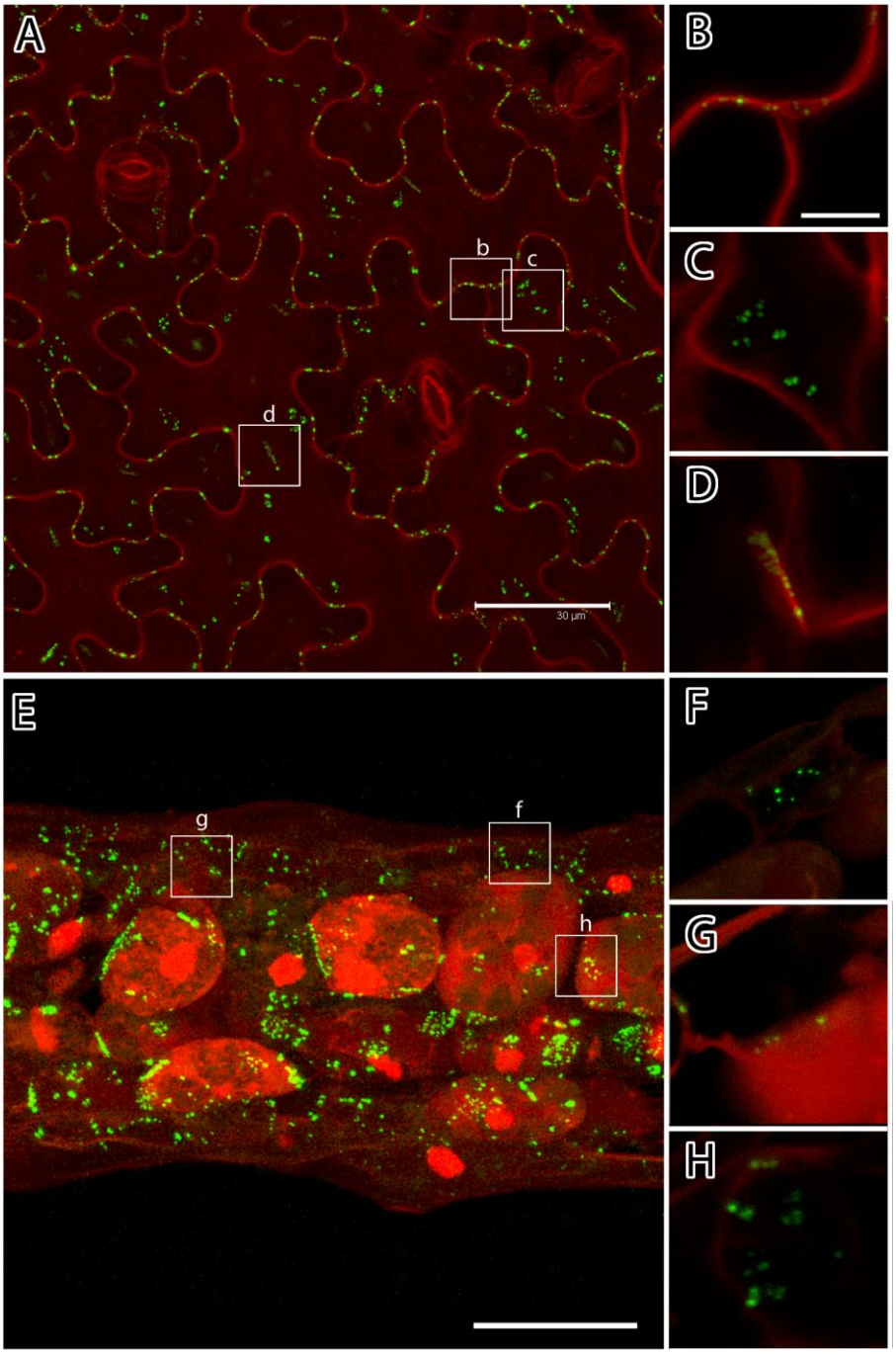

Figure 15: CLSM of *A. thaliana* leaves expressing MP17-GFP (green) and stained with propidium iodide (red). A: Projection of a 1.5 µm step optical stack of longitudinal images taken through the abaxial epidermis and partway into the mesophyll. B-D: Detail of boxed areas in A showing longitudinal stacks through PD at the E-E (B), E-M (C) and M-M (D) interface. E: Cross section through the lamina. The thin cross section caused most cells to be cut, hence the heavy PI staining. F-H: detail of the boxed areas in E showing PD at the E-E (F), E-M (G) and M-M (H) interfaces. Scale bars in A and E = 30 µm, scale bar in B for B-D and F-H = 6 µm.

In interfaces between the epidermal layer and the mesophyll (E-M interfaces), however, MP17-labelled punctae appear in distinct pit fields (Figure 15A, C, E, G). This is most easily seen in the longitudinal views, where groups of punctae, often numbering ten or more, can be seen in well-spaced clusters (Figure 15A and C). Part of this spacing is because contact between the epidermal and mesophyll layer is broken by air spaces, however transverse views show that there are unlabelled areas even where the epidermal and mesophyll cells are in contact (Figure 15E and G).

In contrast, where mesophyll cells are in contact with one another (M-M interfaces) the MP17 label is densely packed across almost the whole of the interface (Figure 15A, D, E and H). Often individual cavities cannot be distinguished, particularly in longitudinal views where the M-M interfaces often appear as a GFP-fluorescent streak that covers the whole interface (Figure 15A and D).

3.3.2 CLSM imaging of general PD markers

Although it is known that both PDLP1 and PDCB1 target PD, their suitability as markers of PD has not yet been assessed. Therefore I imaged leaves from an *A. thaliana* line expressing 35S::PDLP1-mRFP (courtesy of A. Maule) alone or crossed with 35S::MP17-GFP by CLSM as above (Figure 16A-C). Both plant lines showed mRFP-labelled punctae in the cell wall that suggested PD-labelling. However, in both cases there was strong background fluorescence in the wall and vacuole that made PD localisation ambiguous, particularly in smaller cells.

Lines expressing 35S::PDCB1-mCherry (courtesy of A. Maule), either alone or crossed to 35S::MP17-GFP were analysed as for PDLP1. In young leaves, the marker showed localisation to wall punctae as reported (Simpson et al., 2009), albeit with some background wall fluorescence (Figure 16E shows a maximum projection of an optical stack through the depth of the E-E interface). However, as the age of leaves increased, non-specific wall labelling became increasingly prevalent, particularly at the lobe-tips of the epidermal cells (Figure 16F). Spherical aggregations of mCherry also developed, either at walls of the E-E interface or at the epidermal side of the E-M interface.

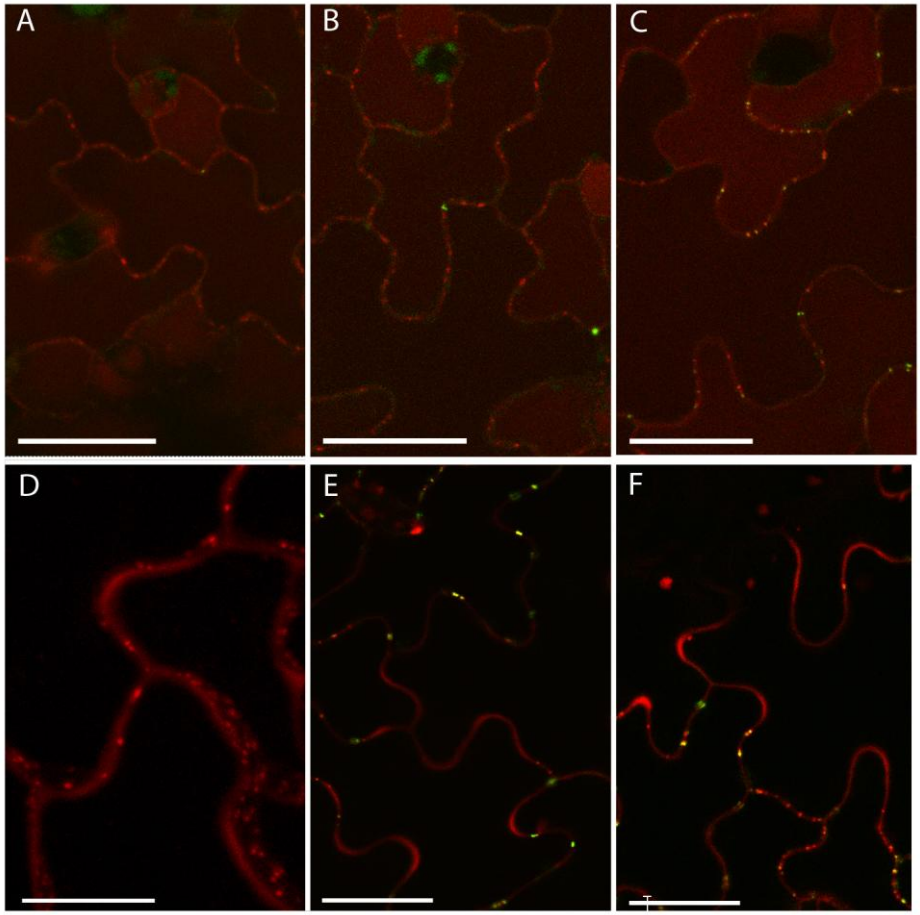

Figure 16: PD markers imaged by CLSM. A-C: PDCB1-mRFP in (A) a young leaf of 2.5 mm length, (B) a transition leaf of 4.5 mm length and (C) a mature leaf of 9 mm length, showing the background red fluorescence that makes it difficult to use this maker to quantify PD. D-F: PDCB1-mCherry. D: a maximum projection of an optical stack taken through angled anticlinal walls in a young leaf, showing acceptable specificity to PD, albeit with some background labelling. E and F: mature leaves from PDCB1-mCherry x MP17-GFP expressing plants showing that in older cells, PDCB1 staining does not form punctae in the walls (E) and sometimes forms spherical aggregations at the periclinal walls of the epidermal cells (F). Scale bars in A-C, E, F = 20 µm, scale bar in D = 10 µm

3.3.3 FESEM Imaging of PD in leaves

The confocal study showed that available markers for simple PD are not specific enough to provide a true assessment of the PD population. Furthermore, while the MP17-GFP label did produce clear punctae in a pattern resembling the expected layout of PD, an MP17-GFP labelled puncta suggests only that a PD with a cavity is present; it gives no information about the number or conformation of the necks of the PD. To gain a fuller picture of the PD population in mature leaves I analysed freeze-fractured tissue by FESEM using two protocols. In one, leaves were attached abaxial-side down to plates using colloidal graphite, and then a panel of steel mesh was fixed to the upper epidermis using more colloidal graphite, before snap freezing the leaves at low pressure. Once frozen, the mesh panels were pulled away, removing part of the tissue underneath. Figure 17A and B shows that this technique exposed adaxial E-M, M-M and abaxial E-M interfaces. The second method was to attach leaves adaxial-side down to slides and freeze as above, and then use a scalpel to shatter the tissue. This method allowed imaging of M-M and, more rarely, E-E interfaces (Figure 17C), which, due to their interlocking shape and tight connections do not readily break along the wall as mesophyll cells do. Both techniques fractured tissue so that the walls were removed and the underlying cell membrane was exposed, allowing PD necks to be seen from their interior. More rarely, the fractures left the wall intact revealing the wall collars of the PD.

On E-E interfaces (Figure 18A-B), PD necks are seen in clusters of ~8, sometimes in a depression resembling a small pit field. As epidermal cells interlock, and are in contact over the whole length of their anticlinal walls, these interfaces were the most technically challenging to fracture, so only a limited number were imaged. These showed small groups of 4-6 necks spaced at intervals along the length of the wall, and concentrated in the lower two thirds of the height of the wall in a pattern very similar to that observed in CLSM (Figure 18, Figure 15F).

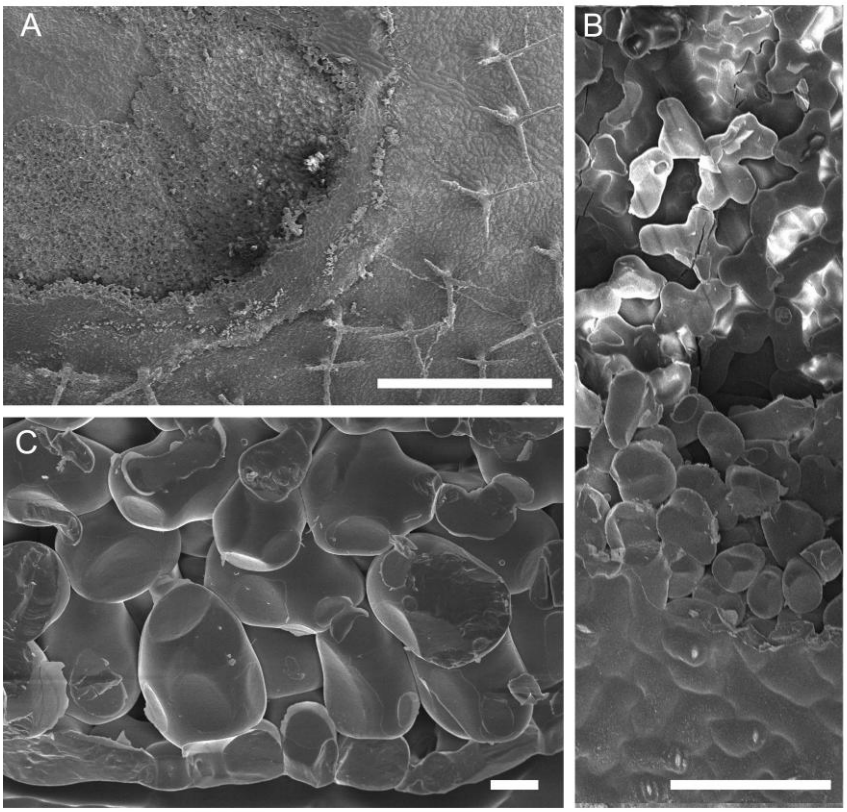

Figure 17: Views of freeze fractured tissue. A) Tissue fractured by the freeze-pull method (see methods) revealing adaxial epidermal-mesophyll interfaces, mesophyll-mesophyll interfaces and mesophyll-abaxial epidermal interfaces. B) Close up of tissue fractures by the freeze-pull method. C) Freeze-shattered leaf, revealing mesophyll-mesophyll interfaces and (rarely) epidermal-epidermal interfaces. Scale bars A = 1 mm, B = 10 µm , C=100 µm

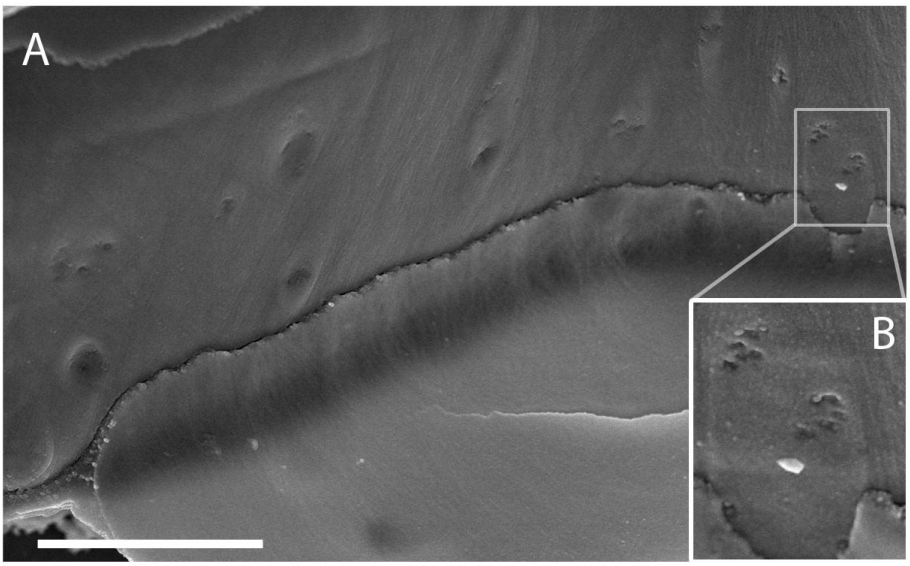

Figure 18: FESEM images of freeze-fractured epidermal cells showing the location and arrangement of PD necks within the walls. A) membrane of an epidermal cell after the wall and neighbouring cell have been removed, showing small clusters of PD necks, some in depressions characteristic of pit fields. B) enlargement of the boxed area in A showing detail and arrangement of necks. Scale bar = 2.5 µm.

Mesophyll cells, having limited, flat contact with neighbours around large air spaces were easier to fracture. E-M interfaces were fractured using the 'peeling' protocol, and showed more numerous pit fields containing ~25 necks in clusters, separated by expansive areas without PD (Figure 19A) similar to the arrangement of complex PD seen in CLSM images. The arrangement of necks in large groups (Figure 19B and C) suggested that each pitfield comprised multiple complex PD clustered together, as seen in the clustered MP17-GFP labelled cavities observed via CLSM (Figure 15A and C).

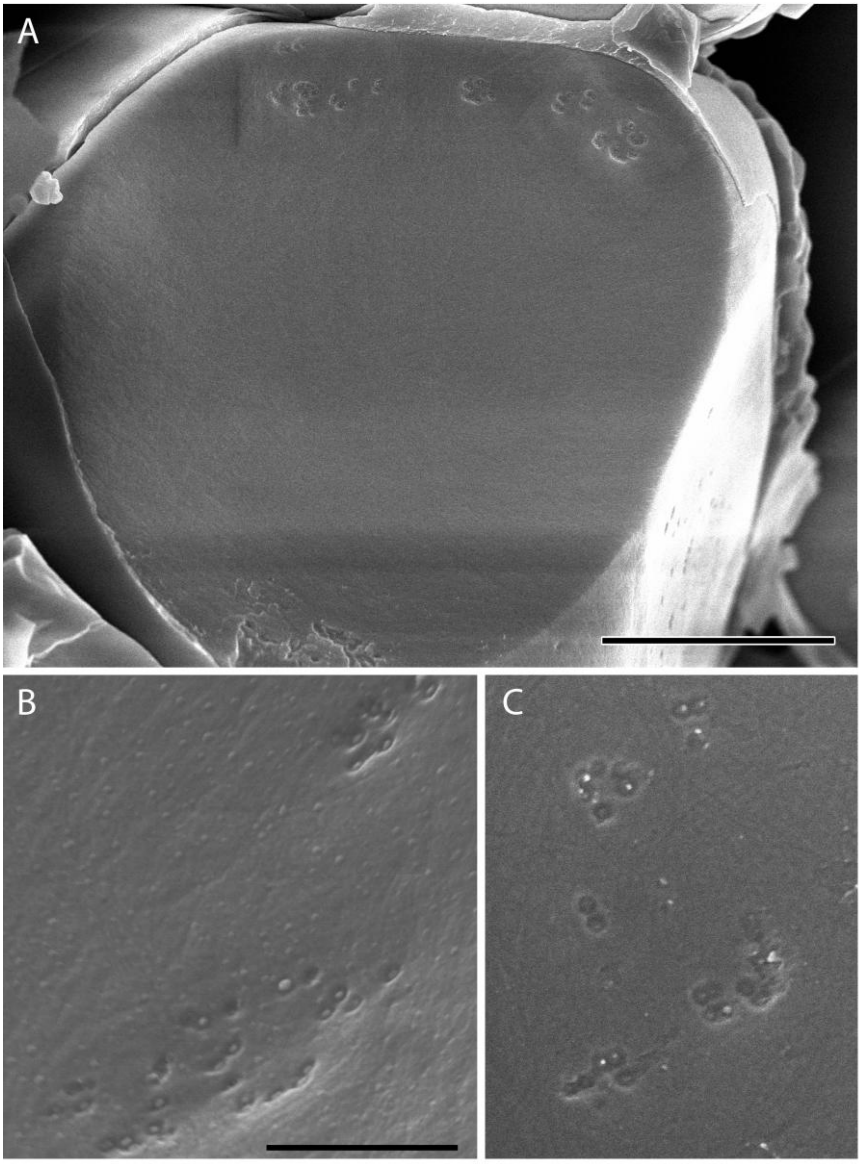

Figure 19: FESEM images of freeze-fractured interfaces between epidermal and mesophyll cells. A) Membrane interface of mesophyll cell after cell wall and overlaying basal epidermal cell has been removed by freeze fracturing. PD groups of PD necks appear in clusters. Wall depressions are minor, if present. B) Close-up of a large pitfield showing one group of >20 necks. C) Pitfield group showing conspicuous PD pairs. Scale bars: A = 5 µm, B-C = 1 µm.

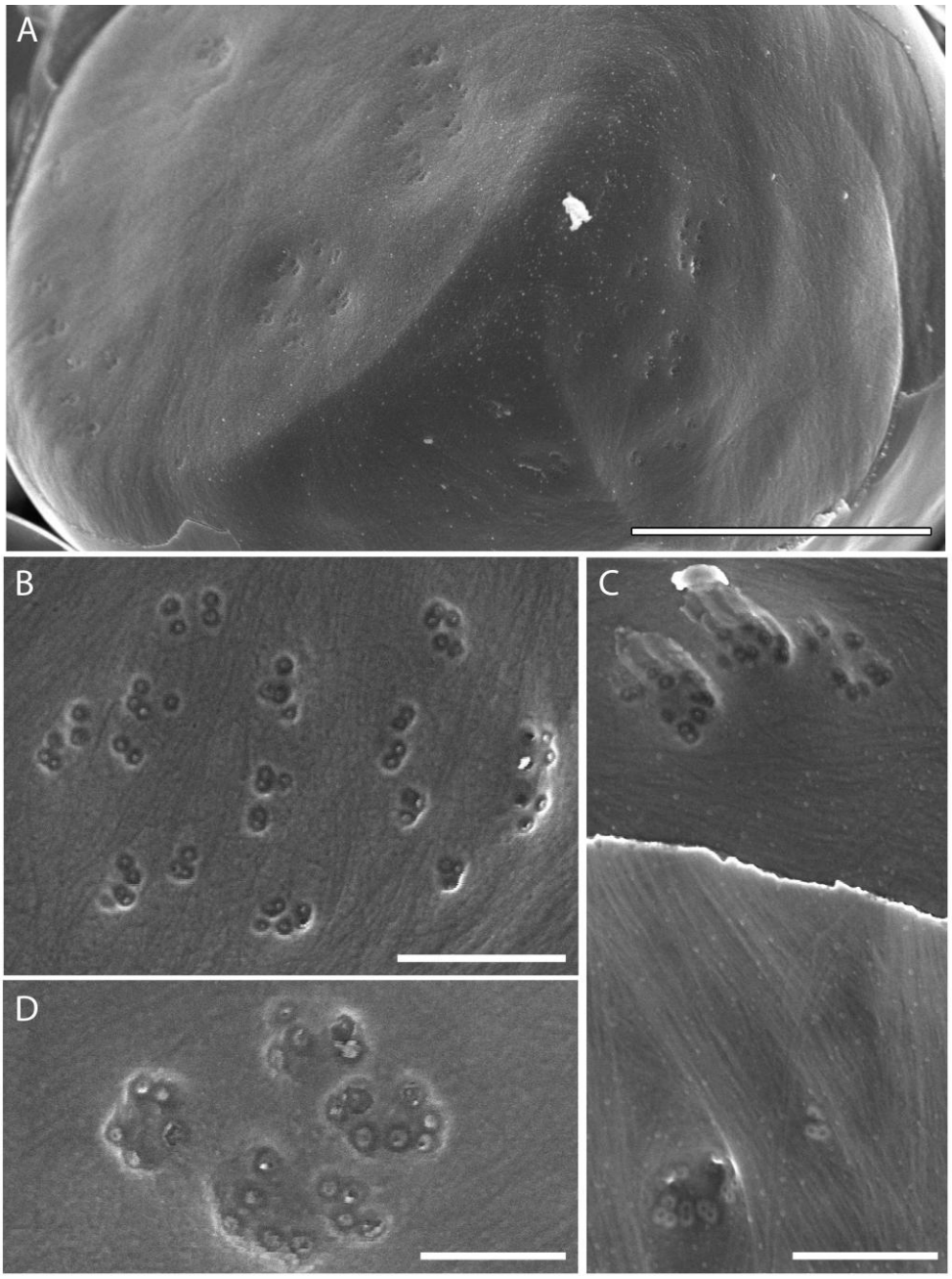

Figure 20: Views of mesophyll-mesophyll interfaces revealed by freeze shattering. View of the membrane of a mesophyll cell with wall and two neighbours removed. Large pit fields are visible. B) Pit field comprising >50 necks. C) View of the inside and outside necks of PD on an interface where the wall has been partially removed. D) Pitfield of >20 necks. Dot in centre of many PD visible. Scale bars: A = 5 µm, B = 1 µm, C = 0.5 µm, D = 1 µm.

Neighbouring mesophyll cells fractured readily along the walls, meaning that M-M interfaces were the most commonly imaged (Figure 20) and showed large pit fields (Figure 20B-D). In these interfaces I was able to observe the greatest level of detail

in the structure of the PD with many of the channels showing a dark central dot, presumably from the desmotubule, not evident in other images (Figure 20D) as well as a dark wall collar surrounding the PD channel. I also observed a few interfaces where the fracture plain had left the wall intact, showing the raised callose wall collars surrounding PD (Figure 20C). PD on these M-M interfaces were organised into large pit fields, often comprising more than 50 necks, again correlating with the expansive pit fields of clustered PD observed in CLSM images of MP17-GFP tissue (Figure 4D,E and H). Of >500 imaged mesophyll PD, 64% were arranged with their wall collar touching at least one other, suggesting that these PD were produced via the twinning principle (Faulkner et al., 2008).

3.3.4 Semi-correlative TEM/CLSM imaging of PD

The next step in the PD survey was to examine the interior ultrastructure of the PD. For this I used a semi-correlative CLSM/TEM approach, where sections from the same leaves of *Arabidopsis* plants expressing MP17-GFP and PDCB-mCherry were processed in parallel for CLSM or TEM imaging (see Figure 21). This allowed me to assess how the pattern of MP17 and PDCB1 accumulation corresponded to the observed structure of the PD. For use in reference to future developmental experiments, I used leaves of different ages: young sink leaves which were expected to have few complex PD, older leaves that were undergoing the sink-source transition and therefore developing complex PD, and mature source leaves with predominantly complex PD (Roberts et al., 2001).

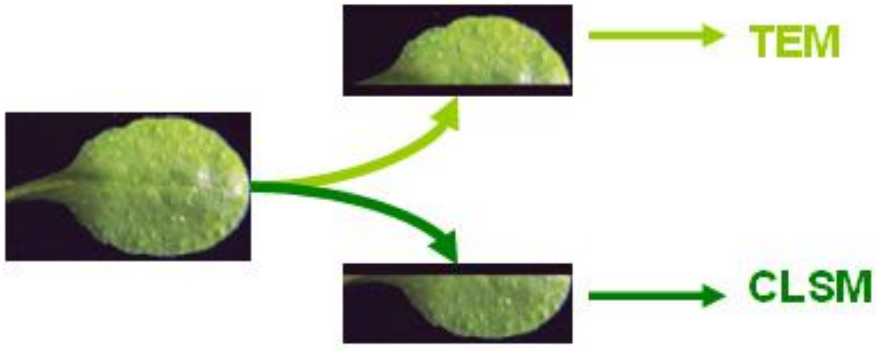

Figure 21: Simplified scheme for semi-correlative imaging. Sections from the same leaves were cut and either fixed, embedded in LR white resin, cut into ultrathin sections and imaged by TEM, or mounted on slides and imaged by CLSM.

In sink tissue, CLSM images showed E-E interfaces labelled with background PDCB1-mCherry fluorescence, with distinct punctae indicating the presence of numerous PD (Figure 22A). MP17 labelling in E-E interfaces was sparse indicating that few of these PD were complex. E-M interfaces showed numerous clustered MP17-GFP spots, suggesting the presence of complex PD pit fields, while M-M interfaces showed denser MP17-GFP labelling (Figure 22B).

TEM imaging of sections from the same leaves showed that the E-E interfaces, which had showed little MP17-GFP labelling under CLSM, correspondingly had simple, single-channelled PD (Figure 22C). These were generally well-spaced with little evidence of clustering. In the mesophyll layer, which showed MP17-GFP at both M-M and E-M interfaces under CLSM, PD with a range of structures were present. In the M-M interfaces simple PD were present, and were often found in pairs (Figure 22D, H and I). There were also numerous small complex PD with 3 or 4 necks arranged in Y, X, or H-shaped configurations (Figure 22E-G). These arrangements were also evident in transverse sections of the E-M interface where PD necks commonly appeared in pairs or tetrads (Figure 22J and K). Although the underlying cavities were not sectioned, it is likely from the neck arrangement, that these PD would appear Y-, X- or H-shaped. These twinned and small complex PD were reminiscent of the PD seen in the expanding trichome base (Faulkner et al., 2008).

In mature source tissue, PDCB1-mCherry labelled punctae could be seen at walls (Figure 23A), although the appearance of large, spherical aggregations of this marker, particularly on the epidermal side of the E-M interfaces, but also on E-E interfaces (Figure 23B), meant that the PDCB1-mCherry label could not be accurately used to indicate PD location. MP17-GFP labelled numerous punctae in the E-E layer, many clustered, as well as pit fields in the E-M interface and highly clustered labelling in M-M interfaces (Figure 23A and B).

TEM imaging of sections from the same leaves showed a range of PD structures in the E-E interfaces including large complex PD (Figure 23C and D), with irregularly shaped electron-dense cavities branching into as many as 6 necks (Figure 23D), even in a single ultra-thin cross section. These PD appeared in prominently thicker areas

of wall, as did, to a lesser extent, other complex PD (Figure 22G). Simple PD were also present at the E-E interface (Figure 23E and F), as were small complex PD (Figure 23F and G). In transverse sections of the E-M layer, small pit fields of less than 10 necks arranged in pairs and tetrads similar to those seen in sink E-M sections were visible (Figure 23H) as well as larger pit fields of >10 necks (Figure 23I) resembling those observed in FESEM images (Figure 19).

Figure 22 (overleaf): Semi-correlative imaging of Arabidopsis sink tissue using CLSM (A, B) and TEM (C-K). A) Single slice through the epidermal layer shows the majority of PD are labelled with PDCB1-mCherry only. B) Maximum projection of 1.5 µm-spaced slices through the epidermal and mesophyll layer show that many PD connecting the epidermal and mesophyll layer and labelled with MP17-GFP. C) TEM section through epidermal cells shows spaced, simple PD. D-H) Simple, branched and twinned PD seen in E-M walls. D) Simple PD. E) Y-shaped PD. F) X-shaped PD. G) H-shaped PD. H) Twinned PD with expanded sleeves in the middle lamella. I) Twinned PD. J) Transverse sections of PD, showing pairs in face-view. K) Close-up view of longitudinally sectioned PD. Scale bars A-B = 25 µm, C = 1 µm, D – I = 0.2 µm, J = 0.5 µm, K = 0.5 µm.

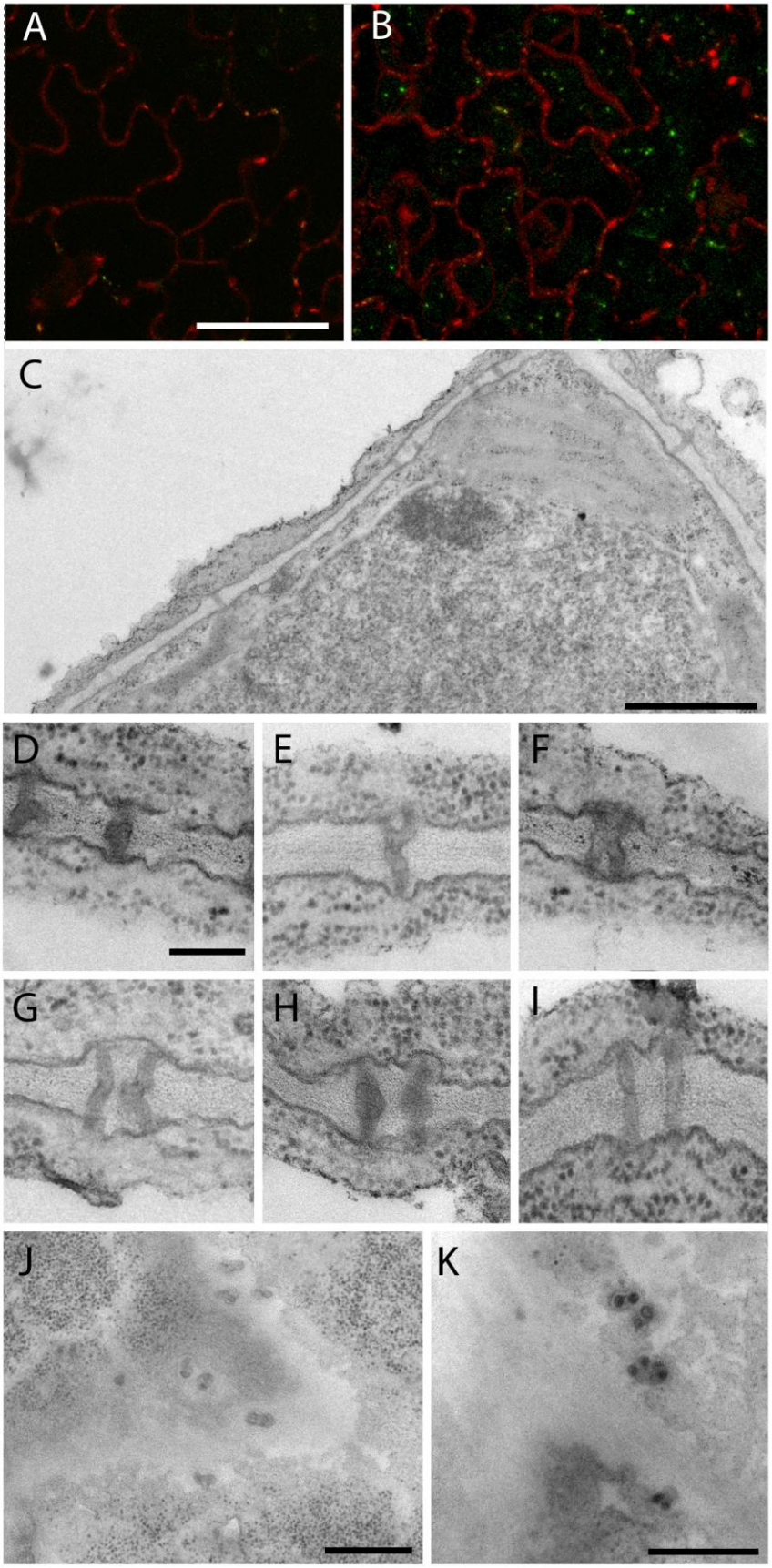

Figure 22: Figure legend on proceeding page.

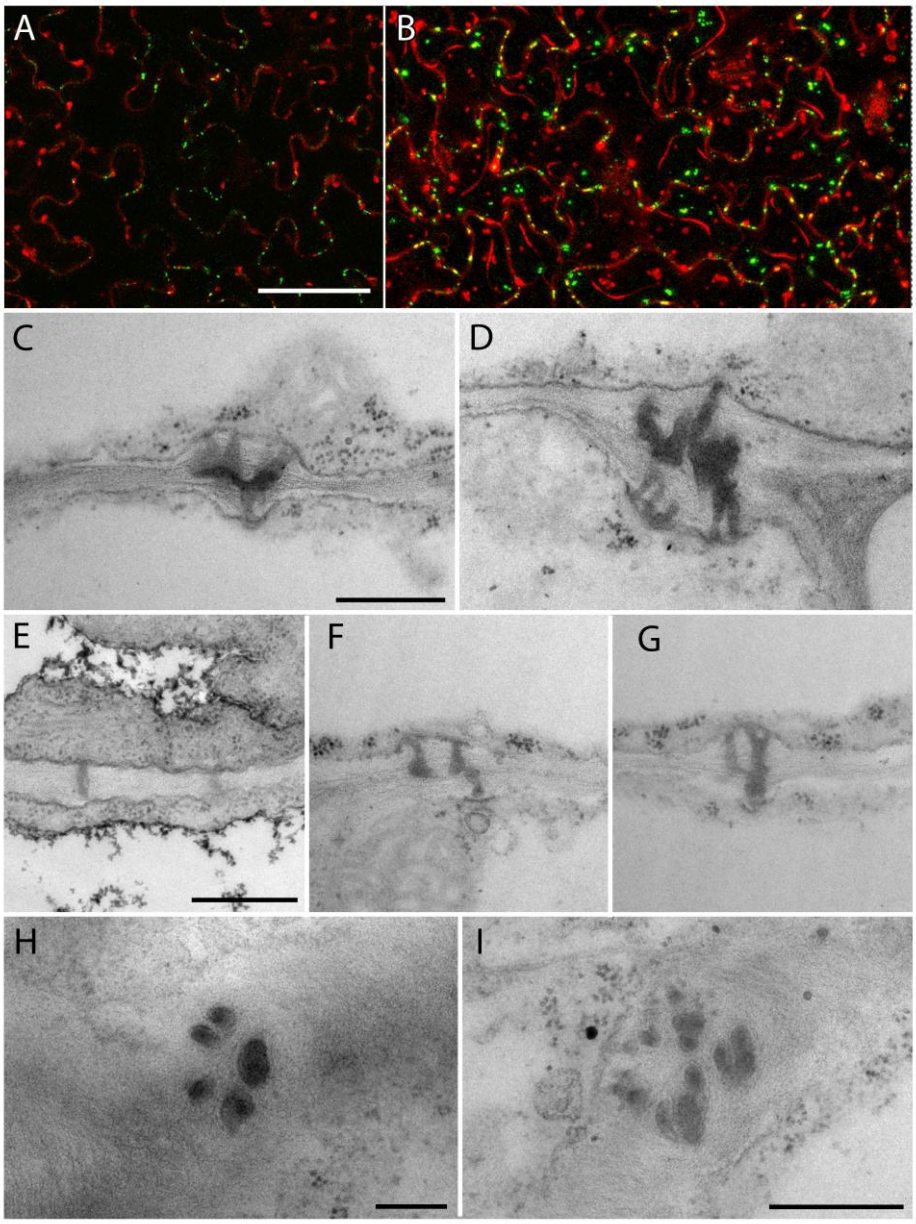

Figure 23: Semi-correlative CLSM/TEM of source leaves using confocal microscopy (A, B) and TEM (C-I). A) Single slice through the epidermal layer of a sink leaf showing numerous MP17-GFP labelled PD in the E-E interfaces. B) Maximum projection of 1.5 µm-spaced slices through the epidermal and mesophyll layer shows numerous MP17-GFP labelled PD in both E-E and E-M interfaces. C-D) TEM imaging shows that many E-E PD have elaborate branched structures, with multiple necks meeting in expanded central cavities. E-G) Simple and twinned PD are also present in these interfaces. Longitudinal sections show groups of PD twins as in sink leaves (H), and also the development of larger pit fields (I). Scale bars A-B = 50 µm, C-D = 0.5 µm, E-G = 0.5 µm, H = 0.2 µm, I = 0.5 µm.

3.3.5 SIM super-resolution imaging of PD structure

The availability of a SIM microscope provided an entirely new way to look at PD using high-resolution, three-dimensional imaging of fluorescently tagged proteins. This allows not only for confirmation of the specificity of candidate PD markers, but may potentially reveal new details about PD structure.

To study PD structure, *N. tabacum* expressing the TMV 30K MP was used, as the tissue can be peeled and sectioned much more easily than *A. thaliana* to allow a thorough investigation of PD structure. Epidermal peels and tissue sections were fixed and immunolabelled with an antibody to callose that was subsequently labelled with a secondary antibody linked to Alexa 594 (Invitrogen). In CLSM, the MP and callose labelling co-localised and each GFP spot appeared to be in the middle of two Alexa 594 spots, representing a PD with a central cavity that has accumulated MP-GFP and multiple necks with callose collars at each wall face. However there was much overlap between the signals and no detail was visible (Figure 24A).

The same samples were subsequently imaged using 3D SIM, providing some of the first super resolution images of plant tissue. Much of the data in the following section has been published (Fitzgibbon and Bell, King & Oparka , 2010, included as Appendix 1). In these experiments K. Bell was involved in experimental design, tissue preparation and imaging, while E. King was involved in development of the SIM system and imaging. Figure 24B shows a single slice through a PD in the E-E interface labelled with MP-GFP and immunolabelled for callose showing that SIM can fully resolve both signals so that the PD structure can be clearly seen. As predicted, the MP-GFP labels a central spot, capped at either side by callose collars, with an unlabelled space between representing the PD necks (Figure 24M). Comparative images of PD imaged by SIM (Figure 24C and E show maximum projections of 125 nm step SIM z-series) and by conventional widefield imaging (Figure 24D and F) show clearly how the improved resolution allows structural details previously only seen with EM techniques to be revealed with fluorescent markers. SIM shows that the ‘dots’ of MP-GFP spheres on widefield images actually represent multi-part- (Figure 24C) and laterally elongated- (Figure 24D) cavities.

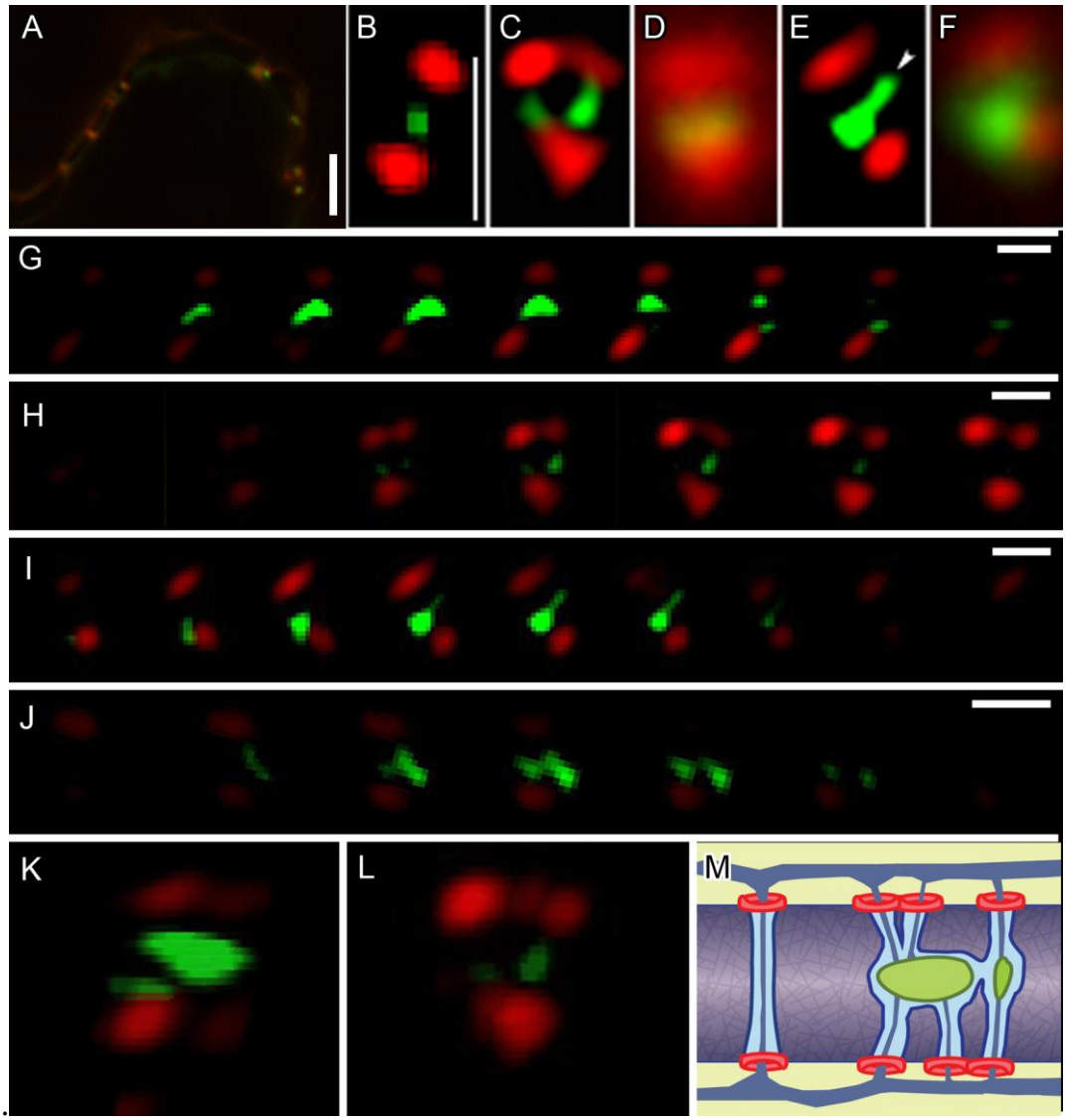

Figure 24: Complex PD labelled with MP-GFP and Alexa 594 to immunolabel callose and imaged with CLSM, widefield fluorescence imaging, and with 3D-SIM. A) CLSM images showing that signals from the MP-GFP and Alexa 594 necks cannot be resolved, so that PD appear as yellow punctae in the walls. B) SIM imaging of the same sections shows that the labels at the cavities and collars can not only be resolved, but have an unlabelled region in between. C and E Maximum projections of a 125 nm step SIM z-series through complex PD showing two aggregations of MP in a single complex PD (C) and a cavity with a lateral extension in the middle lamella region of the wall (E). For comparison, widefield images of the same PD are shown in D and F. G-J: 125 nm step z-series through complex PD showing a range of PD structures: G) An X-shaped PD with two necks on each wall face, connected by a cavity containing a small and a large MP-labelled area. H) A PD with 3 necks on one wall face, and two on the other, connected by a 2-part cavity. I) A Y-shaped PD with an elongated central cavity. J) PD with a horseshoe shaped cavity. K) Frame from a 3D projection of the PD shown in G, showing the X-shape. L) Frame from a 3D projection of the PD shown in H, showing the asymmetric arrangement of necks. Animations of the 3D projections shown in K and L are available in Appendix 2. M) Illustration of where the MP-GFP (green) and callose (red) signals label simple (left) and complex (right) PD. Scale bars: A = 5 µm, B-F = µm , G-J = 5 µm.

Figure 24G-J show a sample of the range of PD structures seen at the E-E interface in the form of serial longitudinal images taken through the PD at 125 nm increments. 3D projections of Figure 24G and H are shown in Figure 24K and L, with full animations available as supplementary files, showing the first 3D views of PD. Each of the PD has 3-5 necks with an average width of 187 ± 6 (n = 32), which is slightly wider than the wall collars imaged with EM (Bell and Oparka, 2011).

The cavities display a range of shapes including approximately spherical (Figure 24G, K), laterally elongated (Figure 24I) or horseshoe-shaped (Figure 24J), and may have more than one part. Between the cavities and collars is an unlabelled region of approximately 136 ± 6 (n = 15), which may correspond to the necks linking the collared pores at the exterior surfaces of the wall with the cavities in the middle lamella (Figure 24M). Further details of PD cavities could be seen in transverse images of PD via 3D SIM, taken in the trichome base-epidermal interface (Figure 25 C-E; comparative widefield images in A and F). The perimeter of the overall pit field is circular, but is composed of clusters of PD arranged in distinct ovals, all elongated along approximately along the same axis. These tissues allowed detailed views of cavity structure (Figure 25G-I)

In sections cut from the stem, fixed and subsequently digested with pectinase, we were able to image pit fields in the elongated parenchyma cells associated with the vascular bundles (Figure 26). A rotated 3D projection indicated clear separation between the callose collars and the cavities, and showed that the pectinase treatment allowed the cells to be pulled apart, hence the presence of necks only on one side of the wall. These pitfields are oval-shaped, elongated along the same axis as the cells (Figure 26A, and B: comparative CLSM image from the same tissue). However, while the necks are found throughout the pitfield, the cavities are concentrated around the edges of each cluster of necks. While in parts the cavities were horse-shoe, circular and oval shaped, as in laminal tissue, these pit fields also contained examples of cavities with large radial elongations in the middle lamella region of over 1µm. These cavities were often seen to lie underneath comparatively few necks (Figure 26D-F), showing that the arrangement of necks on the wall surface may be a poor indicator of the extent of the underlying connectivity.

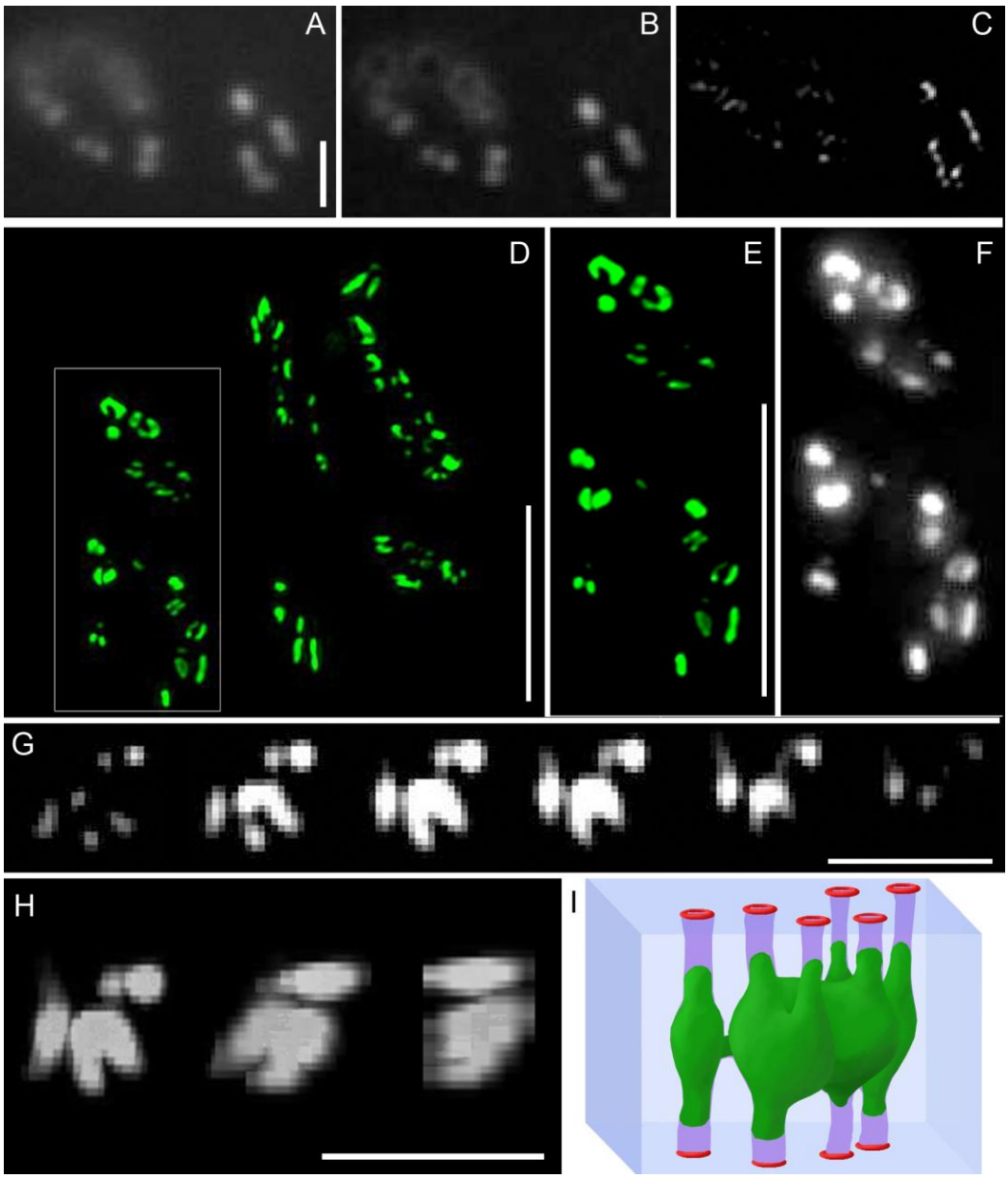

Figure 25: Figure showing details of larger cavities imaged by CLSM, widefield fluorescence imaging and SIM. A-C: widefield (A), widefield image after deconvolution (B) and SIM (C) image of the same pit field. Widefield imaging cannot resolve PD cavities even after deconvolution. SIM imaging allows full separation of individual cavities within a pitfield. D: SIM imaging of an MP-labelled pitfield, showing 6 clusters of PD. E: Close-up of boxed area in D, showing horseshoe shaped cavities. F: comparative widefield image of the area shown in E. G: end-on 125 nm step z-series of a PD in the trichome-epidermal interface with a horse-shoe shaped cavity. The structure of the cavity suggests that 9 necks are present on the trichome face of the PD, with 6 of these merging into a set of 3 cavities linked by thin stands in the middle lamella region, and branching to meet 3 necks on the epidermal wall face H: individual frames of a 3D projection of the PD shown in G rotated 0º, 45º and 90º. An animation of the full 3D rotation is available in Appendix 2. I: interpretation of the full structure of the PD shown in G-H. Scale bars: A-C = 1 µm, D = 5 µm, F-G = 5 µm, G = 1 µm, H = 1 µm.

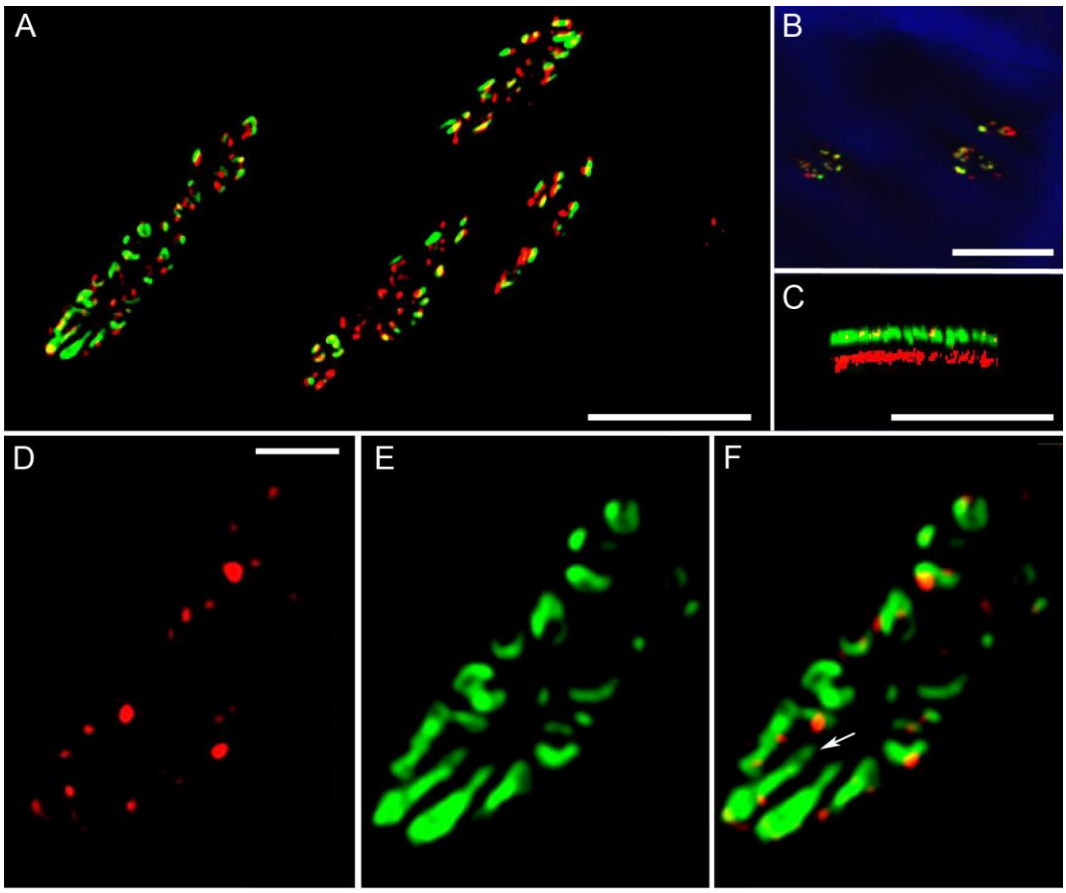

Figure 26: SIM imaging of pitfields from phloem parenchyma cells double labelled with MP-GFP and an Alexa 954 anti-callose antibody, and separated by pectinase treatment. A) A group of elongated pitfields from a phloem parenchyma cell, showing that numerous necks with callose collars are underlaid by, and presumably connected by, a network of large, MP-labelled cavities in the middle lamella region of the wall. B) CLSM image of the same material. The wall has been stained with calcofluor. C) Rotation of 1 3D projection of a phloem pitfield, showing clear separation between callose collars and MP-labelled cavities. Callose collars are only present on one side, as the upper cell has been removed. D-F: enlargement of (A) showing (D) the callose label, (E) the MP label and (F) and overlay of the two signal, showing how a small number of necks can be linked by large cavities. Scale bars A = 5 µm, B = 20 µm, C = 5 µm, D-F = 1 µm.

3.3.6 SIM imaging of PD-specific fluorescent markers

A. thaliana tissue was more challenging to prepare than *N. tabacum*. However the epidermal tissue could be imaged easily as, when thin transverse sections were cut from young MP17-GFP expressing *A. thaliana* leaves and mounted on slides, areas of the epidermis tended to peel away from the mesophyll to lie flat against the coverslip and could be immunolabelled in the same way as the *N. tabacum* tissue (Figure 27).

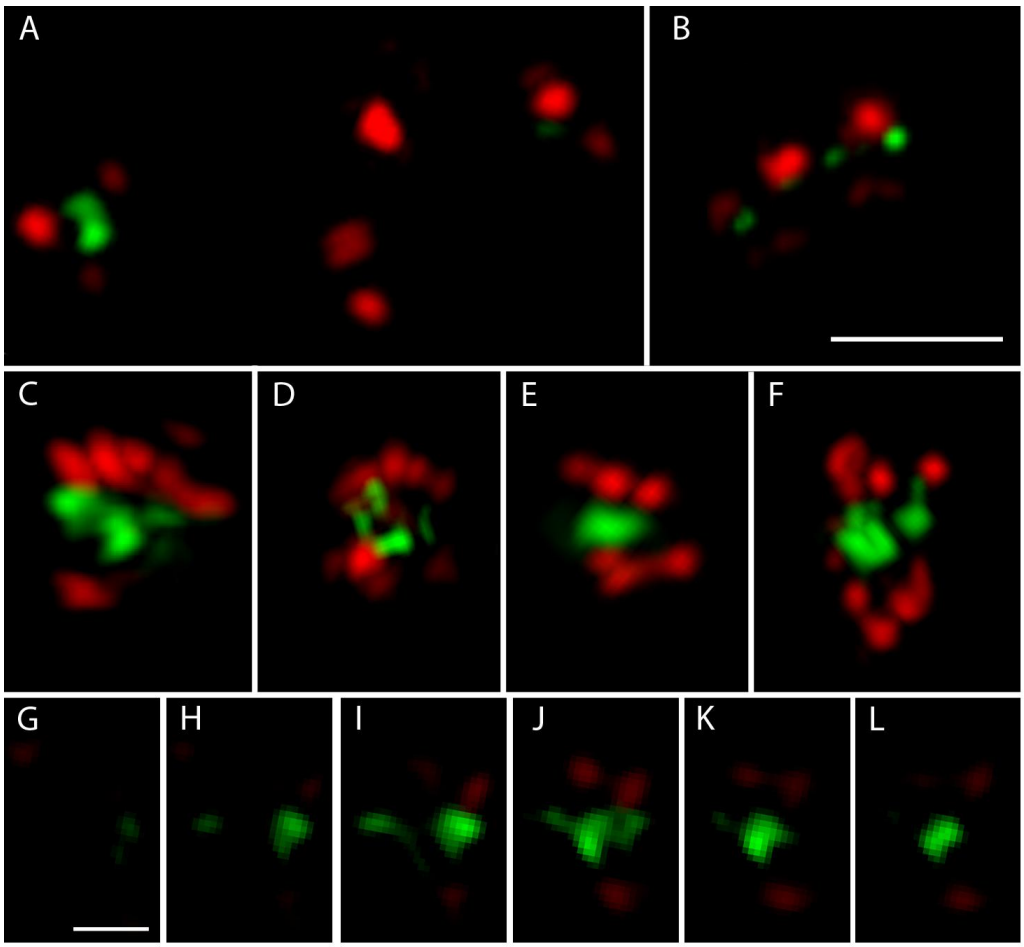

Figure 27: Epidermal PD with central cavities labelled with MP17-GFP (green) and callose immunolabelled with alexa 594 (red). A: maximum projection of three PD in a section of wall running horizontally through the image; complex PD are labelled with MP17-GFP while the simple PD is unlabelled. B: Maximum projection of closely adjacent PD with small cavities. C-F: complex PD with multiple necks and multi-part cavities (C, D and F are images of 3D-reconstructions, E is a maximum projection). G-L: sequential images taken at 125 nm intervals through part of the complex PD shown in C showing details of the internal structure. Scale bar for A-F is shown in B, = 1 µm. Scale bar for G-L is shown in G, = 0.5 µm.

In the young leaves chosen for imaging, cells contained simple PD without MP17-GFP labelling (Figure 27A) while complex PD, including small X- or Y-shaped PD (Figure 27A, B) and large complex PD with ≥9 necks (Figure 27C-L) were labelled with MP17-GFP. This provides more confirmation that MP17-GFP accumulation is specific to complex PD. While smaller complex PD had single spherical accumulations of MP17-GFP at the middle lamella region (Figure 27B), larger PD had cavities with lateral extensions (Figure 27C, shown as individual z-sections in G-L, and E), or were composed of multiple small aggregations of MP17-GFP (Figure 27D, F) similar to those seen in MP30K-GFP labelled tissues.

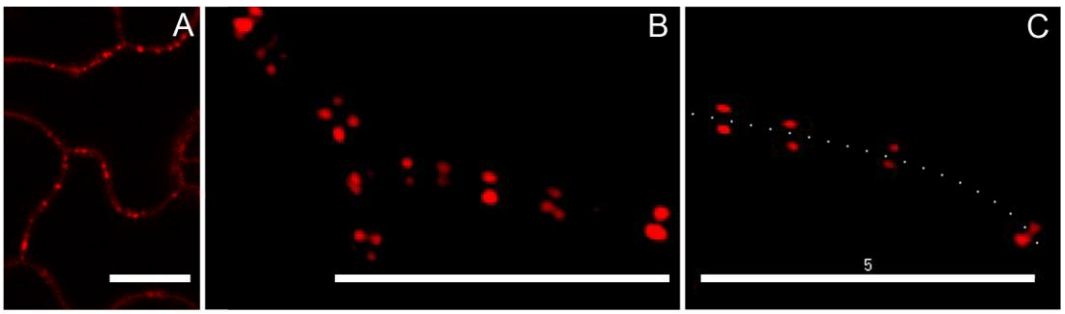

Figure 28: A: PDCB1-mCherry imaged by CLSM shows heavily labelled punctae and background in the cell wall. B: the same tissue imaged using SIM shows that PDCB1 labels PD collars in a pattern identical to immunolabelled callose (Figure 24). C: SIM imaged PDCB1 callose with a dotted line to show the location of the middle of the wall. Scale bars: A = 10 µm, B and C = 5 µm.

The intense laser illumination required by SIM caused photobleaching of PDLP1-mRFP and so this was not suitable for imaging (data not shown). *35S::PDCB1-mCherry* lines proved sufficiently photostable for SIM imaging, which showed that the wall punctae visible in CLSM images (Figure 28A) were actually twin spots of PDCB1 on either side of the wall (Figure 28B and C). PDCB1 had previously been assumed to be a callose binding protein on the basis of its structure alone, as localisation analysis by CLSM could only confirm that the protein was found at PD (Figure 28A), while SIM imaging shows that that it localises to the collar regions of PD in a pattern almost identical to the anti-callose antibody. This work not only strengthens the view that PDCB1 is as a callose-binding protein, it also shows the potential for super-resolution techniques in characterising putative PD proteins by allowing analysis of their precise localisation within the PD pore.

3.3.7 3D-SIM imaging of PD and MP-GFP in the phloem

In our pectinase treated samples, we were also able to gain good views of the phloem strands. As previously discussed, phloem tissue contains notable PD-related structures. The sieve plates that make the end connections between sieve elements in phloem strands contain pores that are evolutionarily derived from PD. These pores are greatly enlarged compared to PD, and have lost much of the interior architecture, including the desmotubule, so that material can flow through unimpeded. However, they do have callose collars and, in our immunolabelled tissue, sieve plates appeared studded with callose dots under CLSM (Figure 29A). The pores are large enough that, with a high magnification objective, some detail of the pores can be seen under

widefield imaging (Figure 29B). SIM reveals the full detail of the sieve plate pores (Figure 29C), showing that they have an internal diameter of 276 ± 16 nm (n = 21), surrounded by callose collars with a diameter of 568 ± 22 nm (n = 21).

With 3D-SIM we were able to show the full shape of the sieve plates in three dimensions by taking optical z-series through the sieve plates that could then be projected. Figure 29D shows a projection of a 25 nm step z-series through two parallel phloem strands, showing a sieve plate angled almost to a face-on view with >100 individual pores (left), and a sieve plate angled at almost a side-on (right) view, showing that plates are slightly curved, and that, as well as possessing callose collars at either opening, the pores are lined with callose, giving a 'cotton-reel' shape. Videos of the 3D projections are available in the supplementary files of Appendix 1.

Between the sieve elements and their companion cells are PPUs, in which the central cavity branches into multiple necks to the companion cell wall face, but only a single pore on the sieve element wall face. This funnel-shaped structure facilitates transfer of materials from the companion cell to the sieve element that is enucleate at maturity and entirely dependent on the companion cell for many of its cellular functions including protein synthesis. These PPUs also label strongly for callose, and in SIM images the pore on the sieve element face can be resolved (Figure 29D, comparative CLSM image shown in Figure 30A) and have an internal diameter of 188 ± 8 nm (n = 26), and callose collars of 510 ± 19 nm (n = 26); although the pores are much smaller than sieve-plate pores, the collars were almost as thick.

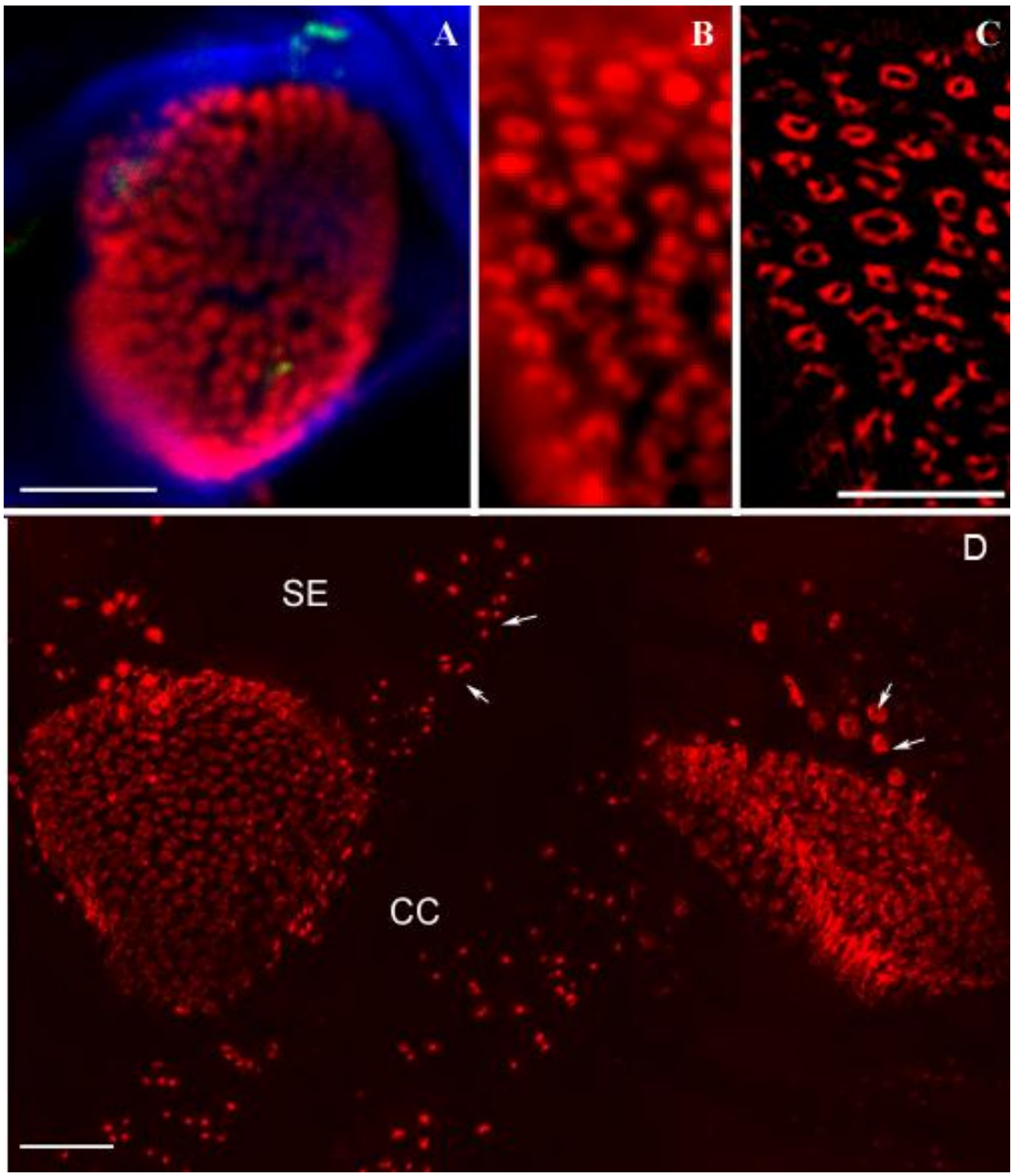

Figure 29: SIM imaging of sieve plates and PPUs. A: CLSM image of a sieve plate showing callose stained red with an alexa-594 linked antibody to callose, blue calcofluor staining the wall, and small accumulations of MP. B: Widefield close-up of sieve plate pores. Although individual pores can be resolved, little detail is visible. C: SIM image of the same sieve plate pores showing each pore surrounded by a ring of callose. D: Image showing two parallel sieve elements, with a sieve plate in face view (left) showing open pores between the callose collars and an angled side view (right) showing that callose lines the entire length of each pore, with a thicker collar at each neck. On the sides of the SE, PPUs connect the sieve elements to their respective companion cells (arrows). Scale bars: A = 5 µm, B-C = 2.5 µm, D = 5 µm.

Sieve elements also showed strong accumulation of MP-GFP. Under CLSM we saw that many sieve elements contained streaks and dots of MP-GFP arranged in a strip along part or all, of the interface with the companion cell (Figure 30A-C). These MP-GFP structures appeared to be in the cytoplasm of the sieve element, rather than in the middle lamella, although sometimes appeared to be associated with the PPUs (Figure 30B).

SIM fully resolved these MP-GFP structures as a fine network of branching strands approximately 144 ± 6 nm thick (n = 30), and sometimes running over 40 µm in length (Figure 30D-I). These strands were strongly associated with the pores of the PPUs, and we saw many examples of the strands touching the pore opening, and apparently entering it (Figure 30E, F, G), although the strands did not appear to actually pass through the pores, and were not seen within the companion cells. Figure 30G-I show 125 nm steps through part of the network, showing a branch of one strand entering a pore, and two strands entering another. These details could not be resolved with widefield imaging (Figure 30J). In other cases the strands seemed to lie around the perimeter of the collar instead of interacting with the pore (Figure 31f)

The MP-GFP strands were also found at the sieve plate (Figure 31A-E), where they adopted a thinner structure of approximately 103 ± 3 nm (n = 30). Figure 31A-E show rotated frames from a 3D-projection of a 125nm step z-series through a sieve plate, showing that MP-GFP labelled strands pass all the way through the sieve plate pores, forming continuity between adjacent sieve elements. As the network is associated with the PPUs of each sieve elements, this network could potentially provide continuity between companion cells of neighbouring sieve elements.

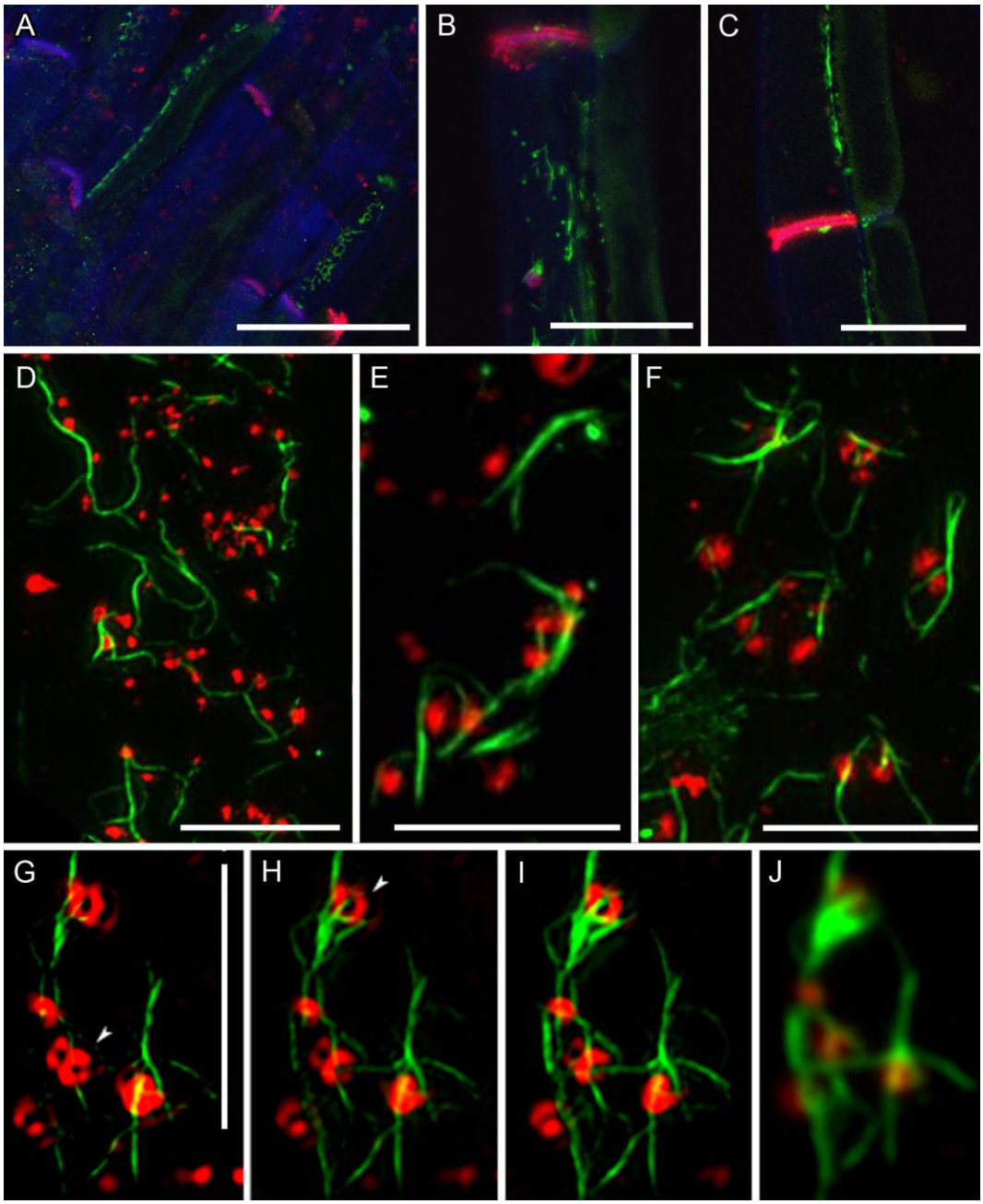

Figure 30: CLSM and SIM imaging of MP in the phloem. A: CLSM image showing multiple phloem stands running in parallel. Walls are stained blue with calcofluor, callose is labelled red with alexa 594, showing sieve plates and PPUs and green shows MP-GFP in a network of fine strands. B-C: CLSM image showing the strands in face-on view and side-on view, showing a strong association with the companion cell. D: SIM image of the MP-GFP labelled strands form an elaborate network associated with the pores of the PPUs. E and F: Close-up of the strands running around and between pores. G-I: 125 nm step z-stack through a section of the network, showing strands running through or across the surface of the pores. J: Wide field image of the network shown in G-I. Scale bars A = 50 µm, B-C = 20 µm, D-I = 5 µm.

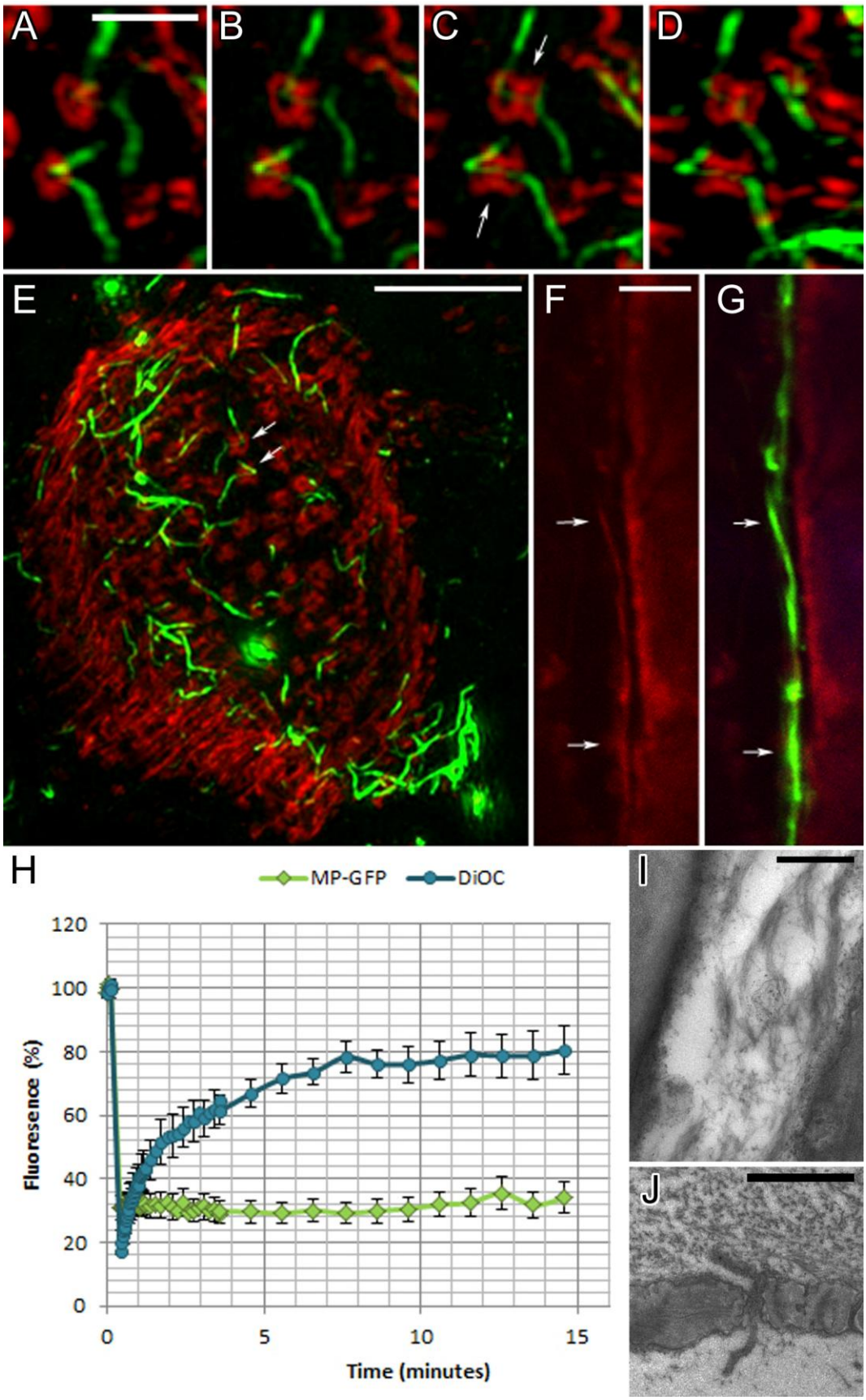

Figure 31: Legend overleaf.

Figure 31: MP-GFP at the sieve plate. A-D: single rotated frames from a 3D projection of a 125nm step z-series showing individual MP-GFP strands running through callose-labelled sieve plate pores. B: maximum projection of a 125 nm step z-series through showing a network of strands on the surface of, and passing through, a sieve plate. The pores shown magnified in A-D are marked with darts. F-G: CLSM images showing that the MP-GFP network (F) co-localises with the ER-specific dye hexyl rhodamine B (G). H: FRAP experiment in which the fluorescence of MP-GFP or $DiOC_6$-labelled SE strands were photobleached and the fluorescence recovery monitored. $DiOC_6$-labelling recovers to 50% after >2minutes, while MP-GFP does not recover. I: FESEM image showing a thread-like network in an *Arabidopsis* SE. J: FESEM image showing thread-like structure passing through an *N. Tabacum* SP pore (image J courtesy of K. Bell). Scale bars: A-D = 1 µm, E = 5 µm, F-G = 5 µm, I = 0.5 µm, J = 1 µm.

As this labelling pattern was only seen in sieve elements it seemed likely that the MP-GFP was labelling a sieve-element specific structure. Sieve elements contain a reduced organelle component and at maturity, have only mitochondria, plastids and a modified endoplasmic reticulum called the sieve element reticulum (SER). These are arranged in a parietal layer close to the plasma membrane, out of the way of the bulk flow through the centre of the cell. EM imaging has shown that the SER forms a tubular network similar to strands observed with MP-GFP and, like the MP-GFP strands, the SER is continuous between individual sieve elements through the sieve plate pores (Figure 31J shows a TEM image by Karen Bell from *N. tabacum* material, showing a fine 80 nm strand of SER in the sieve plate pore). The SER therefore made a likely candidate for the underlying network labelled by MP-GFP.

In support of this, we observed that the MP-GFP network apparently co-localised with the ER specific dye, hexyl rhodamine B. However, FRAP experiments (Figure 31H) showed that the MP-GFP network, after photobleaching using a high intensity 488nm laser, did not recover in a fifteen minute observation period, suggesting that the MP-GFP was not mobile. In contrast, when the SER was stained with the membrane selective dye, 3,3'-dihexyloxacarbocyanine iodide ($DiOC_6$) and bleached under similar conditions, the fluorescence showed rapid recovery; returning to 50% total intensity after less than two minutes, and reaches a plateau of about 80% total intensity after seven minutes. This suggests that if the MP-GFP is associated with the SER it has aggregated in a way that makes it non-mobile.

Other candidates for the identity of the network are still to be investigated. P-proteins form fibrilar networks in sieve elements of many species (Figure 31I shows P-Proteins in *A. thaliana* sieve elements). This remains to be investigated.

3.4 Discussion

3.4.1 MP17 is a suitable marker for studying PD development

This chapter shows that MP17-GFP is a suitable marker for monitoring PD complexity. The accumulation pattern of MP17-GFP, when expressed in *Arabidopsis* and observed by CLSM correlates well with PD observed by EM. These images illustrate that the pattern of PD development is dependent on interface type rather than cell type. This is shown well by mature epidermal cells, where FESEM and TEM show that the anticlinal E-E interfaces have individual, separated complex PD, while the periclinal E-M interfaces of the same cells have small pit fields. This pattern is mirrored in the CLSM images of MP17-GFP accumulation.

The EM images showed some differences from PD imaged in other plants. In the *N. tabacum* trichome basal cell-epidermal cell interfaces imaged by Faulkner and colleagues (2008), the PD necks were spread over the whole interface, forming increasingly concentrated pit fields towards the edges in a manner that could be computationally predicted. However, in the *Arabidopsis* mesophyll-mesophyll interfaces they formed less ordered arrangements. Some interfaces showed more concentrated pit fields in a ring away from the centre of the interface. Other views, however, showed the PD necks located towards one edge of the interface, and large areas with no PD present. The difference in pit field morphology between mesophyll and trichome cells is to be expected as the two cell types mature in different ways; while trichome-epidermal cell interfaces increase in area during wall expansion, the area of mesophyll-mesophyll interfaces decreases as the cells pull apart to form the air-spaces within the leaf.

However, as in the trichome interfaces imaged by (Faulkner et al., 2008) in *Arabidopsis* E-M and M-M interfaces imaged via FESEM, we observed numerous pit fields in which a large proportion of PD were arranged in pairs and tetrads. Although FESEM images of necks do not provide information on how PD are connected within the wall, the high proportion of necks arranged in pairs suggests an abundance of ‘H’ shaped plasmodesmata, as confirmed by the TEM images of the same tissues. The fact that many of the paired PD in a pit field lay in the same

orientation supports the fission model of secondary PD development (Faulkner et al., 2008), suggesting that new PD channels were being formed from existing ones in the direction of cell wall expansion. TEM images showed various arrangements of Y-, X-, H-shaped and paired PD that can be arranged in a sequence mirroring the illustrations of the twinning model (Figure 22).

3.4.2 SIM imaging of PD and related phloem structures

Our work with SIM microscopy showed unambiguously the localisation of the marker proteins used in this project, with the MPs localising in the cavities of complex PD with multiple necks. This work has a broader significance, however, as it not only provides more detailed, higher-resolution images of PD, but has enabled new observations of PD-associated components. SIM imaging of pit fields that had been dual labelled with MP-GFP (targeted to PD cavities) and immunostained for callose (found at the neck regions) resolved individual necks in pitfields and, unlike EM images, allowed correlation of the position of necks with the underlying central cavities. Our images show that the cavities in phloem cells are often elongated, and are largest at the edges of pit fields (Figure 26), suggesting that cavity expansion and branching is most extensive where the pit field is expanding. While EM techniques allow imaging of only a single plane (x, y) through PD cavities, SIM imaging allows high resolution imaging of cavities through x, y and z allowing entirely new views of complex PD structure. This work illustrates the great potential for SIM in PD research, allowing components to be localised precisely within the PD channel. Wider observations of TMV MP 30K show that the protein is not always PD-specific, especially in phloem tissues where we observed the MP-GFP delineating a strand-like network associated with the PPUs. Previously, *N. clevelandii* expressing cucumber mosaic virus MP (MP3a-GFP) showed that it accumulated within sieve elements (Blackman et al., 1998). The pattern of accumulation was slightly different to the GFP-labelled strands observed with TMV MP30K, in that it formed large aggregations connected by a thread-like network; however, CMV MP was imaged using CLSM only, and so the finer details of the structure could not be resolved. Immunogold labelling showed that the CMV MP was seldom found in the cavities of PPUs, but concentrated around the exterior of the sieve element pore.

This sieve element accumulation was not previously a known property of TMV. Indeed, TMV 30K MP has been reported to be absent from vascular tissues in some studies (Ding et al., 1992). Similarly, MP17 has been immunolocalised in PD between the sieve element and companion cell (Hofius et al., 2001), Immunolocalisation of MP17 in infected and transgenic plants expressing the entire PLRV genome showed that the MP localises at the membrane immediately adjacent to the PPUs between sieve elements and companion cells (Schmitz et al., 1997).

The network observed shows a strong resemblance to the SER, as shown in our TEM images and elsewhere, both in its tubular structure (Esau, 1978) and its propensity to pass through sieve plate pores (Evert et al., 1971). We also observed co-localisation with the membrane selective dye hexyl rhodamine B. The SER lacks ribosomes and is therefore not competent for protein translation. Instead it is thought to play a number of roles including as a route for communication and exchange of molecules between adjacent sieve elements and their companion cells separate from the mass flow transport that occurs through the SE. In terms of viral movement, the continuity of ER which connects cells up to and including the phloem cells may mean that viruses encoding MPs that target the ER may spread efficiently throughout the plant.

However, FRAP experiments showed that the MP-GFP network in the sieve elements was non-motile, while the sieve element reticulum is. Other candidates for the MP-GFP-labelled network include the phloem P-proteins that serve to block the sieve-plate pores upon damage, thereby preventing damage to one sieve element causing a major leak in phloem contents. Certain P-proteins form strand-like arrangements in intact sieve elements similar to the network observed here (Ernst et al., 2012). From the known functions of the 30K MP, and the mechanisms by which TMV moves, it is difficult to speculate on how or why the MP would bind P-proteins; however, it is notable that 30K MP is thought to be evolutionarily derived from phloem proteins native to plant hosts (Melcher, 2000).

3.4.3 Final words

The work in this chapter achieved the overall aims and indicated that while PDCB1 and PDLP1 do target PD, they are not specific enough to use as PD markers, while MP17-GFP is suitable for use as a complex marker outside of phloem tissues. The combination of CLSM, FESEM, TEM and SIM gave detailed images of PD in all tissue layers of the leaf, providing a good foundation for developmental studies in leaves. Finally, the SIM experiments provided the first super-resolution images of plant tissues.

3.5 Acknowledgements and thanks

I thank those who supplied materials used in the work in this chapter: F. Vogel for *35S::MP17-GFP* plants, A. Maule and C. Simpson for 35S::PDLP-mCherry plants, A. Maule and C. Thompson for PDCB1-mCherry, and C. Faulkner for the MP17-GFPxPDLP1-mRFP cross, C. Reichel for the *35S::MP30K-GFP N. tabacum*. The EM work was performed with help from the Edinburgh University Rutherford EM Lab, with particular help from C. Jeffree for the FESEM and S. Mitchell for the TEM. I thank E. King and M. Posch for assistance at the OMX SIM facility at the University of Dundee. SIM experiments were done with K. Bell.

4 Chapter 4: Complex PD and Leaf Development

4.1 Introduction

4.1.1 The development of complex PD during leaf maturation.

As discussed in Chapter 1, restriction of intercellular communication by production of complex PD is a common feature of cellular development and shows higher-order organisation and co-ordination in many tissues. This thesis aims to study this using the leaf, where a large scale conversion of PD from simple to complex forms occurs as the leaf switches from a sink, a net importer of carbon, to a source, a net exporter of carbon (Figure 32).

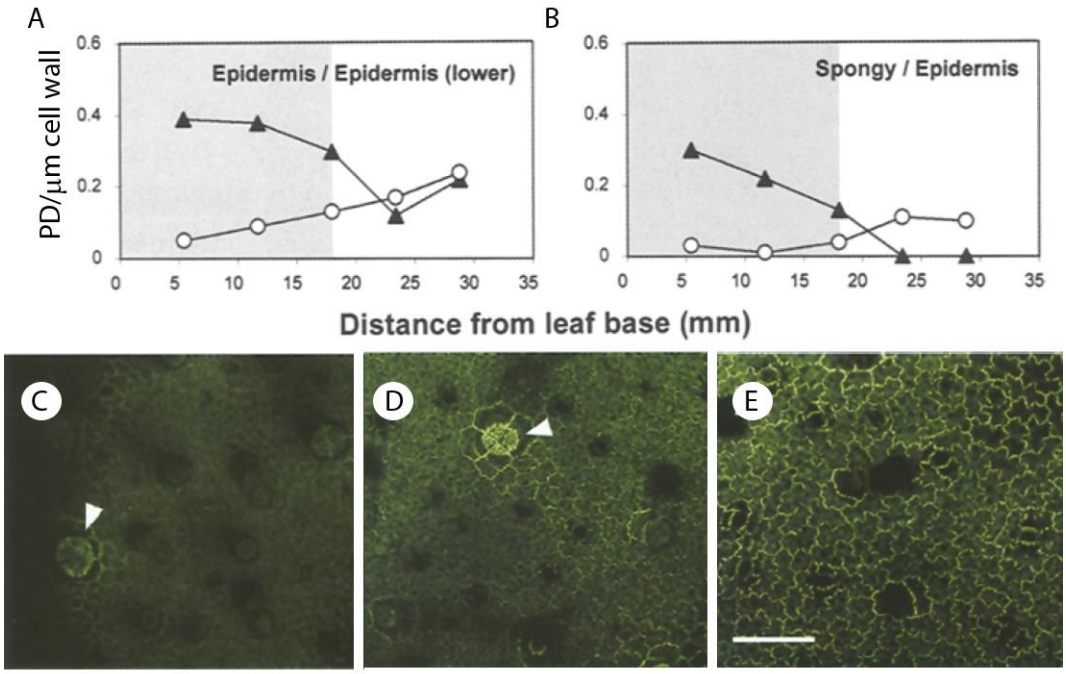

Figure 32: A –B: graphs showing the PD density in E-E (A) and E-M (spongy) (B) interfaces along the length of a leaf mid-way through the sink source transition. Shaded areas show sink leaf regions, unshaded areas show source regions. ▲ = simple PD, ○ = complex PD. C-D: images of 35S::MP30K-GFP epidermis of sink leaf (C), transition (D) and source (E) leaves showing that in the youngest leaf, complex PD are absent in all cells other than those supporting trichomes (arrows), while source leaves show widespread complex PD. Scale bar in C =100 µm. Taken from Roberts et al, 2001).

This phenomenon has been most extensively studied in *Nicotiana* species, where the proportion of simple PD in *N. tabacum* decreases from ~90% of the total PD to ~20% during leaf maturation (Oparka et al., 1999; Roberts et al., 2001). Data for the abaxial epidermis is shown in Figure 32A and B, and as images in C-E. This conversion results in a significant restriction of communication, with 30-46% of sink leaf cells, but only 2-9% of source leaf cells, able to traffic the symplasmically moving 54 kDa probe, 2xGFP (cited in Kobayashi *et al*, 2005). This conversion from simple to complex is also accompanied by a decrease in the overall number of PD due to the expansion of air spaces within the tissue, reducing the average length of shared wall interfaces between mesophyll cells by >50% (Roberts et al., 2001), and the length of shared wall in the transport pathway to the phloem by 63% (Ding et al., 1988). These two processes cause a large net restriction of symplasmic communication.

How this conversion of PD affects leaf development is unknown. What is clear is that many of the primary morphogenesis events of leaf growth are dependent on symplasmically mobile signals and occur while the majority of leaf PD are simple (reviewed in Braybrook and Kuhlemeier, 2010). Maintenance of the SAM and development of the primordium involve symplasmically mobile proteins, including *SHOOTMERISTEMLESS* and knotted-like homeobox (*KNOX)* genes (Kim et al., 2003). In certain species the symplasmically mobile protein KNOXI is also expressed in the early leaf primordium, resulting in complex leaves (Bharathan et al., 2002). The expansion of the leaf from a dome-shaped primordium to a flat sheet is due to a switch from generic expression of developmental genes throughout the whole organ to the polarised expression of genes promoting adaxial fate (*PHABULOSA* (*PHB*)*/PHAVOLUTA* (*PHV*), etc.) and abaxial fate (*KANADI/AUXIN RESPONSE FACTOR*(*ARF*)*/YABBY*, etc.) (Fleming, 2005). The initial spatial restriction of these adaxial- and abaxial- genes in early development appears to be mediated by a mobile signal from the SAM, as isolation of the primordium results in radial leaves (Sussex, 1951). Further dorso-ventral restriction of gene expression occurs through miRNAs that target *PHB/PHV* transcripts (Kidner and Martienssen, 2004) and *ARF* transcripts (discussed in detail in Chapter 1). Trichomes are also

initiated at an early stage of leaf development, and their spacing is controlled by the symplasmically-mobile protein CAPRICE and a mobile signal associated with the gene *TRIPTYCHON*, which act as inhibitors to trichome development (Schellmann et al., 2002; Schnittger et al., 1999).

The secondary morphogenesis events that follow these processes, and the mechanisms controlling them, are less well studied. This stage of development is characterised by successive basipetal waves of development, starting with a general cessation of mitotic activity, first in the adaxial epidermis and then in the palisade mesophyll, which generally takes 8-10 days to cover the whole leaf (Donnelly et al., 1999). The sink source-transition, the development of complex PD, and the later cessation of cell expansion follow, also in basipetal waves.

4.1.2 The sink-source transition

It is not currently known whether the sink-source transition and the widespread conversion of PD are directly linked or merely correlated. As the development of complex PD is a general part of maturation observed in many plant tissues (see Chapter 1), it is entirely possible that the conversion of PD seen in leaves is simply a side effect of synchronised cell maturation rather than attainment of source state specifically. On the other hand, complex PD could potentially play a necessary functional role in the export of photosynthate from mature leaves. In either case the association of complex PD with source tissue has allowed sink/source state to be used as shorthand to infer PD structure, with some studies interchangeably using the terms ‘sink PD’ with ‘simple PD’ and ‘source PD’ with 'complex PD’ (e.g.: Ding et al., 1992; Vogel et al., 2007). However, while the exact correlation is unknown, our limited understanding of complex PD formation in leaves means that the sink-source transition gives the best estimate of general PD structure currently available, so it is relevant to discuss it here.

What determines the timing of the sink-source transition is still unknown. The import capacity of leaves can be demonstrated by feeding exporting leaves with C_{14} and subsequently imaging importing leaves of interest by autoradiography (Turgeon and Webb, 1973), by feeding symplasmically mobile dyes such as carboxy-fluorescein

diacetate into the phloem (Roberts et al., 2001), or by imaging the expression pattern of the *AtSUC2* promoter, which becomes active in mature phloem companion cells (Wright et al., 2003). These methods show that the number of leaves undergoing the sink source transition can vary by species from as many as five in *N. tabacum* (Turgeon and Webb, 1973; Wright and Oparka, 1989), to two in *Beta vulgaris*, to one leaf only in *Cucurbita pepo* (Turgeon and Webb, 1973). The timing appears to be related to the point at which carbon balance is reached, which can vary between species from when the leaf reaches 15%-50% of its total final length (reviewed in Turgeon, 1989). However, carbon balance itself does not trigger the sink-source transition as shown by plants with non-photosynthetic albino leaves, which will transition as normal despite this causing them to starve (referenced in Turgeon, 2006).

4.1.3 High-throughput imaging for PD developmental studies

Plasmodesmata are key to leaf development, and are expected to be required for correct cell differentiation, tissue patterning, and the expansion of leaves as 3D structures. As discussed in Chapters 1 and 3, most of our knowledge of PD development in leaves comes from a combination of monitoring transport capacity via the movement of probes coupled with EM imaging of PD structure. The availability of an accurate marker for complex PD development that can be tracked via CLSM allows for larger scale and more flexible imaging. However, a complete survey of PD development even in a single tissue layer by CLSM is still likely to be problematic for two reasons. First of all, leaf maturation occurs over a timescale of weeks, and so leaves of several different ages would have to be imaged in order to build up a time line of development. Within that large population of sample leaves, a large number of cells require to be imaged. This is because the leaf contains a number of cell types, and even a single layer, such as the abaxial epidermis, contains a heterogeneous population of cells (e.g., pavement, anisocytic and guard cells). Furthermore, meristemoids continue to produce new cells throughout expansive growth of the laminal tissues, meaning that the cells may cover a wide age range. Hence very large samples sizes are required to give a reliable indication of PD density. Such large sample sizes will contain thousands of PD, which causes an

additional complication in that unbiased, reliable counting methods are needed to quantify them.

All of this means that such an experiment would be extremely challenging to perform manually. However, the technology to perform such a study using automated high-throughput systems is becoming available. Over the last decades, biological studies have been operating at increasingly larger scales. Advances in technology allowing the exchange, analysis and storage of large data sets has supported a shift from a reductionist view of biology to a holistic, systems-level approach. Hand-in-hand with this comes the need to automate experimental work to increase the speed and size of experiments, and to standardise conditions and reduce manual handling errors.

Microscopy systems are a somewhat late addition to the streamlining of techniques into automated, high-throughput systems, but are a necessary one as microscopy still provides the best estimate of many aspects of molecular biology, from localisation of proteins to their functional analysis (Pepperkok and Ellenberg, 2006). Automation of fluorescence microscopy has been a challenge because it requires adaptation of several facets of imaging work: sample preparation to produce comparable samples labelled accurately with fluorescent markers; automated acquisition of hundreds of images that are comparable in terms of depth, focus and location without human input; data handling systems to organise large amounts of image data plus the hardware necessary to store it; image processing software for automated image analysis; and the facilities required for mining large image datasets (Pepperkok and Ellenberg, 2006).

Commercially produced, off-the-shelf high-throughput systems have recently become available, but all are designed for analysis of single cell or monolayer systems. However, recent work by Silke Robatzek's group at The Sainsbury Laboratory, Norwich, has shown that such systems can be adapted for analysis of whole-plant tissues (Salomon et al., 2010). By mounting cotyledons in glass-bottomed multiwell plates using a custom-made stamp (Figure 33), this group was able to use a commercial Opera high-content spinning-disc CLSM system (PerkinElmer) to monitor membrane trafficking in living pavement cells. Even with the concession that manual preparation of the plates meant that their overall method

was only semi-automated, this approach still provided an extremely large increase in throughput compared to traditional microscopy.

In practice, preparation of each imaging plate took approximately 15 minutes, and a typical imaging run using the Opera microscope took approximately 30 minutes, and could image three, 2-channel, 24-image stacks in 60 leaves, generating 8640 images per run. To analyse this immense volume of images, custom image analysis scripts for the Acapella software (PerkinElmer) were produced by Ji Zhou (The Sainsbury Laboratory, Norwich). These automatically segmented the images to identify the cell boundaries, measure cellular parameters and count labelled compartments.

The work by the Robatzek group demonstrated that the Opera system could image fluorescently labelled membrane vesicles in cotyledons, suggesting that it should also be able to image PD in leaves. The scripts were designed to quantify fluorescent compartments of similar sizes to MP17-GFP labelled PD, and so could be successfully adapted and expanded to quantify PD in the context of epidermal cells and to distinguish anticlinal and periclinal PD (Figure 34). This opened up the possibility of a thorough investigation of complex PD development in leaf epidermal cells.

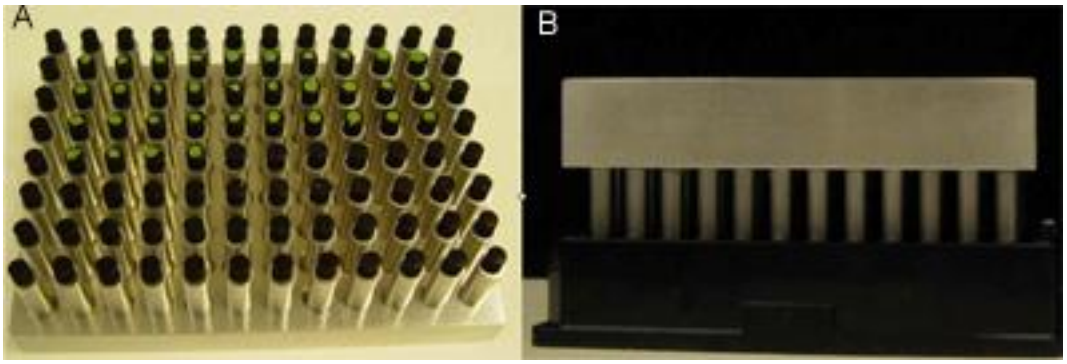

Figure 33: To image whole *A. thaliana* leaves using the OPERA system, leaves are mounted on a custom made stamp (A), which was then inverted and placed into a 96-well glass-bottomed plate (B) so that the leaves were pressed against the glass. The dimensions of the plate are programmed into the automated imaging software, allowing images to be taken of specific areas of each leaf in each well.

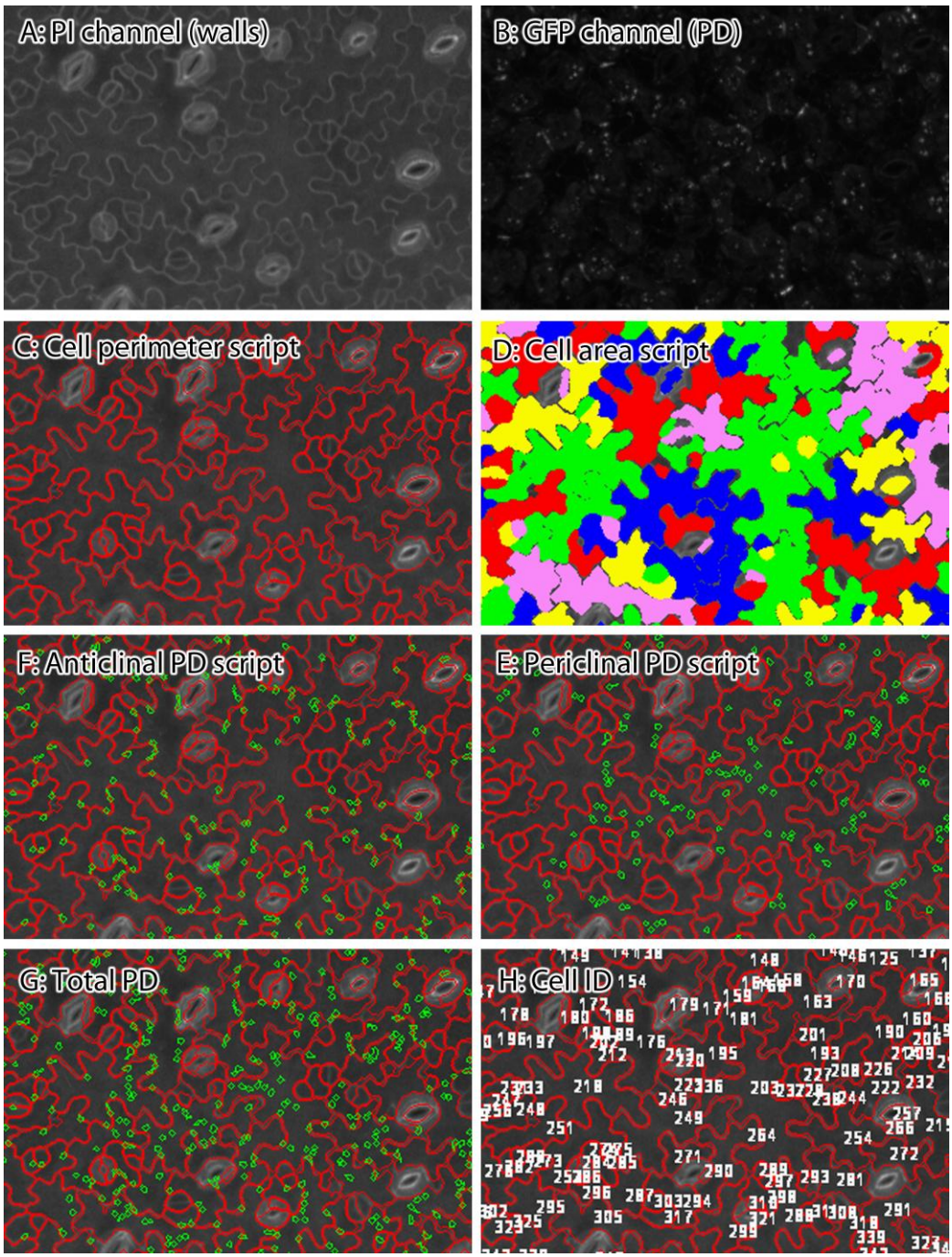

Figure 34: Output images from the custom image analysis written for this project by Ji Zhou. From the original images of the propidium iodide-stained walls (A), the script recognises cell walls, identifies cells and numbers them (H) and calculates the cell perimeter length (C) and cell area (D) (the colours in this image are for clarity only). The script recognises MP17-labelled PD from the GFP image (B), and combines this with the locations of identified walls to count the number of PD on anticlinal walls (F), and the number of PD not on anticlinal walls (E), and the overall number of PD (G).

4.2 Aims

The aims of this chapter are to study the pattern of complex PD development in the abaxial epidermis of *A. thaliana* leaves, using MP17-GFP as a marker for complex PD. Specifically, it aimed to:

- Examine the patterns of complex PD development at the tissue level from the early stages of leaf expansion to leaf maturity using high throughput microscopy and automated image analysis to produce significant datasets.

- Use traditional confocal microscopy to examine complex PD development in detail at the cellular level.

4.3 Results

4.3.1 Complex PD development in the leaf epidermis

As a foundation for this thesis, it was necessary to get a clear picture of the natural developmental pattern of complex PD in leaves. As shown in Chapter 3, complex PD at M-M interfaces rapidly become so densely packed as to be unquantifiable, so my experiments focused primarily on the adaxial epidermal layer and the PD at E-E and E-M interfaces.

As *A. thaliana* has a spiral phyllotaxy, this allows the leaves to be easily sorted chronologically. As I am looking at leaf development, **leaves are numbered reverse chronologically** with leaf 1 being the youngest leaf currently on the plant, contrary to the usual practice. Sequentially imaging leaves from individual rosettes showed the expected pattern of complex PD development (Figure 35): the youngest leaves, leaf 1 and 2, had very few complex PD, while leaf 3 and 4 showed complex PD in some leaf areas and not in others, while the older leaves, leaf 5 and 6, showed heavy MP17-GFP labelling. When regions at the tip, middle and base of each leaf were compared, the expected basipetal wave of PD development was observed: complex PD appear first in the top region of leaf 2-3, but are not visible in basal regions until leaf 4-5.

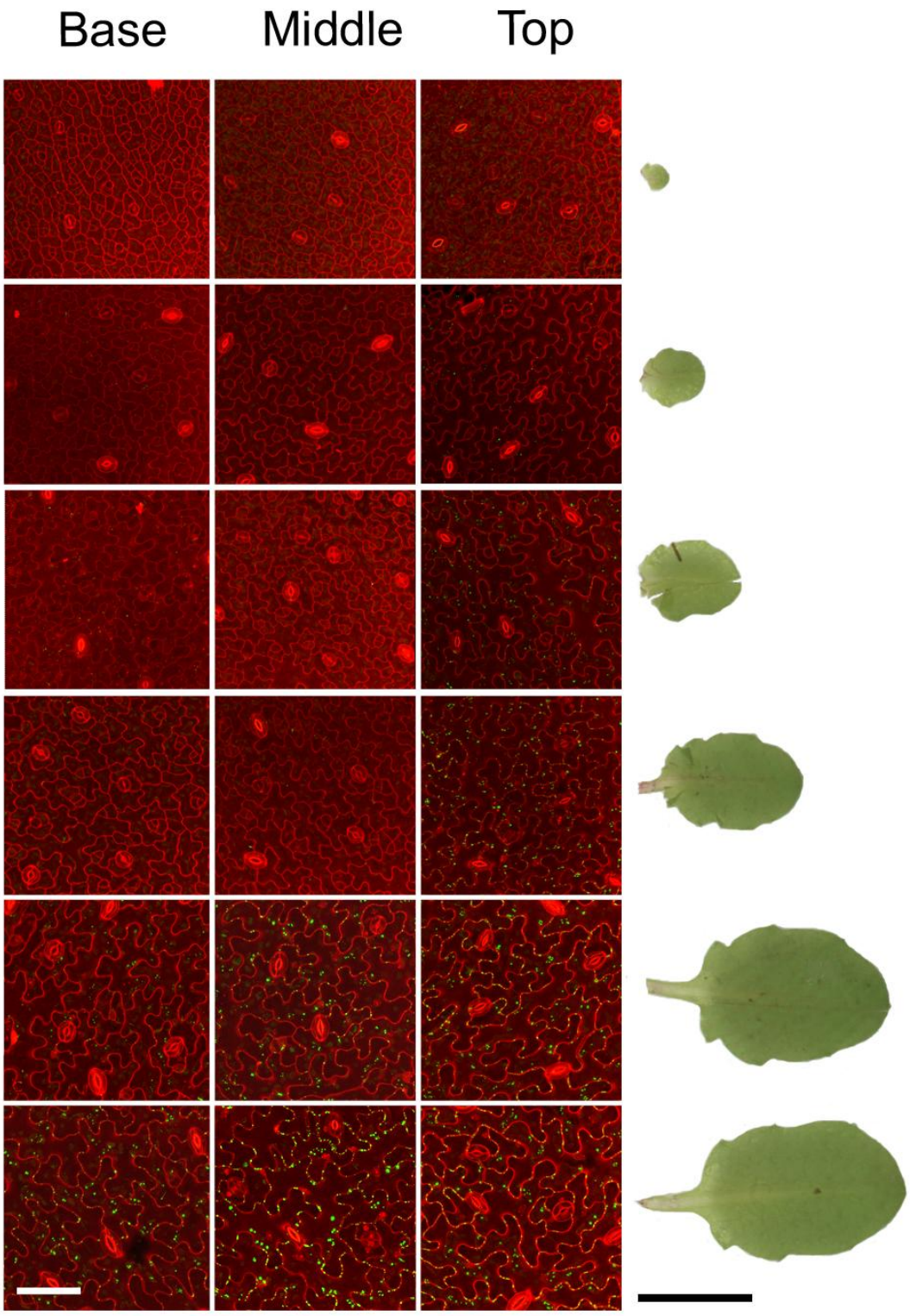

Figure 35: Developmental series showing images from regions at the top, middle and base of the six youngest leaves of a mature 35S: MP17-GFP *A. thaliana*. Cell walls are stained red with PI. Scale bar = 1cm.

To take the variation in developmental rates into account, I scaled leaves by the Leaf Plastochron Index (LPI), a numerical index used to relate leaf age to a developmental time scale rather than a temporal one (Erickson and Michelini, 1957). The index is scaled in terms of plastochrons (the time interval between initiation of successive nodes), which are of regular in duration throughout much of the vegetative growth of many higher plant species. This index is useful as developmental stage can vary widely in a population of plants sown on the same date. The plastochron index has been established as applicable in *A. thaliana* (Groot and Meicenheimer, 2000b) and used to correlate developmental features in this model species (Groot and Meicenheimer, 2000a). However, I found that even when leaves were sorted by their LPI, there was still only a loose correlation with PD number (Figure 36), showing that complex PD development is not simply determined by age, development or growth.

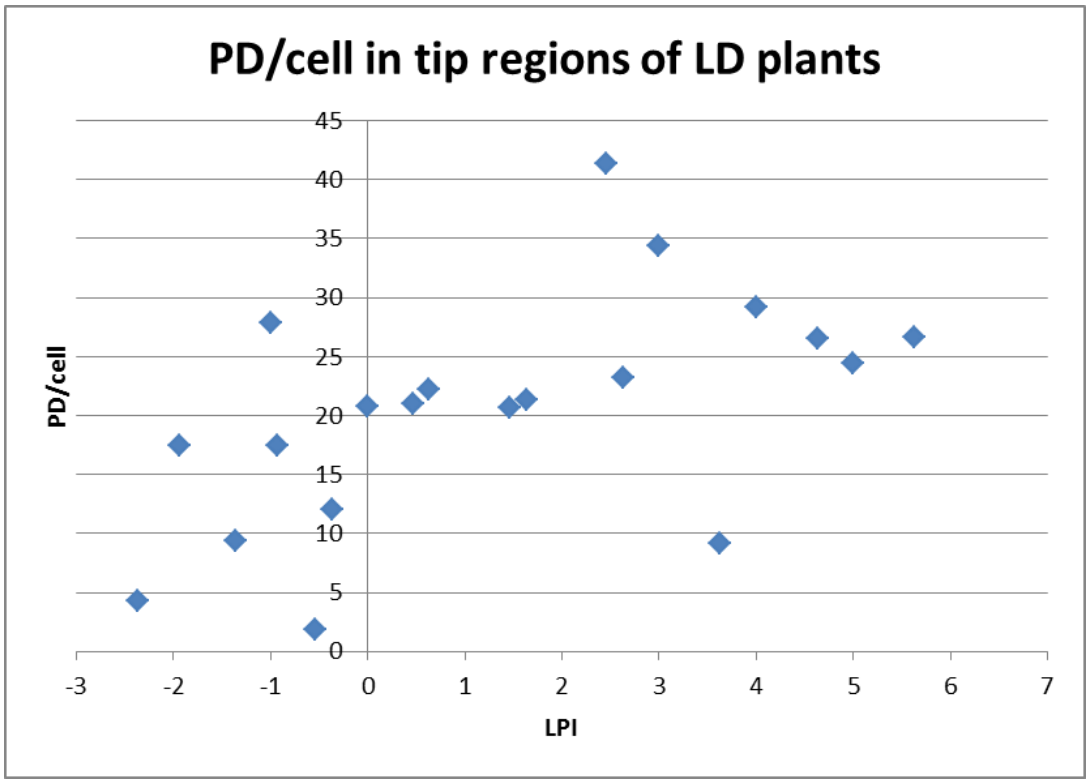

Figure 36: Graph showing the mean PD/cell. Each point represents the mean from an imaged population of 30-60 cells from the tip region of an imaged leaf from long day grown plants.

4.3.2 High throughput confocal analysis of complex PD development in the leaf epidermis

This variability, in addition to the factors outlined in the introduction to this chapter, showed that manual acquisition and processing was therefore not suitable to survey PD development. Instead, the high-throughput OPERA system was used to image the leaves, and automated image analysis software (see Figure 34) used to count PD. In the study, the six youngest leaves of 12 soil-grown *A. thaliana* plants at the 8-leaf stage were mounted in wells in imaging plates, and the confocal system set to take three runs of three 24-image stacks around the centre of each well in order to maximise the chances of obtaining clear images of the leaf lamina. As only complex PD are being observed, 'PD' values given throughout this chapter refer to complex PD only.

As stated in the introduction, the image analysis scripts were written by Ji Zhou from the Sainsbury Laboratory, Norwich. Due to the range of leaves used in this experiment, the cells to be analysed ranged from <50μm to >7000μm^2 with an associated range of wall thicknesses, which made designing a script for complete analysis of all tissues challenging. Two scripts were therefore produced: one for analysis of small cells (50-6000 μm^2) and another for analysis of large cells (200-∞ μm^2). The upper limit of the 'small-cell' script made it unsuitable for analysis of leaves that contained genuine cells over this size threshold (leaves 4-6), and was more likely to artificially split larger cells. On the other hand, the 'large-cell' script had the reverse problem in analysing younger leaves that contained a significant number of cells smaller than 200 μm^2, and was more likely to misrecognise the thinnest cell boundaries and artificially merge cells (Figure 37 A). However, if I used the small cell script for the younger leaves, and the large cell script for the older leaves, the results from the two scripts segregated into two separate groups. It was decided to use the large cell script to analyse all the data, as this would permit counting of PD in the fullest range of cell sizes, and the cells beneath the size threshold would generally contain few complex PD (as shown in Figure 37A, where all the PD present are on boundaries of recognised cells). For comparative purposes, however, the image analysis results for leaves 1-3 using the small cell script are presented in Appendix 3.

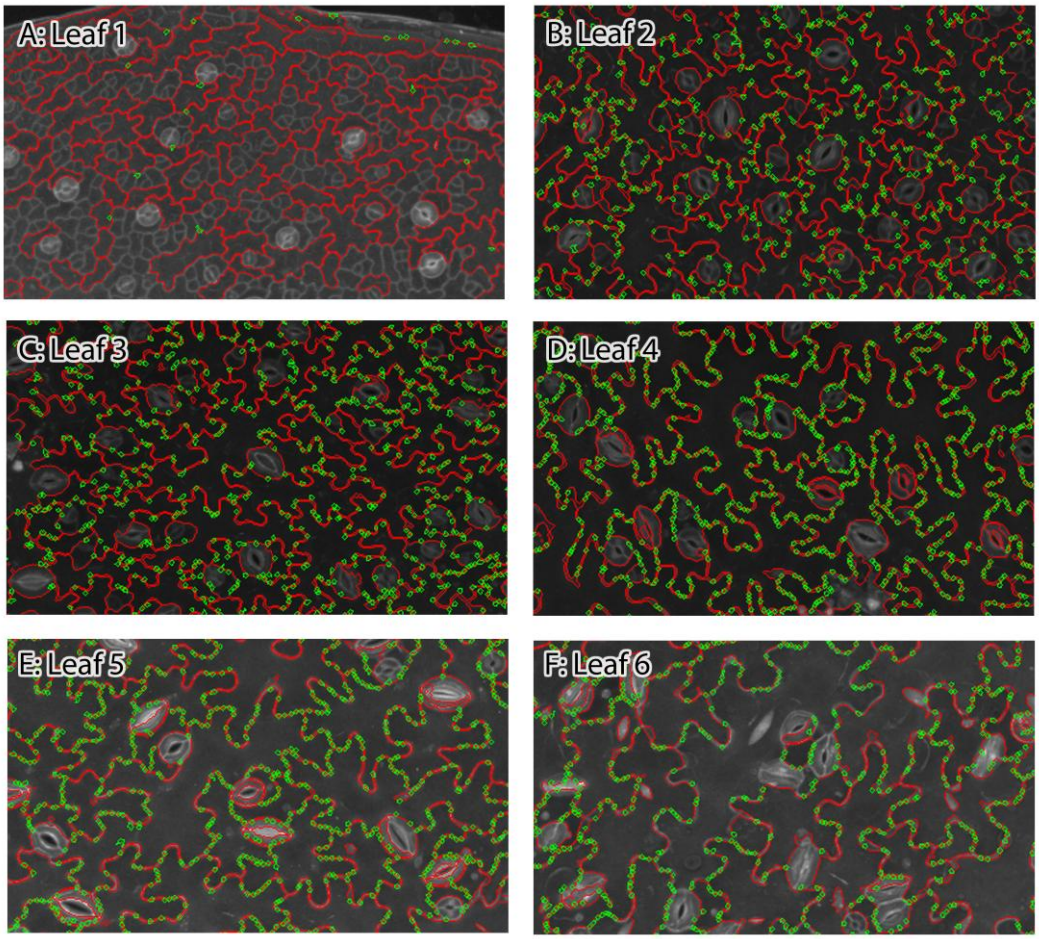

Figure 37: Output images from the 'large-cell' image analysis script, showing the cell wall boundaries outlined in red and the anticlinal PD shown in green. The images shown are the lower epidermis of the six youngest from 8-leaf soil grown *A. thaliana* (images are from equivalent leaves from several plants).

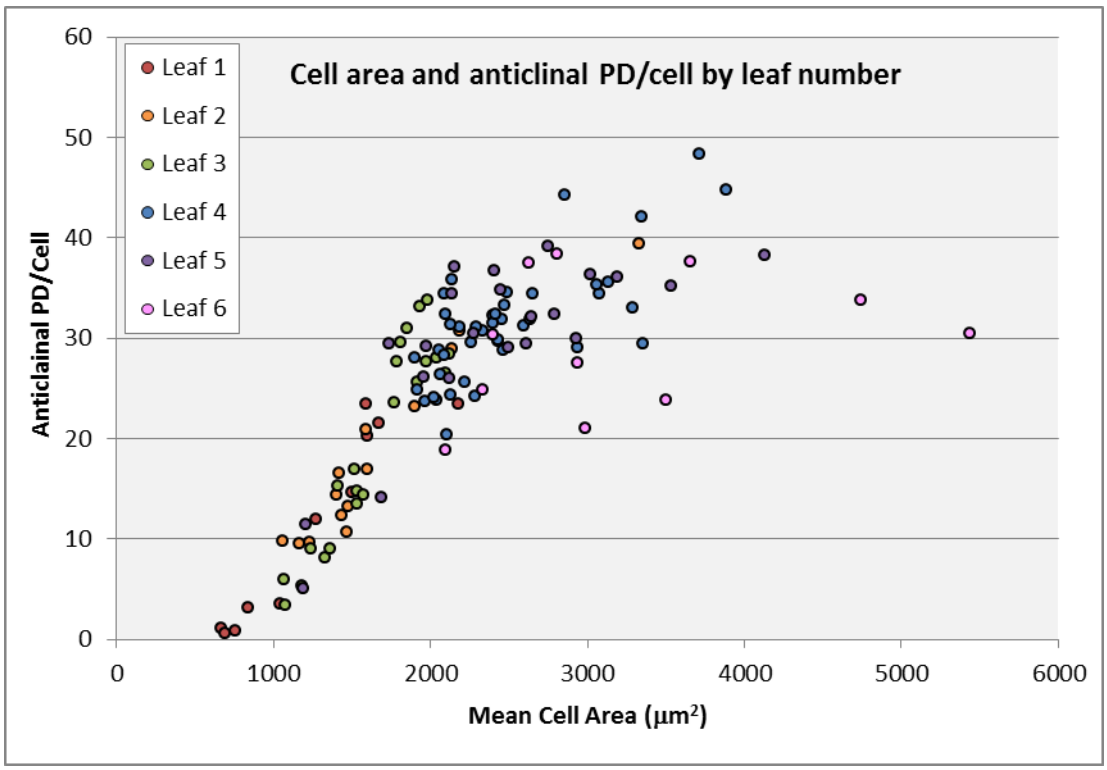

Figure 38: Graph showing the mean cell area and the anticlinal (epidermal-epidermal) PD/cell for the six youngest leaves of 8-leaf soil-grown *A. thaliana*. Each data point represents means from an imaged population of 30-200 cells, and is the raw output from the image analysis script.

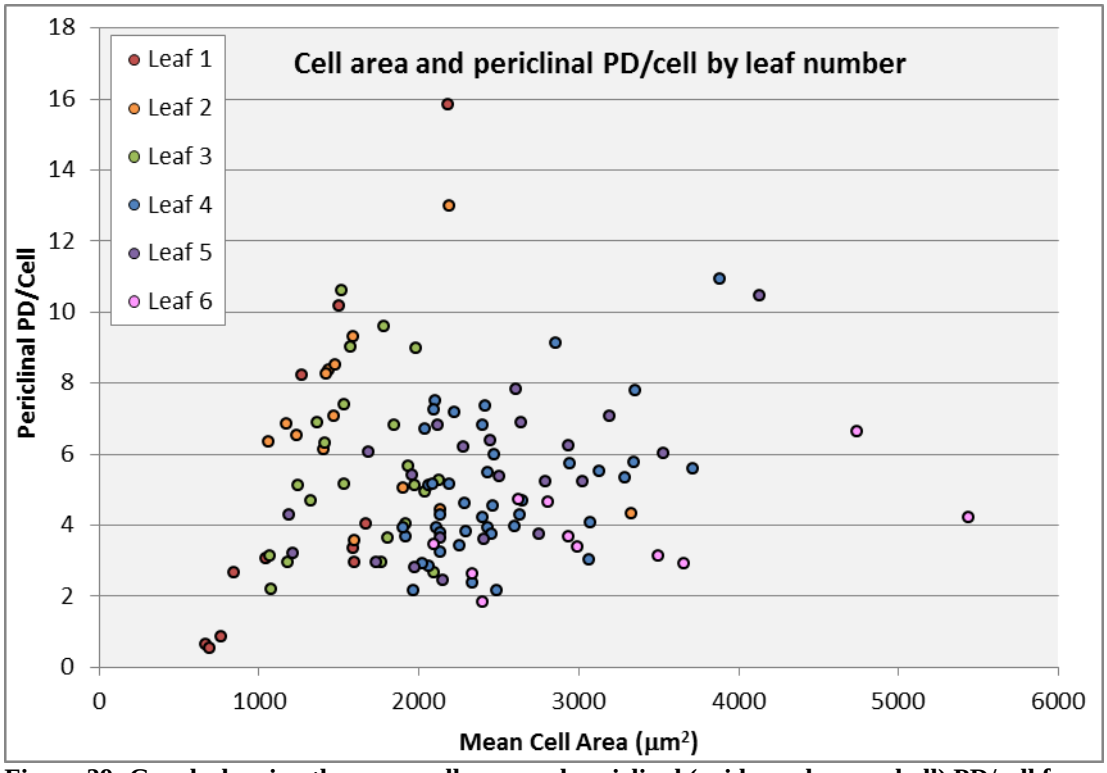

Figure 39: Graph showing the mean cell area and periclinal (epidermal-mesophyll) PD/cell for the same populations shown in Figure 38.

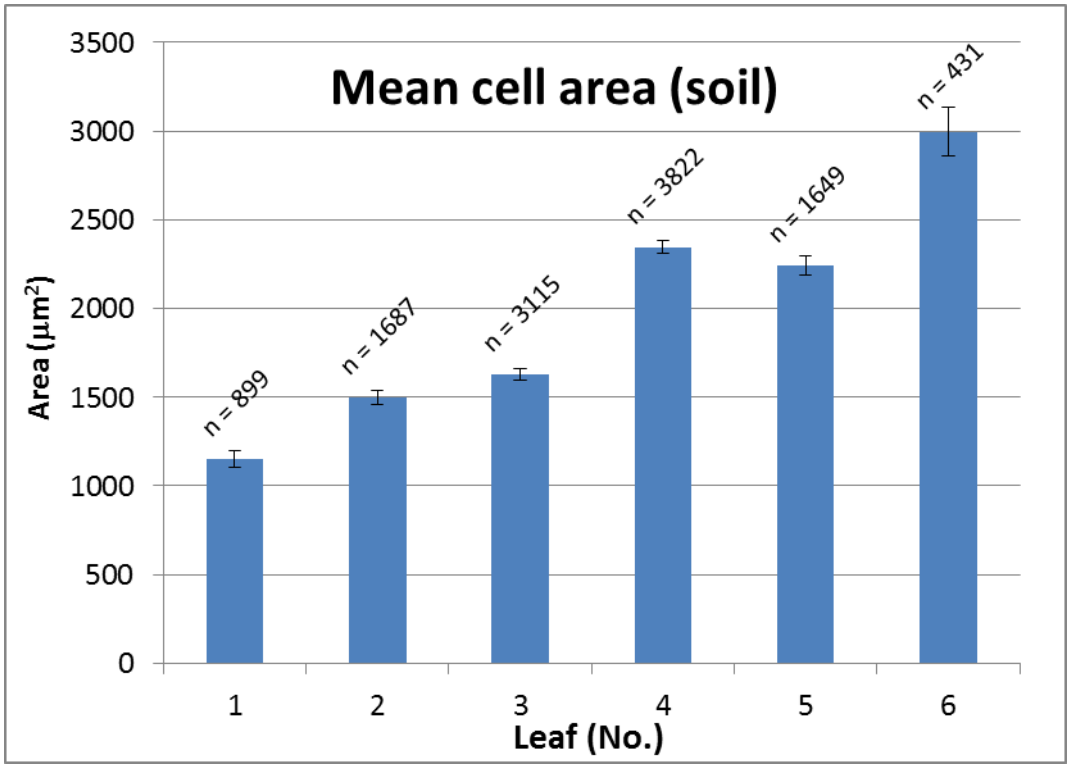

Figure 40: Graph showing the average cell areas of all cells imaged for leaves of each age. Bars are standard errors. 'n' values show the total number of cells analysed.

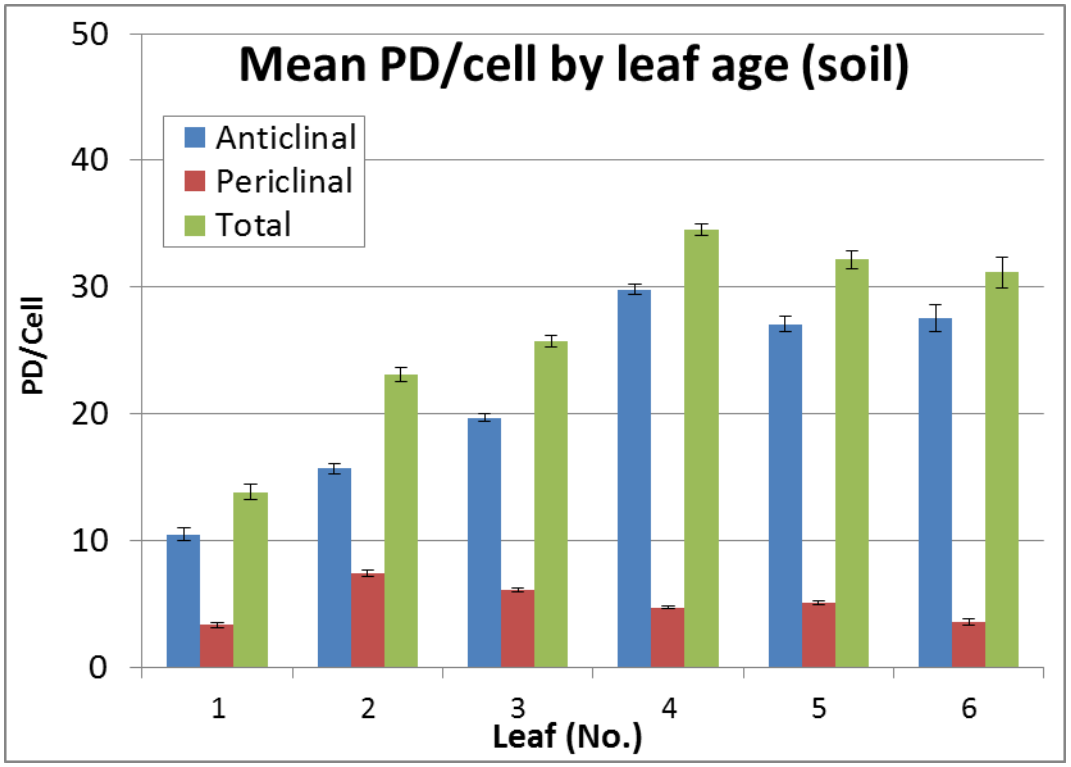

Figure 41: Graph showing the mean number of anticlinal (E-E), periclinal (E-M) and total complex PD per cell by leaf number. Bars show standard errors.

Figure 38 and Figure 39 show the averaged results from each image stack that was suitable for analysis by the image analysis scripts (empty, out-of-focus or images containing below a threshold number of imaged cells were automatically rejected, while analysed but poor quality or misrecognised images were rejected manually), so that each point represents a population of ~30-200 cells, with a mean of 94 cells per image. As each leaf was imaged nine times, several points may correspond to different areas of a single leaf. Smaller leaves (<3mm) were placed whole into the imaging chamber, and so imaged areas may correspond to the tip, middle or base of a leaf. Sections from the middle area of the larger leaves were cut with a cork borer and mounted on the stamp, meaning that for most of the data points for leaf 3, and all leaf 4, 5 and 6, images are taken from the middle region of the leaf. While Figure 38 and Figure 39 show the spread of the imaged populations to demonstrate the plant-to-plant variation, the overall average data from all the cells of all populations imaged for each leaf age are presented in Figure 40 and Figure 41.

Figure 38 and Figure 39 (note different scales on y-axis) shows that cell area and number of complex PD per cell are not strictly correlated and both can show a large range of variation in leaves of equivalent age grown under identical conditions, as suggested from confocal counting experiments (Figure 36). However, the larger populations imaged via the automated confocal system make the patterns of development visible. The cell area and number of anticlinal PD increase linearly up to ~2000 μm^2 or to ~20 anticlinal complex PD/cell, at which point the correlation between area and complex PD number becomes looser, and the mean number of complex PD/cell begins to plateau. In terms of leaf growth, this plateau is generally reached when the leaf is the fourth youngest. When the overall averages are examined, they suggest there may be a slight decline in the number of periclinal complex PD/cell from Leaf 4 onwards. This may represent removal of complex PD, or removal of the MP17-GFP marker by proteasome mediated degradation (Vogel et al., 2007). Equally this phenomenon may be due to the age of the plant. In these 8-leaf plants, leaf 6 would have been only the third true leaf and would have been produced when the first true leaf pair were relatively unexpanded, and so may be expected to develop in a more restricted manner compared to the subsequent leaves.

The complex PD in the periclinal walls connecting the lower epidermis to the spongy mesophyll show a completely different pattern of development. In the youngest leaves surveyed we can see that the numbers of periclinal PD (0.5 and 0.7) are very similar to the numbers of anticlinal PD (0.5 to 0.8), suggesting that anticlinal and periclinal PD begin developing complex forms at roughly the same time and rate (Figure 38, Figure 39). However, increases in the anticlinal PD rapidly outstrip numbers of periclinal (Figure 38 and Figure 39, Figure 41). This is likely due to larger numbers of existing simple PD in the anticlinal walls compared to periclinal walls: the anticlinal walls are formed by divisions of epidermal cells so PD will be regularly inserted by divisions in this plane, whereas the periclinal wall between the L1 and L2 layer is a non-division interface, so almost all of the PD in the periclinal wall will be secondary PD.

The complex PD/cell value reaches a maximum number of around 8-10 periclinal complex PD per cell when the cells are an average size of 1500 μm^2, usually when the leaf is still the first or second youngest on the plant. These 'new' complex PD are likely to arise from simple PD present in the wall, but may also represent further *de novo* insertion of secondary PD. After this point the cells appear to lose complex PD, as the overall number of periclinal complex PD declines to an average of ~5 per cell. From this point onwards the value remains approximately constant suggesting no further insertion or loss of complex PD. This loss of complex PD observed in the young, expanding leaves is likely due to the expansion of air spaces in the spongy mesophyll layer, which results in reduced contact between the mesophyll and epidermis and likely results in destruction of established PD (Roberts et al., 2001).

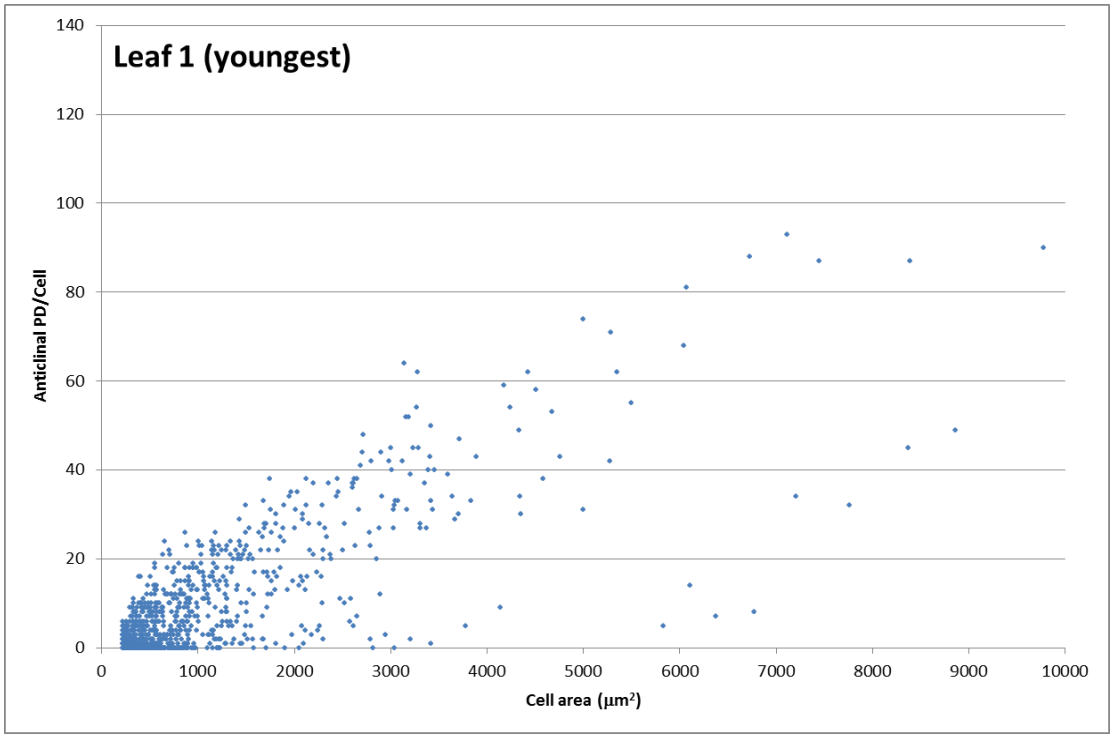

Figure 42: Graph showing the area and number of anticlinal complex PD of individual cells from imaged populations from leaf 1 (youngest leaf) of 8-leaf LD *A. thaliana*. Each datapoint represents values from a single cell.

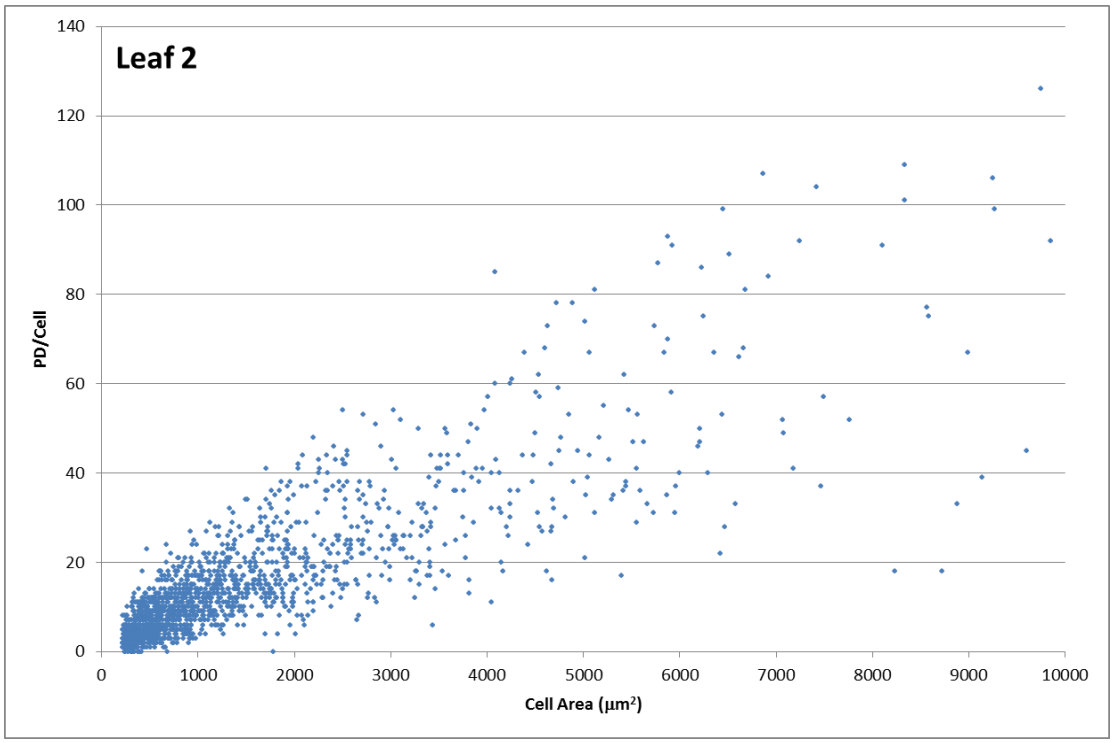

Figure 43: Graph showing the area and number of anticlinal complex PD of individual cells from imaged populations from leaf 2 (second youngest leaf) of 8-leaf LD *A. thaliana.*

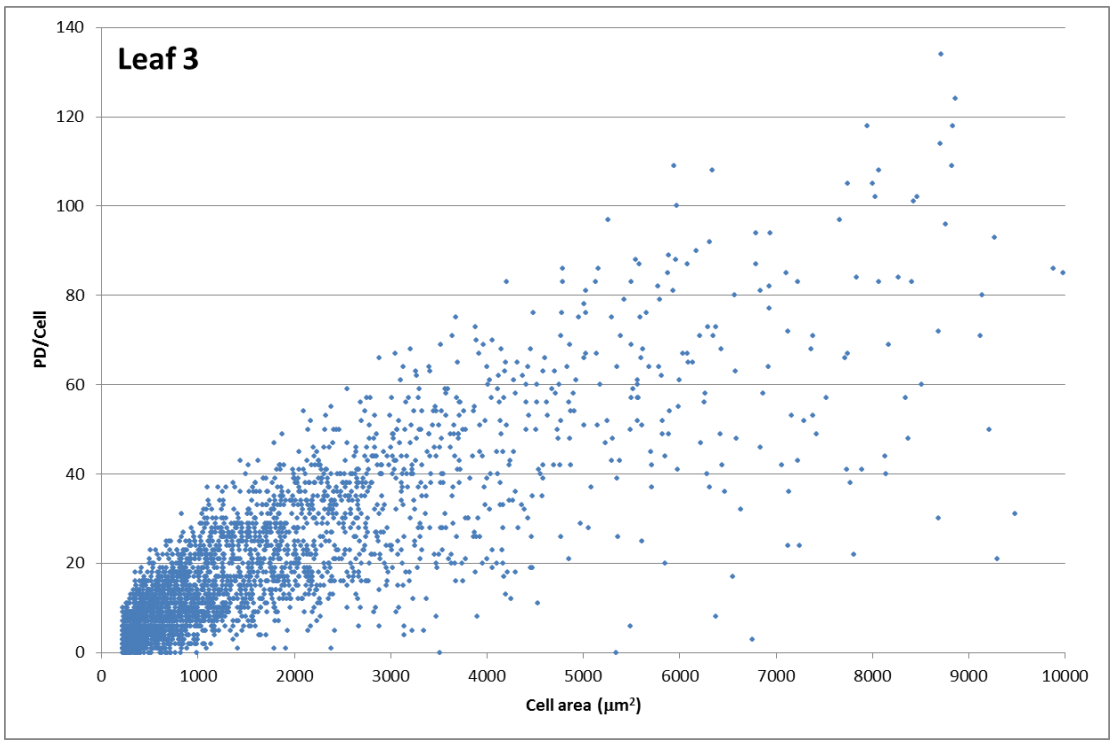

Figure 44: Graph showing the area and number of anticlinal complex PD of individual cells from imaged populations from leaf 3 (third youngest leaf) of 8-leaf LD *A. thaliana.*

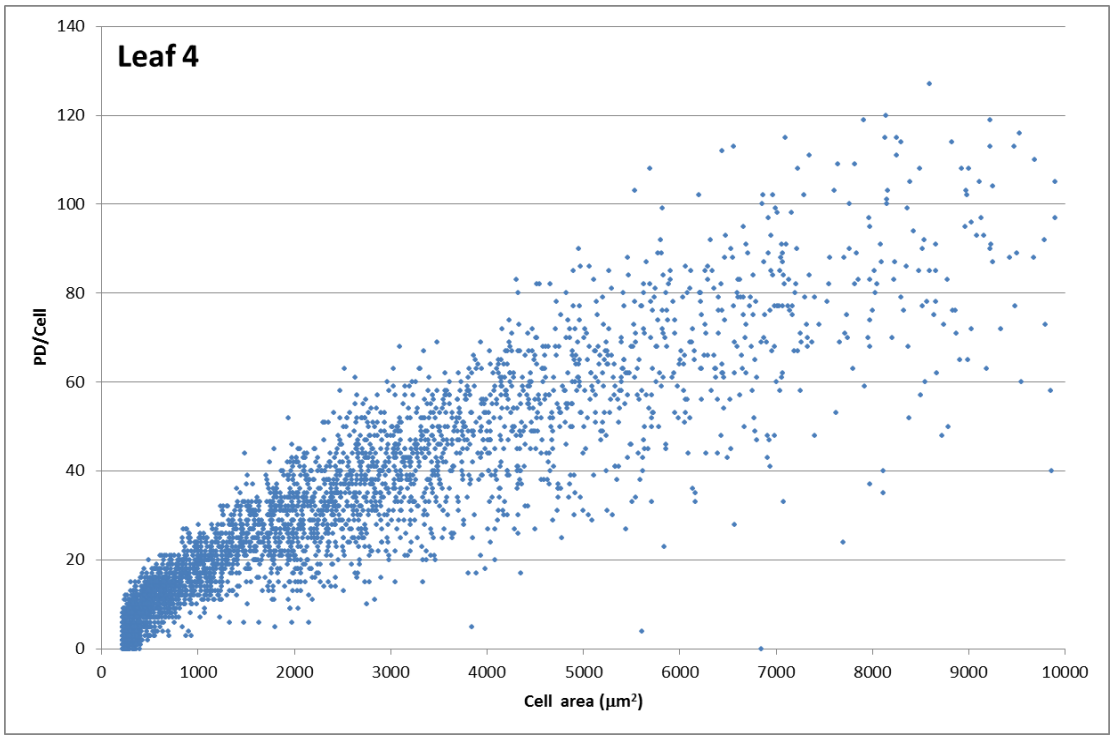

Figure 45: Graph showing the area and number of anticlinal complex PD of individual cells from imaged populations from leaf 4 (fourth youngest leaf) of 8-leaf LD *A. thaliana.*

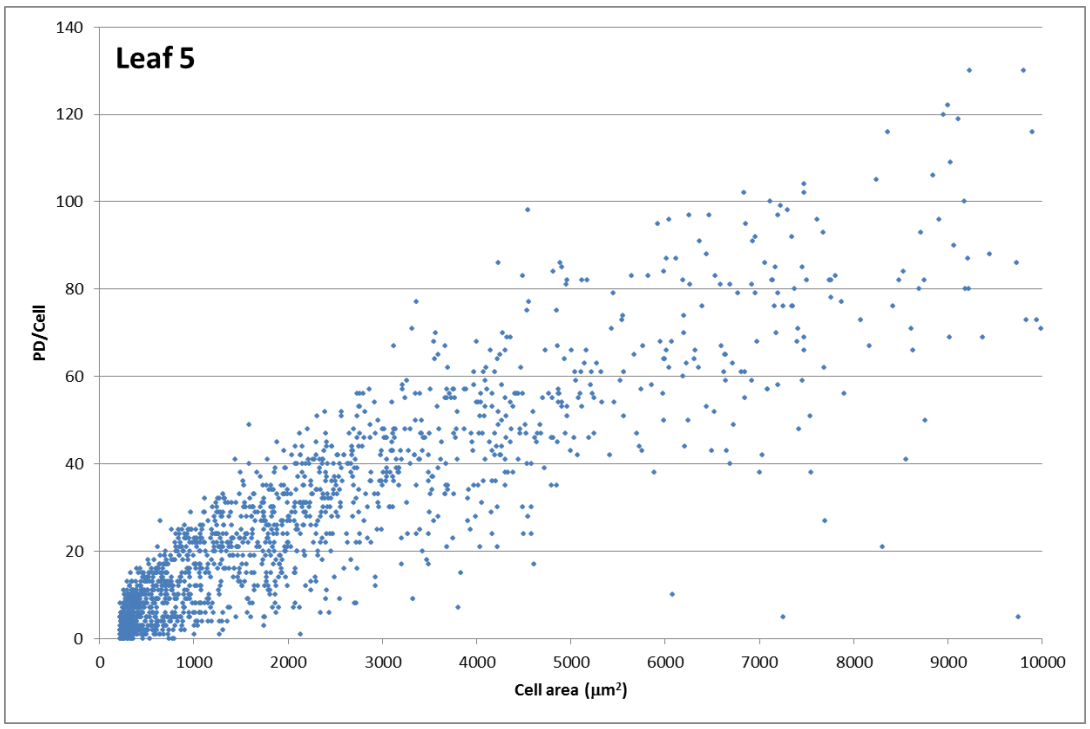

Figure 46: Graph showing the area and number of anticlinal complex PD of individual cells from imaged populations from leaf 5 (fifth oldest leaf) of 8-leaf LD *A. thaliana.*

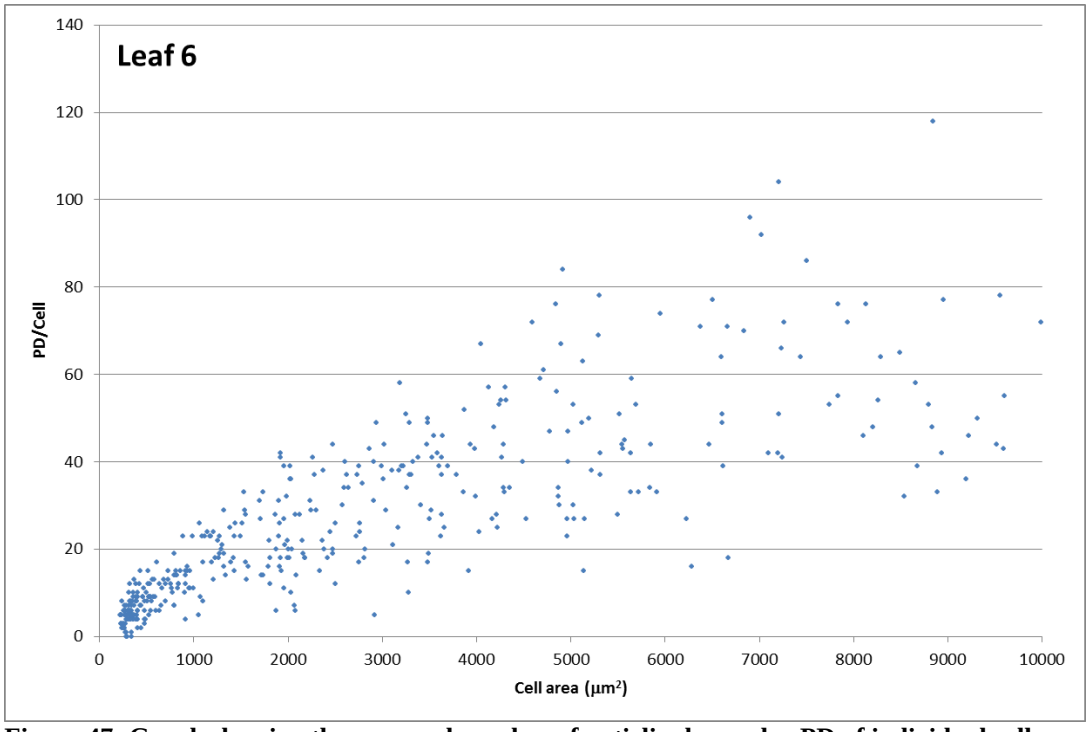

Figure 47: Graph showing the area and number of anticlinal complex PD of individual cells from imaged populations from leaf 6 (sixth oldest leaf) of 8-leaf LD *A. thaliana.*

Table 1: Trendline data for the graphs of anticlinal complex PD/cell and cell for leaves 1-6 shown in Figure 42 to Figure 47.

Leaf No.	Gradient of trendline	Intercept of trendline	R^2	Number of cells
1	0.0086	0.5273	0.6284	899
2	0.0084	3.1342	0.7076	1687
3	0.0093	4.5083	0.6883	3115
4	0.0098	6.7821	0.8229	3822
5	0.0096	5.4793	0.7772	1649
6	0.006	9.6688	0.6429	431

The graphs in Figure 42 to Figure 47 show the complete datasets, with each datapoint representing the actual area and number of complex PD in the E-E interfaces of an individual cell. These graphs reveal the range of values for both parameters and how they are linked in leaves of the same age. Due to space restrictions, the graphs have been thresholded to remove points >10,000 μm^2 or >140 PD/cell, but in the entire dataset, this resulted in deletion of ~20 points. The data for leaves 1-5 show clear trends in complex PD development over time. The trends are shown less strongly in leaf 6, which shows a reduction in number of complex PD compared to younger leaves, as was observed in Figure 38 and Figure 41.

The cell area and PD/cell increase in an approximately linear pattern, although the lower limit of the size threshold of the 'large cell' script means that cells <200 μm^2 are ignored, which gives the impression of a curve at the base of the graph. Analysis of the images with the 'small cell' script that includes these values shows that the data continue to the origin in a linear fashion (see Appendix 3). The gradient of the line shows a gradual increase from <0.009 in leaves 1 and 2 to >0.009 from leaf 3 onwards. This suggests that the rate of development of complex PD is slow at the onset of leaf expansion, but increases as leaves mature.

During leaf development, we see an increase in both the mean cell area (Figure 40) and the maximum cell area (Figure 42 - Figure 47). However, all leaves, including the most mature, maintain a population of cells of <1000 μm^2, which will include many specialised epidermal cells such as meristemoids, guard cells and the smallest cells of the anisocytic complexes. In the youngest leaves, many of the cells <1000 μm^2 contain few or no complex anticlinal PD, but looking at leaves of increasing age, shows that cells in this size range contain progressively more PD. This is shown in

the increase in the x-axis intercept value of the trendline from 0.53 complex PD in the youngest leaf, to 5.4-9.66 in the oldest leaves. This indicates that while the smallest cells in the youngest leaves include many immature cells, the older leaves maintain a population of unexpanded cells that, although small, are mature and possess complex PD.

When comparing the R^2 values of each plot, the range of PD/cell values seems restricted in the older leaves. However, this effect is not clear cut and trends may be enhanced or masked by the differing numbers of cells imaged for different leaf categories. In the youngest leaves, fewer cells were observed as the small leaves did not cover the entire imaging well and therefore may have been missed by the automated confocal system. In older leaves, increased cell area meant that fewer cells were imaged per stack.

4.3.3 Development of complex PD in periclinal interfaces

The corresponding cell-by-cell datasets for periclinal complex PD in the E-M interface/area are shown in Figure 48 to Figure 53. The overall trends for periclinal complex PD development, as shown by means of imaged populations in Figure 39 and as overall means in Figure 41, is that the maximum number of periclinal PD occur at the 2nd or 3rd leaf stage, when the cells have an average area of 1000-1500 μm^2. The cell-by-cell datasets confirm this, as the gradient of the trendline increases from 0.0037 in the youngest leaves to 0.0042 in leaf 3, and then decreases to ~0.0025. However, the individual PD/cell values for each leaf age (Figure 48 - Figure 53) show a linear trendline with no fall in PD numbers in cells over 1000-1500 μm^2 , as seen from the overall means for all leaf categories (Figure 39, Figure 41). This suggests that removal of periclinal PD occurs on a leaf-by-leaf basis rather than a cell-by-cell basis; i.e.: it is not a case of individual cells losing complex PD after they reach a certain size threshold, but that leaves lose complex PD in cells of all sizes after they reach a certain developmental threshold. This occurs approximately when they become the third youngest on the plant.

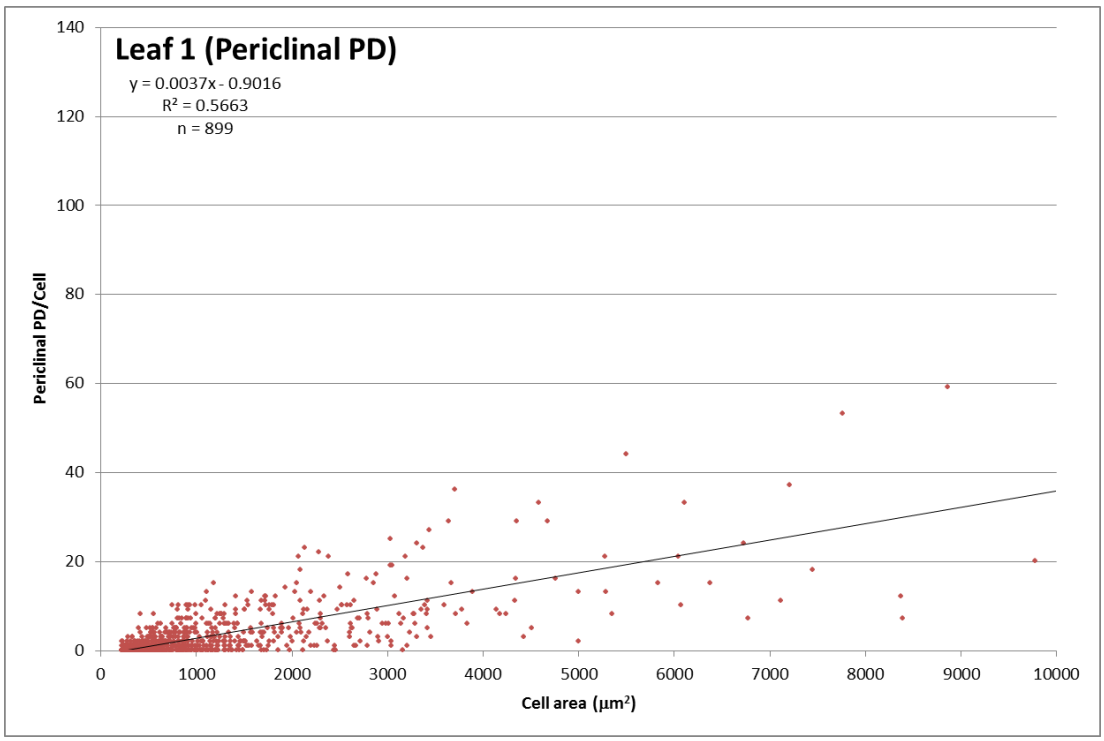

Figure 48: Graph showing the area and number of periclinal complex PD of individual cells from imaged populations from leaf 1 (youngest leaf) of 8-leaf LD *A. thaliana.*

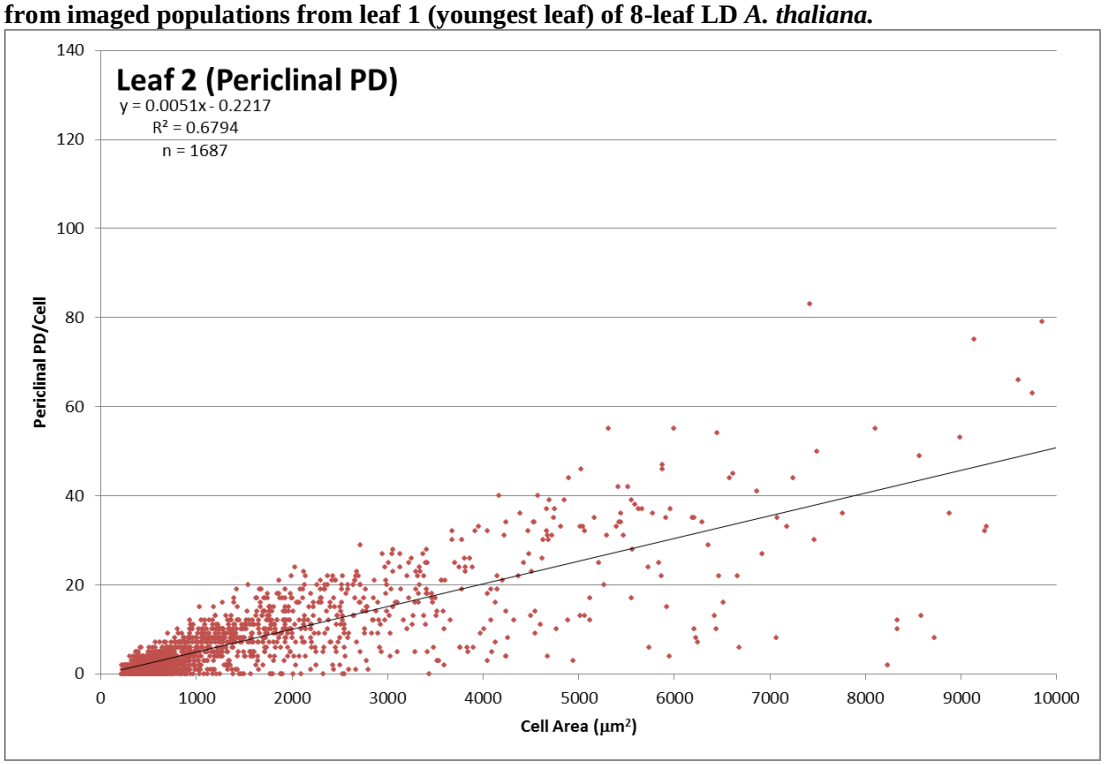

Figure 49: Graph showing the area and number of periclinal complex PD of individual cells from imaged populations from leaf 2 (second youngest leaf) of 8-leaf LD *A. thaliana.*

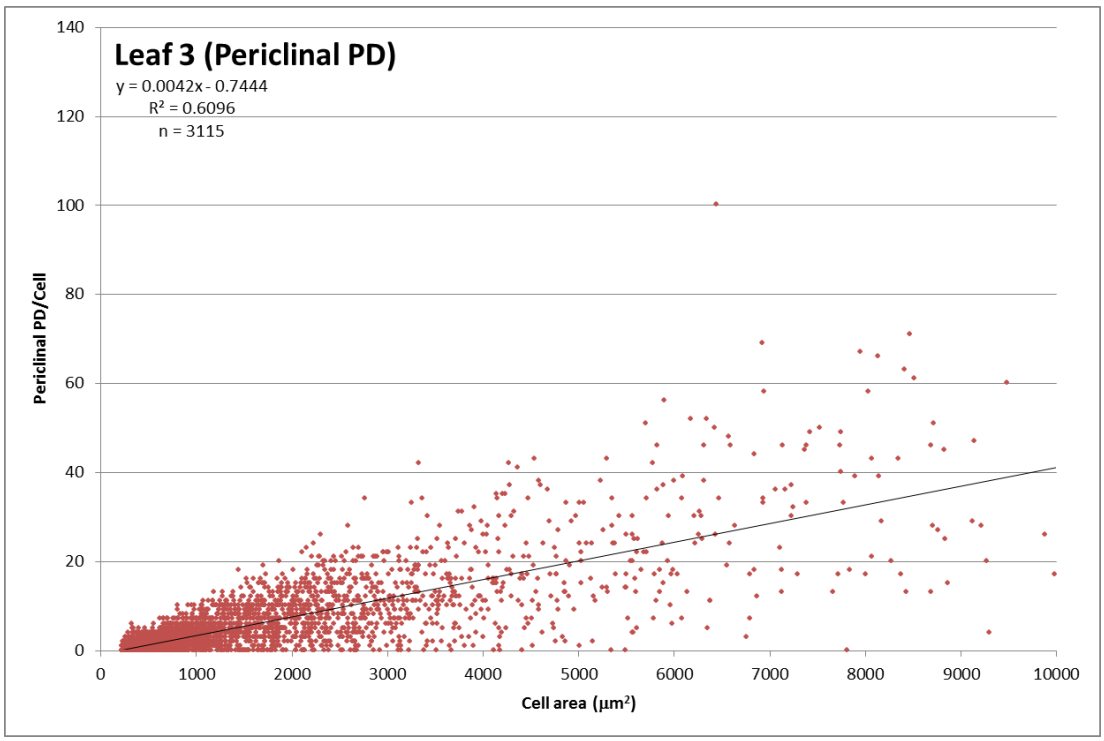

Figure 50: Graph showing the area and number of periclinal complex PD of individual cells from imaged populations from leaf 3 (third youngest leaf) of 8-leaf LD *A. thaliana.*

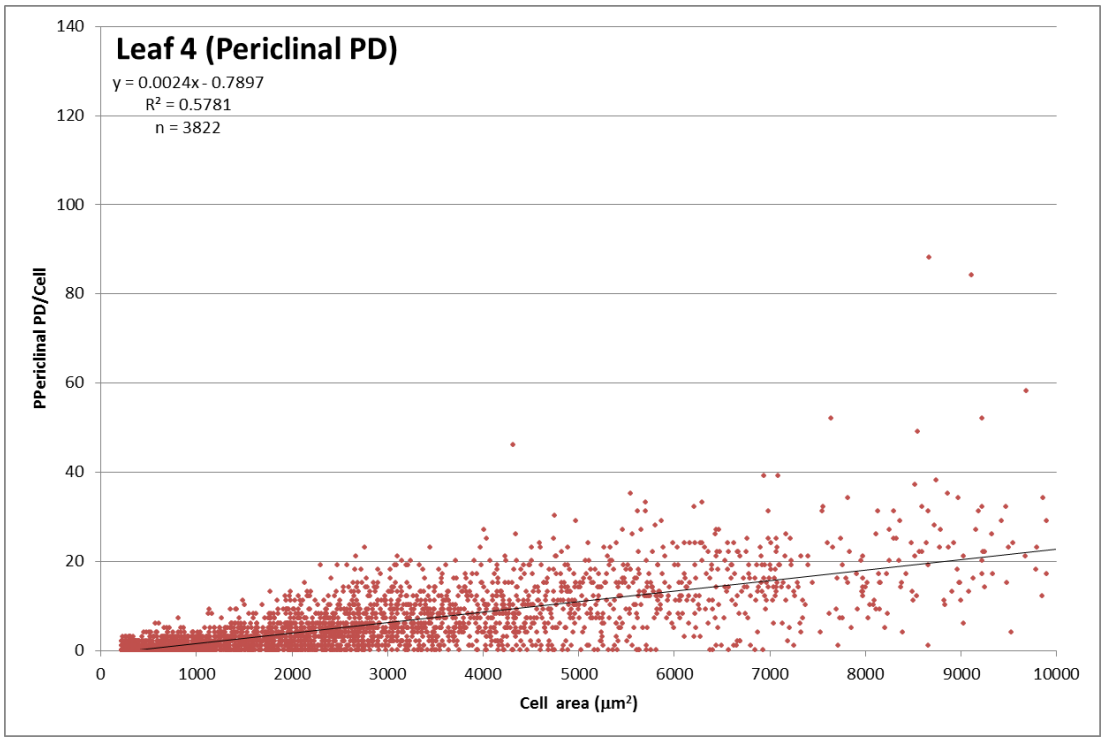

Figure 51: Graph showing the area and number of periclinal complex PD of individual cells from imaged populations from leaf 4 (fourth youngest leaf) of 8-leaf LD *A. thaliana.*

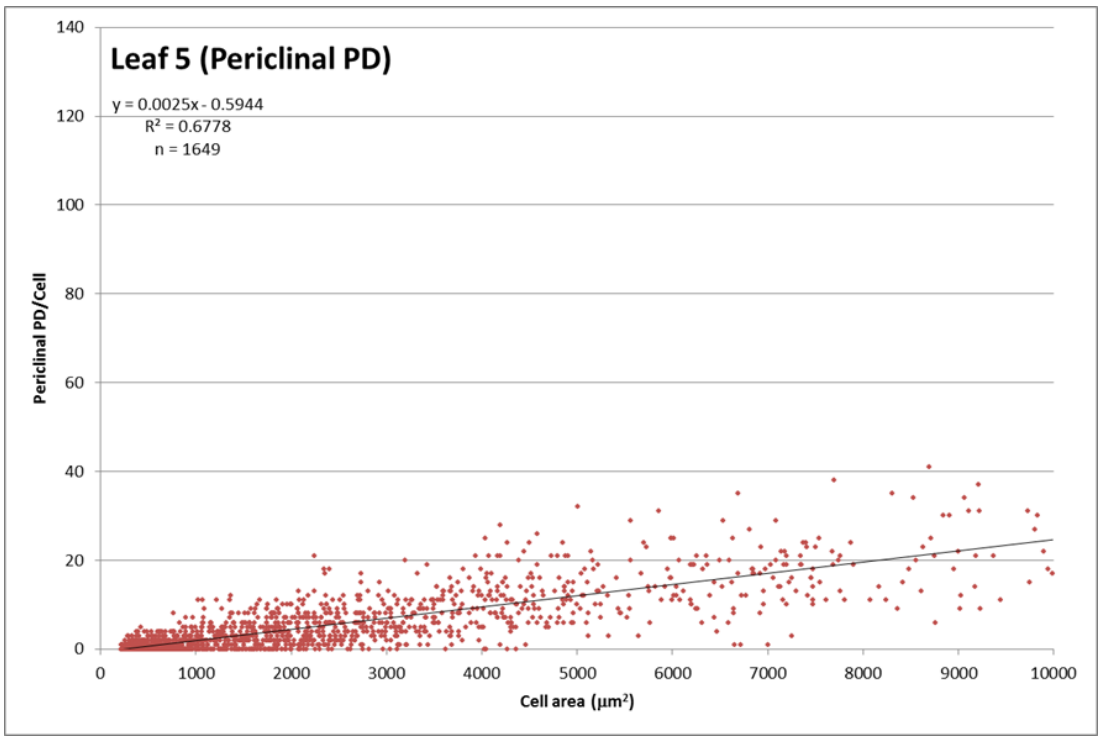

Figure 52: Graph showing the area and number of periclinal complex PD of individual cells from imaged populations from leaf 5 (fifth youngest leaf) of 8-leaf LD *A. thaliana.*

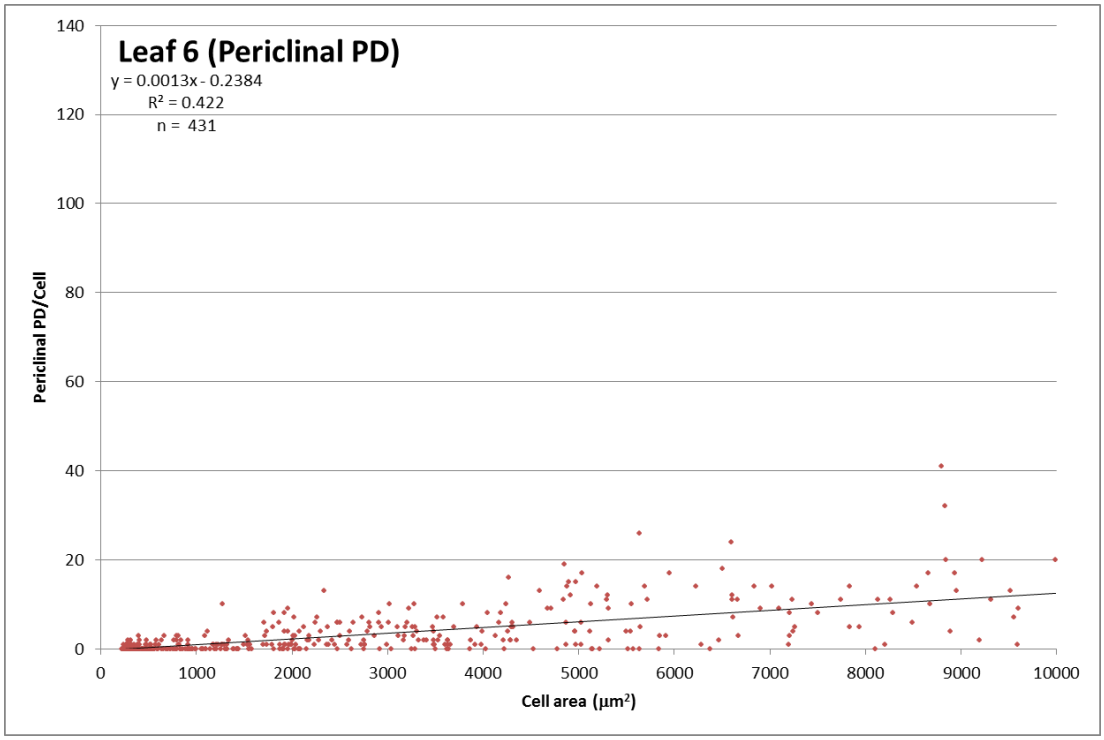

Figure 53: Graph showing the area and number of periclinal complex PD of individual cells from imaged populations from leaf 6 (sixth youngest leaf) of 8-leaf LD *A. thaliana.*

Table 2: Trendline data for the graphs of periclinal complex PD/cell and cell area for leaves 1-6 shown in Figure 48 to Figure 53.

Leaf No.	Gradient of trendline	Intercept of trendline	R^2	Number of cells
1	0.0037	-0.9016	0.5663	899
2	0.0051	-0.2217	0.6794	1687
3	0.0042	-0.7444	0.6096	3115
4	0.0024	-0.7897	0.5781	3822
5	0.0025	-0.5944	0.6778	1649
6	0.0013	-0.2384	0.422	431

Unlike the data for anticlinal PD, when PD/cell values are plotted for each leaf type, intercept values for the trendlines are all negative (Table 2), as are the intercept values given by the small cell analysis script that contains counts for cells <200μm^2 (L1 = -0.49, L2 = -0.50, L3 = -0.50) see Appendix 3. This shows that a large number of small cells in leaves of all ages possess few or no complex periclinal PD.

4.3.4 Development of complex PD in plate-grown plants

For comparison and use in experiments using plants grown on plates, six *A. thaliana* plants grown on 0.5 MS medium to the 7-leaf stage were imaged in the same way as the soil-grown plants above, and Figure 54 and Figure 55 show the mean cell area and PD/cell of the six youngest leaves. Each data point represents means from an imaged population of 30-200 cells, derived from the raw output from the 'large cell' image analysis script. The dataset contains fewer imaged populations than in the study of soil-grown plants because fewer plants were used. Furthermore, plants grown on plates had smaller and thinner leaves than soil-grown plants, making them more prone to damage during staining and mounting. Particularly, this dataset contained very few good images for the second leaf of the plant, with all of the datapoints for this dataset coming from populations on a single leaf.

Growing plants in culture results in a reduction of leaf length and overall organism size, and biolistic bombardment experiments have indicated that leaves of plate grown plants are more restrictive in terms of symplasmic communication than in equivalent soil-grown plants (Crawford and Zambryski, 2001). In this study, the overall patterns for cell area and PD/cell for the imaged populations of plate-grown

plants (Figure 54 and Figure 55) look very similar to the equivalent datasets from soil-grown plants (Figure 38 and Figure 39). The development of complex PD increases at a linear rate up until the leaf is the fourth youngest on the plant and its cells are an average size of around 2000-3000μm^2, after which point the number of PD/cell plateaus with a maximum of ~40-50 complex PD/cell. However, the plate-grown plants exhibit higher PD/cell values than soil-grown plants, with anticlinal PD reaching a maximum value of about 40 PD/cell in plate-grown plants compared to 35 PD/cell in soil-grown (Figure 38 compared to Figure 57).

Periclinal PD also show very similar tends between plate-grown and soil-grown plants, with the number of PD/cell reaching its maximum value (>8/cell) when the leaves are the second oldest on the plant with cells of ~1500 μm^2, and then subsequently declining to <8/cell for the remainder of leaf development. There is an abrupt split in the data between points corresponding to Leaf 1 and points corresponding to leaf 2. This is likely to be due to the points for leaf 2 coming from a single leaf, as discussed above.

More broadly this high-throughput confocal data indicate that the overall patterns of complex PD development are not strictly determined by growth of the leaves, either in terms of temporal age, developmental age, or size, but do show clear trends over a population of plants. The data also show that complex PD development is not determined on a cell-by-cell basis, but is modified as a population on a leaf-by-leaf basis.

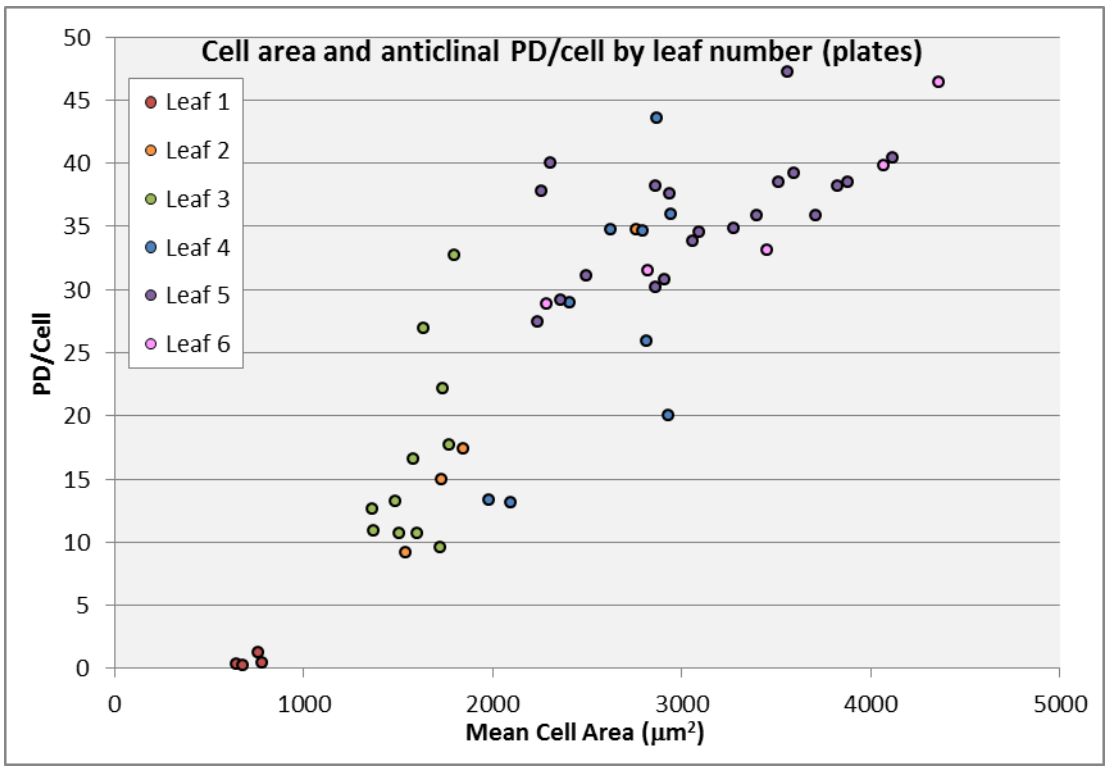

Figure 54: Graph showing the mean cell area and anticlinal (epidermal-epidermal) PD/cell of the six youngest leaves of *A. thaliana* at the 6-7 leaf stage grown on 0.5 MS agar plates. Each data point represents means from an imaged population of 30-200 cells, and is the raw output from the image analysis script.

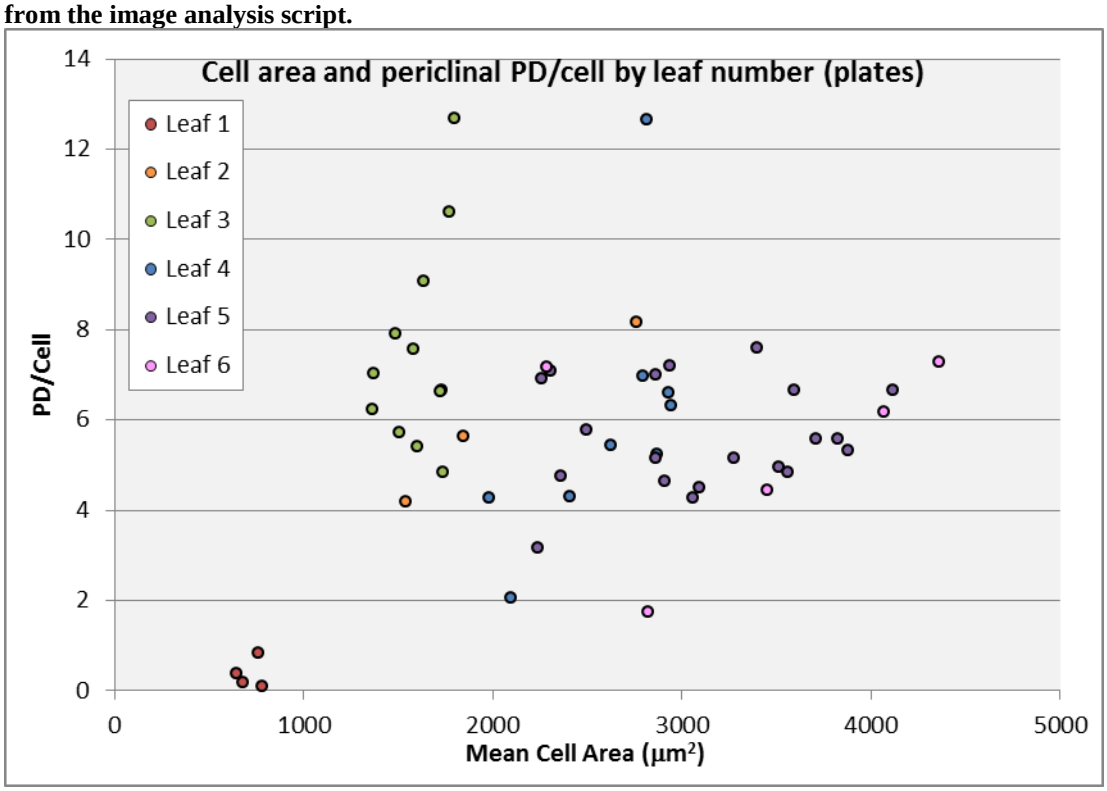

Figure 55: Graph showing the mean cell area and periclinal (epidermal – mesophyll) PD/cell of the six youngest leaves of *A. thaliana* at the 6-7 leaf stage grown on 0.5 MS agar plates. Each data point represents means from an imaged population of 30-200 cells, and is the raw output from the image analysis script.

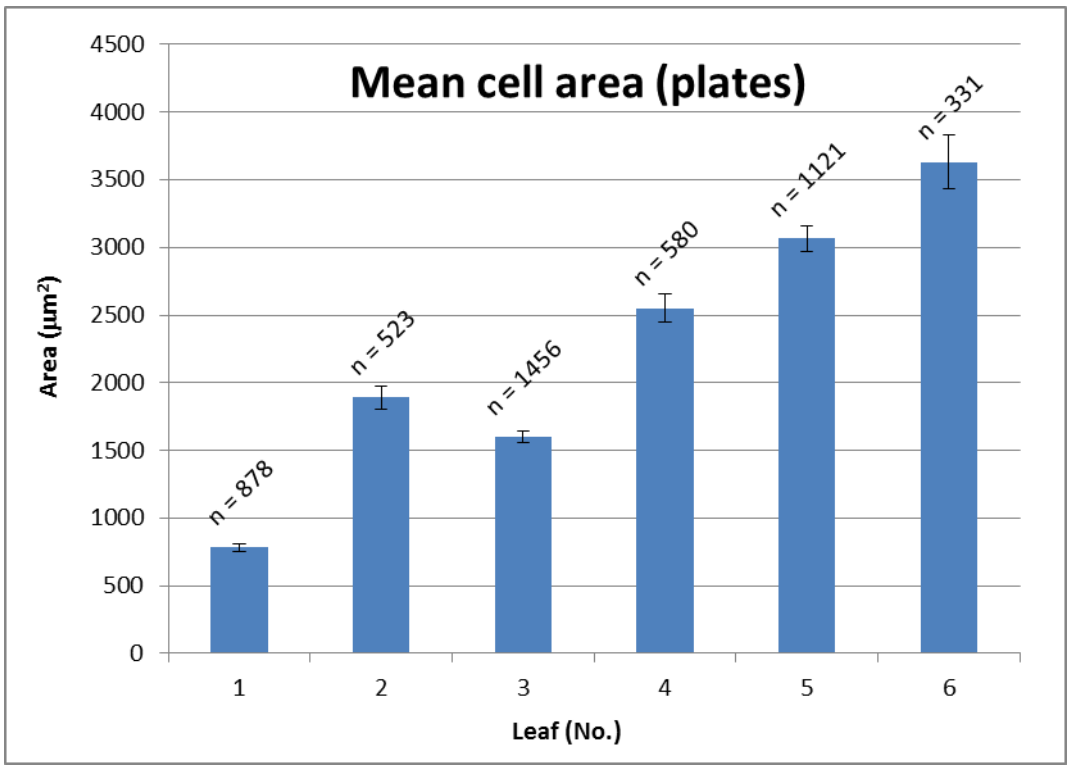

Figure 56: Mean cell area by leaf age for MP17-GFP plants grown on media plates. Bars are standard errors. Graph showing the average cell areas of all cells imaged for leaves of each age. To indicate the range of cell sizes observed, standard errors are given. N values are the total number of cells analysed,

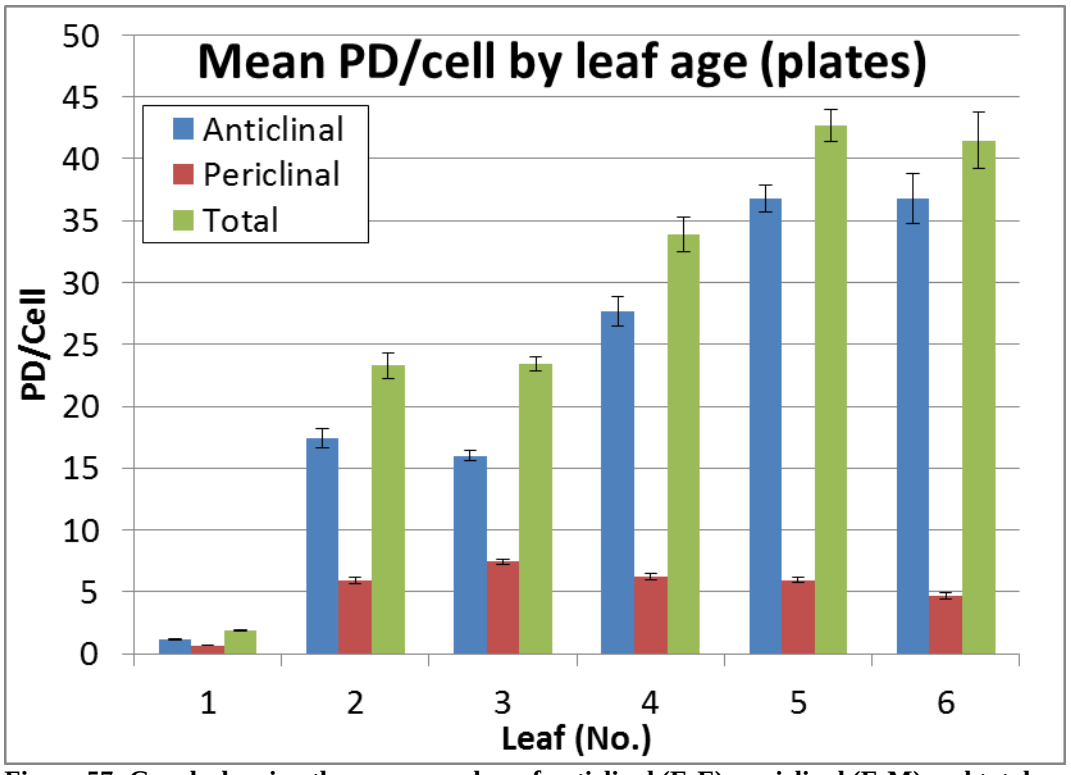

Figure 57: Graph showing the mean number of anticlinal (E-E), periclinal (E-M) and total complex PD per cell by leaf number. Bars show standard errors.

4.3.5 Spatial locations of complex PD within cells

High-throughput microscopy was eminently suitable for studying PD development in leaves at the level of organ and tissue development. However, to observe the details of complex PD development at the cellular level, traditional manual CLSM was required as it allows more precise imaging of the tissues of interest. Additionally, while automated image processing is an advantage for studying developmental trends, there are other patterns of PD development that automated imaging is unlikely to detect. Observation of the spatial location of anticlinal PD within cells showed that they are not inserted randomly around the cell periphery, and occurred in three discrete areas (Figure 58).

The first category was the 'corners' where three cells meet (Figure 58A). All leaves observed, including the very youngest sink leaves, showed MP-labelling at a subset of these corner interfaces, and these appeared to be maintained consistently throughout leaf growth. EM images of the cells show that each cell meets the others in a rounded corner, resulting in a thickened core of cell wall between them with an expanded middle lamella region (Figure 23D). While no PD have been imaged in these regions to my knowledge, it is expected that a PD passing through this region of the wall must be extended compared to PD in other epidermal walls. If these PD connect all three cells at the corner then they must be branched by necessity. These MP17-GFP labelled spots are likely to represent true PD rather than accumulations of MP within the apoplast, as there is no evidence of accumulation of MP at wall regions outside of PD.

The first PD to develop outside of these corners do so slightly in advance of the large-scale conversion of PD from simple to complex forms, and are inserted specifically at the lobe tips of jigsaw-shaped epidermal cells (Figure 58B). Later, when the cells are more expanded and the leaves are becoming sources, further PD appear generally around the periphery (Figure 58C). This can be confirmed using image analysis software. From samples in which the walls were stained with PI (Figure 58D), the cells can be mapped and measured (Figure 58E), and the cell bodies reduced to skeletons that accurately identify the lobed shape (Figure 58F and

G). Here, PD were defined as being at the lobe tip if they were at the end of one of these skeleton lines or in arcs within ten degrees to either side.

When the data is graphed by scaling the leaves by LPI, no pattern is clear (data not shown). As before, the natural variation in the onset and rate of complex of PD development will obscure developmental patterns. However, when imaged populations are arranged by their total number of complex PD, a clear trend for preferential insertion of complex PD at the lobe tips early in development is observed, prior to PD insertion generally around the periphery (Figure 59). This occurs even though the area of wall accounted for by the lobe tips is still less than the remaining area of wall. Over the course of development, complex PD continue to appear at the lobe tips while the complex PD at the corner interfaces are maintained. However, both of these categories of complex PD contribute progressively less to the total number of PD as the overall numbers increase.

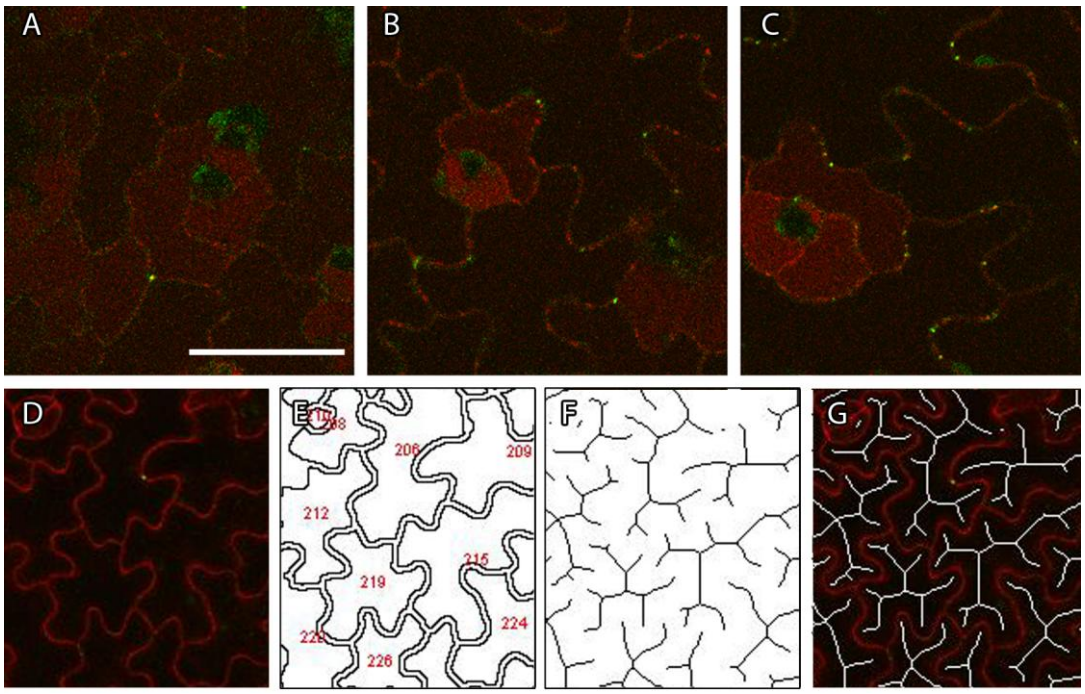

Figure 58: Plasmodesmata locations. A-C: images from MP17-GFP PDLP1-mRFP (scale bar in A = 25µm). A) Complex PD in young leaves at the corner interfaces between three cells, B) Complex PD in older leaves at the lobe tips of the epidermal cells and C) complex PD in yet older leaves at all areas of the wall. D-G image analysis. D: PI stained cell walls, E: cell map, F: cell skeletons, G: cells and skeletons overlaid. Scale bar = 25µm.

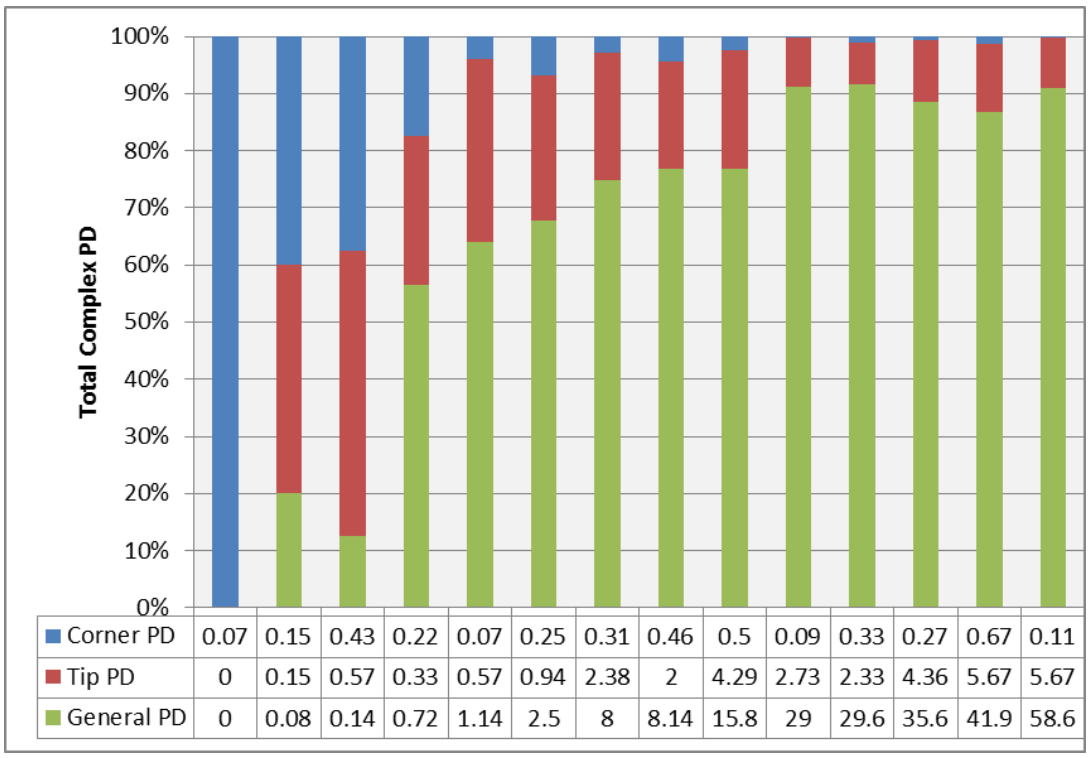

Corner PD	0.07	0.15	0.43	0.22	0.07	0.25	0.31	0.46	0.5	0.09	0.33	0.27	0.67	0.11
Tip PD	0	0.15	0.57	0.33	0.57	0.94	2.38	2	4.29	2.73	2.33	4.36	5.67	5.67
General PD	0	0.08	0.14	0.72	1.14	2.5	8	8.14	15.8	29	29.6	35.6	41.9	58.6

Figure 59: Graph showing the percentage of PD found at the corners (blue), the tips (red), or generally around the periphery (green) in apical regions of leaves of increasing age. Each bar represents data from a section of a different leaf, sorted by average numbers of PD/cell.

4.3.6 Complex PD at anisocytic complexes

The lower leaf epidermis is perforated with stomata for gas exchange. In *A. thaliana*, many of these are in anisocytic complexes, which result from progressive spiral divisions of a meristemoid initial cell, resulting in each pair of guard cells being surrounded by three monoclonal cells of increasing size (Figure 60A)(Nadeau and Sack, 2002). This pattern helps ensure that stomata are always one cell apart to maximise the efficiency of gas exchange, and to ensure guard cells have pavement cell neighbours for ion exchange.

Mature guard cells have no functional PD; these are degraded during development. However, the other cells in the anisocytic complex develop complex PD at a faster rate and to a higher density than other pavement cells (Figure 60B, Figure 61) The number of MP17-GFP tagged PD per unit cell wall between members of anisocytic complexes is generally double that found in interfaces between pavement cells. This suggests that cells associated with the stomata may specifically restrict communication with surrounding cells.

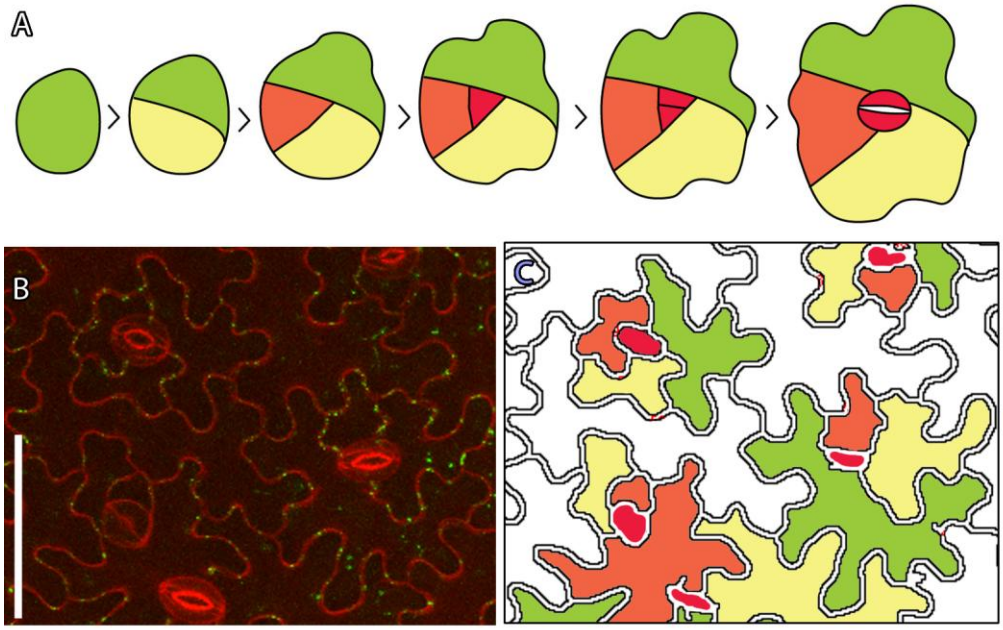

Figure 60: A: Illustration of the production of guard cells (red) in an anisocytic complex formed by progressive divisions of a meristemoid. B: Epidermis in a maturing MP17-GFP-expressing leaf, with walls stained red with PI, showing high numbers of complex PD at anisocytic complexes. Scale bar = 50µm. C: Illustration of cells in B, with anisocytic complex cells coloured as in A and pavement cells white.

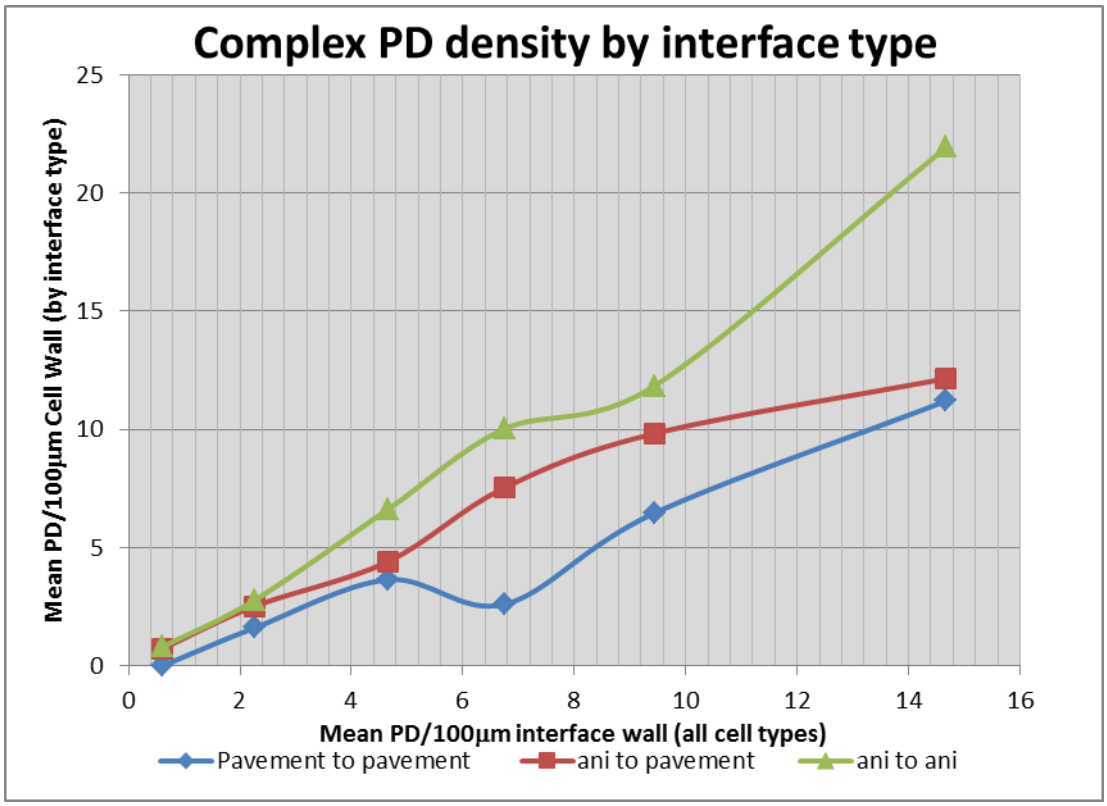

Figure 61: Graph showing the average PD/100µm in three types of interface: walls between cells of an anicytotic complex (green), walls between anicytocic complex cells and pavement cells (red) and walls between pavement cells(blue). Each vertical group of three measurements is from a separate leaf.

4.4 Discussion

While we know from studying individual plants that the onset and rates of complex PD development are not strictly determined by growth, either in terms of age, development or size, high throughput technology allows us to see that when leaves and cells are surveyed in a broader scale, patterns do emerge. The epidermal cells of *A. thaliana* show two clear patterns of PD development: one for the anticlinal walls, connecting epidermal cells in the L1 layer; and one for the periclinal walls connecting epidermal cells to the spongy mesophyll. Anticlinal development of complex PD continues for over three plastochrons, rather than one or two for periclinal PD, numbers of PD reaching a much higher overall density.

The difference between PD in the anticlinal and periclinal walls lies in the origin of the PD. Anticlinal cell divisions in both the epidermal and mesophyll layers are common, whereas periclinal divisions resulting in an L2 cell being produced from an L1 cell (or vice versa) are rare. The lack of cytokinesis between these layers means that very few of the PD connecting the mesophyll and the epidermis are primary in origin, and hence the vast majority of the periclinal PD counted in this study data must therefore be secondary PD, i.e.: inserted *de novo* across an existing cell wall. In contrast, many more PD in the anticlinal interfaces will be primary in origin due to the frequent cell division in this layer early in leaf development.

Interface dependent numbers of PD are also seen in the root, which is likewise composed of cell files produced by anticlinal divisions, with restricted periclinal divisions (Zhu et al., 1998), and in the vasculature, with companion cells in some species forming different numbers of PD with their associated sieve element compared to surrounding cells (Ding et al., 1988).

4.4.1 Complex PD and epidermal cell morphogenesis

The distribution of complex PD in the anticlinal walls of epidermal cells indicates an insertion of complex PD at the lobe tips of epidermal cells prior to insertion at other areas of the cell wall.

Notably, the pattern of PD development in epidermal cells correlates with current models of epidermal cell morphogenesis. *A. thaliana* epidermal cells develop their characteristic, intercalating 'jigsaw' shape by co-ordination of the cytoskeleton to control localised wall thickening (Panteris and Galatis, 2005). Cortical microtubules (MT) form bundles down the anticlinal walls of developing epidermal cells, which meet with radial microtubule arrays at the periclinal wall towards the surface. The wall around each MT bundle then becomes thickened, creating areas where cell wall expansion is restricted. As the epidermal cells expand, the differential growth between the thickened and non-thickened areas of wall causes the lobed shape to develop (Figure 62).

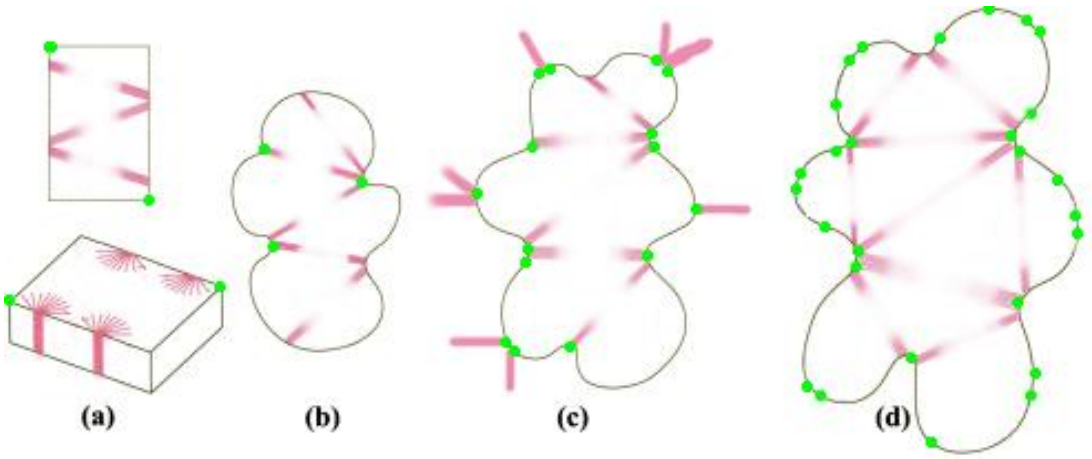

Figure 62: Model of epidermal cell development adapted to show PD distribution as an epidermal cell develops from an unexpanded immature cell (a) to fully expanded mature cell (d); microtubule bundles shown in pink, complex PD shown in green. Microtubule bundles form along the anticlinal walls of unexpanded epidermal cells (a) shows the same cell from surface view (top), and side-view (bottom)). In these young cells complex PD are limited to corner interfaces where three cells meet. As cells expand, the thickenings around the microtubule bundles cause localised areas of restricted growth, allowing the lobed shape to develop (b) and (c). In these cells, complex PD develop at the lobe tips where expansion is minimal. In more mature cells, where expansion is slow, complex PD begin to develop around the entire cell periphery. (Figure adapted from Panteris and Gelatis, 2005).

The radial arrays of MTs along the periclinal walls that promote the arc-shaped lobes are assisted by the development of patches of filamentous actin in the lobe tips, although the importance of these in determining the final cell shape is debated (Fu et al., 2002; Fu et al., 2005; Panteris and Galatis, 2005). Growth is co-ordinated so that the lobes of adjacent cells interdigitate, with no spaces between cells. This could suggest two possible reasons for preferential PD development at these regions. The first is that conversion of PD occurs in areas where wall expansion is limited. This may be due to PD branching only being initiated when cell wall expansion drops below a certain threshold level. Equally, it has been postulated that secondary PD may act as 'rivets' (Roberts et al., 2001), and therefore these complex PD may be involved in development of the cell shape. However, this possibility seems unlikely and, in the case of *Arabidopsis* at least, lobes appear prior to the appearance of complex PD.

Also relevant is the mechanical stress that the cells experience. That the lobe tips are sites of restricted expansion is just one of several hotly-debated theories to explain epidermal morphogenesis. Other models allow for expansion at the lobe tips and consider the epidermis as part of a flat sheet of turgid cells pulling away from one another. In this way, much of the mechanical stress across the leaf will be felt at the lobe tip due to the way that the cells fit together. It is also been established that stretching may promote complex PD development and that PD branches are inserted in the direction of wall expansion (Faulkner et al., 2008).

The idea that mechanical forces are involved in PD development is attractive because mechanical forces have a major influence on overall leaf development. That plants can sense and respond to forces is most obviously illustrated macroscopically by the phenomenon of thigmonasty, but stress and strain more subtly influence all aspects of development in the conversion of gene expression into 3D shapes (Boudaoud, 2010). At the cell level, growth itself is induced by turgor pressure acting on the walls, which influences not only the rates of expansion but also shape: microtubules orientate in response to stress, and the arrangement of microtubules in turn influences how cellulose microfibrils are laid down (Boudaoud, 2010). Modelling analyses suggest that many elements of morphogenesis are not directly programmed by genes

per se, but act as guidelines that are interpreted through the constraints of growth and mechanical restraints (Boudaoud, 2010; Prusinkiewicz and de Reuille, 2010) allowing individual organs to be tailored to the plant's needs. A good example of this is the development of the reticulate vasculature seen in the leaves of many species, which seems largely determined by mechanics rather than programmed directly. Although auxin has been shown to have significant effects on vein formation in leaves, models of vein differentiation based on auxin canalisation generally do not produce reticulate, looped networks unless apparently unrealistic assumptions and modifications are made (Laguna, et al., 2008). Models where auxin signalling provides the germs of procambium from which the formation of an interconnecting vein network proceeds as dictated by the mechanical stresses present in the mesophyll produce reticulate vein networks similar to those observed in leaves (Bohn et al., 2002; Corson et al., 2009, Laguna et al., 2008). The vein networks of individual leaves of the same species will have a similar pattern, but will be individually unique, suggesting a process of self-organisation (Bohn et al., 2002). If PD were also able to respond to mechanical forces, this would allow PD to develop in co-ordination with other mechanically-determined aspects of leaf development and permit some elements of the flexibility of PD development observed in different plants.

This results in two contradictory hypotheses: that restriction of wall stretching at tips promotes PD complexity, or conversely that enhanced wall stretching at the tips promotes PD development. The latter is more likely, as we know that wall stretching can indeed promote PD development (Faulkner et al., 2008).

4.4.2 Stomatal development and complex PD

I observed that the anisocytic complexes around stomata develop complex PD at a higher rate and to a higher overall density than other leaf cell types. The evidence suggests that these cells specifically develop complex PD in order to promote correct patterning and development of the stomatal complex. Stomatal guard cells themselves are one of few plant cell types to be symplasmically isolated. However, before they mature developing guard cells are symplasmically connected to one another, and to all surrounding cells, and so are able to exchange positional

information and developmental signals with their neighbours. It is only once the guard cells are developmentally specified that they occlude their PD (Willmer and Sexton, 1979)

That anisocytic cells develop complex PD in order to control tissue patterning is suggested by disrupted stomatal patterning in plants mutant for the glucan synthase gene *CHORUS* (Guseman et al., 2010). *chorus* mutant lines accumulate significantly less callose at PD, and therefore have increased SELs that allow exchange of molecules as large as 3xGFP. Among other growth effects, these lines exhibit increased production and division of meristemoids resulting in ~10% of stomata developing in contact with another, compared to <1% in the WT. Upregulation of movement causes aberrant patterning in these mutants, strongly suggesting that the patterns of complex PD deposition I see during WT plant development are important for correct stomatal development.

The fact that the rate of complex PD development in anisocytic complexes is increased with respect to other epidermal cells makes sense in the context of when these cell types mature. Stomatal development, including the division of meristemoids and the development of guard cells, occurs as series of basipetal waves during leaf development, and these waves begin significantly in advance of other leaf maturity events as shown by the presence of stomata in relatively young tissues (Nadeau and Sack, 2002). Hence the anisocytic cells may mature early and therefore develop complex PD faster than surrounding cells.

That anisocytic complex cells develop complex PD to a higher density compared to other cell types is more challenging to explain. One possibility is related to function. The anisocytic complex cells are essential to stomatal function as guard cells undergo ion exchange with their neighbours in order to control their turgor (Nadeau and Sack, 2002), and increased PD contacts may be necessary to co-ordinate this.

4.4.3 Final words

This chapter achieved the overall aim of studying PD development at both a detailed and a broad scale, from the level of cells to organs. The overall picture of PD development during leaf maturation indicates that there are 'layers' of input that govern how a cell's programme of PD development proceeds, just as a cell has several classes of identity. For example, the cells of an anisocytic complex in a young leaf are also epidermal cells, and also sink tissue cells and also leaf cells. All of these identities will influence plasmodesmatal development in different ways. As an epidermal cell, this hypothetical cell will follow a layer-specific program of PD development common to all epidermal cells, resulting in development of complex PD and pitfields on the E-M interface, followed by complex PD on the E-E interface, while no PD develop on the exterior wall. The PD on anticlinal and periclinal interfaces will proceed at different rates influenced in part by stresses and stretching in the walls and in the neighbouring cells, and by the overall growth rate of the leaf. As an anisocytic complex cell, this cell will experience role-specific regulation of that PD development program, resulting in accelerated development of complex PD on interfaces with other anisocytic cells, mildly accelerated development with neighbouring pavement cells and occlusion of PD on the interface shared with the guard cell. As a cell of *x*-location with respect to veins, the midrib, symplasmic domains and boundaries, the cell may be influenced by PD-development programs at the level of cell groups to control flux through the leaf.

Additionally, this work illustrates the possibilities for study of PD development using high-throughput approaches, and these will be explored further in Chapter 7. With suitable hardware and software, PD can now be studied at a much broader scale than was possible previously, allowing observation of trends that would be obscured by natural variation in smaller samples. That said, automated imaging methods were not suitable for identifying patterns of development at the cellular level, which was instead performed using manual microscopy and imaging. Despite massive advances in technology over the past few decades, the human eye remains by far the most valuable tool in modern microscopy.

4.5 Acknowledgements and thanks

The high-throughput work in this chapter was performed in collaboration with Silke Robatzek and her group members from The Sainsbury Laboratory, Norwich. Martina Beck assisted with experimental design, imaging and grew the plate-grown plants used for the study. Ji Zhou designed, wrote and optimised the image analysis scripts.

5 Chapter 5: Dynamic Views of Plasmodesmatal Development

5.1 Introduction

The work presented in Chapter 4 followed PD development by examining leaves of different ages, allowing me to piece together a timeline of when and where complex PD develop in leaves. The work in this chapter aimed to go a step further and observe and observe PD development in real time.

The ideal conditions to image development are those that represent the true physiological state as closely as possible. Some systems have been developed for imaging attached leaves *in situ*, usually using large-leaved plants with long, flexible stems and petioles such as the fava bean *Vicia fava* (Knoblauch and van Bel, 1998) and the sunflower *Helianthus annuus* (Endo and Omasa, 2007). Imaging *A. thaliana* leaves *in situ* is more technically challenging, and the few published methods are restricted to specific circumstances and relatively low resolutions (Sawchuk et al., 2007). To image PD development in attached leaves makes for logistical difficulties due to the small size of the leaves (2 mm-8 mm), and their proximity to the stem, SAM and other tissues in the rosette. The natural curvature of the leaves, which is enhanced when leaves are grown on solid medium as in published *in situ* methods, is also problematic. Repetitive, high-resolution imaging of specific areas is difficult without holding the leaves flat using a coverslip or an adhesive, and repeated removal and mounting can cause extensive damage to the delicate leaf tissues. As I wished to continue my experiments using *A. thaliana*, I therefore had to consider alternative options to *in situ* imaging.

The most promising strategy was to use an imaging chamber system. Such chambers allow specimens to be maintained and imaged repeatedly, and have been used throughout biology for studying developmental processes. They allow groups of cells to be easily monitored over relatively extended time periods, without the stress and damage to tissues that would result from repeated transfer between growth conditions and imaging conditions.

Chambers come in a plethora of designs, but are generally based on a ‘simple’ chamber modified from a typical coverslip and a microscope slide (Dailey et al., 2012). An O-ring or other spacer creates a gap between the slide and the coverslip in which cells or tissues can be maintained in medium. The assembled chambers are then sealed with a suitable adhesive to hold the coverslip on the slide and prevent contamination, leakage or evaporation of the medium. Simple chambers are easy to construct and can be made to suit most tissue types and sample sizes, but with this simplicity comes restrictions. The sealed environment within the chamber not only prevents access to or manipulation of the tissues during the experiment, it also prevents media from circulating or being replaced, allowing chemical and gas gradients to build up around the tissue.

A range of increasingly sophisticated imaging chambers are available commercially, many of which are designed to counteract the restrictions of simple imaging chambers (Dailey et al., 2012). Some allow control of experimental parameters, such a temperature control, and access for adding reagents. Also available are perfusion chambers that incorporate a pump to allow a medium to flow through the chamber. Most of these are designed for use with cultured cells, but some have been used successfully with whole plant tissues, for example (Schwarzlaender et al., 2008).

A. thaliana has been the subject of many imaging chamber experiments, although the leaves have seldom been studied. For almost all chamber types, obtaining good images from leaves requires them to be detached from the plant. This introduces restrictions in what can be studied, and even detached leaves will continue to expand in length and thickness and therefore move and curve within the chamber, making imaging difficult. For this reason most chamber studies of leaves have used relatively short time periods (for example, Schwarzlaender et al., 2008). However, other tissues have been frequently used with success. Roots are particularly suitable for imaging in chambers as they are thin, transparent, and grow in well-defined patterns in a single dimension. *A. thaliana* plants are small enough to be grown on slides for extended periods so that roots can be observed while still attached to the plant. With an appropriate set-up, roots can be grown and imaged at near physiological conditions (Maizel et al., 2011). Simpler coverslip-and-slide chambers have also provided

excellent images and insights into root development (De Rybel, et al., 2010). Hypocotyls share many of the qualities that make roots suitable for chamber imaging, and have also been successfully imaged in chambers. Again, some groups have used complex, custom-made setups such as that used by Sauret-Güeto et al. (2011), which was a perfusion chamber with a mesh support to hold the hypocotyl close to a coverslip, but simpler chambers are also successful. Work by Chan et al. (2007) used a chamber system made from a coverslip and a gas permeable membrane held in a supporting plastic frame to conduct a detailed study of microtubule movements during wall expansion. This chamber system is as straightforward to construct and maintain as a typical simple imaging chamber but allows for some degree of gas exchange within the chamber itself. Gas exchange is obviously an important consideration when imaging leaves in closed conditions and so I decided to adapt this simple membrane chamber for the starting point of my work to study the dynamics of PD development.

5.1.1 Biological studies using detached leaves

In *A. thaliana*, the size and position of the leaves of interest on the plant meant that attached leaves could not be put into chambers. Work with detached leaves seemed a viable option as they may be successfully maintained for extended periods (Reis et al., 2000, Yarwood, 1946), and detached leaves have been used successfully in imaging chambers (Schwarzlaender et al., 2008).

Many aspects of the biology of detached leaves have been well studied, particularly in the early twentieth century when there was much interest in leaf cuttings from both a scientific and horticultural perspective. Yarwood (1946) provides an excellent review of the early literature regarding leaf detachment and culture, summarising many papers that are not available in English. Early researchers established that while detached leaves die swiftly if allowed to wilt, they can often be maintained for extensive periods provided they are kept hydrated, sometimes longer than they would naturally persist on the plant. Most species may be maintained for at least three weeks, although the full range runs from about two weeks in plants such as lettuce and corn, to several months in plants such as apple and mint, and many years in the case of a few plants, such as ivy (reviewed in Yarwood, 1946). In many cases, the

cause of death of a detached leaf kept in culture is often fungal or bacterial infection (Yarwood, 1946).

Detached leaves in culture are not simply maintained, in the sense that death is being postponed, but are living independently of the parent plant. While translocation from the leaf is halted, most cellular process including respiration, protein synthesis and photosynthesis continue (Yarwood, 1946). Many leaves continue to grow in length and thickness, sometimes at comparable rates to attached leaves for a limited period, with some species showing a size increase of over 60%. In some cases, leaves which have attained their full size on the plant resume growth once detached. This observed growth is mostly due to continued cell expansion rather than division (Yarwood, 1946). Supplying leaves with sucrose solutions (1-20%) can cause increased growth and prolonged life (Böhm, 1877, reviewed in Yarwood, C. E. 1946). Work by Nadson established that detached leaves from a range of species can metabolise starch from substances containing alcohol groups, including dextrose, lactose, glycerin and dextrin (reviewed in Yarwood, 1946). Associated with detachment, however, are changes to certain aspects of leaf biology. Cut and sliced tissues undergo a range of developmental phenomena, including an expansion in the ER network and changes in the properties of ribosomes (Van Steveninck, 1975) and the metabolism and uptake of organic solutes (Sakr et al., 1993).

With this in mind, I expected that PD development would proceed in detached leaves, but that the rates and patterns might be modified in response to detachment and the additional stresses imposed by the imaging chamber. While this proved to be correct, detached leaves actually proved to be an effective system in which to study PD development, with many of the patterns described in Chapter 4 retained, but with certain aspects of the variability in timing reduced. The patterns observed not only reinforced many of the conclusions drawn in Chapter 4, but allowed some aspects of the development of cut leaves, and leaves in general, to be understood in a way that would not have been possible without the chamber.

5.1.2 Aims

- To develop an imaging chamber system to allow repeated imaging of *A. thaliana* laminal tissues, allowing observation of PD development in specific areas over relatively long time periods.

- To record the development of MP17-labelled complex PD in real time, taking into account of the stresses and restrictions of a closed chamber system.

- To use real-time imaging of PD development to complement the work in Chapter 4 to construct a timeline of PD development during the sink-source transition.

5.2 Results

5.2.1 Imaging Chambers allow PD development to be followed for over 48h

A chamber system adapted from Chan *et al* (2007) was developed using a standard coverslip and a section of breathable membrane, with a ring of double-sided adhesive tape forming a spacer between, all supported by a custom-made plastic frame (see Chapter 2 for full method). Larger versions were tried which could contain a whole seedling, but expansion and growth in the restricted area of the chamber inevitably caused imaged areas to move out of focus. A few different media were tried instead of water, including PBS, but all resulted in poorer imaging conditions or showed no improvement in tissue preservation. Flooding the chamber with water proved to be the most reliable method of maintaining leaves, as chambers with the lamina in air and the petiole covered in wet filter paper or gels resulted in wilting.

The chamber shown in Figure 63 allowed microscopic observation of PD development in detached leaves, giving images of a similar quality to fresh tissue mounted on slides with coverslips. Leaves could be maintained for as long as five days or more within the chamber, although many samples showed fluorophore bleaching, clustering of fluorescent proteins and other symptoms of cell necrosis (Frigault et al., 2009) after three days.

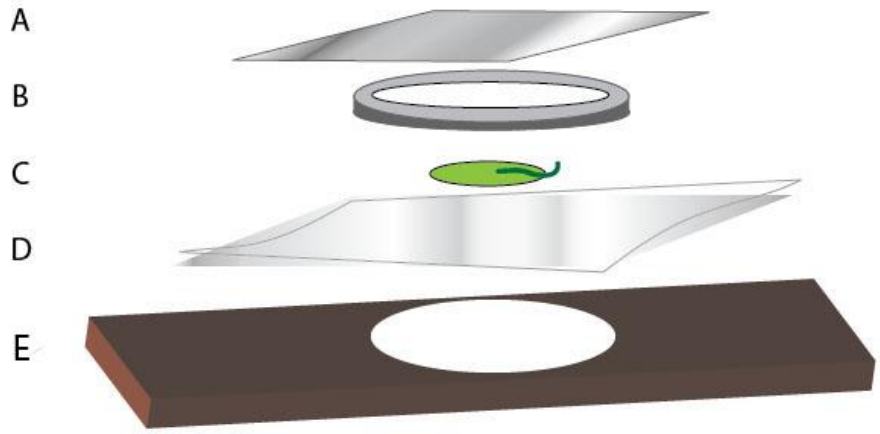

Figure 63: The constituent parts of a simple imaging chamber comprising of A: a standard coverslip through which the tissue can be imaged, B: a ring of double-sided adhesive to act as a sealant and a spacer, C: the leaf to be imaged in a droplet of medium, which is placed with its abaxial side to the coverslip and sits in the space in the centre of the ring of adhesive, D: a section of breathable membrane, E: a supporting plastic frame. These components are assembled in the order shown, and the coverslip and film sealed to the frame with adhesive tape.

Observations showed that complex PD formation and cell expansion continued after leaf detachment. Figure 64 shows an enlarged section of a typical image series from a PDLP1-mRFP x MP17-GFP leaf, showing that new complex MP17-GFP labelled PD continued to develop for up to 72h after detachment. PDLP1-mRFP often marked wall punctae but also, as discussed in Chapter 3, produced cytoplasmic background fluorescence. PDLP1-mRGP labelling therefore was not specific enough to show whether new secondary PD were being inserted, although new MP17-GFP labelled-PD were often seen to arise from areas heavily labelled with RFP, suggesting that many of the new complex PD developed from existing simple PD (Figure 64 arrows). However, this cytoplasmic RFP fluorescence was useful in that it highlighted the shape of the cells without any application of dyes which would have harmed the live tissue, and these plants were used in preference to plants expressing *35S::MP17-GFP* alone for most experiments. As only complex PD are being observed, 'PD' values given throughout this chapter refer to complex PD only.

Control experiments with free GFP linked to the same 35S promoter as used in the PDLP1-mRFPxMP17-GFP plants showed no obvious increase in fluorescence, indicating that the additional labelling was not due to increased abundance of the MP17-GFP protein caused by leaf detachment (data not shown).

5.2.2 Detachment accelerates PD development in laminal tissues

When the populations of MP17-GFP labelled PD were monitored in detail over time, I saw that not only were new complex PD being inserted after the leaves were detached, but that this happened at an accelerated rate. Figure 65 shows PD counts from monitored areas taken from leaves of 4.5-6 mm length. These had between 1 and 11 PD per cell at the time of detachment, when averaged over the total number of whole cells in the monitored region, which varied from 8 to 26 cells.

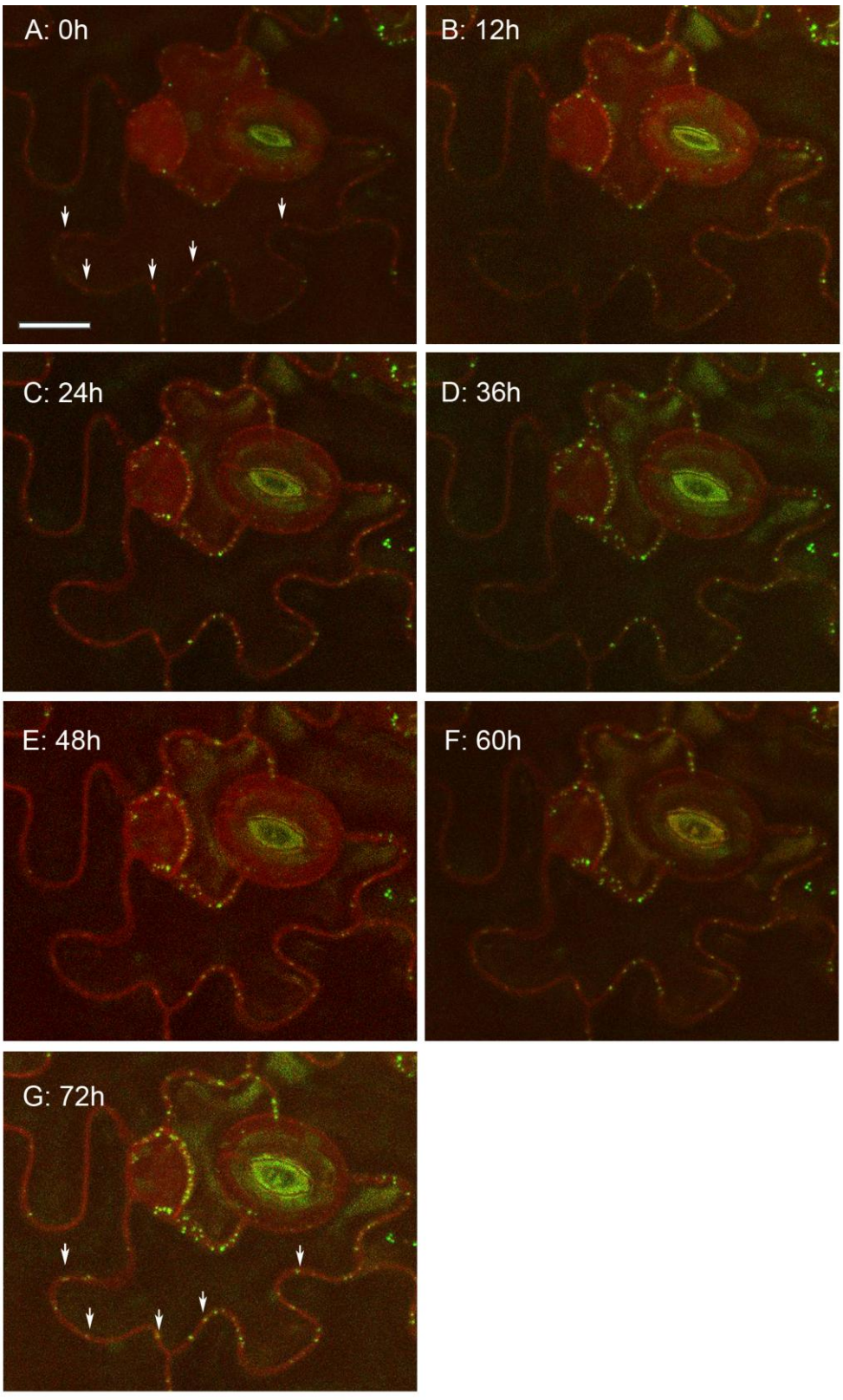

Figure 64: Area from the tip region of a 5 mm MP17-GFPxPDLP1-mRFP leaf detached and maintained in an imaging chamber and imaged every 12h. Each image is a maximum projection of the entire epidermal layer. Arrows show PD that have only PDCB1-mRFP labelling at 0h, and subsequently develop MP17-GFP labelling. Red=PDLP1-mRFP; green = MP17-GFP. Scale bar =10 µm.

PD counts showed that in all monitored areas the number of MP17-GFP labelled PD had doubled and sometimes tripled after 48h observation. In the youngest leaves, which had less that 3 PD per cell at 0h, the number of MP17-GFP-labelled PD often doubled within 24h. This is a rate of PD development much faster than suggested by the work shown in Chapter 4. After 36 h the number of PD appeared to decrease in some areas, although this was most likely due to photobleaching from prolonged imaging periods rather than the removal or fusion of PD. Ignoring the timepoints that showed decreased counts, PD in leaves maintained in chambers were appeared at an average rate of 0.18 PD per cell per hour.

The fact that all young leaves, including those with very few MP17-GFP labelled epidermal PD at the initial timepoint, were observed to develop PD at a faster rate and to a higher total density than *in situ* leaves of similar developmental stages suggested that some aspect of either the chamber or detachment was promoting PD development.

To confirm this, I imaged leaves of less than 1 mm in length and at the youngest stages of development at which they could be detached and manipulated (see Figure 66). As expected, at 0 h these leaves had very few complex PD, with distinct MP17-GFP punctae only appearing at 'corner' interfaces (arrow), as described in Chapter 4. However, within 30 min, new MP-17 GFP-labelled PD could be observed in the mesophyll layer. PD insertion continued so that at 3 h post detachment, many mesophyll-mesophyll interfaces had densely packed MP17-GFP labelled PD, resembling more mature mesophyll cells. However, the location of the PD in the mesophyll layer, the close proximity of the PD in these small interfaces and the bleaching and autofluorescnece caused by repeated imaging prevented these PD from being counted accurately.

This result confirmed that some aspect of the chamber conditions stimulated PD insertion. It also showed that PD may develop complexity with unexpected speed, with new MP17-GFP appearing in under 1 h.

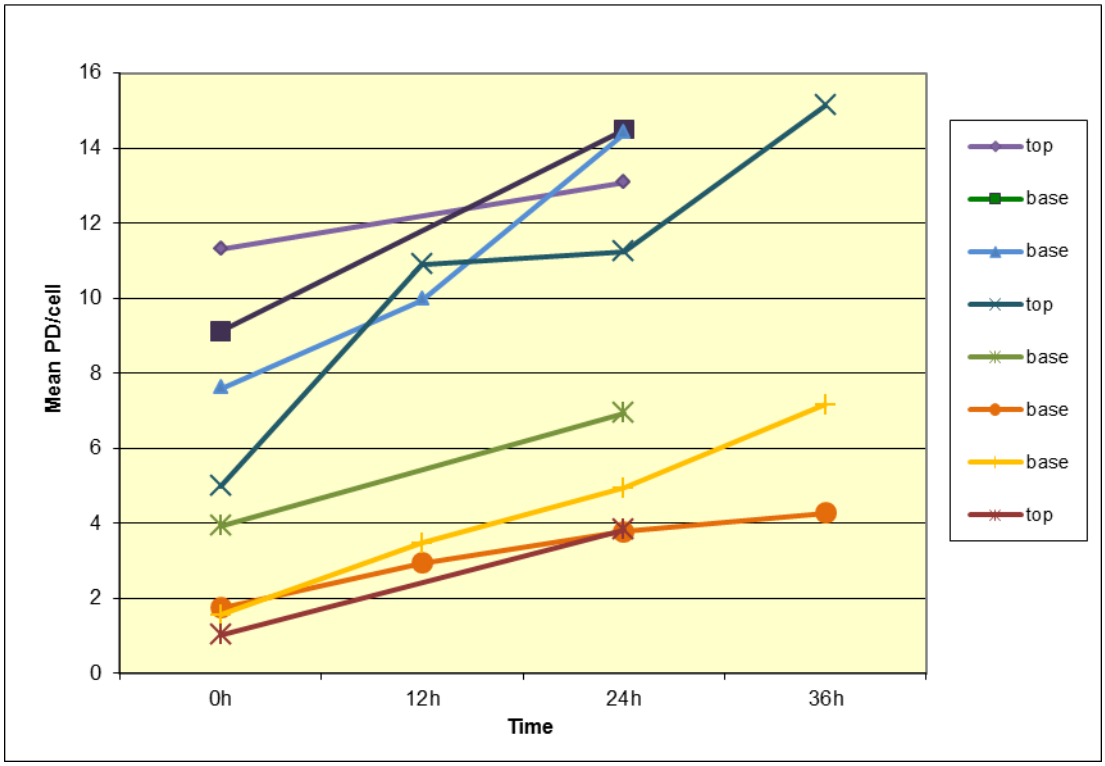

Figure 65: Graph showing number of MP17-GFP labelled PD in specific sections of monitored leaves of between (3-8 mm) maintained in chambers and observed at 12 h or 24 h intervals. Graph shows PD/cell values; counts are presented in Table 3. 'top' indicates the imaged area was near the leaf tip, ' base' signifies the images were taken at an area near the large hydathodes at the base of the leaf, so usually ¾ down the length of the leaf rather than at the very base of the leaf.

Table 3: PD counts from monitored areas in PDLP1-mRFPxMP17-GFP leaves maintained in chambers.

	Cell No.	0h	12h	24h	36h	48h
6mm leaf top	12	135.5	-	157	-	-
4.5mm leaf top	10	76	-	144	-	131
6mm leaf base	8	73	-	116	-	-
5mm leaf, top	10	50	109	112.5	151.5	149
5mm leaf, base	26	45.5	76.5	98.5	111	105
4.5mm leaf base	8	31.5	-	55.5	-	103.5
5mm leaf, base	16	25	55.5	79	114.5	135.5
4.5mm leaf base	15	15.5	-	57.5	-	95

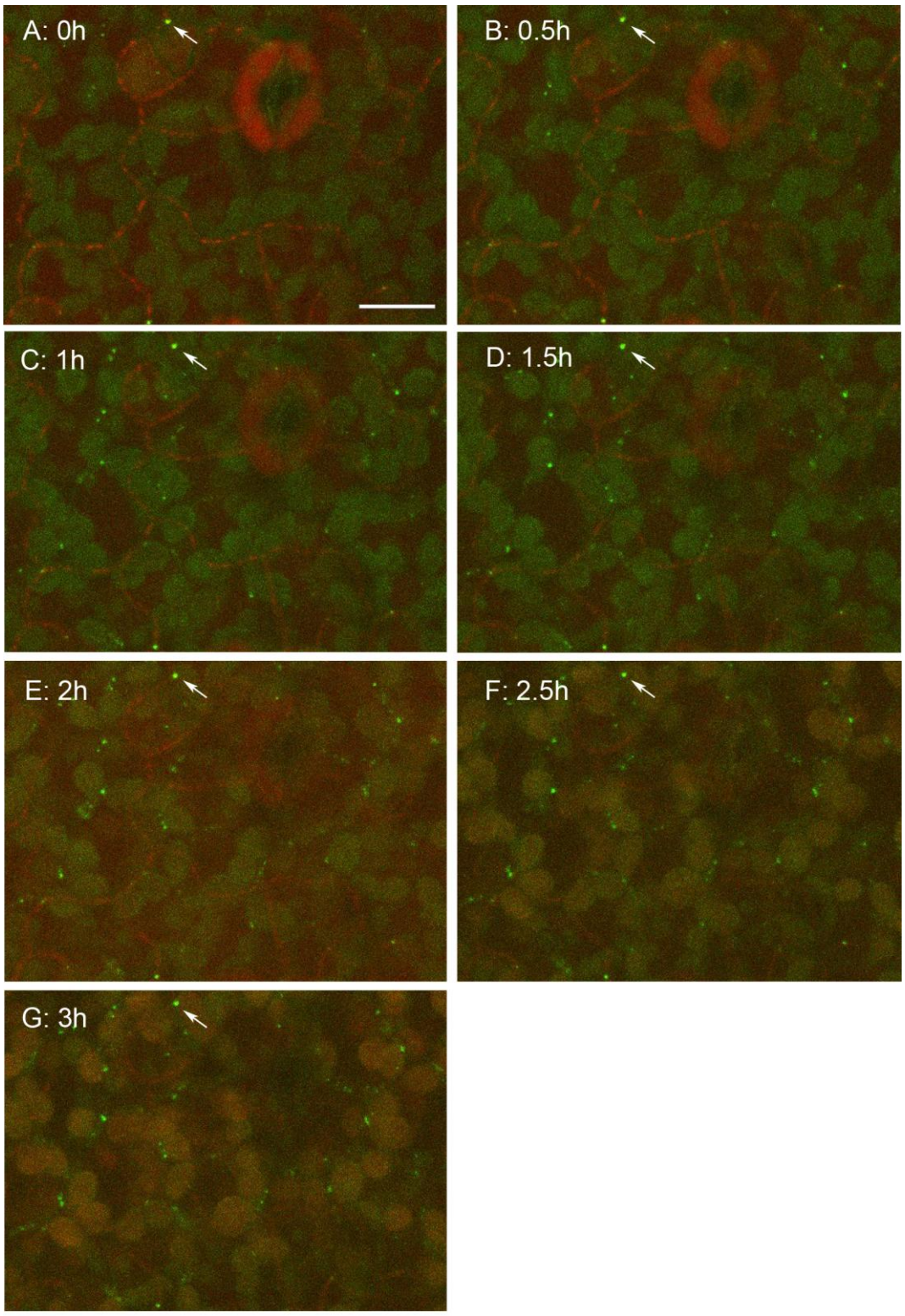

Figure 66: Images from a 1mm MP17-GFPxPDLP1-mRFP leaf detached and maintained in a chamber. Images are maximum projections of stacks taken at 30 min intervals. Most of the MP17-GFP labelled PD are in the mesophyll layer. Intense and frequent imaging caused mRFP to bleach, so the arrow points to an MP17-GFP labelled 'corner' PD present in all images for orientation purposes. Scale bar = 10 µm.

5.2.3 Patterns of PD development in detached leaves

When I examined the patterns of PD development in leaves maintained in chambers I saw that some of the patterns observed in *in situ* leaves in Chapter 4 were maintained while some were not.

The accelerated development of PD was seen to occur in both basal and tip regions of leaves after detachment (Figure 65,

Table 3) suggesting that if the transition of PD from simple to complex forms was occurring as a basipetal wave, it was doing so at a rate greater than that associated with the sink-source transition . Rather than the rate of insertion being dependant on the position within the leaf (i.e.: top or base), it seemed more dependent on the number of MP17-GFP labelled PD present in the tissue at the time of detachment. Figure 65 shows that areas in which there were relatively few PD (<4 PD/cell) had rate of insertion of 0.115 PD/hour, half that of areas which had >4 PD at 0h, which developed new MP17-GFP labelled PD at an average rate of 0.221 PD/h. This suggests that many of these new MP17-GFP labelled complex PD were developing from unlabelled simple PD that were already present, rather than from newly inserted secondary PD.

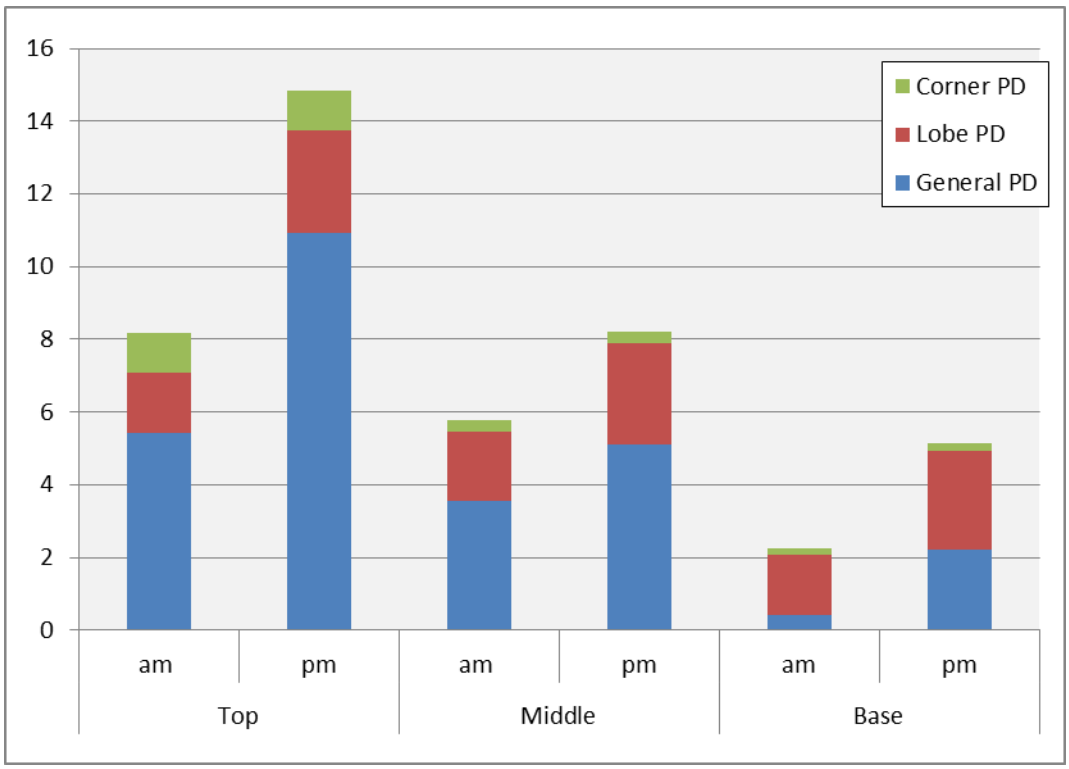

Figure 67: average PD/cell at cell corners, lobe tips or other areas of the cell perimeter (general) in populations of 8-10 cells sampled at the top, middle or base of a detached leaf in a chamber. Time interval was 6 h between measurements.

Furthermore, mapping the locations of complex PD as 'general' or 'lobe tip' as in Chapter 4 did not reveal a preference for insertion of complex PD at lobe tips (Figure 67). Cells also continued to expand after detachment, although the cell area and number of new PD were not strongly linked.

Mapping the interface types where complex PD developed suggested that, despite the fact that the PD were no longer preferentially inserted at lobe tips, PD were not being inserted randomly. Within a single cell, complex PD appeared at different frequencies in walls shared with different neighbours (Figure 68, A-C). Mapping these by interface type showed preferential development of complex PD at interfaces related to the stomatal anisocytic complexes (Figure 68 D), as had been suggested by my observations of attached leaves (see Chapter 4).

In all areas analysed, the total combined length of pavement-pavement interfaces is lower than other interface types. When I scaled for this by expressing counts as number of PD per µm of interface length I observed that, as shown in Chapter 4,

anisocytic-anisocytic interfaces contain the most PD at all timepoints, with an average of 0.120 PD/µm wall at 0 h, compared to 0.057 PD/µm in anisocytic-pavement interfaces and 0.023 PD/µm in pavement-pavement interfaces. Observations with the imaging chamber revealed that the rate of insertion of MP17-GFP labelled PD is also highest in anisocytic-anisocytic interfaces, with an average of 0.0056 PD inserted/µm of interface/ h compared to anisocytic-pavement interfaces at 0.0040 PD/µm/h, and pavement-pavement at 0.0022 PD/µm/h. This gave anisocytic-anisocytic interfaces an average of 0.323 PD per µm wall after 36 h in the chamber, compared to anisocytic-pavement interfaces at 0.201 PD/µm and pavement-pavement at 0.102 PD/µm.

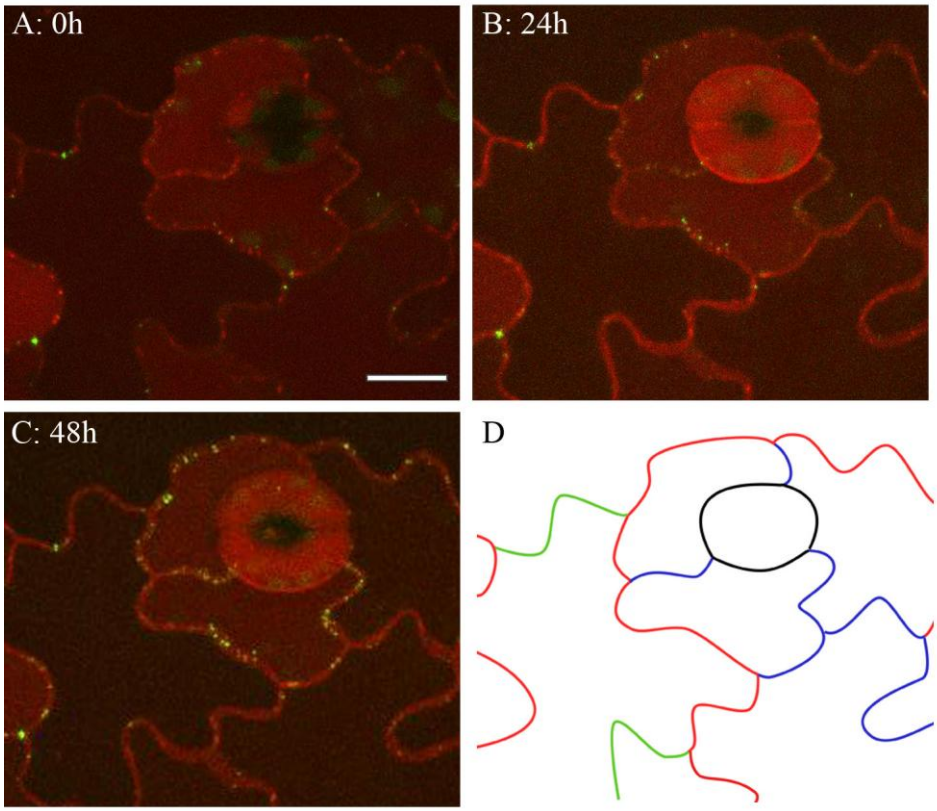

Figure 68: Anisocytic complex in an MP17-GFPxPDLP1-mRFP leaf imaged at 24 h intervals. D shows diagrammatic representation of interface types: Blue = interfaces between anisocytic cells, red = interfaces between anisocytic cells and pavement cells, green = interfaces between pavement cells, black = interfaces between anisocytic cells and guard cells. Scale bar: 10 µm.

Figure 69: Graphs showing data from expressed as PD/µm wall interface.

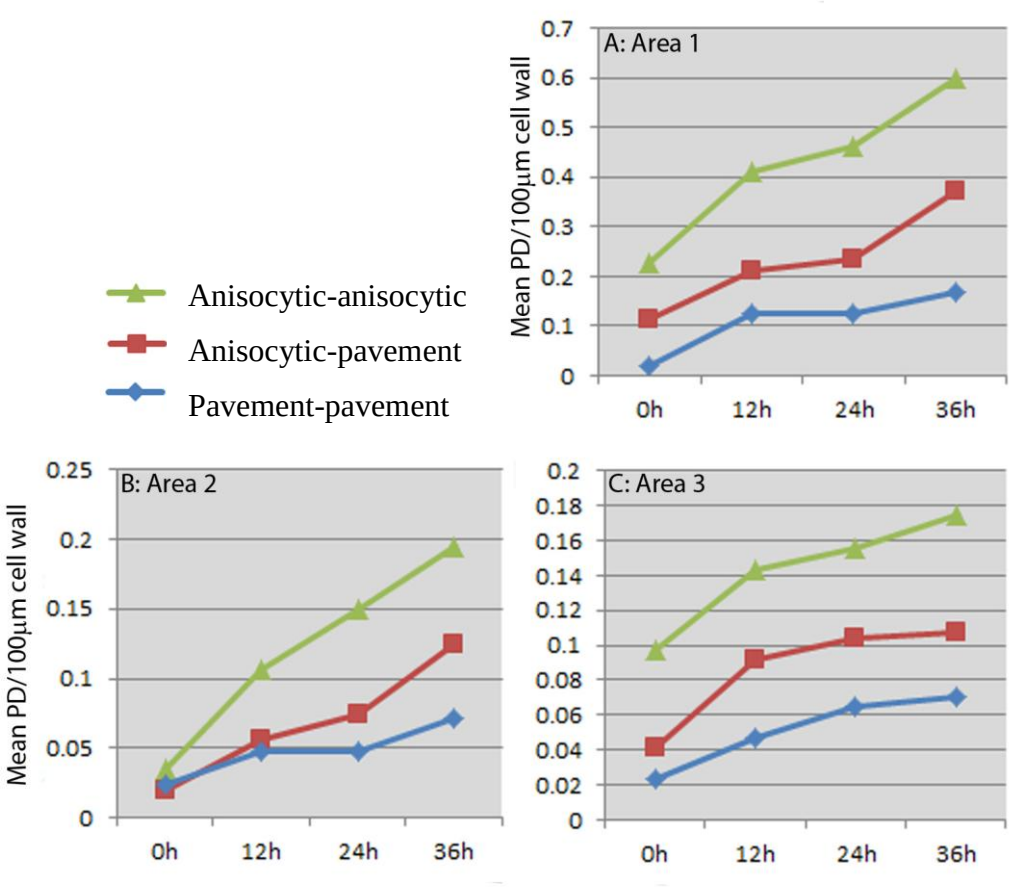

Table 4: Table showing the length epidermal interfaces of different types and the number of MP17-GFP labelled PD present at 12h time intervals. PD counts are average values from two independent manual counts. Area 1 is from a tip region, and areas 2 and 3 are from base regions of a 5 mm leaf.

	Interface length (µm)	PD at 0h	PD at 12h	PD at 24h	PD at 36h
Area 1					
Anisocytic-anisocytic	96.54	22	39.5	44.5	58
Anisocytic-pavement	80.65	9	17	19	30
Pavement-pavement	48.145	1	6	6	8
Area 2					
Anisocytic-anisocytic	113.005	4	12	17	22
Anisocytic-pavement	257.51	5	14.5	19	32
Pavement-pavement	42.24	1	2	2	3
Area 3					
Anisocytic-anisocytic	286.77	28	41	44.5	50
Anisocytic-pavement	241.35	10	22	25	26
Pavement-pavement	85.035	2	4	5.5	6

5.2.4 Accelerated PD development in detached leaves is accompanied by an accelerated sink-source transition.

The observation that leaves in chambers exhibit rapid development of MP17-GFP labelled PD similar to attached leaves undergoing the sink-source transition suggested that the sink-source transition itself might have been promoted by the detachment/chamber system. To test this, I used plants expressing GFP from the *AtSUC2* promoter, which expresses a sucrose-H^+ symporter in companion cells, and only becomes active in the minor veins following the transition to the source state (Truernit and Sauer 1995; Wright et al., 2003). The normal pattern of expression is shown in Figure 70, from *A. thaliana* plants in which GFP is expressed from the SUC2 promoter. To monitor the sink source transition in detached leaves, youngest leaves of *pSUC2::GFP* plants were mounted in water inside imaging chambers. At 0h, detached leaves showed strong GFP fluorescence in class I (midrib) and class II veins, and in a gradient from the veins into the surrounding leaf tissue (Figure 71A, showing a leaf the same age as Figure 70i). The diffuse pattern of GFP emanating from the major veins is characteristic of GFP unloading. (Wright et al., 2003). The absence of fluorescence in the lower order vein classes confirms that these leaves are full sinks. After 24 h the GFP fluorescence in the class I and II veins had become lighter and broken, presumably due to the cessation of import, while GFP fluorescence had become visible in class III veins and, at 48 h, in class IV veins, suggesting that the *pSUC2* promoter in these detached leaves had become active, and hence the leaf has converted from a sink to a source. At 36 h, the leaf displayed a *pSUC2::GFP* expression pattern resembling a mature source leaf (compare the detached leaf in Figure 71 A at 24h with the attached leaf 4 in Figure 70iv), while still only a few millimetres in length.

Together, the observed changes in detached leaves, both in terms of development of complex PD and *pSUC2* activation suggest that upon detachment, sink leaves spontaneously and precociously undergo a sink-source transition to resemble mature leaves.

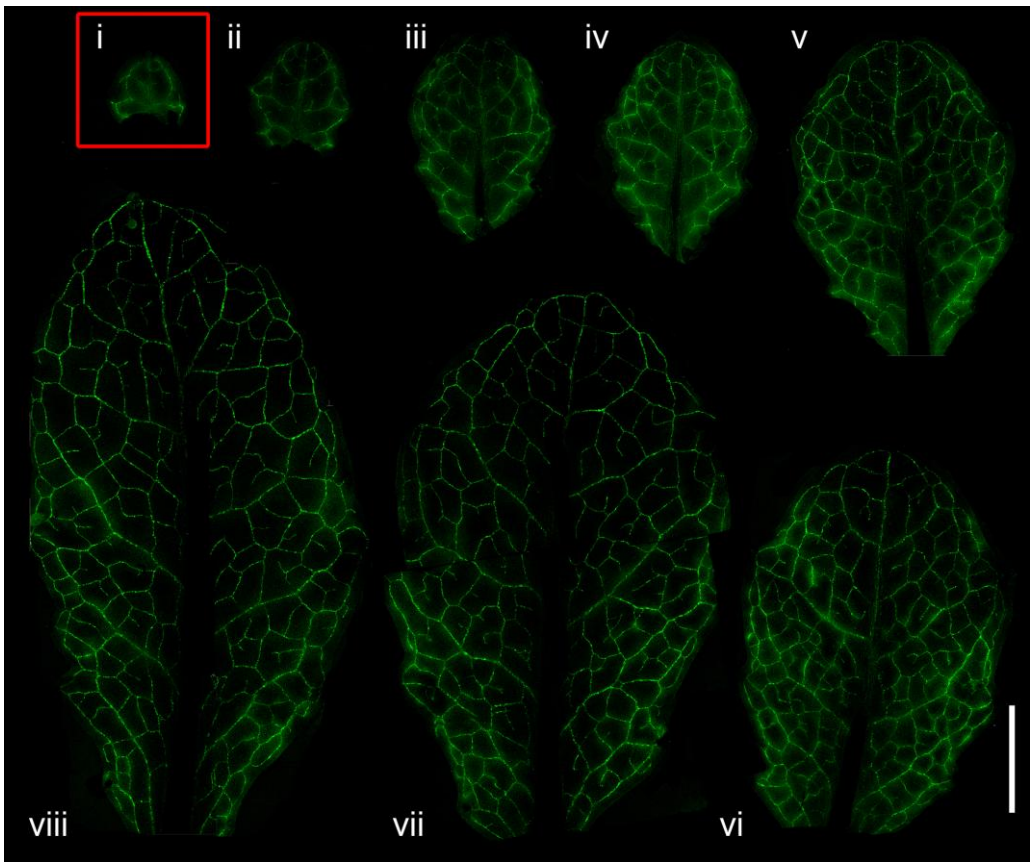

Figure 70: The youngest 8 leaves of a mature *pSUC2::GFP* plant, showing the normal progression of the sink source transition as marked by GFP expression. The leaves used for detachment experiments were leaf 1 (boxed). Scale bar = 2cm.

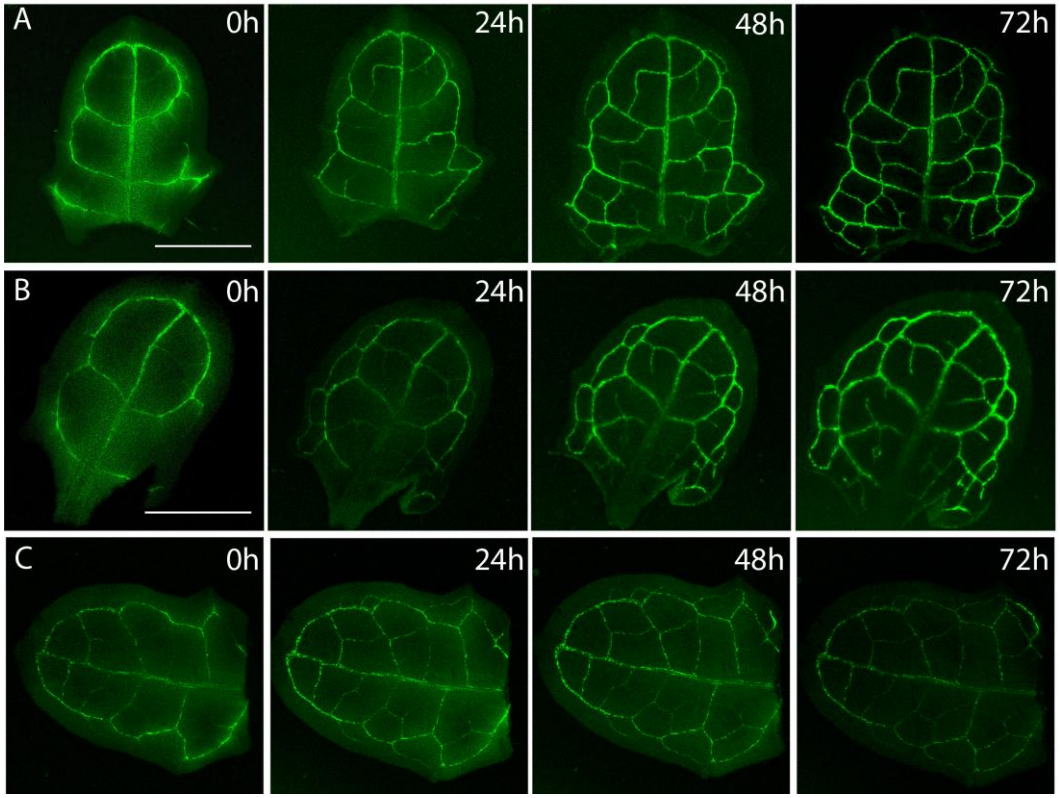

Figure 71: leaf 1 from *pSUC2::GFP* plants detached and maintained in chambers in either H_2O (A) or 1% sucrose (B), or in H_2O in the dark (C). Scale bar = 500 µm.

5.2.5 Detachment alone promotes the sink-source transition

Having established that some aspect of my imaging chamber experiments prompted leaves to develop traits of source leaves, with the associated conversion of PD from simple to complex forms, the next step was to examine whether this was a response to detachment or an artefact caused by the additional stresses of the imaging chamber. To test this leaves were detached from SD-grown *pAtSUC2::GFP A. thaliana* and maintained upright in slits cut into wet filter papers as in Reis et al., (2000) within Petri dishes. This method maintained the detached leaves in a hydrated state without flooding and with air circulation. Although the same plants could not be imaged over time, leaves which had been detached for ≥24h showed GFP fluorescence in the lower order veins as seen in the chamber experiments, showing that they had undergone a sink-source transition as in leaves maintained in chambers (Figure 72).

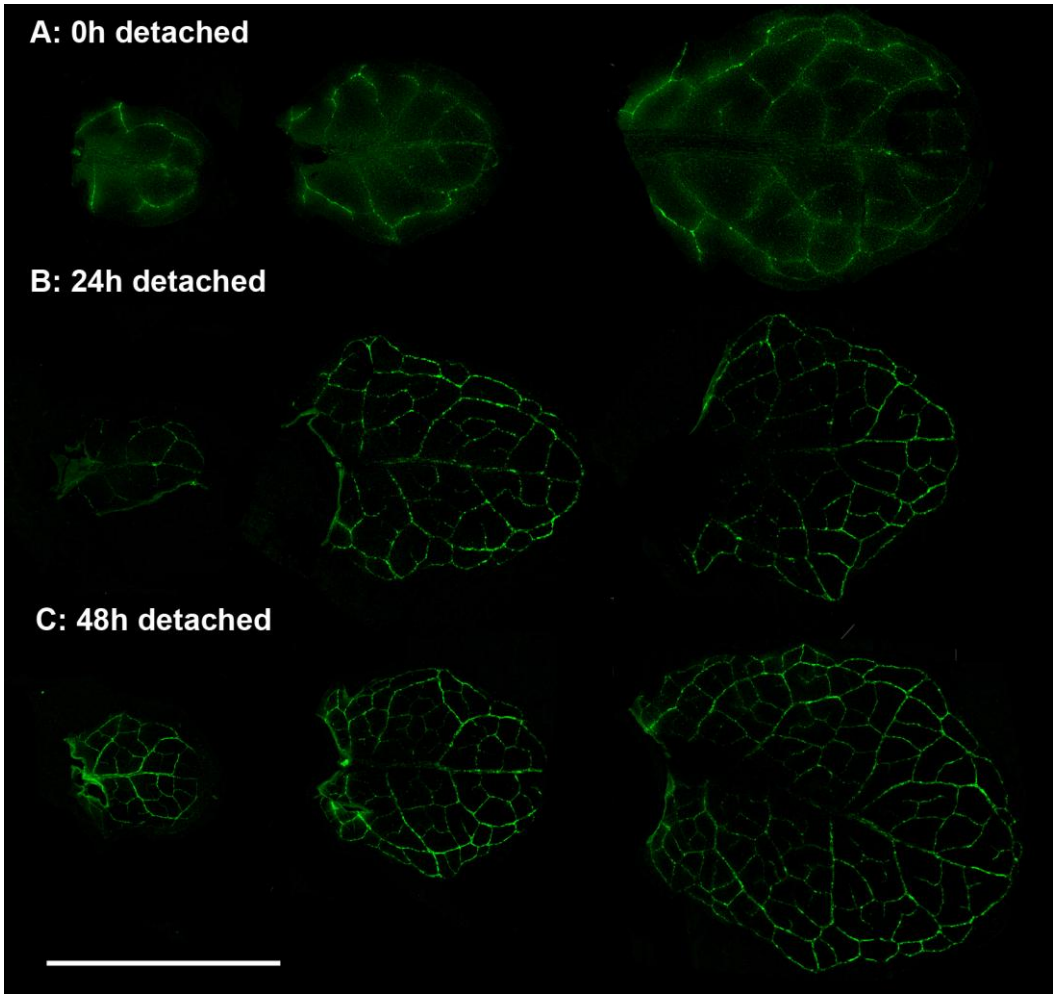

Figure 72: Leaves 1-3 (left to right) detached from pSUC2::GFPs plant and imaged (A) immediately, or maintained outside of chambers for 24 h (B) or 48 h (C). Scale bar = 2 cm.

5.2.6 Factors promoting the sink-source transition in response to detachment.

Upon detachment, sink leaves, that were previously reliant on other plant organs to supply them with sucrose, underwent transitions to resemble source leaves, which are presumably capable of producing their own photosynthate supply.

It seemed possible that the rapid sink-source transition might therefore be prompted specifically by removal of other sources of imported sugar. To test this, I removed all source leaves from mature, soil-grown *pSUC2::GFP* plants, leaving only the three youngest leaves, which were all sink leaves (Figure 73A). Within 24 h and 48 h (Figure 73B and C) the attached leaves showed strong GFP expression in the veins, identical to that seen in detached sink leaves (Figure 72).

Detached leaves have been reported to survive for long periods on sugar solutions suggesting that they can take up exogenous sugars through the cut petiole (Yarwood, 1946). However, maintaining *AtSUC2::GFP* leaves inside chambers containing 1% sucrose showed that they developed GFP fluorescence in the importing veins at a rate indistinguishable from leaves maintained in water (Figure 71B). Leaves maintained in the dark also showed activation of the *AtSUC2* promoter in the importing veins at the same rate, although they showed increasingly lower fluorescence after 24h, showing that this sink-source transition occurred whether the leaves were able to photosynthesise or not (Figure 71 C). Quantifying the effects on PD development in response to sugars was not directly possible because sugar-containing medium within the chambers made for difficult imaging conditions. To examine the effects on PD, I therefore maintained MP17-GFP plants on detached leaves on filter papers in Petri dishes as in (Reis, et al., 2000), using 12%, 6%, 3%, 1%, 0.5% and 0.1% sucrose solutions instead of water, or alternatively by floating leaves on sucrose solutions of the above concentrations (Mita et al., 1995). At higher concentrations (12% and 6%), leaves showed visible accumulation of anthocyanins, and turned purple at their base. Although the amount of variation observed was such that statistically significant counts of PD could not be obtained, numbers of complex PD at all sugar concentrations leaves appeared to be within a similar range as the H_2O control (Figure 74).

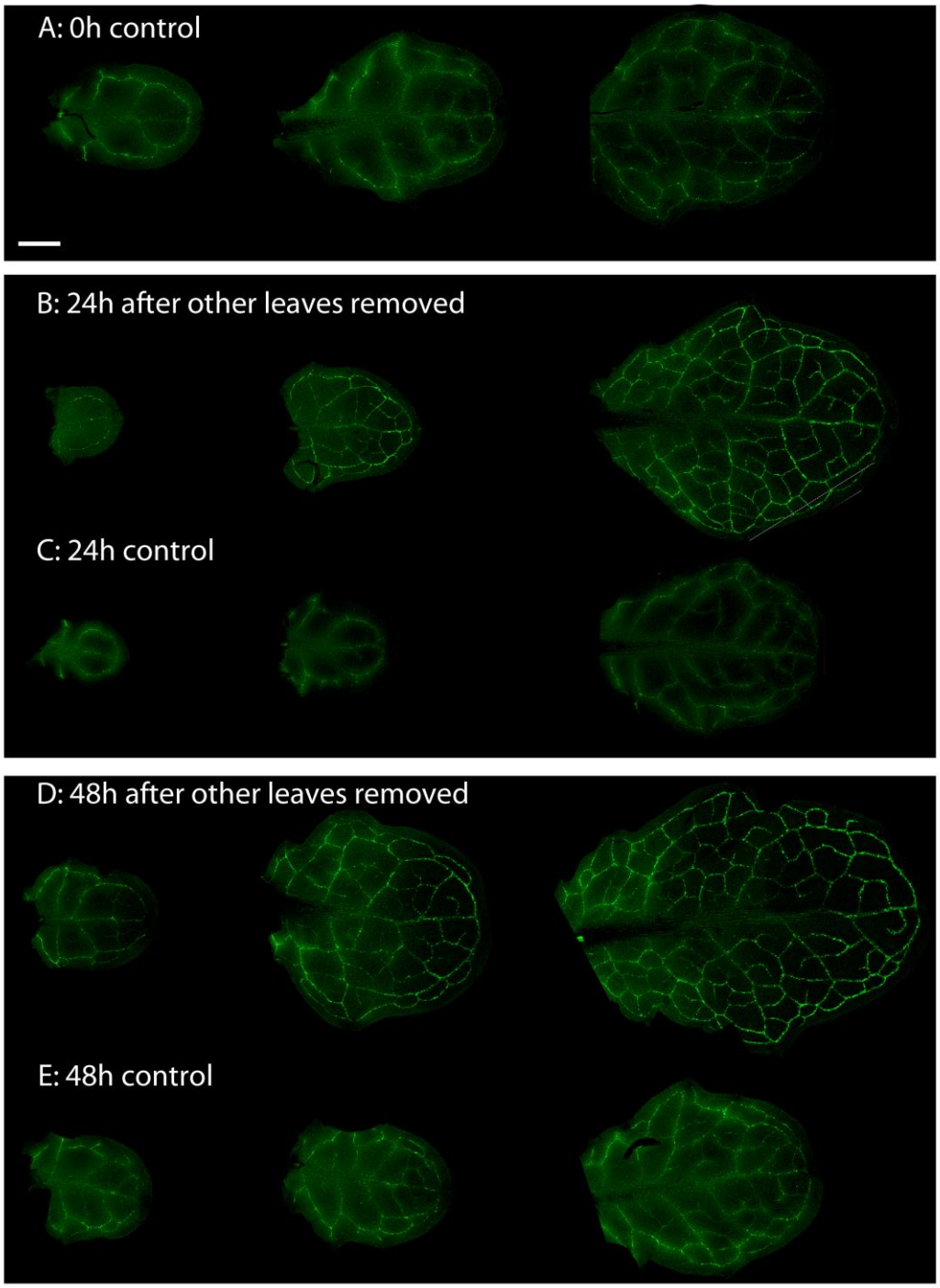

Figure 73: shows the youngest 3 leaves (left to right) from pSUC2::GFP plants. At 0 h, the plants shown in B and D had all leaves but the youngest 3 removed. A) the youngest 3 leaves or a plant at 0h. B and C) plants at 24 h: showing the youngest leaves of plant which had all other leaves removed 24 h previously (B) or was left intact (C). D and E) plants at 48 h: showing the youngest leaves from a plant that had all other leaves removed 48 h previously (D) or was left intact (E). Scale bar = 500 µm.

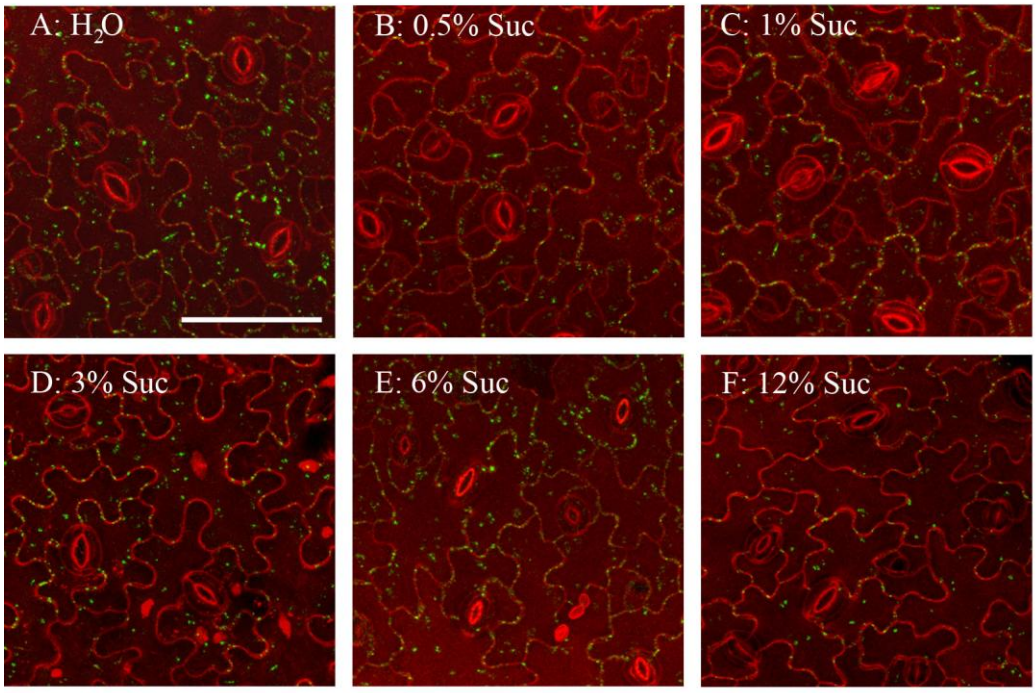

Figure 74: Images from MP17-GFP leaves detached from soil-grown plants and maintained on solutions of increasingly concentrated sucrose on filter papers for 24 h. Leaves shown were the second youngest and all between 3.0-4.75 mm length. Walls have been stained with propidium iodide. Scale bar = 50 µm.

5.3 Conclusions and Discussion

5.3.1 PD development viewed in real time

PD development has historically been studied as 'snapshots' of PD populations within individual tissues at single time points. The aim of this chapter was to study PD development in real time using a chamber imaging system that allowed me to observe PD development in living leaves. Using fluorescent PD markers, I was able to image PD converting from simple (PDLP1-mRFP labelled) to complex (PDLP1-mRFPand MP17-GFP labelled) in the context of the sink-source transition. The data showed that the plant may modify the fundamental structure of its PD in less than an hour. These results challenge the standard view of PD as static structures whose immediate responses to stresses are limited to basic constriction or blockage of the pore.

My other aim was to use these real-time studies to complement my longer-term 'static' studies (Chapter 4) to complete the timeline of PD development in leaves as they mature from sink to source. Using detached leaves proved to be particularly

useful due to the unexpected finding that detachment itself prompts young leaves to rapidly transition from sink to source. The chamber can therefore be used as a simplified system to observed PD development and the sink-source transition without the complicating factor of variability in timing.

The work in Chapter 4 identified two patterns of development at the cell wall: one related to the type of cells connected by PD, and the other related to the position of the PD in the wall. While cells do continue to expand in the chamber, growth is slowed considerably, while other aspects of leaf maturation, such as the sink-source transition, are accelerated. This system therefore gives a unique view of PD development uncoupled from factors related to growth and stretching forces in the wall. As expected, the preferential insertion of PD at interfaces within the anisocytic stomatal complexes occurred as observed in *in situ* leaves, confirming that this is an aspect of PD development that is not reliant on the physical growth of the cell walls, but is dependent on cell identity. Meanwhile, the observed trend of preferential insertion at the lobe tips of epidermal cells was thought to be primarily determined by stress and stretching forces present in the wall environment around the PD; accordingly, this pattern is reduced in detached leaves.

5.3.2 Plasmodesmata and the response of leaves to detachment

The chamber also gave some new insights into the biology of detached leaves. The discovery that detached sink leaves undergo accelerated development, both in terms of complex PD formation and the sink-source transition, is in some ways unsurprising as the general response of leaves upon detachment is not death, but survival. As discussed in the introduction to this chapter, detached leaves continue to carry out most biological processes, including photosynthesis and respiration. This work shows that this survival reaction is just as strong in leaves of an immature developmental state. Within an hour of detachment, these small leaves use the limited resources they have to undergo major physiological changes and convert to independent source organs. By 48h, microscopic analysis showed that these leaves have many features of mature source leaves, while still only a few millimetres in length. These miniature ‘adult’ leaves, with their mixture of juvenile and mature

characteristics, are an intriguing example of the plasticity and adaptability of plant development and could form a useful system for wider studies of leaf development.

This dramatic survival response is likely to be the first step in the detached tissue to become self-sufficient. In many species, survival of a detached leaf may produce an independent plant, as organogenic callus may form at the cut region to regenerate a whole, reproductively viable plant. In a survey of 1024 species by Hagemann in 1932, detached leaves from 289 species developed shoots and roots, 501 species developed roots only, and 25 shoots only (reviewed in Yarwood, 1946). Of the surveyed species, only 46 were observed to spontaneously form buds or roots on whole, attached leaves, showing that this is generally a response to detachment. Some species require treatment with hormones to regenerate organs from leaves (such as are supplied by commercial rooting powders), but many species may do so when supplied with water only (reviewed in Yarbrough, 1936). Regeneration from cut leaves has found various uses. Propagating whole plants from leaf cuttings is a routine gardening procedure for certain plants including species from *Streptocarpus* and *Kalanchoe* (Royal Horticultural Society, 2012) and has been widely used in production of horticultural cultivars of species such as *Begonia,* as plantlets develop from a single epidermal cell and so are non-chimeric (reviewed in Broertje et al., 1968). Detached and rooted leaves or cotyledons have also been used as experimental systems (Lovell et al., 1970; Yarwood, 1946), particularly for studying plant-pathogen interactions.

5.3.3 Final words

Work done in the course of this chapter achieved my aim of observing PD in real time. This dynamic imaging revealed that PD themselves are dynamic structures, and that the plant may modify PD structure as a rapid response to extreme changes in circumstances. However, many natural patterns of PD development are preserved. The chamber system presented therefore provides an intriguing window through which many of the natural patterns of leaf development can be observed and studied.

5.4 Acknowledgements and thanks

The chamber system used was adapted from one developed by Jordi Chan at the John Innes Centre, Norwich, and I thank him for helpful discussions about chamber usage. *pSUC2::GFP* plants were courtesy of N. Sauer. University of Edinburgh Darwin Building Workshop produced the plastic frames for the chambers.

6 Chapter 6: Control of PD development

6.1 Introduction

6.1.1 Co-ordination of PD development

The work presented so far in this thesis has built up a picture of the pattern of complex PD development during leaf maturation. Chapter 4 showed that under normal growth conditions, the structural modification of PD from simple to complex forms occurs over a relatively extended developmental period and is co-ordinated on an interface-, cellular-, tissue- and organ-specific level. It also illustrated that the rate of PD development can be variable within a population of genetically similar plants grown under the same conditions, and that complex PD numbers were not strictly correlated with plant growth rate when measured in terms of either size or by the plastochron index. This suggests an inherent flexibility in PD development that allows it to be tailored to the needs of individual leaves. The work in Chapter 5 showed that the natural pattern of complex PD development is highly co-ordinated and can be rapidly and synchronously induced. These observations together suggest that PD development in leaves is co-ordinated in response to the complex network of stresses and stimulants in a plant's growing environment.

While we understand how development and modulation of PD themselves influence wider development through control of symplasmic signalling, we understand very little about the factors that control PD development itself. The large-scale co-ordination observed in PD development suggests that it is tailored to wide range of stresses, stimuli and growth parameters, although the identity and contribution of these is as yet unknown. Indeed, few factors have been identified that result in direct modification of PD structure.

The most extensively studied factors known to affect PD development are reactive oxygen species (ROS). These effects were discovered by analysis of mutants in the mitochondrial genes *ise1*and *ise2*, and the plastid gene *gat1*, that display altered SELs. As described in Chapter 1, all of these lines have increased cellular ROS levels, and all have increased numbers of complex PD in the embryonic tissues: an increase of 15% in the case of *ise1 ise2* (Kobayashi et al., 2007), and a 9% increase

in the case of *gat1* (Benitez-Alfonso et al., 2009). If ISE1 expression is knocked down by VIGS in leaf tissues, a 13% increase in the number of complex PD is observed (Burch-Smith and Zambryski, 2010). The modification of PD could be a direct effect of an increase in cellular redox levels as hydroxyl radicals have been shown to promote wall loosening, which could theoretically facilitate production of complex PD. However, it is also clear that general increases in cellular ROS levels may affect many aspects of cellular function, and will cause a general stress response. In illustration of this, Stonebloom et al. (2012) were able to mimic the ROS-production and transport phenotypes of *ise* and *gat* lines using low concentrations of two metabolic inhibitors: salicylhydroxamic acid, which inhibits a mitochondrial oxidase and mimics *ise*; and paraquat, which directly oxidises plastid reductants and mimics *gat1*. At higher concentrations these inhibitors are used in oxidative stress experiments and may cause severe tissue damage. It is therefore likely that their effect on PD may be indirect, and part of a general stress response that results in restriction of symplasmic communication.

Hormones are also known to have effects on PD development. Direct application of the cytokinin benzyladenine (BA) to the vegetative SAM of *Sinapsis alba* caused increases in the numbers of PD observed (Ormenese et al., 2006), mimicking the effects of floral induction by exposure to LD growth conditions (Ormenese et al., 2000). The additional PD observed all had a simple architecture, and could be seen within 22 h of exposure to BA, although the mechanism responsible for this has not been identified.

Other factors are expected to modify PD, such as defence signalling pathways (Lee and Lu, 2011), but this has not yet been shown. This presented an intriguing field to study as, to put the patterns of development observed in Chapter 4 in context, it would be useful to understand the factors that guide them.

6.1.2 A high-throughput approach to PD development

As discussed in Chapter 4, investigating PD development through traditional microscopy is challenging due to the large sample sizes required, the heterogeneous cell constitution of the tissues of interest, and the intricate and variable growth patterns of the leaves. To study the coordination of this developmental pattern is

even more challenging as the range of factors that can be expected to affect PD is extensive. Host signals such as hormones, abiotic stresses such as drought and salinity, and defence responses triggered by pathogen attack all have the potential to influence PD development.

However, work in Chapter 4 also established that high-throughput imaging approaches can be applied to the study of PD. Using the Opera high-content microscopy system for automated imaging, and custom-written Acapella scripts (Ji Zhou, The Sainsbury Laboratory, Norwich), it was possible to image, measure and quantify over 3,500 cells and 100,000 PD from 60 leaves in a single 40 minute run of the system. These numbers make a screen of complex PD development feasible, and opened the possibility to test the effects of various stresses and treatments on PD development.

6.2 Aims

The aim of this chapter is to investigate the network of factors that contribute to the precise co-ordination of PD development seen in *A. thaliana* leaf epidermal cells. This was done by comparing rates of complex PD development under different growth treatments, including:

- Plant hormones: auxin, cytokinin.
- Defence related signals: salicylic acid, methyl jasmonate, flg22 and H_2O_2.
- Salinity and osmotic stress
- Sugars: sucrose, glucose and sorbitol
- An inhibitor: BFA.

6.3 Results

6.3.1 Preliminary study to investigate PD response to treatments

Because my access to the Opera microscope was relatively limited, it was not feasible to use it for a full initial screen of PD responses to a large range of treatments, each of which was to be tested at a minimum of two concentrations.

Instead, I chose to perform a preliminary study using manual processing, image acquisition and analysis before repeating the most promising experiments using the Opera system.

The purpose of the preliminary experiments was twofold. Firstly, it would enable optimisation of the experimental design, including plant growth conditions, selection of sample tissues for analysis, and use of dyes to ensure that the samples would image well and give meaningful results on the Opera system. Secondly, although the time-consuming work could use only small sample sizes, it would provide an indication which treatments were having an effect on PD development, allowing me to prioritise the experiments to be analysed using the Opera system.

For the preliminary study, plants were grown on 0.5x MS medium for five days to allow germination and seedling establishment to proceed under standard conditions. At day five the seedlings, which had expanded cotyledons and a visible but unexpanded first leaf pair, were transferred to 0.5x MS plates with or without treatments, and grown for further five days (see Chapter 2 for a fuller description of the methods used). Treatment media that produced plants with four leaves by day ten were used for the study, with the third leaf used for analysis as it was large enough to manipulate with tweezers and had been grown entirely during the treatment period. The list of treatments used is shown in Table 5. In general, at least two concentrations of each treatment were used: a medium-high concentration known to have measurable effects on growth parameters, and a lower concentration expected to have minimal effects on growth. The high concentration was expected to show any effects on complex PD development strongly enough to be identifiable. The lower concentration would help establish to what extent the observed effects were caused indirectly by alteration of other growth parameters.

By applying the treatments through the medium, the plants for all treatments could be grown under the same conditions, with the same tissues exposed to the treatments for the same time period, in a manner that would not require direct manipulation of the leaves until imaging. As the tissues of interest are not directly exposed to the treatment, a negative result in this test does not mean that a particular treatment does not have any effect on PD if applied through different means.

6.3.2 Effects of treatments on growth parameters

To monitor possible indirect effects on PD development due to growth inhibition caused by the treatments, seedling fresh weight (Figure 75), length of the third leaf (Figure 76), root length (Figure 77) and number of lateral roots (Figure 78) were recorded. As only complex PD are being observed, 'PD' values given throughout this chapter refer to complex PD only.

In practice most treatments showed some effects on growth, usually as inhibition of root growth (Figure 77), which was expected as the roots were exposed directly to the treatments. Most of the treatments showed more minimal effects on overall fresh weight and leaf length and so, except in the cases discussed in more detail below, the effects on leaf epidermal cells and PD were in many cases not linked to major changes in leaf growth rate.

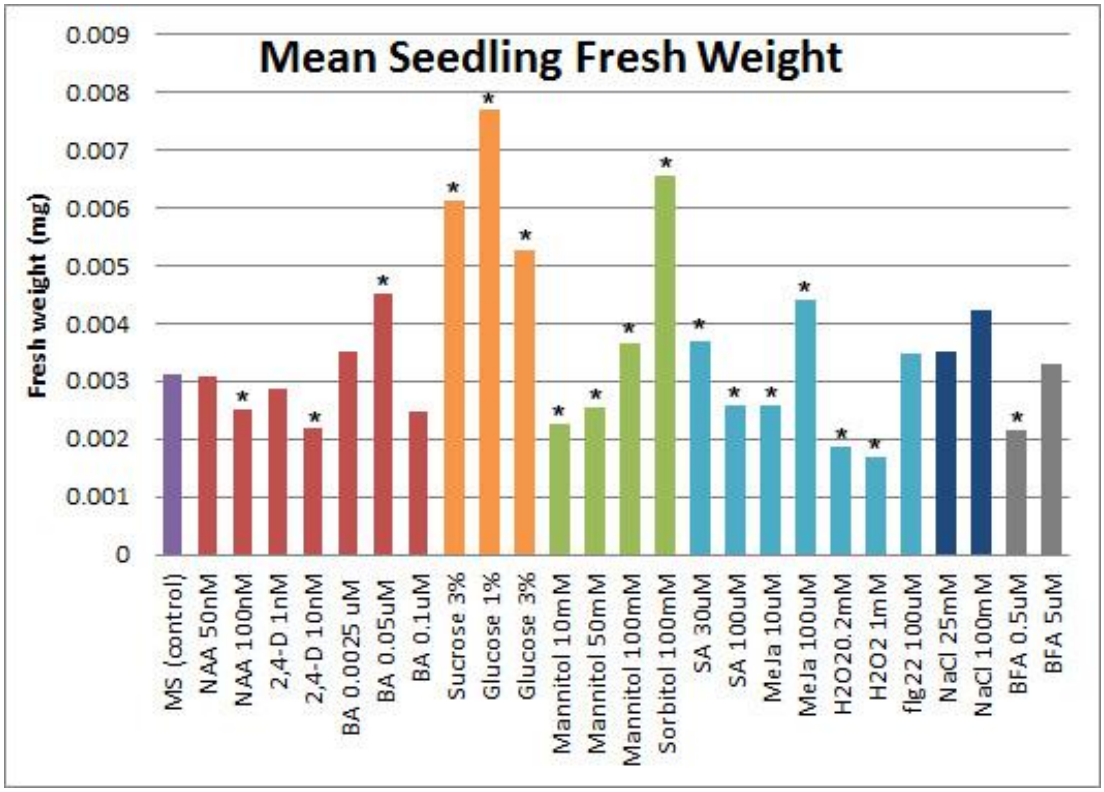

Figure 75: Bar chart showing mean seedling fresh weight. Bars are marked with an asterisk where a t-test showed the mean differed significantly from the control at the 5% level. Purple: control plants, red: hormone treatments, orange: sugars, green: sugar alcohols, cyan: defence treatments, blue: salinity, grey: inhibitors.

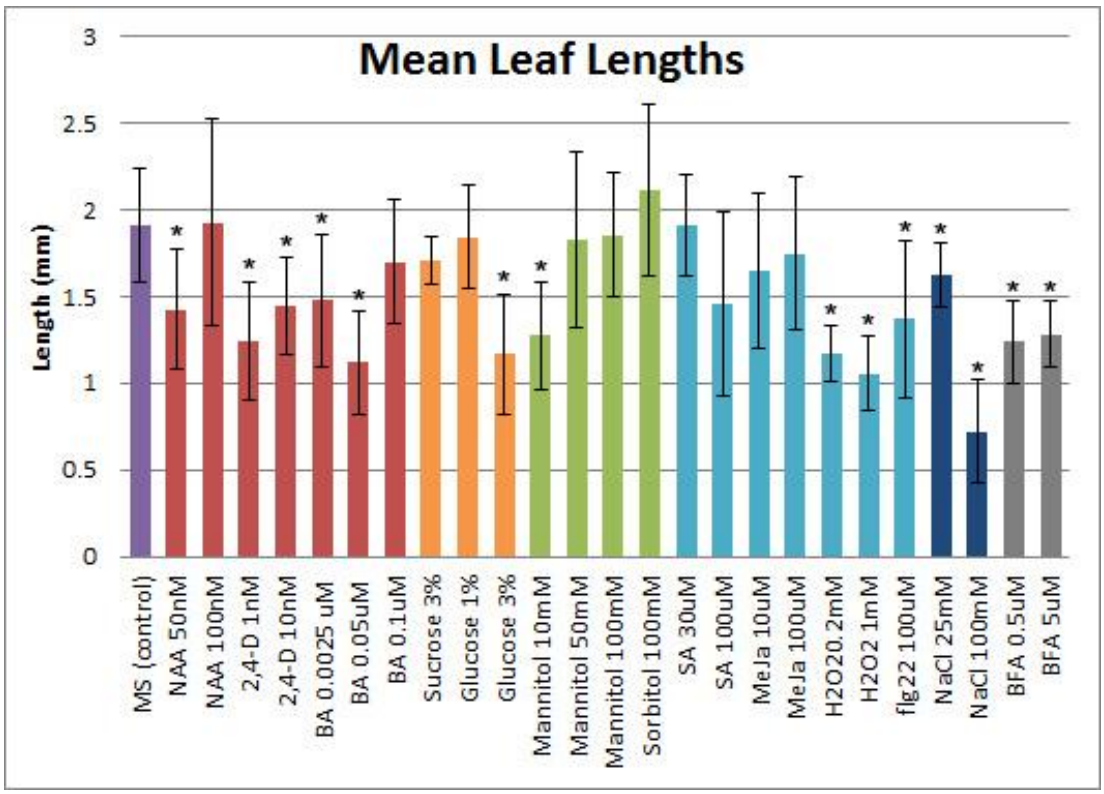

Figure 76: Bar chart showing mean length of the third leaf of plants at 10 days growth. Error bars show standard deviations. Bars are marked with an asterisk where a *t*-test showed the mean differed significantly from the control at the 5% level

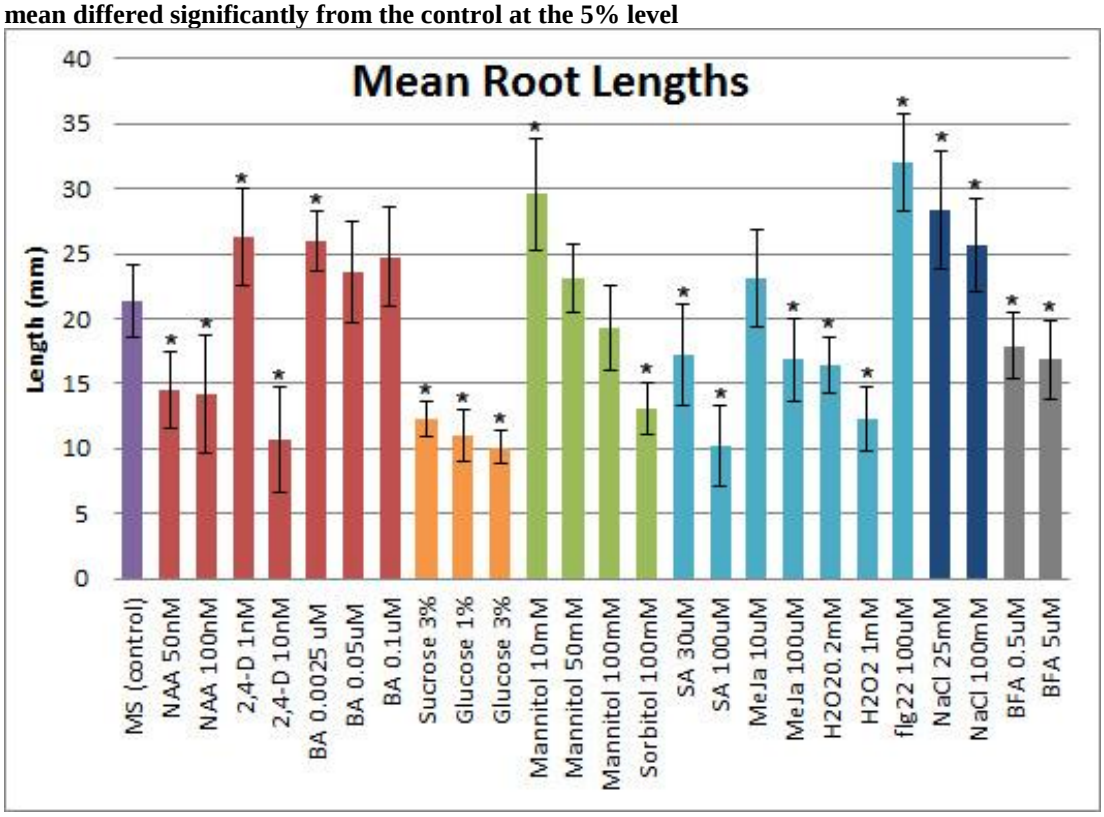

Figure 77: Bar chart showing mean root length of plants at 10 days growth. Error Bars are standard deviations. Bars are marked with an asterisk where a *t*-test showed the mean differed significantly from the control at the 5% level

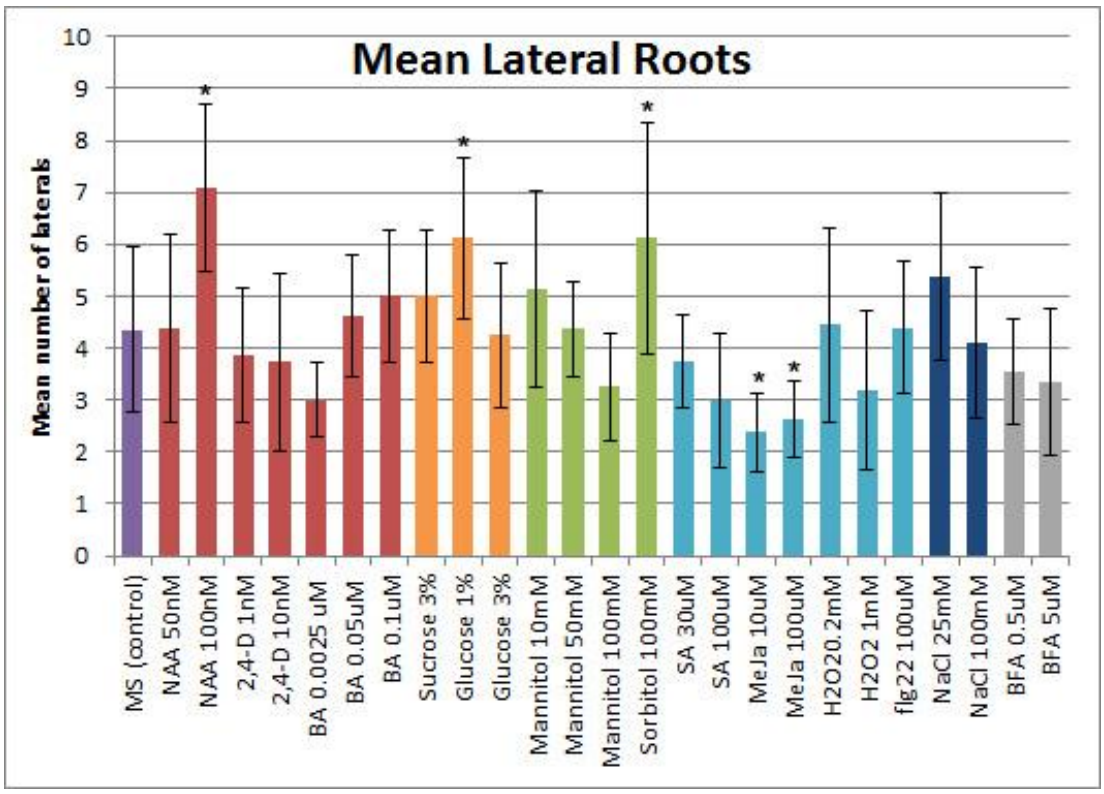

Figure 78: Bar chart showing mean number of lateral roots of plants at 10 days growth. Error bars are standard deviations. Bars are marked with an asterisk where a *t*-test showed the mean differed significantly from the control at the 5% level

6.3.3 Effects of treatments on epidermal PD.

The overall trends for effects of treatments on epidermal cell size and the number of PD per cell are summarised below in Table 5.

Table 5: Table showing the complete list of treatments tested during the preliminary experiment. The column '4 leaves' records whether plants grown on the treatment had 4 leaves after 5 days growth on control medium and 5 days on the treatment medium; those that did not were not analysed. The column 'cell size' and 'PD/cell' records an increase or decrease with respect to control plants that is significant at the 5% level according to a *t*-test. The full data is shown in graphical form in Figure 79

Treatment	Conc.	4 leaves	Cell size	PD/cell
Hormones:				
Auxin, NAA	10 nM	Yes	No change	Increased
	100 nM	Yes	No change	Increased
Auxin, 2-4-D	1 nM	Yes	No change	No change
	10 nM	Yes	No change	No change
Cytokinin, BA	0.025 µM	Yes	No change	No change
	0.05 µM	Yes	No change	No change
	0.1 µM	Yes	Increased	Increased
Sugars				
Sucrose	3%	Yes	No change	Increased
	6%	No	N/A	N/A
Glucose	1%	Yes	No change	No change
	3%	Yes	No change	Increased
Sugar alcohols				
Mannitol	10 mM	Yes	Decreased	No change
	50 mM	Yes	Decreased	Increased
	100 mM	Yes	Decreased	Increased
	300 mM	No	N/A	N/A
Sorbitol	100 mM	Yes	No change	No change
	400 mM	No	N/A	N/A
Defence				
Salicylic acid	30 µM	Yes	Increased	Increased
	100 µM	Yes	No change	Increased
Methyl Jasmonate	10 µM	Yes	No change	No change
	100 µM	Yes	Increased	No change
H_2O_2	0.2 mM	Yes	No change	No change
	1 mM	Yes	No change	Increased
Flg22	100 µM	Yes	No change	No change
Salinity				
NaCl	25 mM	Yes	Increased	No change
	100mM	Yes	Increased	No change
Inhibitor				
BFA	0.5 µM	Yes	No change	No change
	5 µM	Yes	No change	No change

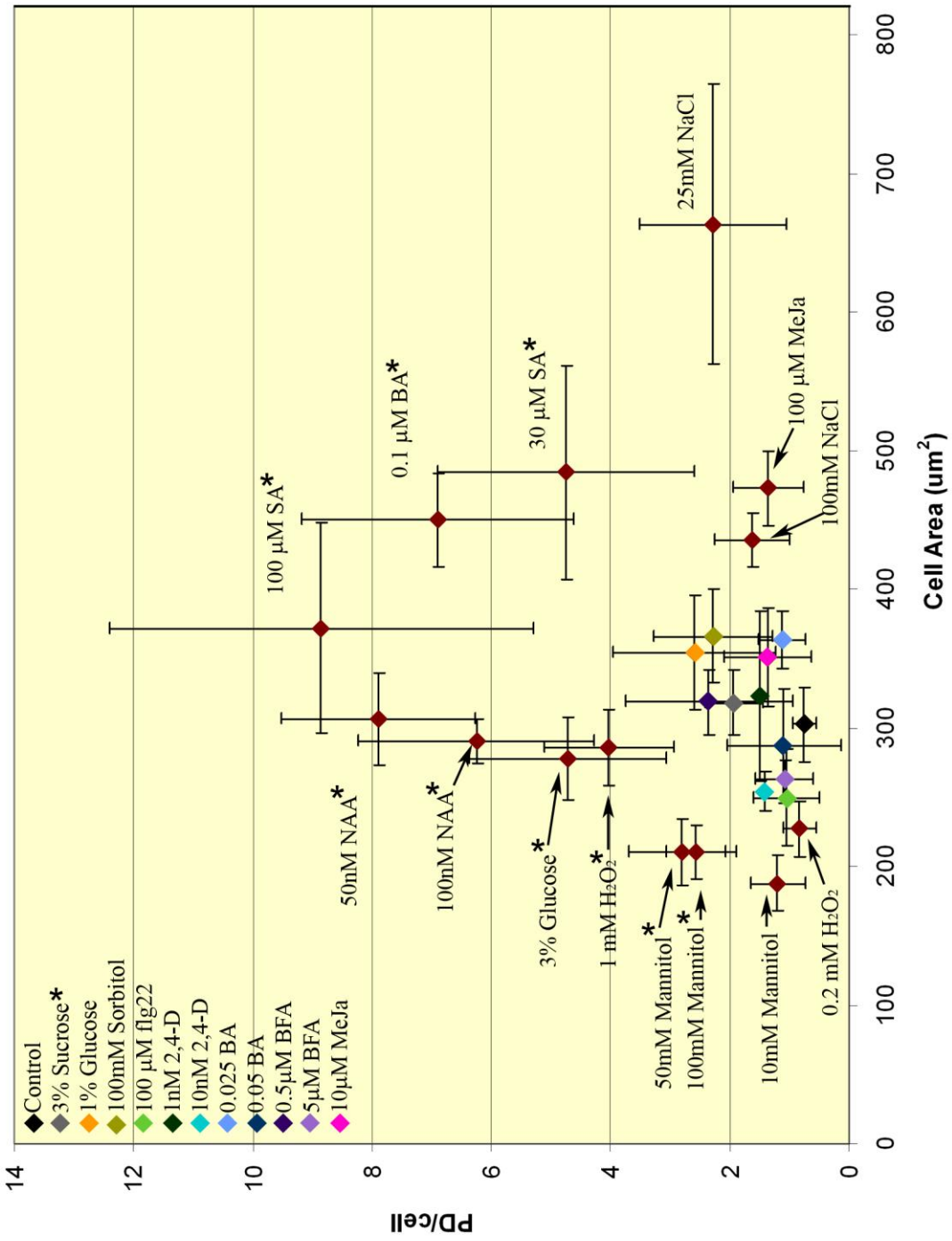

Figure 79: Graph showing mean cell area and mean numbers of complex PD/cell in the leaf epidermis of *A. thaliana* grown on root medium supplemented with treatments. Compared to the control group (black marker), 1mM H_2O_2, 3% glucose, 3% sucrose, 100nM and 50nM NAA and 100µM SA increase frequency of complex PD without significantly altering cell size. 0.1 µM BA and 30 µM SA increase PD number while increasing cell size. 50mM mannitol and 100mM mannitol increase complex PD numbers while decreasing cell size. Several treatments show no significant effect on numbers of complex PD while increasing cell area (25 and 100mM NaCl and 100 µM MeJa) or decreasing it (10mM mannitol). Bars are standard errors. Treatments marked with an asterisk significantly increased the numbers of complex PD/cell at the 5% level.

Notably, all treatments caused in increase in the mean number of PD, although analysis via a *t*-test showed that these were significant at the 5% level in only 40% of cases (Figure 79). This shows the sensitivity of the mechanisms influencing PD development, and shows that modification of complex PD is a general response to a broad range of challenges and stresses.

6.3.4 Treatments: control data

The control data from plants that were transferred to untreated x0.5MS medium shows an average cell size of 302.5 μm^2 and an average of 0.8 PD/cell. As indicated in data from previous chapters, the number of PD and cell size can vary significantly even in a control population grown under standard conditions and, while the majority of the control plants cluster around the mean values, the sample contains two outliers that have an average cell size of >500 μm^2 and a further outlier which had 3 PD/cell.

6.3.5 Hormone treatments: auxins and cytokinins

Due to their multifaceted roles in development, the two major phytohormones, auxin and cytokinin, were analysed for their effects on PD development. Due to difficulties in getting the major endogenous auxin, indole-3-acetic acid, to stay reliably in solution, two synthetic auxins were used: 1-naphthaleneacetic acid (NAA), and 2,4-dichlorophenoxyacetic acid (2,4-D). 50 nM and 100 nM NAA medium was used based on root growth assays which showed that NAA caused minimal effects on root elongation at 10-100 nM (Marchant et al., 1999). In this preliminary experiment, both concentrations caused significant increases in the frequency of complex PD, with a *t*-test at 95% confidence showing that 50 nM NAA caused an increase of 4.8-9.5 PD/cell compared to the control sample (Figure 79). Plants grown on 100 nM NAA showed significant effects on all growth parameters, while plants grown on 50 nM NAA only showed significant decreases to leaf and root lengths (Figure 75-78).

2,4-D was used at concentrations of 1 nM and 10 nM, based on root growth assays which showed that 2,4-D caused minimal effect on root elongation at 1nM and 60% reduction in growth at 10nM (Mussig et al., 2003). This auxin caused no significant changes to either cell size or development of complex PD (Figure 79).

The cytokinin 6-benzyl aminopurine (BA) was used at concentrations of 0.0025 µm, 0.05 µm and 0.1 µm, based on root growth assays that showed that very low concentrations of BA (>5 nM) causes reduced root elongation (To, J. P. C. et al., 2004). The lowest concentrations of BA used caused little effect to PD development or cell growth. However, plants grown on 1 µM BA showed an increase in both PD/cell of between 3.2 and 9.1 PD/cell (95% confidence) (Figure 79) with no significant effects on other measured growth parameters (Figure 75-78).

6.3.6 Sugar treatments: sucrose and glucose

In order to further test the link between leaf carbon balance and PD development, I tested the effect of exogenously applied sugars on the development of complex PD.

MS medium generally contains added sucrose: standard MS medium contains 0.3%, while the recipe I used, which is adapted to reduce leaf curling in plate-grown plants, contains 0.6%. Experiments by others showed that sucrose concentrations could be increased up to 3% with only subtle effects on plants, e.g.: the mild alteration of circadian rhythm observed by Dalchau et al. (2011). Higher sucrose concentrations give much stronger effects, e.g.: 12% sucrose represses germination rates (Cho and Yoo, 2011). Under my conditions, plants grown on 3% sucrose showed a small but significant increase in PD frequency of between 0.3-2.1 PD/cell compared to the control population, as shown by a *t*-test at 5% confidence (Figure 79) as well as significant root inhibition and gains in fresh weight, while plants grown on 6% sucrose showed strongly repressed growth rates and so were not analysed.

To test glucose, a constituent monomer of sucrose, I used media containing 1% and 3% glucose as higher concentrations cause strong growth inhibition (Cho and Yoo, 2011). In this experiment, both concentrations of glucose caused root inhibition and an increase in fresh weight (Figure 75, Figure 77) and a *t*-test on the PD counts of plants grown on 3% glucose suggested at 95% confidence that it caused an increase of between 1.6 and 6.3 PD/cell compared to the control sample (Figure 79).

6.3.7 Sugar alcohol treatments: mannitol and sorbitol

To test for the effects of osmotic or drought stress on PD development, I used mannitol at concentrations of 10-300 mM. Initially I used only 50 mM and 100 mM

medium, based on root growth assays that suggested concentrations of 50-100 mM mannitol may cause ~20% inhibition of root growth (Deng et al., 2009; Zhu et al., 2002) while higher concentrations of 350 mM and above cause severe osmotic shock effects (Schulz, 1995).

Growing plants on mannitol-containing medium showed an unexpected effect on cellular and plant morphology. While gross plant morphology was largely unchanged (Figure 80A-D), and most growth parameters including leaf length were unaffected (Figure 75-78), the young leaves were significantly narrower (Figure 80E, F and G). Mannitol treatments caused a decrease in cell size (Figure 79), and the cells themselves were uniformly square or oblong shaped, a contrast to the normal jigsaw-shaped cells (Figure 81 A-C). The third leaves also showed a large number of stomata at the leaf tips, on the adaxial epidermis as well as the abaxial (Figure 81, G and I). These same cell-shape effects were observed in Col-0 WT plants grown on media supplemented with mannitol (Figure 81H, I).

To expand these experiments I extended the range of concentrations tested by using 10 mM and 300 mM mannitol medium. 10 mM mannitol caused a more attenuated effect on leaf shape (Figure 80G), but the cells showed a similar size and shape range as plants grown on higher concentrations (Figure 81A). 300 mM mannitol caused growth inhibition when the plants were only at the two or three leaf stage (10 days post transfer), and so were not analysed.

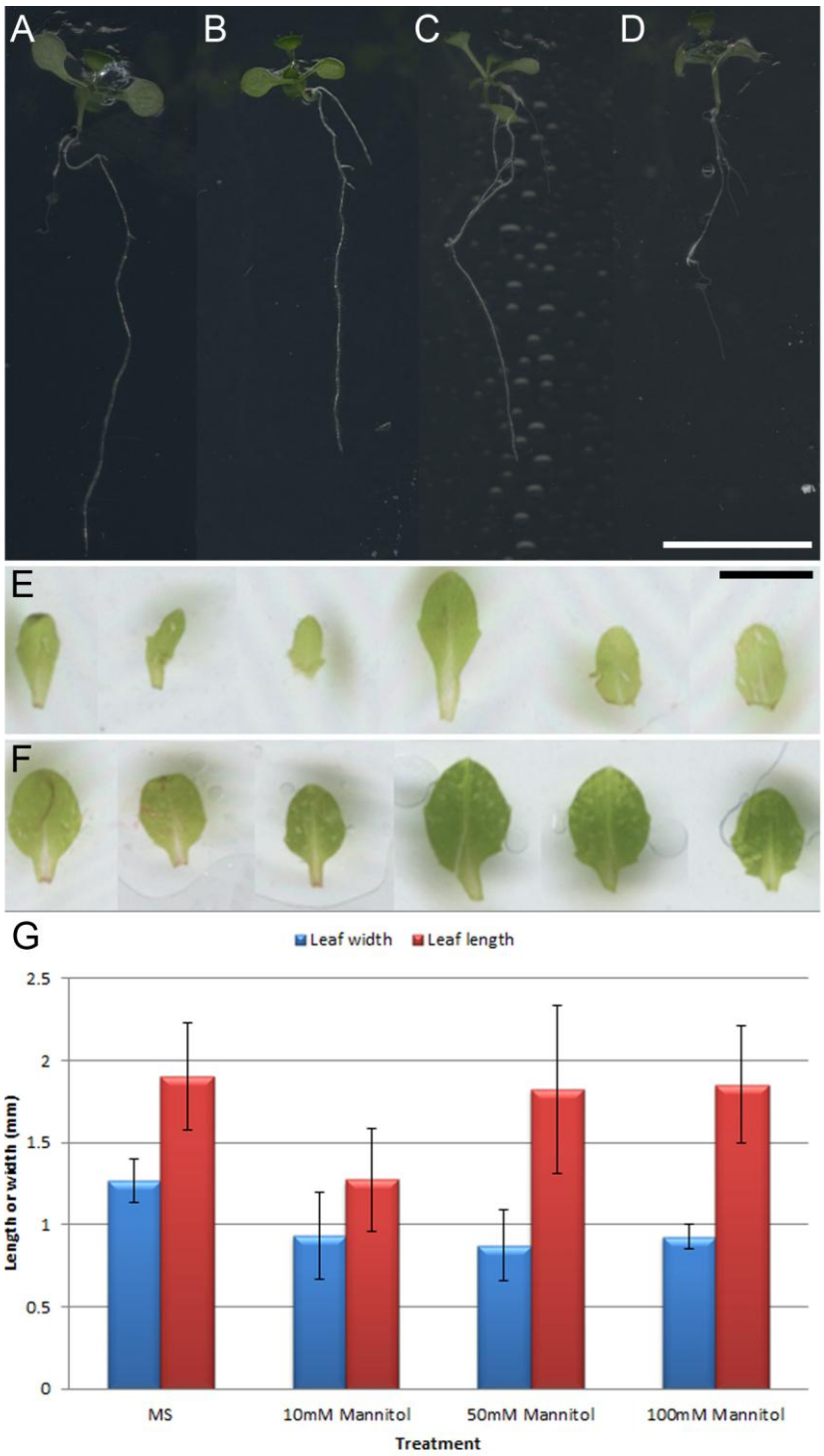

Figure 80: plants grown on mannitol. A-D: MP17-GFP plants on 0.5x MS (A) or 10 µM (B), 50 µM (C) or 100 µM (D) mannitol. E-F: Montage of sample third leaves taken from MP17-GFP plants grown on 50 µM mannitol (E) or 0.5x MS (F). G: graph of leaf lengths and widths of plants grown on increasing mannitol concentrations. Scale bar A-D = 1 cm, scale bar E-F = 2 mm.

Although the cells had expanded less than controls, to an average of only 210.2 μm^2 compared to 302.5 μm^2 in control plants, the number of complex PD was higher. A *t*-test of the data suggests an increase of 0.7-3.4 PD/cell in 50 mM mannitol-grown plants compared to control plants at 95% confidence. In some cases, the MP17-labelled PD appeared to divide the tissue into groups (Figure 81 D-F), with 'barriers' of complex PD encircling blocks of cells with few complex PD in the interior crosswalls. This pattern of complex PD development could represent either the formation of symplasmic domains, or be related to the pattern of cell division, with the labelled wall representing the oldest walls in the tissue.

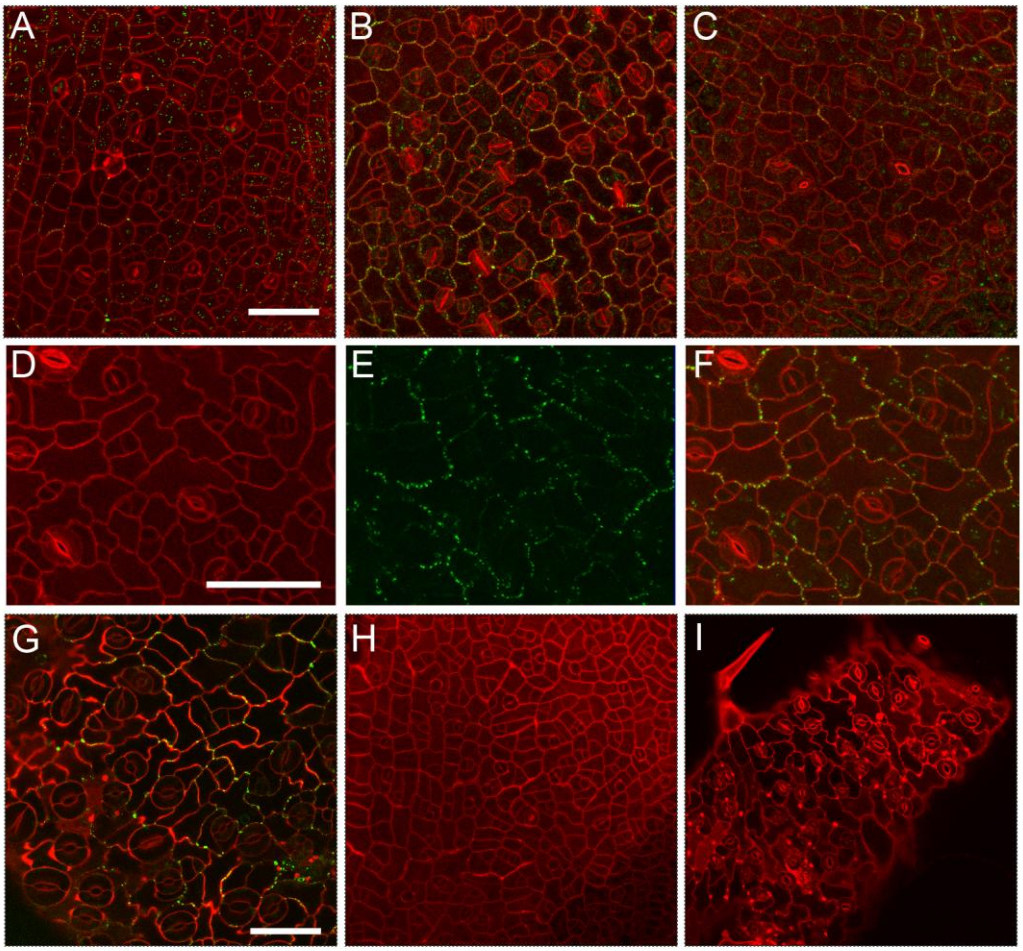

Figure 81: Mannitol treated plants. A-C: MP17-GFP *A. thaliana* treated with (A) 10 mM, (B) 50 mM or (C) 100 mM mannitol and stained with propidium iodide (red). D-F: detail of plant treated with 50 mM mannitol (D) shows the propidium iodide wall only, (E) shows the GFP-labelling only, and (F) is an overlay of both signals. Note the MP17-labelled PD divide the tissue into sections. (G) Tip region of a plant grown on 300 mM mannitol. (H) WT Col-O plant grown on 100mM mannitol. I) Upper epidermis at leaf tip of a WT plant grown on 100 mM mannitol. Scale bars A-C, D-E, G-H = 50 µm.

For a comparison, I also tested the effects of growth on sorbitol, an isomer of mannitol and another sugar alcohol sometimes used for osmotic stress experiments. I used sorbitol at 100 mM and 300 mM based on experiments by (Schluepmann et al., 2003) which showed that 100 mM sorbitol had no detectable effect on growth when either supplied in solid medium or fed directly to plants.

Unlike plants grown on mannitol-containing medium, plants grown on medium containing 100 mM sorbitol showed no significant change in cell size, cell morphology, leaf morphology or PD number (Figure 79). Instead, 100 mM sorbitol treated plants had a significantly larger mass and shorter roots than the controls, similar to plants grown on sucrose- and glucose-containing medium (Figure 75-78). Plants grown on 300 mM sorbitol showed strong inhibition of growth and so were not analysed.

6.3.8 Defence treatments: SA, MeJa, H_2O_2 and Flagellin

In a natural environment, plants are constantly challenged by pests and pathogens, and have complex network of responses to defend themselves. Pathogens from viruses to fungi are known to target PD in order to spread from the initial infection site, and so plants are expected to modify PD in order to counteract this *Achilles*' heel in their defence. I used a range of treatments related to different aspects of the defence responses to test for possible links between defence response and PD development.

Salicylic acid (SA) is the long-range signal that moves from the site of infection to produce systemic acquired resistance, and application of exogenous SA may stimulate defence response directly. It was used at concentrations of 30 and 100 μM, based on experiments by (Tiryaki and Staswick, 2002) in which WT plants showed growth inhibition on media containing 50 μM SA. SA treatment gave the largest increases in PD number in this study (Figure 79). Compared to the control value of 0.756 PD/cell, plants treated with 100 μM salicylic acid developed an average of 8.85 PD/cell, and a *t*-test of the data shows a difference in population means of between 3.5 and 12.7 PD/cell at 95% confidence. The increase in complex PD frequency for plants grown on 100 μM was not coupled to a significant change in

cell size (Figure 79) or leaf length, but significant decreases in fresh weight and root length (Figure 75-78).

Methyl Jasmonate (abbreviated to MeJa in figures) is another component in the plant defence signalling response, and may directly stimulate defence responses in plants exposed to it. It was used at concentrations of 10 and 100 μM based on a root growth assay by Yan et al. (2007), which suggested that medium containing 25 μM methyl jasmonate caused root inhibition. Plants grown on methyl jasmonate showed significant alterations to most growth parameters (Figure 75-78) and PD/cell numbers similar to controls.

H_2O_2 forms part of the redox burst produced as part of the plant defence response to a broad range of pathogens and, as has been discussed, may alter patterns of complex PD development (Stonebloom et al., 2012). I used H_2O_2 at 0.2 and 1 mM based on root growth assays which showed that plants transferred to medium containing H_2O_2 exhibited ~15% inhibition of root growth at 0.2 mM and ~40% growth at 1 mM (Bai et al., 2007). Under my conditions both the high and low concentration used caused mild growth inhibition of all parameters tested except lateral root production (Figure 75-78). While low concentrations had no significant effect on PD development, a *t*-test showed that growth on 1 mM H_2O_2 medium caused a increase of between 1.5 and 5 PD/cell (95% confidence), while not significantly altering the size of the cells.

flg22 is a constituent of the prokaryote flagellum and is a potent elicitor of plant defence responses. Plants respond to exogenously applied flg22 as they would to bacterial pathogens. For the flg22 treatments, a slight variation of the method was used as flg22 is unsuitable for long applications. Instead of being transferred to medium containing flg22, roots were soaked in liquid 100 μM flg22 solution and rinsed prior to transfer to fresh 0.5MS medium plates (see Chapter 2 for detailed method). This method was based on experiments that used short exposure to flg22 (Navarro et al., 2004; Sun et al., 2006; Jacobs et al., 2011). However, in the present test flg22 treatment caused no significant change in PD development (Figure 79).

6.3.9 Salt treatment: NaCl

NaCl was used to monitor the effect of PD in response to salinity stress, a typical environmental stress that plants experience in many habitats. I used 25mM and 100mM based on growth assays that showed that 25 mM NaCl causes 5% root growth inhibition (Zhu, et al., 2002), and experiments by (Xu and Shi, 2007) using 80-150 mM NaCl, which showed that higher concentrations caused significant inhibition of many growth parameters . Under my conditions, NaCl treatment caused significant increases in root length and decreases in leaf length and (Figure 75-78). Plants exhibited a significant increase in epidermal cell size (Figure 79) with a *t*-test confirming with 95% confidence that a low concentration of NaCl (25 mM) caused an increase in cell area of between 209-514μm^2. Note, however, that the cell size was variable, hence the large standard error. This large increase in epidermal cell size was also unlinked to an increase in PD development, as mean numbers of PD were similar to controls (Figure 79).

6.3.10 Inhibitor treatment: BFA

Although not a typical stress plants would experience, the inhibitor BFA was also tested as a point of interest. The mechanism by which complex PD develop is unknown, but most models assume a contribution of proteins and membranes delivered by the secretory pathway. There are few experiments testing longer-term growth effects of BFA, with most published studies using short (<24h) applications. For my growth study I used BFA at 0.5 µM and 5 µM,based on work by (Qi et al., 2005) which showed 50% reduction in root growth in seedlings grown for an extended period on medium containing 5 µM BFA. Both concentrations of BFA used showed no effect on PD development or cell expansion in leaves (Figure 79), however.

6.3.11 Treatments and the sink source transition

Chapter 5 illustrated that accelerated complex PD development can be linked to acceleration in the onset of the sink-source transition. I therefore grew *AtSUC2::GFP* plants on x0.5 MS for 5 days and then transferred them to medium containing treatments for a further five days, exactly as had been performed for the treatment experiments. The treatments tested included those that caused increased numbers of complex PD in the preliminary experiment (SA 100 μM and 30 μM, Mann 100mM, NAA 50nM), treatments that caused alterations in cell size (NaCl 25mM and methyl jasmonate 100 μM), and 0.5MS as a control. In all cases, the pattern of GFP fluorescence observed in treated plants was similar to controls (Figure 82 shows sample leaves).

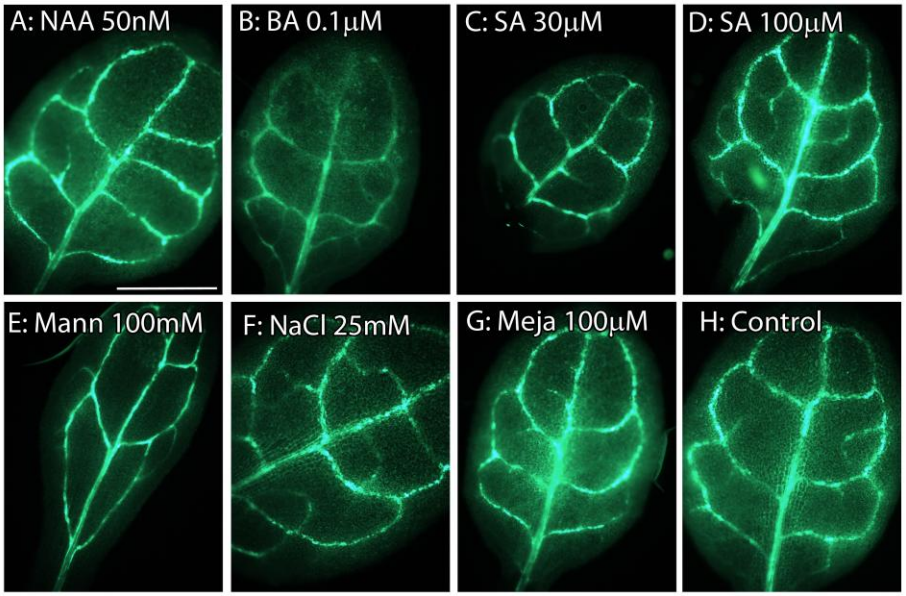

Figure 82: 3rd leaf of sample *pSUC2::GFP* plants grown for 5 days on control medium and then on treatment containing media for five days. The pattern of GFP fluorescence observed is similar in all treatments and the control.

6.3.12 Longer term effects of treatments

As young leaves were used for the study it was not possible to say from these experiments whether increases in the number of complex PD caused by treatments was due to an increase in the rate of production of complex PD, or an increase in the total overall numbers of complex PD. To test this, I used the treatment that caused the largest overall increases in complex PD numbers, 100 µm salicylic acid, and allowed the plants to grow on the treatment-containing medium for 10 days rather than 5, before imaging the 3rd oldest leaf. A graphical representation of the data (Figure 83) suggests a possible increase in the overall numbers of complex PD, but a *t*-test showed that this was not statistically significant at the 5% level.

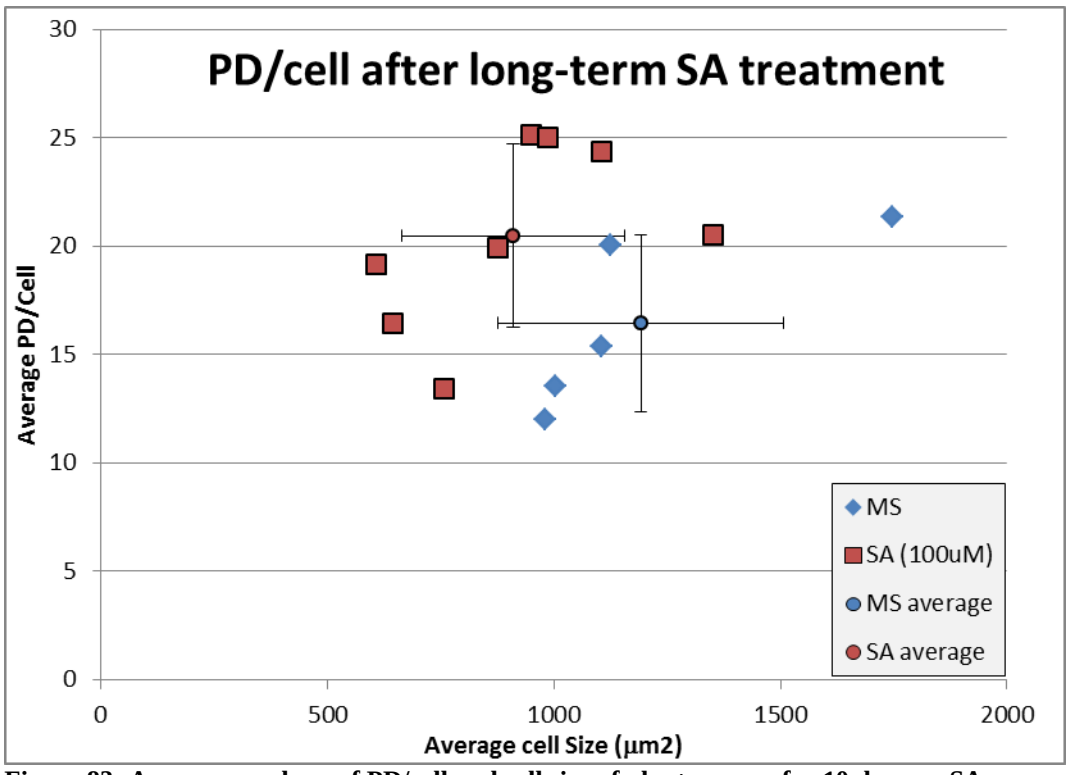

Figure 83: Average numbers of PD/cell and cell size of plants grown for 10 days on SA-containing or control medium. Each point represents an average from 12 touching cells from an imaged population of cells from the middle of the leaf, and the overall average and standard deviation of all points is shown.

6.3.13 Treatments selected for the Opera high-throughput study

From the preliminary study, 9 treatments were selected for analysis using the Opera high-throughput system (Table 6).

Table 6: Treatments from the preliminary study selected for high-throughput analysis, and the changes to PD/cell frequency or cell area observed during the preliminary experiment. Two of the selected treatments caused addition growth retardation when grown for the high through put study and so were not analysed.

Treatment	Conc.	Cell size	PD/cell	Imaged?
Hormones:				
Auxin, NAA	100 nM	No change	Increased	Yes
Cytokinin, BA	0.1 µM	Increased	Increased	No
Sugars				
Glucose	1%	No change	Increased	No
Sugar alcohols				
Mannitol	10 mM	Decreased	Increased	Yes
Mannitol	100 mM	Decreased	Increased	Yes
Defence				
Salicylic acid	30 µM	Increased	Increased	Yes
Salicylic acid	100 µM	No change	Increased	Yes
H_2O_2	1 mM	No change	Increased	Yes
Salinity				
NaCl	25 mM	Increased	No change	Yes

From the hormone treatments, the auxin NAA was selected because auxin is a major phytohormone involved in multiple aspects of leaf development and so the increases in PD numbers seen in the preliminary experiment could represent one of the endogenous signals promoting conversion of PD from simple to complex forms. The cytokinin BA was chosen because not only is it another major phytohormone, but has been shown to increase PD numbers when applied directly to SAM tissues (Ormenese et al., 2006). There is therefore the possibility that the increases in complex PD number observed in the preliminary experiment were significant, and that cytokinins could act as endogenous signals involved in co-coordinating PD development.

Glucose was chosen because experiments in previous chapters have indicated a strong relationship between sink/source state and PD development. Mannitol was chosen for the study due to the unusual combination of modified cell expansion

resulting in small, square cells and a notable increase in the number of complex PD. A high concentration (100 mM) which caused a strong effect on growth, and a lower concentration (10 mM) which caused a more attenuated effect were used for analysis at high-throughput.

From the defence-related treatments, salicylic acid was selected for analysis due to the very large increase in complex PD frequency observed. Again, two concentrations were chosen for the study (30 and 100 μM) in order to observe an attenuated and strong phenotype for comparison. H_2O_2 was also selected because ROS species have been reported to have several effects on development of complex PD, and so the increases in PD number seen in the preliminary study were of potential interest.

Finally, NaCl treatment was selected because it caused a significant increase in cell size that was not coupled to an increase of complex PD frequency. This indicates limitations in the linkage between wall stretching forces and complex PD formation, and I wished to explore this in more depth.

For the Opera experiments, certain alterations had to be made to the experimental procedure. Although seeds, media, and growth conditions were standardised as far as possible between those used at Edinburgh University for the preliminary study and those grown at The Sainsbury Laboratory for the high-throughput study, plants at the Sainsbury laboratory showed slightly slower growth. Although 10 days total growth did provide leaves of a size suitable for individual manipulation in a preliminary Opera trial performed by Martina Beck at the Sainsbury laboratory (data not shown), in the final experiment, when hundreds of leaves needed to be detached, stained, and individually mounted in precise locations, the small size was unpractical. Growth on the treatment-containing medium was therefore extended from 5 days to 6 days, which gave leaves of a similar size to those used in the preliminary experiment. Even with the 24h extension, however, plants grown on medium containing 3% glucose and 0.1 μM BA, did not produce leaves of an appropriate size to image.

Due to the difference in equipment between the preliminary experiment and the high-throughput experiment, there were also some differences in the imaging conditions.

In the preliminary experiment the imaging site could be manually selected and so images were consistently taken from the middle region of the leaf lamina. The automated imaging system takes images in the same positions in each imaging well, and as leaves were placed manually in the wells, it was not possible to position them precisely enough to ensure the same tissue regions were always imaged. Instead, nine images were taken from each leaf in a grid pattern in the centre of the imaging well to maximise the chances of obtaining images of high quality for analysis, and so provide a large range of images that should incorporate all areas of the leaf. The automated imaging analysis allowed the use of a smaller objective so that more cells could be included in each image, further increasing the population size compared to the preliminary study. However, this also meant that many images included either the vein or the edge of the leaf.

The script used for analysis was the 'small-cell' script described in Chapter 4 (Figure 34). The script produced output data in the form of a *Microsoft Excel* spreadsheet with each cell identified with a number, and parameters including total PD, cell perimeter, cell area, anticlinal PD, periclinal PD measured, and also shown as images (as an example Figure 84 shows perimeter and anticlinal PD). Although counts of periclinal PD were also made, only anticlinal PD numbers were analysed. As each cell was individually numbered, I could test the overall accuracy of the scripts by manually refining the raw data by removal of values from artefactual split or merged cells, from guard cells, the elongated cells over the midrib, trichome cells, and cells at the leaf edge. As shown in Table 7, the ratio of the raw data values to the manually refined data values is always close to 1, showing the high accuracy of the scripts.

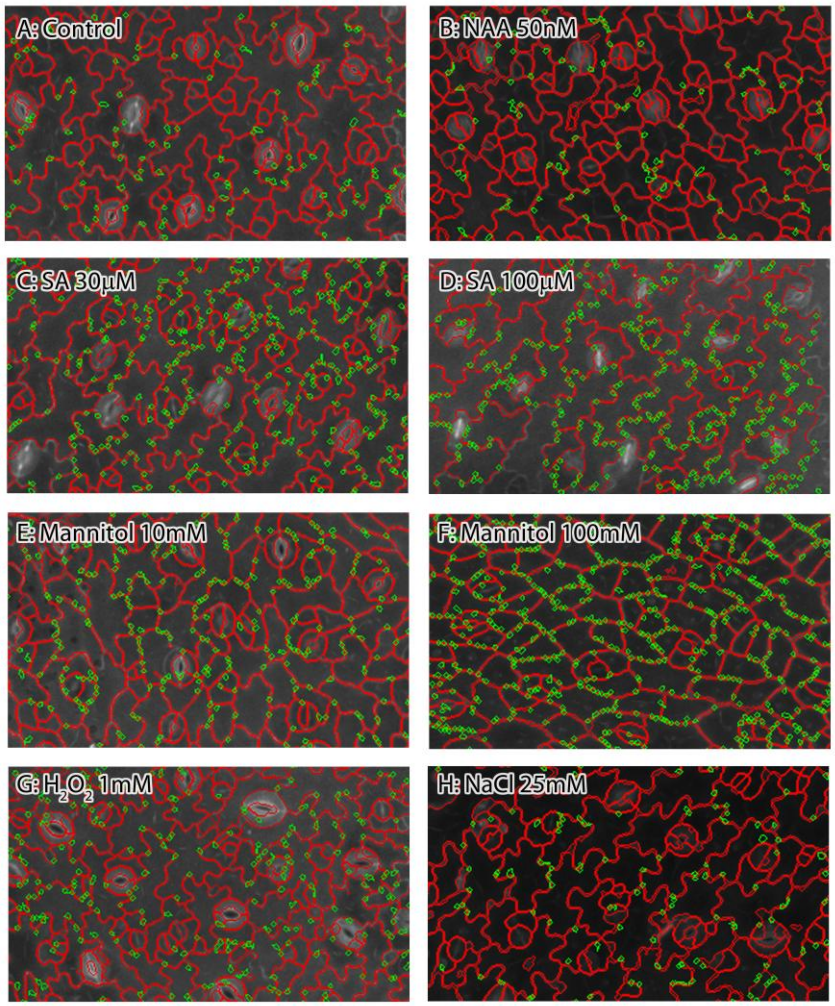

Figure 84: Sample output images from the analysis scripts showing the cell perimeters (red lines) and the locations of PD coinciding with the cell wall (green circles) for each of the treatments and the control.

Table 7: Table showing the ratio of the means from the raw data and the means from 5-11 manually refined population datasets is close to 1 for all treatments tested.

Treatment	PD per cell Raw/Refined data	Cell area Raw/Refined data
Control (overall)	1.338955	1.019784
Control (NAA)	1.055537	1.077692
NAA 50 nM	1.039462	1.037027
Control (mannitol)	1.009417	1.058217
Mannitol 100 mM	1.001337	1.016099
Man 10 mM	1.182589	1.863348
Control (SA)	1.016116	1.03475
SA 30 uM	0.921523	0.992185
SA 100 uM	0.911685	1.00136
Control (H_2O_2)	1.124912	1.068114
H_2O_2 1 mM	1.018894	1.082151
Control (NaCl)	0.984959	1.016084
NaCl	0.965011	0.966148

6.3.14 High-throughput study of treatment effects of PD development

Controls were performed in parallel with each treatment to allow direct comparison between treatment and control plants imaged at exactly the same time. These individual control populations showed some variation to one another (shown in Figure 85), with the NaCl control showing an overall smaller maximum cell size and the mannitol control showing a larger cell area; in these cases the results below are compared to the complete control dataset (reffered to as the 'overall control' population) rather than the parallel control alone. The 52 raw control datasets produced a combined analysis of >19,000 cells. Overall they had a mean cell area of 453 μm^2, an increase from that seen in the preliminary experiment of 302.07 μm^2. Likewise, the mean PD/cell values increased to 2.1 from the 0.76 as observed in the prelimary dataset. Some of this increase is to be expected because, as described, the plants were grown for an additional 24 hours before imaging.

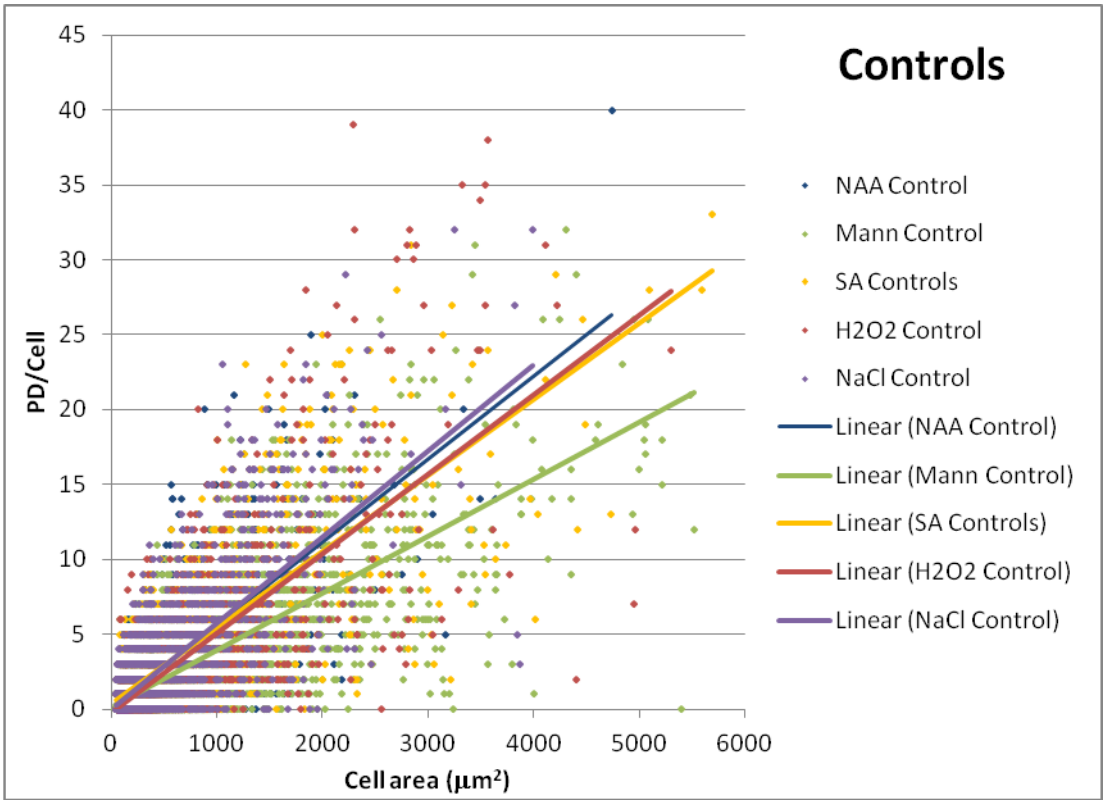

Figure 85: Graph showing individual PD/cell and area data for analysed cells from the controls done in parallel to each high-throughput experiment.

6.3.15 High throughput: auxin

High-throughput analysis of complex PD numbers from 15,000 cells from plants grown on 50 nM NAA compared to >1,400 cells from plants in the parallel control (Figure 86) show similar numbers of PD, with small decreases of 0.5-0.9 PD/cell, determined by a *z*-test at 95% confidence (Figure 93). A graphical representation against the parallel control suggests an increased cell size (Figure 86), but this is not significant (at 5%) and the cells actually show a decreased cell size when compared to the overall control of 19 – 40 μm^2 (95% confidence).

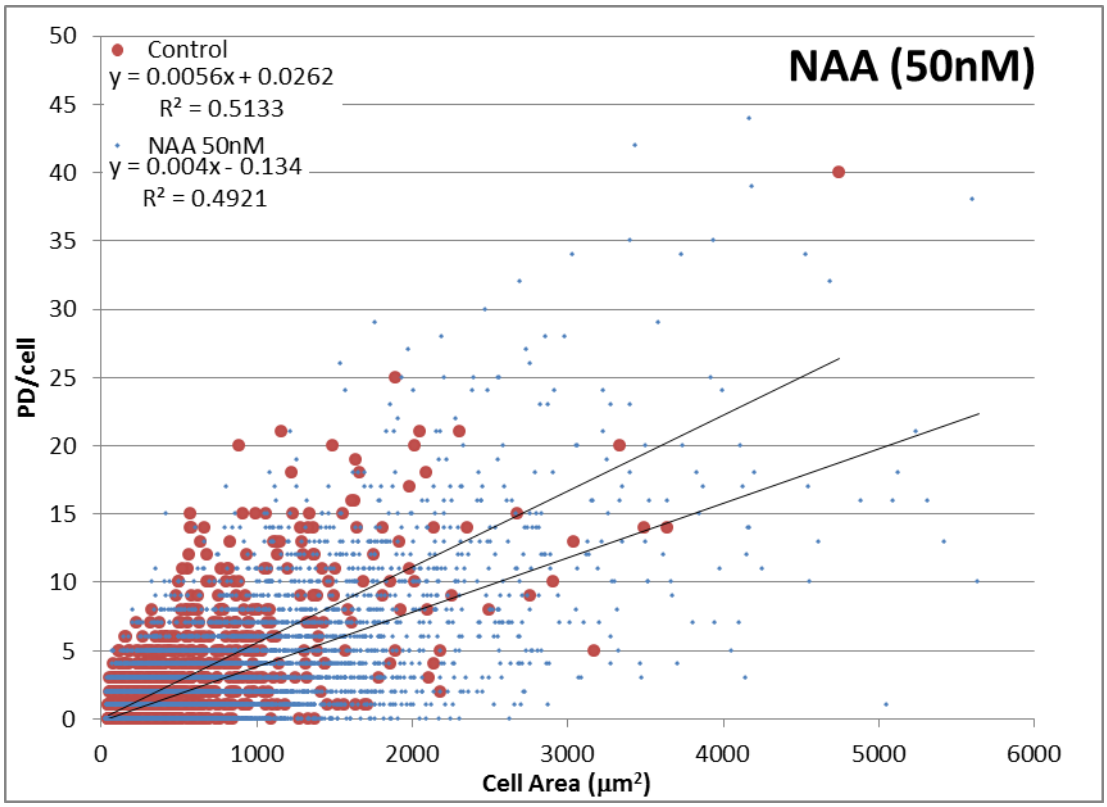

Figure 86: Graph showing anticlinal PD numbers and area for individual cells of plants grown on medium containing 50 nM NAA (blue) or grown on control medium (red) in parallel.

6.3.16 High-throughput study: mannitol

Plants grown on mannitol for the high-throughput experiments exhibited similar growth effects to those observed in the preliminary study: plants grown on a high mannitol concentration (100 mM) had narrow leaves with uniformly square or oblong epidermal cells that completely lacked the interdigitating lobes which give the epidermal cells their characteristic jigsaw appearance (Figure 84). However, at low concentrations of mannitol (10 mM), the cell shape effect was more attenuated in the population grown for the high-throughput study, with cells showing some lobing (Figure 84E), rather than the square cells observed in the preliminary study (Figure 80A). Unlike the preliminary study, however, both concentrations caused a small but significant increase in the overall cell size compared to the parallel control (Figure 79), of 85-112 μm^2 in 10 mM- and 44-67 μm^2 in 100 mM mannitol-treated plants (95% confidence). The controls grown in parallel with this experiment had unusually large cell sizes (Figure 85), and the mannitol-treated plants show much larger cell sizes compared to the overall control population, with increases of 105-127 μm^2 (10 mM) and 65-81 μm^2 (100 mM) observed (95% confidence).

Both concentrations produced an increase in complex PD frequency. From plants grown on 10 mM mannitol >22,000 cells were imaged and quantified versus >9,000 cells from the parallel control populations (Figure 87). A *z*-test, showed that the difference between the mannitol-grown sample mean and the control lies within 2.71 and 2.89 PD/cell (95% confidence) (Figure 93). From plants grown on 100 mM mannitol, >19,000 cells were imaged and quantified against the same parallel control population (Figure 88) the difference between the test sample mean and the control lies within 2.79 and 2.95 PD/cell (95% confidence) (Figure 93). Similar increases of 2.5-2.7 PD/cell was seen when both 10 mM and 100 mM mannitol treated plants were compared against the overall control (95% confidence) (Figure 93). A linear regression of the data when plotted against cell area shows that the gradient of the trendline is increased for both low and high concentrations of mannitol (Figure 87-Figure 88). This suggests that increased PD numbers were coupled to cell area, with the largest cells showing the greatest relative increase in complex PD numbers relative to the control population.

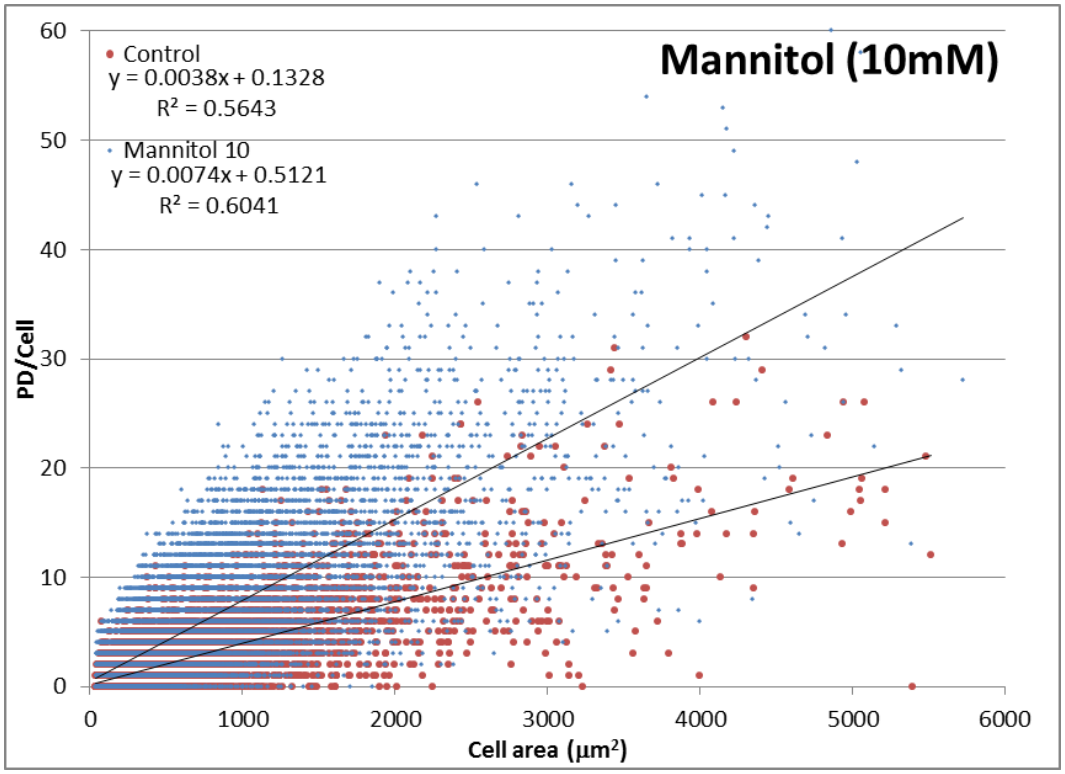

Figure 87: graph showing anticlinal PD numbers and area for individual cells of plants grown on medium containing 10 mM mannitol (blue) or control medium (red).

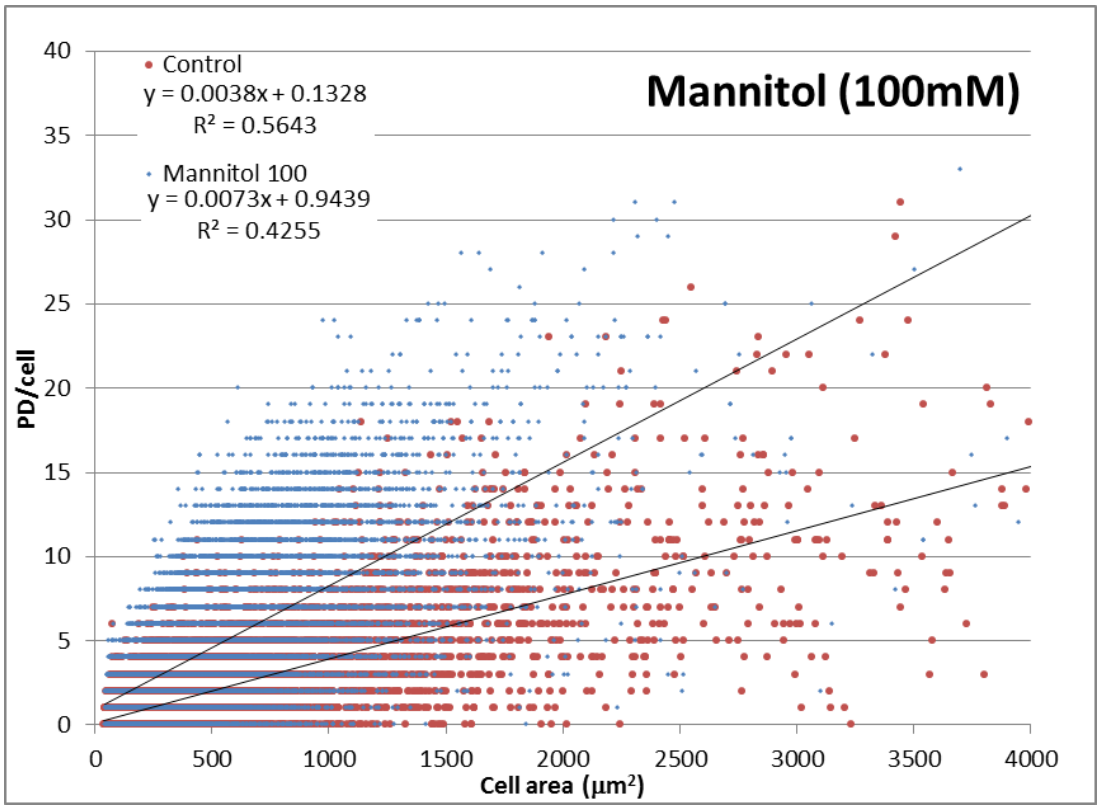

Figure 88: graph showing anticlinal PD numbers and areas for individual cells for plants grown on medium containing 100 mM mannitol (blue) or control medium (red).

6.3.17 High-Throughput study: Salicylic Acid

The high-throughput data for plants grown on 30 µM SA, the lower concentration used, showed a small but statistically significant (from a *z*-test at 95% confidence) increase of 0.4 - 0.9 PD/cell compared to the mean of the control data (Figure 93). The plants grown on 100 µM SA showed a much larger increase in PD numbers in the >800 cells from plants grown on 100 µM salicylic acid versus >1,500 cells in the parallel control population (Figure 90). From this data a 'z'-test shows with 95% confidence that the difference between the means of the 100 µM SA grown and control plants is between 2.2 and 3.1 PD/cell (Figure 93). This reinforces the strong increase in PD/cell observed in the preliminary experiments using plants treated with SA (Figure 79).

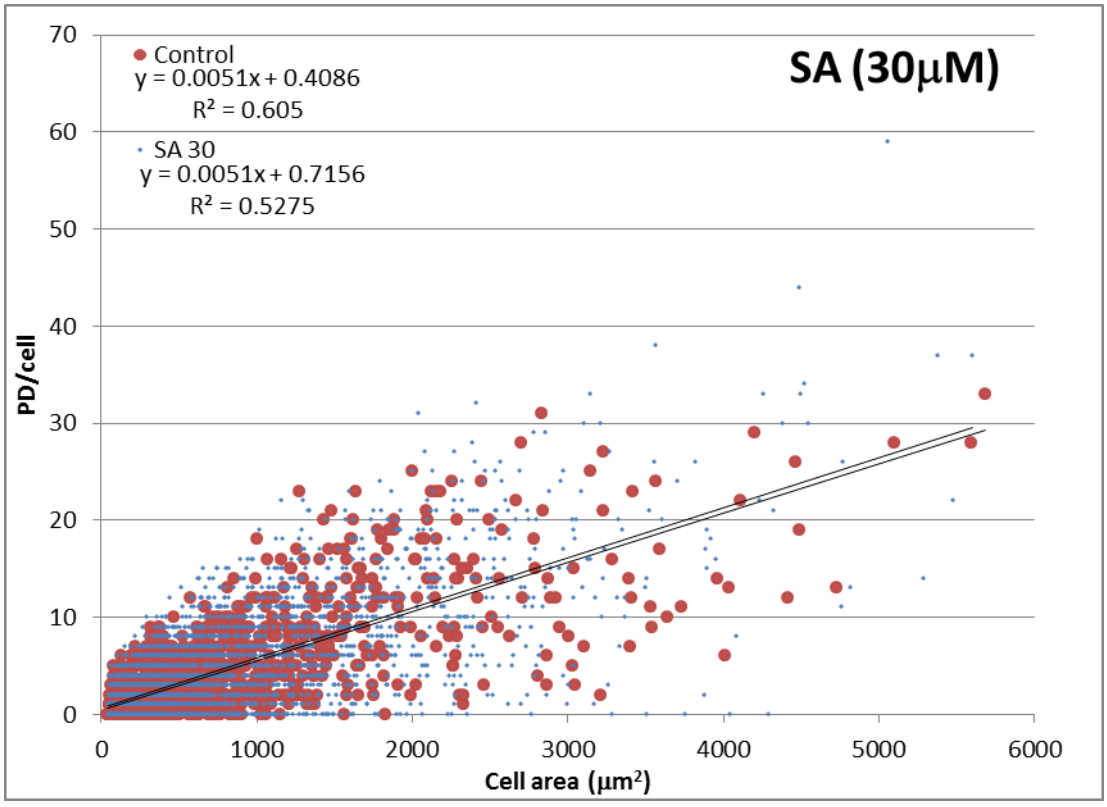

Figure 89: graph showing anticlinal PD numbers and areas for individual cells for plants grown on medium containing 30 µM SA (blue) or control medium (red).

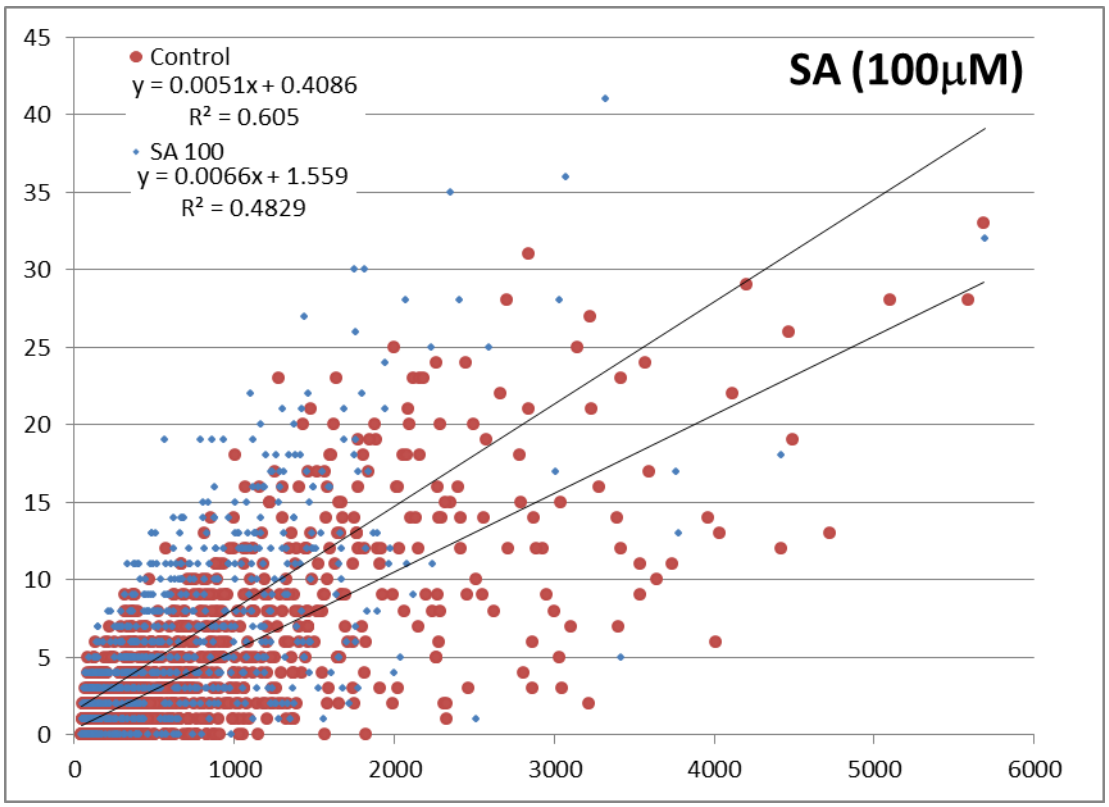

Figure 90: graph showing anticlinal PD numbers and areas for individual cells from plants grown on medium containing 100 µM SA (blue) or control medium (red).

6.3.18 High throughput study: H_2O_2

Analysis of >2,100 cells from plants grown on 1mM H_2O_2 compared to >3,800 cells from control plants grown in parallel produced very similar datasets (Figure 91), with H_2O_2-grown plants showing a small increase of 0.5-0.8 PD/cell (95% confidence) (Figure 93) unlike the larger increase observed in the preliminary experiment.

6.3.19 High throughput study: NaCl

When analysed at high throughput, a comparison of >9,500 cells from plants grown on 25 mM NaCl with >1,400 cells from the parallel control population (Figure 92) showed a small decrease of 0.2-0.6 PD/cell (from a *z*-test at 95% confidence) (Figure 93), as expected from the preliminary experiment which showed very similar numbers of PD in NaCl-grown and control plants (Figure 79). When analysed at high-throughput, NaCl grown plants showed only a small increase in cell size of 45-88 µm^2 (95% confidence), a reduction from the approximate doubling of size observed in the preliminary experiment (Figure 79).

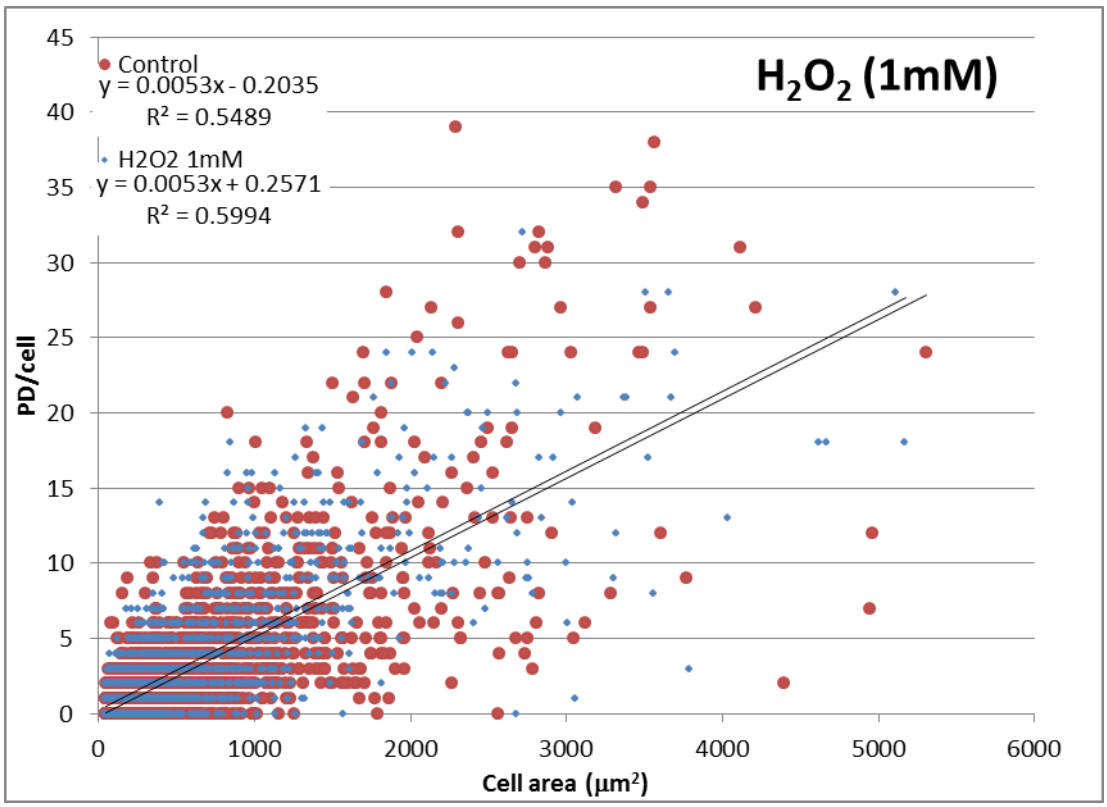

Figure 91: graph showing anticlinal PD numbers and areas for individual cells from plants grown on medium containing 1 mM H_2O_2 (blue) or control medium (red).

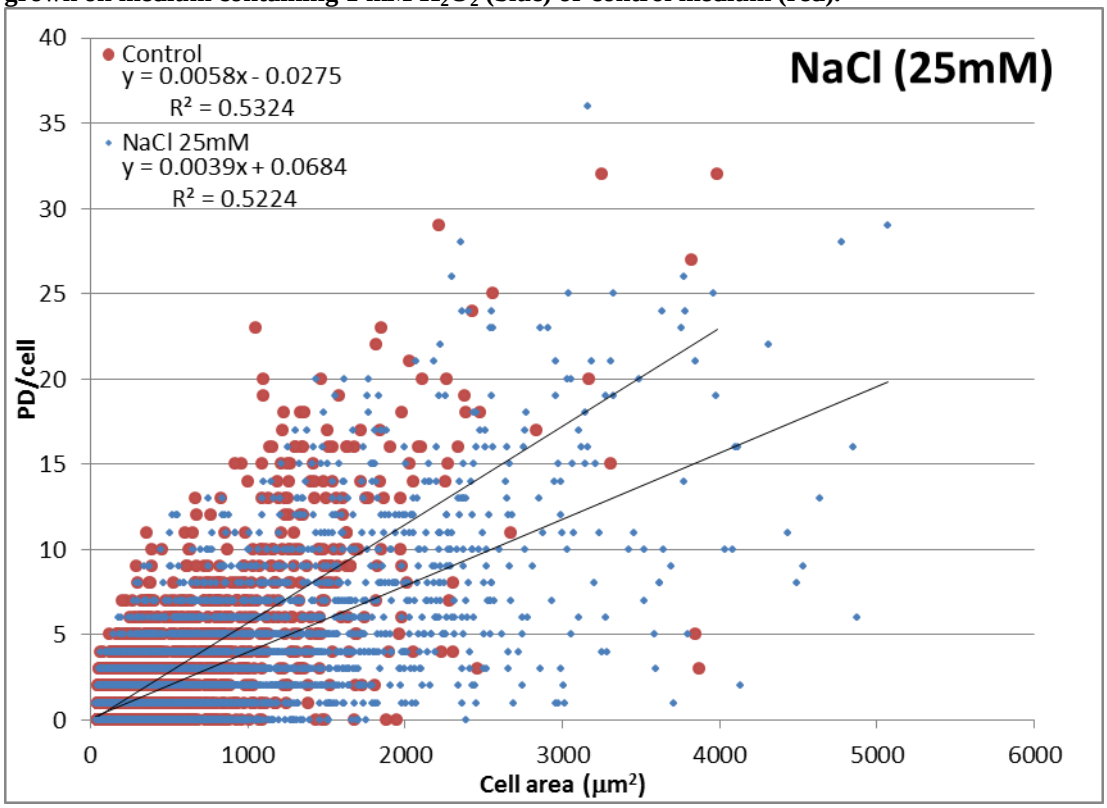

Figure 92: graph showing anticlinal PD numbers and areas for individual cells from plants grown on medium containing 25 mM NaCl (blue) or control medium (red).

6.3.20 Overall results from the high-throughput study.

The high-throughput system showed unambiguously that treatment of plant roots with SA and mannitol causes an increase of complex PD development (Figure 93) Other treatments which had shown strong effects in the preliminary experiment, either on complex PD development (H_2O_2 and the synthetic auxin NAA), or on cell expansion (NaCl) (Figure 79), showed weaker effects when analysed using high-content screening (Figure 93). The results of the preliminary and high-throughput study are compared directly in Table 8, showing how high-throughput study reduced the rage of variations in both cell area (from 188-634 to 424-625 μm^2) and complex PD numbers (from 0.8-8.9 to 1.6-5.7 PD/cell).

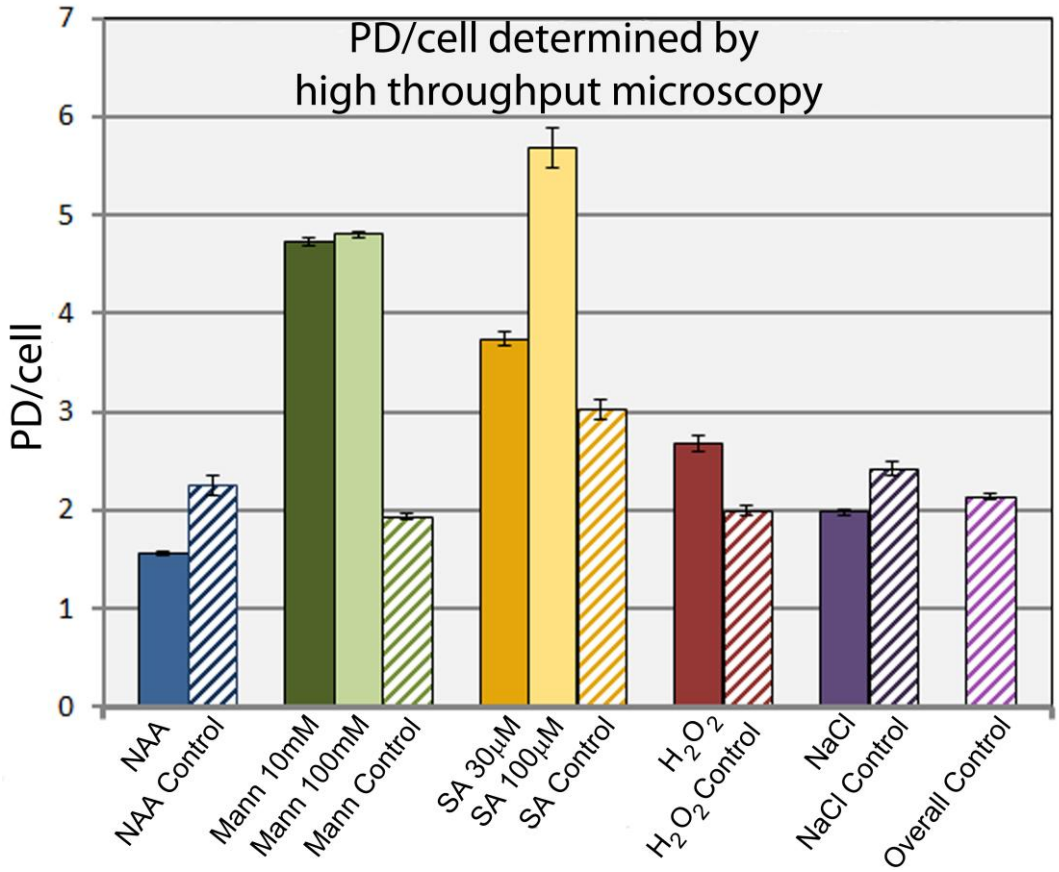

Figure 93: histogram showing the mean PD/cell for each treatment in the high-throughput experiment compared to a parallel control. Bars are standard errors.

Table 8: Table comparing the values for mean cell area and mean PD/cell from the preliminary and high-throughput experiments. Orange indicates a decrease in the high throughput study compared to the preliminary study, and light green indicates an increase.

Treatment	Preliminary cell area (µm^2)	High throughput cell area (µm^2)	Preliminary PD/cell	High throughput PD/cell
Control	302	453	0.8	2.1
NAA 50nM	306	424	7.9	1.6
Man 10mM	188	570	1.2	4.7
Man 100mM	210	527	2.6	4.8
SA 30uM	484	588	4.7	3.7
SA 100uM	372	625	8.9	5.7
H_2O_2 1mM	285	457	4	2.7
NaCl 25mM	663	491	2.3	2

6.4 Discussion

6.4.1 High-throughput imaging for PD developmental studies

The results demonstrate the possibilities of high-throughput microscopy for studying PD development in a way not previously possible. Using the Opera system, the complete anticlinal cell walls of over 70,000 cells were imaged and analysed, allowing clear effects on the development of complex PD caused by growth conditions to be observed and quantified.

The results also indicate the risks of inferring effects on PD from small sample sizes. Traditionally, EM approaches have been used in studies of PD structure and development, and these necessitate small sample sizes (e.g. Stonebloom et al., 2009). My preliminary study using CLSM imaging represented a large increase in sample size compared to many EM studies, as typically the full depth of all anticlinal cell walls of at least 100 cells were analysed per treatment. This preliminary study indicated strong effects on PD and/or cell size that were not always substantiated by a high-throughput analysis looking at larger populations.

The experiments described also indicate how the high variability of PD development in plants can complicate analysis. Due to the equipment used, the preliminary study and the high-throughput study were performed in two separate laboratories, the former at Edinburgh University and the latter at the Sainsbury Laboratory, Norwich. Despite using standard growth conditions, medium, seeds and method, the plants

used for the high-throughput experiment grew more slowly than those used in the preliminary study, necessitating extension of the growth period by and additional 24h to produce leaves large enough to be imaged. Plants grown on two treatments that had been imaged reliably in the preliminary study, the cytokinin BA and 3% glucose, did not produce leaves of sufficient size to be imaged and were not included in the experiment. Despite the decreased size of leaves grown for the high-throughput study, however, the cells of these leaves were consistently larger than those analysed in the preliminary experiment (Table 8), including those of mannitol-treated plants that had shown a clear and reliable size decrease in the preliminary study with a very little standard deviation. The variation in growth rates of plants grown under standardised conditions in different laboratories has been shown to be significant (Massonnet et al., 2010). This variation is likely to be even more exaggerated in terms of PD development, which Chapter 4 demonstrated may vary significantly in populations grown in a single laboratory. It is therefore expected that the some of the inconsistency between the two experiments may not be due to the population size, but also to changes in growth parameters.

6.4.2 Complex PD and exogenous hormone treatments

Both auxin and cytokinin were tested as these two phytohormones are considered 'master regulators' of multiple facets of plant development.

Auxin is involved in wide array of developmental processes, particularly in leaves. Polar auxin flow through polarised PIN protein localisation produces auxin maxima in the SAM from which leaf primordia develop, and canalisation of auxin within the primordia determines the positioning of the midrib and influences vein structure. Auxin accumulation acts in different contexts to determine various aspects of leaf development including the 3D-shape of the leaf, the position of leaflets and adaxial-abaxial patterning (Scarpella et al., 2010). A relatively large increase of between 4.8-9.5 PD/cell compared to controls was suggested by the preliminary test, but this was not borne out by the high-throughput data which showed a much smaller increase of 0.5-0.9 PD/cell. However, as with all of the treatments in this experiment, this does not prove that auxin has no role in PD development. Although it was expected that the auxins applied in these experiments would be able to act directly on leaves (as

exogenously applied auxin is transported through the xylem and can also move radially from xylem to phloem) and so was likely to reach the tissues of interest (Zamski and Wareing, 1974, and references therein), this was not tested. Further, more direct experiments would be required to unambiguously show the effects on auxin.

Cytokinins were one of the more promising candidates for a potential co-ordinator of PD development, as they are one of the few known factors to promote changes in PD populations when applied exogenously (Ormenese et al., 2006), and they are known to be transported from roots to shoot and may promote modification of leaf physiology in response to stresses (Bradford 1983; Ghanem et al., 2011). An increase of between 3.2 and 9.1 complex PD/cell was observed in plants grown on medium supplemented with the highest concentration of cytokinin in the preliminary experiment. However, when the experiment was repeated for the high-throughput experiment, the plants showed retarded growth that prevented imaging. The effect of cytokinin on plant development therefore requires further testing.

6.4.3 Complex PD and exogenous sugars

The link between complex PD and source function in leaves made sugars attractive potential candidates for factors able to coordinate PD development. Chapter 5 showed that sink leaves could be induced to mature and produce complex PD if all of the source tissues were removed from the plant. This suggested the possibility that cessation of import might stimulate PD development, although in my detachment experiments (Chapter 5) exogenous sucrose could not compensate for removal of source tissues.

The preliminary experiment suggested that exogenous sucrose treatment caused only small increases in complex PD development of 0.3-2.1 PD/cell, but suggested that one of the component monosaccharides of sucrose, glucose, could promote caused relatively large increases of between 1.6 and 6.3 PD/cell compared to the control. As with plants grown under the influence of cytokinins, plants grown on 3% glucose medium showed an unexpected growth retardation that prevented them from being imaged for the high-throughput experiment to confirm this.

6.4.4 Complex PD and osmotic stresses using sugar alcohols

Mannitol consistently increased numbers of complex PD in leaves in both the preliminary and high-throughput studies. These significant increases of 2.79 and 2.95 PD/cell compared to controls (for 100mM mannitol-grown plants) as much as double the number of complex PD per cell, while the lobing of the cells is highly reduced. Mannitol was used in this study with the intention of showing the effect of osmotic shock on PD development as mannitol (and, to a lesser extent, other sugar alcohols) have long been used by researchers to investigate effects of osmotic stress on plants. Sugar alcohols can be added to growth media to increase the osmotic potential and, it is assumed, will penetrate tissues slowly on account of the six hydroxyl groups in the structure, and should not be metabolised by the plants (Cram, 1984). Mannitol does cause a measurable osmotic effect on many plant tissues and these can affect PD; treatment of pea roots with 350mM mannitol caused a transient widening of PD and an increase in symplasmic connectivity in affected tissues ~1hr after application (Schulz, 1995). Mannitol naturally functions in many species as a non-metabolised 'compatible solute' produced in response to osmotic stresses as it can accumulate in cells as an osmolyte without disrupting metabolism (Stoop et al., 1996). Mannitol functions in some species as an osmoprotectant (Zhifang and Loescher, 2003, and references therein), increasing resistance to salinity stress. Certain species, such as celery, can metabolise mannitol, and translocate a proportion of their photoassimilate as mannitol (discussed in Trip et al., 1964, and Turgeon, 1989). *A. thaliana* is not one of these, and does not naturally contain mannitol (Zhifang and Loescher, 2003).

Osmotic shock generally results in a reduction in leaf growth, usually due to a combination of factors; a reduction in cell expansion due to lowered cell turgor or reduced uptake of water into the cells, or a reduction in cell division. Leaf narrowing and epidermal cell shape alteration as observed here are not common reactions to osmotic stress, and effects on division are usually compensated for by changes in growth rates (discussed in Fricke and Peters, 2002). Skirycz et al. (2011) also observed this kind of growth compensation in experiments that used a low concentration of mannitol (10mM) to investigate the effects of continuous low-intensity stress on plants in a set-up very similar to my treatment experiments. Upon onset of stress conditions they observed an acute growth response where expression

of cell-cycle related genes was down regulated, ethylene-related genes were upregulated and cell division rates were drastically reduced. However, within 72h of mannitol treatment, cell division rates returned to normal and, later, even showed a compensatory increase compared to controls, referred to as an adaptive growth response. Some of this compensative growth appeared to come from increased division activity of meristemoids, resulting in more pavement cells. This group also observed that growth on mannitol-containing medium reduced the lobing of cells, but as the researchers were using low concentrations of mannitol (25 mM) the effect was not pronounced.

However, the suitability of mannitol as a ubiquitous osmoregulator has long been questioned, and there is much evidence to show that it may have additional effects. Lipavska and Vreugdenhil (1996) showed that mannitol is taken up from the growth medium by some species and transported to shoots. Etxeberria et al. (2007) showed that mannitol may enhance fluid-phase endocytosis in certain cell types. Brainerd and Fuchigami (1982) showed that mannitol causes closure of stomata in detached leaves. Trip et al. (1964) fed leaves of different species with [^{14}C] mannitol and showed that of the 26 species tested, 15 appeared to metabolise mannitol, 4 of which (including potato, which has been used in many mannitol-driven osmosis studies) had not been previously shown to naturally contain mannitol. This itself is not too surprising as it has been shown that certain plants can metabolise entirely artificial sugars not found in nature, such as allose (cited in Trip et al., 1964). The metabolism may also be related to defence; some fungal pathogens secrete mannitol in the presence of the host plant to, it is thought, quench ROS produced by the plant defence response (Jennings et al., 2002; Stoop et al., 1996). Mannitol has been shown to activate plant defence genes and many plants which do not themselves produce mannitol have functional mannitol dehydrogenase enzymes, including *A. thaliana*.

To try and gain better understanding of the observed effects of mannitol treatment, plants were grown on sorbitol, a sugar alcohol isomeric to mannitol. Like mannitol, sorbitol is naturally produced in plants and some species use it as a major transport sugar (Turgeon, 1989), and it can be added to growth media to induce osmotic stress

in experimental systems (Jain et al., 2010). In practice, plants grown on 100mM sorbitol did not show either the altered cell shape or the increased numbers of complex PD observed in mannitol grown plants. Also, unlike mannitol treatment, sorbitol caused root inhibition and gain of fresh weight similar to that observed in plants grown on sucrose and glucose containing media, suggesting that in this context sorbitol is not comparative to mannitol.

High-throughput technology has therefore identified mannitol as a substance capable of significantly altering PD development, and has shown again that complex PD development can be completely unlinked to cell wall expansion patterns. Due to the unusual effects on cellular and leaf morphology, this experiment does not show directly that osmotic stress is the cause of the changes to PD development, however, presenting an avenue for future research.

6.4.5 Complex PD and treatments related to defence responses

Although it is expected that PD must be modified as part of the defence responses of plants, no examples of changes to PD frequency or architecture are known other than deposition of callose at pores (Lee and Lu, 2011). To test this, I exposed plants to a range of substances expected to stimulate various aspects of the defence response: salicylic acid, which caused a significant increase in complex PD numbers, and H_2O_2, methyl jasmonate and the flagellin peptide flg22.

Salicylic acid caused a significant increase in the numbers of complex PD in leaves of treated plants in both the preliminary and high throughout experiments, more than doubling the numbers of complex PD observed. SA was used because it is integral to the development of systemic acquired resistance (SAR): the broad-spectrum resistance that develops in uninfected tissue after a localised infection. SA is produced at sites of infection as part of the local defence response and then is exported through the phloem as methylsalicylic acid, and then converted back to SA in distal tissues where it promotes the expression of genes involved in defence responses such as Pathogenesis Response (PR) genes (Ryals et al., 1996; Spoel and Dong, 2012). Application of exogenous SA induces SAR to develop, and as restriction of PD SEL is a known aspect of the plant defence response, conversion of existing PD from simple to complex could function in plant defence. However,

salicylic acid is also a major plant hormone and plays numerous roles, including signalling response to a wide range of abiotic stresses such as high and low temperatures, salinity, osmotic and heavy metal stresses (reviewed in Rivas-San and Plasencia, 2011). This means that the acceleration in complex PD numbers could be part of a defence response against stress, rather than infection in particular.

The idea that the SA response may not be related to plant defence is supported by the fact that the other defence related treatments caused no notable effect on complex PD development. Methyl jasmonate acts as an inter-plant signal in defence, produced as a gas from the leaves of infected plants that promotes pre-emptive PR gene expression in neighbouring plants (Farmer and Ryan, 1990). Methyl jasmonate can be taken up from root growth medium to inhibit root elongation and induce accumulation of nutrient storage proteins in leaves (Staswick, et al., 1992), but may not function in defence in the same way as gaseous methyl jasmonate. Hence the fact that no effects on complex PD numbers were observed is not necessarily informative about the effects of the defence response on PD development. The bacterial peptide flg22, however, is a potent elicitor of defence responses, both as part of the flagellum of a pathogenic bacterium and as an isolated peptide. This 22 amino acid motif is recognised by plant resistance genes (R-genes), which then activate plant defence responses including the hypersensitive cell death response and the development of SAR. The absence of an effect on complex PD numbers after exposure to flg22 suggests that upregulation of complex PD development is not an integral part of the SAR defence response. However, due to the strong response induced by flg22, in this experiment it was administered as a single application rather than added to the growth medium as SA was, and so the two experiments are not directly comparable. Further work will be required to determine which of the many roles played by SA is involved in promoting the development of complex PD.

Plants grown on H_2O_2 treatment media showed a mild increase of between 1.5 and 5 PD/cell in the preliminary experiment, but <1 PD/cell when the experiment was repeated at high-throughput. H_2O_2 was tested because it is part of the local response to infection, and is one of the ROS produced as part of the oxidative burst that following pathogen detection to induce the hypersensitive cell death response

(McDowell and Dangl, 2000) and to activate PR gene expression (Chen et al., 1995). As well being involved in defence, ROS have been shown to cause increases in the number of complex PD through analysis of *gat* and *ise* mutants (Stonebloom, et al., 2012), as discussed in the introduction of this chapter. H_2O_2 itself has not been shown to be directly responsible for the PD phenotype seen in these mutant lines but paraquat, a metabolic inhibitor which induces H_2O_2 production, was shown to mimic the effects of *gat* (Stonebloom, et al., 2012). However, as the application of H_2O_2 was indirect in my experimental system, the small effect on PD does not mean that H_2O_2 does not cause the effects observed in the *gat* line.

6.4.6 Complex PD and salinity stress

Growth of plants on media containing a relatively low concentration of NaCl in the preliminary experiment caused no significant effect on PD, but caused a highly significant increase in cell size. I chose to repeat the experiment at high-throughput for two reasons. The first was that it would provide another example of complex PD development being uncoupled from cell expansion and stretching forces in the wall. The second was that this increased cell expansion effect of salt stress was unexpected as salinity stress causes inhibition of leaf and cell expansion under most circumstances. Salt stress has multiple effects on plants, directly disrupting the nutrient, ionic and osmotic balance of tissues. This has multiple knock-on effects to many aspects of cell function and growth, including a large effects on photosynthesis and respiration, as shown by various physiological and proteomic studies (reviewed in (Zhang et al., 2012). The turgor effects of salt stress are compensated for by modifications to the cytoskeleton: salinity stress can stabilise actin microfilaments and bundles, while microtubules depolymerise on exposure to salt and, upon repolymerisation, display altered growth orientations (reviewed in Wang et al., 2011). Expression levels of wall-modifying enzymes are also altered (reviewed in Zhang, et al., 2012), although this would not usually promote cell expansion.

When the experiment was repeated at high throughput, NaCl-grown plants showed only a relatively small increase in cell size. As the growth conditions used for the preliminary and high-throughput experiments did not result in comparable growth

rates, the cell size effect I observed in the preliminary experiment could have been genuine, and should be investigated further.

6.4.7 Final words

In this chapter, I took advantage of newly available high-throughput microscopy methods to survey the effects of various additives to root growth media on complex PD development. The unprecedented breadth of this study, which measured complex PD numbers in over 70,000 cells from 118 different plants allowed me to identify highly significant increases in PD numbers induced by salicylic acid and mannitol. The underlying causes of these effects remain to be elucidated, and much further research could be done to build on the results presented here.

The high throughput experiments presented here and in Chapter 4 demonstrated that we now have the technology to quantify PD, and reliably screen for effects on their development. This technology therefore holds great potential for the future of PD research, and opens the door for further treatment screens as presented here, and also genetic screens to identify mutants with PD development phenotypes. The advent of new technology in light microscopy is now lowering the barriers to our understanding of the structure and development of PD.

6.5 Acknowledgements and thanks

The high-throughput work in the chapter was again done in collaboration with Silke Robatzek at The Sainsbury Laboratory, Norwich. I am very grateful for the assistance of Martina Beck in experimental design, optimisation and imaging and maintenance of plants, and of Ji Zhou for the design, optimisation and production of the scripts. Additional thanks to Gary Loake for advice on defence-related treatments.

7 Discussion & Conclusions

The overarching aim of this project was to investigate long-standing questions about the development of plasmodesmata using a light microscopy approach facilitated by a combination of recent advances in microscopy techniques and the availability of new and established markers for labelling PD. In particular, a specific marker for complex PD allowed for me to investigate the development of these PD at a much broader scale than has previously been possible. This enabled me to examine the development of these complex PD at a range of different levels; from individual cells to whole leaves; to look both statically and dynamically; and to understand the factors that co-ordinate their development from those at the level of individual walls, to those affecting whole leaves over time.

7.1.1 The aims of this project

My aims, as described in Chapter 1, were:

- **Aim 1: Investigate the suitability of available fluorescent markers and microscopy techniques for studies of PD development, and investigate the structure of PD using super resolution microscopy techniques**
- **Aim 2: Survey the development of PD in leaves, particularly during the large scale development of complex PD that accompanies the sink source transition**
- **Aim 3: Follow complex PD development in real time.**
- **Aim 4: Investigate the factors that control and co-ordinate the development of complex PD in leaves.**

This thesis has presented the experimental programme through which each of these aims was challenged and discussed the significance of the results obtained at the end of each respective chapter. However, to briefly summarise the rationale and overall findings:

The first part of Aim 1 was addressed in *Chapter 2: Imaging Plasmodesmata*. In this chapter I conducted an imaging survey of two PD-localised proteins that were potential markers for both simple and complex PD in A. *thaliana*. These were; the endogenous plant proteins PDLP1 and PDCB1, and two markers specific for complex PD; the viral proteins MP30K and MP17. However, I found that both of the

available simple PD markers were not specific enough for accurately quantifying PD. However, analysis of transgenic plants expressing MP17-GFP using CLSM, FESEM, TEM and SIM produced high-resolution images showing the locations, arrangements and ultrastructure of MP17-GFP labelled PD. These experiments provided strong evidence that this marker is specific to complex PD in epidermal cells.

The second part of Aim 1 was also addressed in *Chapter 2*, where MP17, MP30, callose, and PDCB1- labelled PD were all imaged using Structured Illumination Microscopy. This work presented the first published super-resolution images of PD, and some of the first SIM images of plant tissues in general. In particular this work gave new insights into the structure of complex PD, providing the first three-dimensional views of PD, and was able to image the fine detail of PD cavities and necks both in small complex PD with ~2-3 necks, larger branched PD with >5 necks, and in expanded pitfields containing >15 necks.

Aim 2 was addressed in Chapter 2 and in *Chapter 3: Complex PD and Leaf Development*. Chapter 2 showed the fine detail of PD in the epidermal and mesophyll layer, as discussed above. Chapter 3 used MP17-GFP to conduct the largest scale survey of PD development undertaken to date. Using high-throughput confocal microscopy I was able to image and analyse ~11,600 cells and 330,000 PD. By studying such large populations of PD I was able to accurately observe developmental trends during leaf maturation that would normally be obscured by the natural variation that occurs during PD development. This work illustrated that the overall pattern of complex PD formation in plate- and soil-grown plants was very similar regardless of the differential growth rates and sizes of plants. It also showed that there were separate developmental patterns of PD in different interfaces of the same cells, and that these trends were controlled at the level of the leaves, rather than the component cells. Using conventional CLSM I was able to observe PD development at the cellular level, and saw that complex PD development is influenced by the position of the PD in the walls, by the identity of the cells sharing the wall, and by the location of the cell-cell interface within the leaf.

Aim 3 was addressed in *Chapter 4: Dynamic views of PD development*, which presented the first views of complex PD development in real time. This was conducted using detached leaves maintained in a semi-enclosed imaging chamber. The use of detached leaves was expected to be a restriction of the system. Instead, it led to the unexpected finding that detachment stimulates early maturation of sink leaves, causing the precocious onset of the sink-source transition, vein maturation and the widespread development of complex PD from cells previously displaying only simple PD. This made the system especially suitable for studying PD, and I was able to observe PDLP1-labelled (simple) PD converting to PD labelled with both PDLP1 and both MP17 (complex). This showed, for the first time, that PD architecture may be modified rapidly by the leaf if required. This challenges the prevailing view of PD as static structures that respond slowly to change. It also provided additional support for the cell-based control of complex PD development observed in Chapter 3, as I was able to observe patterns of PD development related to cell-identity developing in real-time.

Aim 4 was addressed in Chapter 4 and *Chapter 5: Co-ordination of Complex PD Development*. Chapter 4 showed that the programme of complex PD development can be accelerated when required, and is stimulated upon leaf detachment. *Chapter 5* investigated the effect on PD development using a range of phytohormones, defence-related signals, exogenous sugars, salt, and an inhibitor. This was done first in a preliminary study, and then in a more focused study using high-throughput microscopy. This work suggested broadly that a wide range of factors may influence complex PD development, both positively and negatively. Significant effects were observed in plants treated with mannitol, which caused changes in cell and leaf expansion rates possibly due to osmotic stress, and salicylic acid, which is a signal involved in responses to a range of stresses and infection. It also showed that cell expansion and PD development may be unlinked, treatments causing changes in one parameter not always causing changes in the other.

I believe this experimental programme successfully achieved the aims as outlined in the introduction, giving new data and insight into the development of complex PD using a novel light microscopy approach.

7.2 Overall trends observed in this work

The interpretation and significance of individual experiments was discussed in depth at the end of each appropriate chapter. However, there were several over-arching patterns regarding complex PD and their development that emerged over the course of the project as a whole, and some important findings deserve special emphasis.

7.2.1 The importance of complex PD

That PD are essential to plant function has been established beyond doubt. PD are fundamental to a vast array of cellular processes and underlie many of the features intrinsic to plant function. Mutational studies have confirmed that even tangential effects on PD function may be lethal. However, the significance of *complex* PD is less well understood, mainly because there is no reliable way of perturbing complex PD specifically, and because PD architecture has been difficult to survey on a broad scale. One can infer that complex PD are important to higher-plant function due to the correlation of mature PD with mature cells (Roberts et al., 2001), although the significance or necessity of this is not understood.

My experiments using detached leaves provide strong evidence that complex PD are vital to tissue maturation in general and leaf function in particular. When young leaves, ranging from the youngest sink leaves of <1mm length to older leaves approaching maturity, were detached they began an immediate 'fight for survival'. All leaves converted immediately from dependent sink organs to self-sufficient source organs, presumably in order supply their own energy requirements as the first steps to potential organ regeneration and long-term survival. It is telling of the importance of complex PD to tissue maturation in general and leaf function in particular that one of the first responses of these leaves upon detachment is to modify their PD. Equally, these minute leaves have only limited stored resources and photosynthetic capacity to fuel this rapid maturation. Therefore, conversion of simple to complex PD must represent significant energy costs in terms of wall modification, membrane remodelling and the production of proteins for PD construction. Despite this, the extent of PD modification in these leaves is similar to that observed in much larger maturing attached leaves that are still supplied with photosynthate by the supporting plant.

7.2.2 Support for the 'Twinning' model of PD development

Prior to 2008, the exact mechanism by which complex PD develop had largely escaped detailed study. It was known that the majority of primary PD forming at cytokinesis were simple, and it was largely assumed that the complex PD that appeared during development were new secondary PD that were inserted into the wall by an unknown mechanism that largely rendered them branched by default (Ehlers and Kollmann, 2001). However, in 2008 work by my host lab produced the twinning model of PD development, showing that new PD necks are often inserted immediately adjacent to existing necks in a direction parallel to wall expansion. This suggested that complex, and possibly new secondary PD, may arise from simple primary PD by production of additional branches from existing pores (Faulkner et al., 2008). A similar idea had been proposed in the 1960s by Krull (1960) based on her interpretations of 'X' and 'Y' shaped PD as intermediates in the production of branched or secondary PD from simple PD. However, the prevailing view of these PD with low-order branches as *fusion* rather than fission profiles meant that the idea did not gain acceptance and was forgotten.

My real-time studies of PD development give strong support to the twinning model of PD development, as I was able to observe that the same PD that were initially labelled with PDLP1 became labelled with MP17-GFP during leaf development. More indirectly, my studies of complex PD development in the non-dividing interface between the epidermis and the mesophyll showed that periclinal PD reach a peak density while the leaves are still relatively young and unexpanded, after which they decrease, suggesting that at this interface the insertion of secondary PD occurs only at an early stage of development.

7.2.3 Programmes of PD development are highly co-ordinated

The exquisite co-ordination of PD development to control wider developmental events has been observed throughout plant biology, from the development of symplasmic domains to define future organs in the embryo, to the waves of PD modifications that accompany the maturation of the vegetative shoot apical meristem to the floral shoot apical meristem. Leaves were chosen as the focus of this study due to the wave of structural PD modification that accompanies the sink-source

transition. In the course of this study, I was able to not only define this pattern, but to provide insights into just how many 'layers' of regulation feed into co-ordinating the behaviour of PD within a leaf.

Detailed CLSM imaging showed that the precise position of PD within an interface influenced development of their architecture, with PD located at the tips of the interdigitating epidermal cell lobes developing complex PD more quickly than other PD in the walls. This may be related to stress and stretching forces felt in the walls, and so would be influenced by the overall growth rate of the cells in general and the lobes in particular, and the presence of cell-wall modifying enzymes and cytoskeletal elements involved in development of the lobe.

At the next level, the wall type within which the PD is embedded may influence its development, with PD in anticlinal and periclinal walls of epidermal cells undergoing entirely separate developmental programmes. This is likely to be controlled by a range of factors, including: the individual rates of expansion of different wall types, the directions of expansion, and the removal of some PD as cells become pulled apart by expansion of the air spaces in the mesophyll. The different developmental patterns may also be related to the origin of the PD, as many of the epidermal-epidermal PD will be primary PD, inserted during division, while the restriction of cell division between the mesophyll and epidermal layer would mean that the majority of PD in the periclinal interface are expected to be secondary in origin.

At the next level, the identity of the cells sharing the interface influences the development of PD. This has been illustrated in other tissues, particularly in the root, but my work shows that this phenomenon occurs in the leaf even when the specialisation of cells is very subtle, as in the anicyctotic cells and pavement cells which are objectively very similar but experience different rates of development and overall densities of PD. The location of the PD in relation to the leaf as a whole will also influence its development. This includes the timing and rates of overall maturation events, especially those related to the sink-source transition, and the cell's location with respect to transport structures such as trichomes and veins.

7.2.4 Programmes of PD development are flexible and tailored to the needs of individual leaves

I also observed that while PD development occurs in specific patterns, these are inherently flexible, and can vary widely even in populations of genetically identical plants grown under the same conditions. This is in agreement with work studying the sink-source transition in *N. tabacum* that showed that the size of a leaf could not be used to predict its transition state (Wright et al., 2003). My work showed that PD development is not strictly linked to leaf size, average cell size, by the age of the leaf or its position on the plant, or by leaf developmental age as shown by the plastochron index.

However, the flexibility of PD development can also be considered from another angle, as my experiments show that the standard developmental patterns of complex PD are strongly preserved in plants maturing under highly different circumstances. An example of this is shown in Chapter 4, where almost identical patterns of complex PD formation were observed in plants grown in soil and plants grown on solid media plates, despite significant changes in growth rate, plant size and environmental conditions between the two samples. In Chapter 5, I observed that complex PD formation may occur in leaves of any age or size if required by the plant. Despite major changes in the rate of maturation, the growth rate, and the resources available to the tissues, the fine patterns of PD development proceeds as normal. In Chapter 6, I observed that PD development in plants treated with relatively high concentrations of salts, defence-related compounds and inhibitors proceeded as usual, and that similarly inhibition of root growth, leaf growth, or overall biomass production did not necessarily cause any effect on the development of complex PD in leaves.

7.2.5 Technological advances have great potential for the study of PD

One of the main aims of this project was the use of new light microscopy techniques to study PD development. PD were discovered using traditional light microscopy, thanks to the detailed observations of Eduard Tangl in 1880 (discussed in Kohler and Carr, 2006). However, the inherent resolution limit of the light microscope means

that little was known of PD structure until the advent of electron microscopy in the 1950s. EM provided revolutionary high-detailed images of the intricate ultrastructure of PD (e.g. the work of Katherine Esau, reviewed in Bell and Oparka, 2011). However, while EM techniques provided the means to view PD structure, they presented limited opportunities to define structural components. EM is also restricted to single-plane images from viewing thin sections or surfaces, providing limited information about the three-dimensional structure of complex PD. The revolution in light microscopy caused by the discovery of GFP and the subsequent development of fluorescent tags has been much slower to have an effect on PD research. Primarily, fluorescence microscopy has been used only to determine if a fluorescently-tagged protein is present at PD by the co-localisation with callose at punctae in the walls. However, the work in this thesis has shown that new 'super-resolution' techniques, which circumvent the resolution limit of light microscopy, have the means to identify structural components of plasmodesmata and view them *in situ*.

For studying development, the traditional approach has been to use light microscopy and EM in combination. Light microscopy can be used to assess the symplasmic connectivity of cells by following the movement of differently sized probes vs. selectively trafficked probes. EM can then be used to correlate the trafficking properties of the tissue with the frequency and structure of PD. EM is also limited with respect to studying this facet of PD development as, due to the heavy processing coupled with manual analysis, only restricted populations of PD can be analysed. My work has shown that light microscopy can be used to quantify PD frequency and structure and, thanks to the advent of high-throughput CLSM, can be used to analyse large sample sizes using automated-image acquisition, processing and analysis. My work has also illustrated just how necessary large sample sizes are for the study of PD by demonstrating the inherent variability and flexibility of complex PD development.

The success of these techniques has broad implications for the future of PD research. At the start of this project in 2009, when most of the SIM imaging was undertaken, super-resolution imaging was just becoming established and the system used, the *OMX* at the University of Dundee, was one of the first SIM microscopes available in

Europe. At the time of writing, several manufacturers are offering off-the-shelf systems capable of a combination of SIM, STED, PALM and other super-resolution techniques, and so the accessibility and reliability of these techniques is increasing dramatically. With the current rate of progress it is likely that super-resolution microscopes will shortly become mainstream in many microscopy facilities. This, coupled with a recent push in the effort to identify PD protein constituents (Fernandez-Calvino et al., 2011) offers the potential for a further revolution in our understanding of PD structure. Meanwhile, the use of high-throughput confocal systems means that PD can finally be analysed in sufficiently large numbers to provide statistically significant data regarding their frequencies and locations.

7.3 Future work & scope for expansion

7.3.1 Future work

In addition to the experiments presented, there are also further experiments which would have strengthened the current data and the conclusions drawn, but I was not able to perform due to time constraints or the access to and availability of materials. Equally, the results suggest further avenues of enquiry that I would like to have pursued directly.

The major limitation of this work is that it only considers complex PD. When this project was designed, I planned to look at PD of all structural types, using a fluorescently tagged protein that localises to all PD in combination with a viral protein that would target complex PD specifically. In practice neither of the candidate 'general' PD markers, PDLP1 and PDCB1, proved to be specific enough to quantify PD. In 2012, PDLP5 was identified as a further possible 'general' PD marker, and it is likely that continuing efforts to identify PD-specific proteins will soon yield a protein that can be used to label all PD, or simple PD only, for CLSM analysis.

The focus on complex PD alone meant that it was not possible to identify the origin of the PD of interest, and so I was only able to provide limited developmental information on primary and secondary PD. My work with time-lapse imaging

indicated that many of the complex PD that appear during leaf maturation arise from a previously existing simple PD. However, I could not determine if some of the complex PD arose from *de novo* insertion of secondary PD and, if so, what proportion of the total PD population these constitute in a mature leaf. When a specific marker for simple PD becomes available, high-throughput experiments, similar to those presented in Chapter 4, will be able to quantify the relative proportions of simple and complex PD at different stages of development. This would allow for definitive assessment of the contributions of conversion and *de novo* insertion in the production of complex PD. However, full understanding of the role of secondary PD in leaf development would require an accurate method of differentiating primary and secondary PD directly. As far as is known, there are no structural differences between these PD types, and so it seems unlikely that appropriate labels for these PD will appear in the foreseeable future.

Another facet of PD development that I would have liked to study was changes to the connectivity of the PD during development. It has been well established that complex PD have restricted trafficking properties compared to simple PD, but I feel it would have strengthened my results if I could have shown that directly. This was something I hoped to include in the developmental survey in Chapter 4 and the treatment experiments presented in Chapter 6 so that I could directly correlate changes to the structure of the PD with the connectivity of the tissues. This could have been done using an assay similar to the DANS assay (Lee et al., 2011), by spotting a symplasmically mobile tracer such as CFDA onto single cells, or groups of cells, on the lower epidermis and monitoring the extent of movement after a set period. However, I was not able to accommodate these in the time available.

7.3.2 Scope for expansion

The experiments presented in this thesis provided scope for future work, both in terms of new work building from the knowledge established and using the techniques developed, for further studies of PD development and function.

In particular, PD proved to be very suitable for SIM imaging. Their fixed location meant that they remained static during the relatively long image acquisition times

required, and their wall location meant that material could be prepared using a variety of techniques including epidermal peeling and vibroslice-cut sections. With SIM, I was able to image a combination of transgenically expressed fluorescently-tagged molecules, immunostaining, and fluorescent dyes to view structures. Due to the optical sectioning capacity, I was able to image PD from a variety of locations, and produce full 3D rotations, allowing structures to be viewed from any angle. Newer SIM microscopes have even greater flexibility, with additional laser lines for imaging a broader range of fluorophores. This offers great potential for future imaging studies of PD. If a molecule within PD can be stably labelled with a fluorescent marker resistant to photobleaching, then SIM should be able to produce super resolution images of its location. Further advances in our understanding of PD structure should produce a library of fluorescent markers suitable for SIM analysis.

Additionally, high-throughput microscopy presents similar possibilities for PD developmental studies, as they allow a magnitude difference in the number of PD and cells that can be analysed compared to EM studies. For this project, custom image analysis scripts for counting PD and measuring epidermal cells were written by Ji Zhou (The Sainsbury Laboratory, Norwich) suitable for use with high-throughput data produced by the OPERA high-throughput system (Perkin Elmer). These scripts could be used for a variety of studies on leaf tissue, and could potentially be adapted for studying PD in other tissues and contexts.

The discovery that leaf detachment stimulates the sink source transition presents further possibilities for the study of leaf maturation in general, and PD maturation in particular, as this is the first known system able to reliably induce PD development and modification. Imaging chambers are simple and inexpensive to produce and reliably maintain leaves for periods long enough for maturation to proceed significantly. This system therefore presents an intriguing base for further study.

The discovery in Chapter 6 that growth of plants on root medium supplemented with mannitol or salicylic acid causes a doubling of the numbers of complex PD observed an early stage of leaf development presents an intriguing avenue for future work. Plants are reliant of precise control of their PD for correct maturation and function.

Determining the underlying causes and mechanisms for these alterations of PD developmental patterns would provide the first understanding of the genetic and cellular factors that plants use to control and coordinate PD development

7.3.3 Final words

In the introduction to this project, I stated that PD are interesting because they are one of the structures that make plants what they are. The structure and development of complex PD lies at the heart of many of the biological processes unique to the plant way of life, and have been incorporated into processes that are performed without symplasmic connectivity in other organisms. In this work I was able to provide fresh insights on these fundamental but often inaccessible structures, allowing me to observe detail of their 3D structure, define their developmental patterns, and to follow their development. The technology that facilitated this work will continue to provide further advances in our understanding of the form and function of PD, meaning that answers to many of the long-standing questions about PD are finally within reach.

Appendix 1

A PDF of the manuscript “Super-resolution Imaging of Plasmodesmata using Three-Dimensional Structured Illumination Microscopy” by J. Fitzgibbon J & K. Bell, E. King and K. Oparka. (Plant Physiology, 2010, volume 154: p1453-63) is included on a CD.

Appendix 2

Animations of the 3D projections shown in Figure 24K and L and 25 H are included on a CD.

Appendix 3

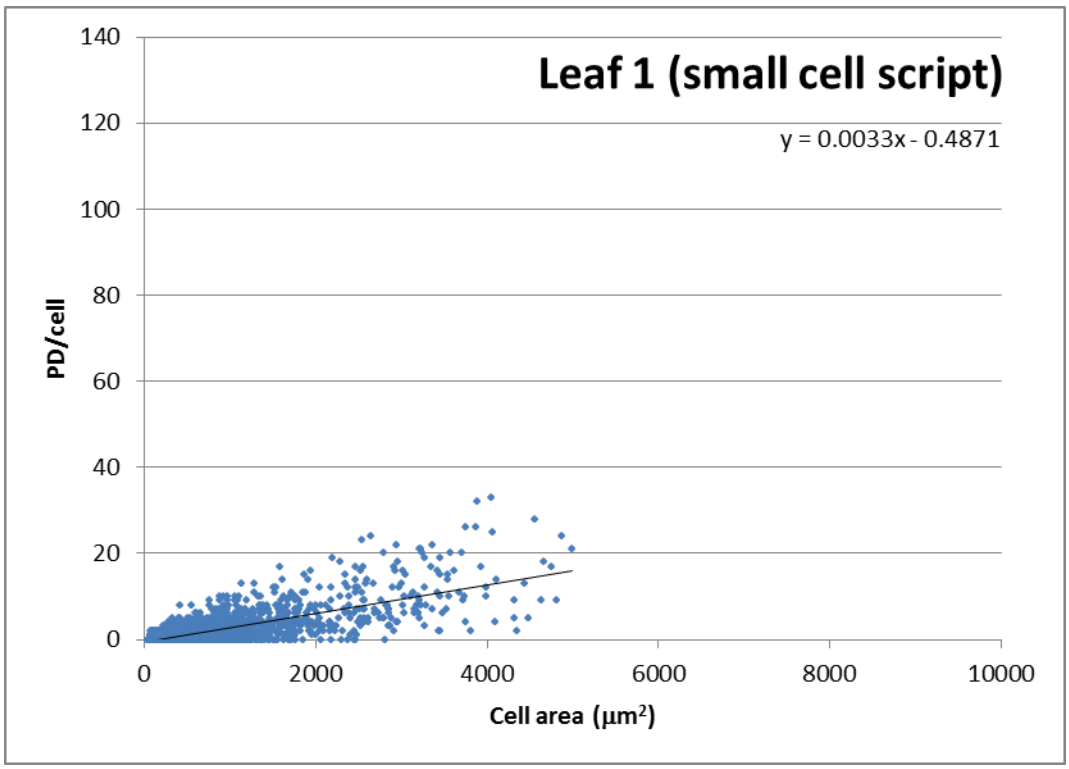

Figure 94: Graph showing the area and number of anticlinal complex PD of individual cells from imaged populations from leaf 1 (youngest leaf) of 8-leaf LD *A. thaliana* analysed using the ‘small cell’ script.

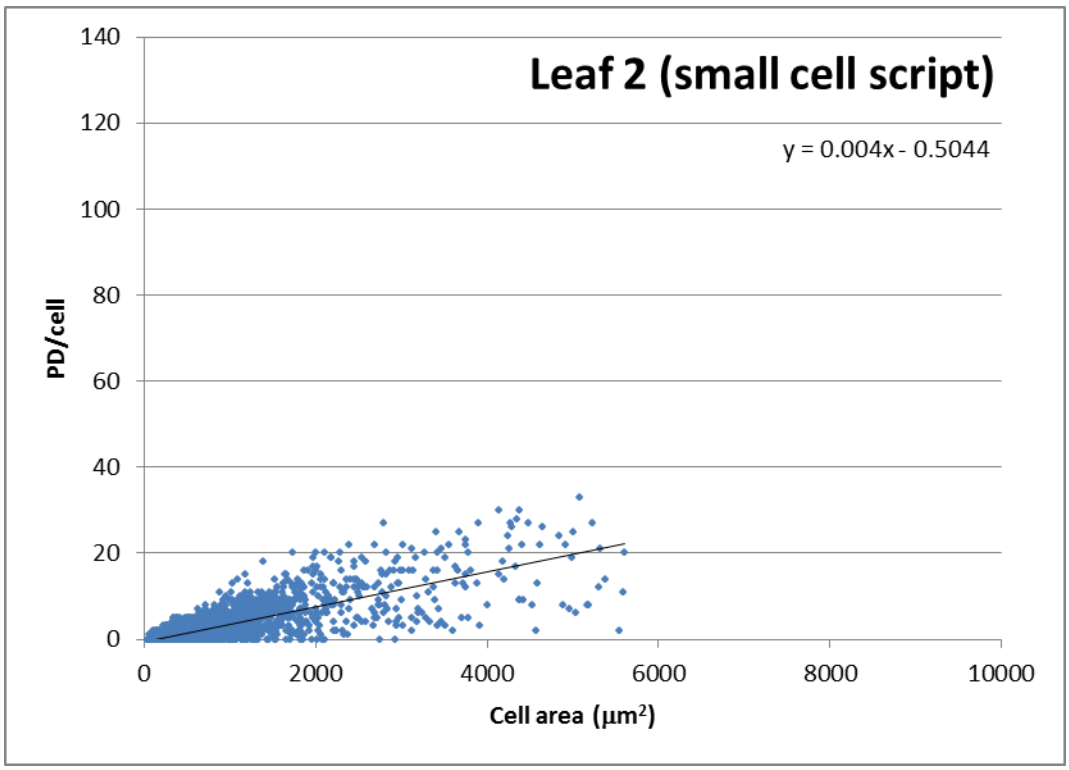

Figure 95: Graph showing the area and number of anticlinal complex PD of individual cells from imaged populations from leaf 2 (2nd youngest leaf) of 8-leaf LD A. thaliana analysed using the 'small cell' script.

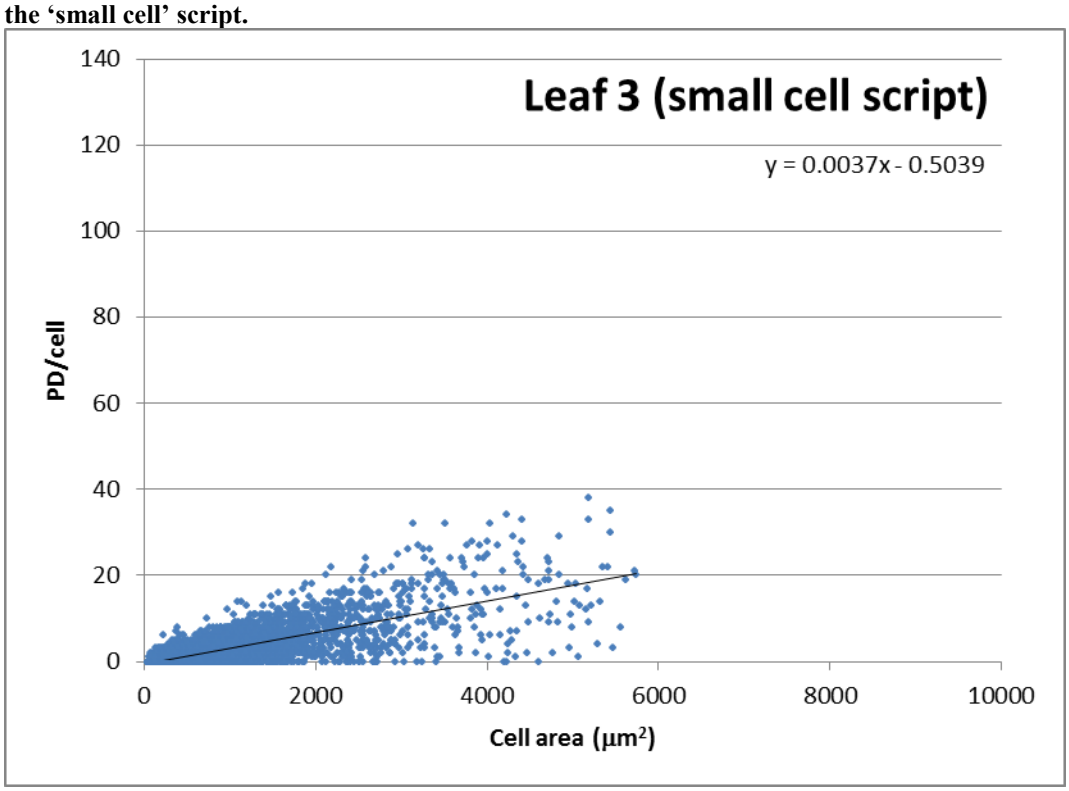

Figure 96: Graph showing the area and number of anticlinal complex PD of individual cells from imaged populations from leaf 1 (youngest leaf) of 8-leaf LD A. thaliana analysed using the 'small cell' script.

Bibliography

Aaziz,R., Dinant,S., and Epel,B.L. (2001) Plasmodesmata and plant cytoskeleton. Trends in Plant Science 6:326-330.

Anastasiou,E., Kenz,S., Gerstung,M., MacLean,D., Timmer,J., Fleck,C., and Lenhard,M. (2007) Control of plant organ size by KLUH/CYP78A5-dependent intercellular signaling. Developmental Cell 13:843-856.

Atkins,D., Hull,R., Wells,B., Roberts,K., Moore,P., and Beachy,R.N. (1991) The Tobacco Mosaic Virus-30K Movement Protein in Transgenic Tobacco Plants Is Localized to Plasmodesmata. Journal of General Virology 72:209-211.

Badelt,K., White,R.G., Overall,R.L., and Vesk,M. (1994) Ultrastructural Specializations of the Cell-Wall Sleeve Around Plasmodesmata. American Journal of Botany 81:1422-1427.

Bai,L., Zhou,Y., Zhang,X., Song,C., and Cao,M. (2007) Hydrogen peroxide modulates abscisic acid signaling in root growth and development in Arabidopsis. Chinese Science Bulletin 52:1142-1145.

Bayer,E., Thomas,C., and Maule,A. (2008) Symplastic domains in the Arabidopsis shoot apical meristem correlate with PDLP1 expression patterns. Plant signaling & behavior 3:853-855.

Bell,K. and Oparka,K. (2011) Imaging plasmodesmata. Protoplasma 248:9-25.

Benitez-Alfonso,Y., Cilia,M., Roman,A.S., Thomas,C., Maule,A., Hearn,S., and Jackson,D. (2009) Control of Arabidopsis meristem development by thioredoxin-dependent regulation of intercellular transport. Proceedings of the National Academy of Sciences of the United States of America 106:3615-3620.

Bharathan,G., Goliber,T.E., Moore,C., Kessler,S., Pham,T., and Sinha,N.R. (2002) Homologies in leaf form inferred from KNOXI gene expression during development. Science 296:1858-1860.

Blackman,L.M., Boevink,P., Cruz,S.S., Palukaitis,P., and Oparka,K.J. (1998) The movement protein of cucumber mosaic virus traffics into sieve elements in minor veins of Nicotiana clevelandii. Plant Cell 10:525-537.

Böhm,J. (1877) Über die Aufnahme von Wasser und Kalksalzen durch die Blätter der Feuerbohne. Wiener Landwirthsch. Versuchsstation.

Bohn,S., Andreotti,B., Douady,S., Munzinger,J., and Couder,Y. (2002) Constitutive property of the local organization of leaf venation networks. Physical Review e 65.

Boudaoud,A. (2010) An introduction to the mechanics of morphogenesis for plant biologists. Trends in Plant Science 15:353-360.

Bradford,K.J. (1983) Involvement of Plant-Growth Substances in the Alteration of Leaf Gas-Exchange of Flooded Tomato Plants. Plant Physiology 73:480-483.

Brainerd,K.E. and Fuchigami,L.H. (1982) Stomatal Functioning of Invitro and Greenhouse Apple Leaves in Darkness, Mannitol, Aba, and Co2. Journal of Experimental Botany 33:388-392.

Braybrook,S.A. and Kuhlemeier,C. (2010) How a Plant Builds Leaves. Plant Cell 22:1006-1018.

Broertje,C., Haccius,B., and Weidlich,S. (1968) Adventitious Bud Formation on Isolated Leaves and Its Significance for Mutation Breeding. Euphytica 17:321.

Burch-Smith,T.M., Stonebloom,S., Xu,M., and Zambryski,P.C. (2011) Plasmodesmata during development: re-examination of the importance of primary, secondary, and branched plasmodesmata structure versus function. Protoplasma 248:61-74.

Burch-Smith,T.M. and Zambryski,P.C. (2010) Loss of Increased Size Exclusion Limit (Ise)1 Or Ise2 Increases the Formation of Secondary Plasmodesmata. Current Biology 20:989-993.

Cantrill,L.C., Overall,R.L., and Goodwin,P.B. (1999) Cell-to-cell communication via plant endomembranes. Cell Biology International 23:653-661.

Chan,J., Calder,G., Fox,S., and Lloyd,C. (2007) Cortical microtubule arrays undergo rotary movements in Arabidopsis hypocotyl epidermal cells. Nature Cell Biology 9:171-U57.

Chen,Z.X., Malamy,J., Henning,J., Conrath,U., Sanchezcasas,P., Silva,H., Ricigliano,J., and Klessig,D.F. (1995) Induction, Modification, and Transduction of the Salicylic-Acid Signal in Plant Defense Responses. Proceedings of the National Academy of Sciences of the United States of America 92:4134-4137.

Chitwood,D.H., Nogueira,F.T., Howell,M.D., Montgomery,T.A., Carrington,J.C., and Timmermans,M.C. (2009) Pattern formation via small RNA mobility. Genes & Development 23:549-554.

Cho,Y.H. and Yoo,S.D. (2011) Signaling Role of Fructose Mediated by FINS1/FBP in Arabidopsis thaliana. Plos Genetics 7.

Christensen,N.M., Faulkner,C., and Oparka,K. (2009) Evidence for Unidirectional Flow through Plasmodesmata. Plant Physiology 150:96-104.

Corson,F., Adda-Bedia,M., and Boudaoud,A. (2009) In silico leaf venation networks: Growth and reorganization driven by mechanical forces. Journal of Theoretical Biology 259:440-448.

Cram,W.J. (1984) Mannitol Transport and Suitability As An Osmoticum in Root-Cells. Physiologia Plantarum 61:396-404.

Crawford,K.M. and Zambryski,P.C. (2000) Subcellular localization determines the availability of non-targeted proteins to plasmodesmatal transport. Current Biology 10:1032-1040.

Crawford,K.M. and Zambryski,P.C. (2001) Non-targeted and targeted protein movement through plasmodesmata in leaves in different developmental and physiological states. Plant Physiology 125:1802-1812.

Dailey, Michael E., Focht, Daniel C., Khodjakov, Alexey, Rieder, Conly L., Spring, Kenneth R., Claxton, Nathan S., Olenych, Scott G., Griffin, John D., and Davidson, Michael W. Nikon MicroscopyU: Culture Chambers for Live-Cell Imaging. http://www.microscopyu.com/articles/livecellimaging/culturechambers.html . 24-1-2012.

Dalchau,N., Baek,S.J., Briggs,H.M., Robertson,F.C., Dodd,A.N., Gardner,M.J., Stancombe,M.A., Haydon,M.J., Stan,G.B., Goncalves,J.M., and Webb,A.A. (2011) The circadian oscillator gene GIGANTEA mediates a long-term response of the Arabidopsis thaliana circadian clock to sucrose. Proceedings of the National Academy of Sciences of the United States of America 108:5104-5109.

Day,S.J. and Lawrence,P.A. (2000) Measuring dimensions: the regulation of size and shape. Development 127:2977-2987.

De Rybel,B., Vassileva,V., Parizot,B., Demeulenaere,M., Grunewald,W., Audenaert,D., Van Campenhout,J., Overvoorde,P., Jansen,L., Vanneste,S., Moeller,B., Wilson,M., Holman,T., Van Isterdael,G., Brunoud,G., Vuylsteke,M., Vernoux,T., De Veylder,L., Inze,D., Weijers,D., Bennett,M.J., and Beeckman,T. (2010) A Novel Aux/IAA28 Signaling Cascade Activates GATA23-Dependent Specification of Lateral Root Founder Cell Identity. Current Biology 20:1697-1706.

Deng,K., Wang,Q., Zeng,J., Guo,X., Zhao,X., Tang,D., and Liu,X. (2009) A Lectin Receptor Kinase Positively Regulates ABA Response During Seed Germination and Is Involved in Salt and Osmotic Stress Response. Journal of Plant Biology 52:493-500.

Denk,W. and Horstmann,H. (2004) Serial block-face scanning electron microscopy to reconstruct three-dimensional tissue nanostructure. Plos Biology 2:1900-1909.

Ding,B., Haudenshield,J.S., Willmitzer,L., and Lucas,W.J. (1993) Correlation Between Arrested Secondary Plasmodesmal Development and Onset of Accelerated Leaf Senescence in Yeast Acid Invertase Transgenic Tobacco Plants. Plant Journal 4:179-189.

Ding,B., Haudenshield,J.S., Hull,R.J., Wolf,S., Beachy,R.N., and Lucas,W.J. (1992) Secondary Plasmodesmata Are Specific Sites of Localization of the Tobacco Mosaic-Virus Movement Protein in Transgenic Tobacco Plants. Plant Cell 4:915-928.

Ding,B., Parthasarathy,M.V., Niklas,K., and Turgeon,R. (1988) A Morphometric Analysis of the Phloem-Unloading Pathway in Developing Tobacco-Leaves. Planta 176:307-318.

Donnelly,P.M., Bonetta,D., Tsukaya,H., Dengler,R.E., and Dengler,N.G. (1999) Cell cycling and cell enlargement in developing leaves of Arabidopsis. Developmental Biology 215:407-419.

Ehlers,K. and Kollmann,R. (2001) Primary and secondary plasmodesmata: structure, origin, and functioning. Protoplasma 216:1-30.

Endo,R. and Omasa,K. (2007) 3-D cell-level chlorophyll fluorescence imaging of ozone-injured sunflower leaves using a new passive light microscope system. Journal of Experimental Botany 58:765-772.

Erickson,R.O. and Michelini,F.J. (1957) The Plastochron Index. American Journal of Botany 44:297-305.

Ernst,A.M., Jekat,S.B., Zielonka,S., Muller,B., Neumann,U., Ruping,B., Twyman,R.M., Krzyzanek,V., Prufer,D., and Noll,G.A. (2012) Sieve element occlusion (SEO) genes encode structural phloem proteins involved in wound sealing of the phloem. Proceedings of the National Academy of Sciences of the United States of America 109:E1980-E1989.

Erwee,M.G. and Goodwin,P.B. (1985) Symplast Domains in Extrastellar Tissues of Egeria-Densa Planch. Planta 163:9-19.

Esau,K. (1978) Developmental Features of Primary Phloem in Phaseolus-Vulgaris l. Annals of Botany 42:1-&.

Etxeberria,E., Gonzalez,P., and Pozueta-Romer,J. (2007) Mannitol-enhanced, fluid-phase endocytosis in storage parenchyma cells of celery (Apium graveolens; Apiaceae) petioles. American Journal of Botany 94:1041-1045.

Evert,R.F., Eschrich,W., and Eichhorn,S.E. (1971) Sieve-Plate Pores in Leaf Veins of Hordeum-Vulgare. Planta 100:262-&.

Farmer,E.E. and Ryan,C.A. (1990) Interplant Communication - Airborne Methyl Jasmonate Induces Synthesis of Proteinase-Inhibitors in Plant-Leaves. Proceedings of the National Academy of Sciences of the United States of America 87:7713-7716.

Faulkner,C., Akman,O.E., Bell,K., Jeffree,C., and Oparka,K. (2008) Peeking into pit fields: A multiple twinning model of secondary plasmodesmata formation in tobacco. Plant Cell 20:1504-1518.

Fernandez-Calvino,L., Faulkner,C., Walshaw,J., Saalbach,G., Bayer,E., Benitez-Alfonso,Y., and Maule,A. (2011) Arabidopsis Plasmodesmal Proteome. Plos One 6.

Fernandez-Suarez,M. and Ting,A.Y. (2008) Fluorescent probes for super-resolution imaging in living cells. Nature Reviews Molecular Cell Biology 9:929-943.

Fleming,A.J. (2003) The molecular regulation of leaf form. Plant Biology 5:341-349.

Fricke,W. and Peters,W.S. (2002) The biophysics of leaf growth in salt-stressed barley. A study at the cell level. Plant Physiology 129:374-388.

Frigault,M.M., Lacoste,J., Swift,J.L., and Brown,C.M. (2009) Live-cell microscopy - tips and tools. Journal of Cell Science 122:753-767.

Fu,Y., Gu,Y., Zheng,Z.L., Wasteneys,G., and Yang,Z.B. (2005) Arabidopsis interdigitating cell growth requires two antagonistic pathways with opposing action on cell morphogenesis. Cell 120:687-700.

Fu,Y., Li,H., and Yang,Z.B. (2002) The ROP2 GTPase controls the formation of cortical fine F-actin and the early phase of directional cell expansion during Arabidopsis organogenesis. Plant Cell 14:777-794.

Galbraith,C.G. and Galbraith,J.A. (2011) Super-resolution microscopy at a glance. Journal of Cell Science 124:1607-1611.

Ghanem,M.E., Albacete,A., Smigocki,A.C., Frebort,I., Pospisilova,H., Martinez-Andujar,C., Acosta,M., Sanchez-Bravo,J., Lutts,S., Dodd,I.C., and Perez-Alfocea,F. (2011) Root-synthesized cytokinins improve shoot growth and fruit yield in salinized tomato (Solanum lycopersicum L.) plants. Journal of Experimental Botany 62:125-140.

Gillespie,T., Boevink,P., Haupt,S., Roberts,A.G., Toth,R., Valentine,T., Chapman,S., and Oparka,K.J. (2002) Functional analysis of a DNA-shuffled movement protein reveals that microtubules are dispensable for the cell-to-cell movement of Tobacco mosaic virus. Plant Cell 14:1207-1222.

Grabski,S., Defeijter,A.W., and Schindler,M. (1993) Endoplasmic-Reticulum Forms A Dynamic Continuum for Lipid Diffusion Between Contiguous Soybean Root-Cells. Plant Cell 5:25-38.

Groot,E.P. and Meicenheimer,R.D. (2000a) Comparison of leaf plastochron index and allometric analyses of tooth development in Arabidopsis thaliana. Journal of Plant Growth Regulation 19:77-89.

Groot,E.P. and Meicenheimer,R.D. (2000b) Short-day-grown Arabidopsis thaliana satisfies the assumptions of the plastochron index as a time variable in development. International Journal of Plant Sciences 161:749-756.

Gunning,B.E.S. (1978) Age-Related and Origin-Related Control of Numbers of Plasmodesmata in Cell-Walls of Developing Azolla Roots. Planta 143:181-190.

Guseman,J.M., Lee,J.S., Bogenschutz,N.L., Peterson,K.M., Virata,R.E., Xie,B., Kanaoka,M.M., Hong,Z., and Torii,K.U. (2010) Dysregulation of cell-to-cell connectivity and stomatal patterning by loss-of-function mutation in Arabidopsis CHORUS (GLUCAN SYNTHASE-LIKE 8). Development 137:1731-1741.

Gustafsson,M.G.L. (2000) Surpassing the lateral resolution limit by a factor of two using structured illumination microscopy. Journal of Microscopy-Oxford 198:82-87.

Hamant,O. and Traas,J. (2010) The mechanics behind plant development. New Phytologist 185:369-385.

Hell,S.W., Dyba,M., and Jakobs,S. (2004) Concepts for nanoscale resolution in fluorescence microscopy. Current Opinion in Neurobiology 14:599-609.

Hofius,D., Herbers,K., Melzer,M., Omid,A., Tacke,E., Wolf,S., and Sonnewald,U. (2001) Evidence for expression level-dependent modulation of carbohydrate status and viral resistance by the potato leafroll virus movement protein in transgenic tobacco plants. Plant Journal 28:529-543.

Huang,B., Bates,M., and Zhuang,X. (2009) Super-Resolution Fluorescence Microscopy. ANNUAL REVIEW OF BIOCHEMISTRY

Itaya,A., Woo,Y.M., Masuta,C., Bao,Y.M., Nelson,R.S., and Ding,B. (1998) Developmental regulation of intercellular protein trafficking through plasmodesmata in tobacco leaf epidermis. Plant Physiology 118:373-385.

Jackson,D. (2005) Transcription factor movement through plasmodesmata. PLASMODESMATA

Jacobs,S., Zechmann,B., Molitor,A., Trujillo,M., Petutschnig,E., Likpa,V., Kogel,K.H., and Schaefer,P. (2011) Broad-Spectrum Suppression of Innate Immunity Is Required for Colonization of Arabidopsis Roots by the Fungus Piriformospora indica. Plant Physiology 156:726-740.

Jain,M., Tiwary,S., and Gadre,R. (2010) Sorbitol-induced changes in various growth and biochemical parameters in maize. Plant Soil and Environment 56:263-267.

Jennings,D.B., Daub,M.E., Pharr,D.M., and Williamson,J.D. (2002) Constitutive expression of a celery mannitol dehydrogenase in tobacco enhances resistance to the mannitol-secreting fungal pathogen Alternaria alternata. Plant Journal 32:41-49.

Kaplan,D.R. and Hagemann,W. (1991) The Relationship of Cell and Organism in Vascular Plants - Are Cells the Building-Blocks of Plant Form. Bioscience 41:693-703.

Kempers,R., Ammerlaan,A., and van Bel,A.J.E. (1998) Symplasmic constriction and ultrastructural features of the sieve element companion cell complex in the transport phloem of apoplasmically and symplasmically phloem-loading species. Plant Physiology 116:271-278.

Kidner,C., Sundaresan,V., Roberts,K., and Dolan,L. (2000) Clonal analysis of the Arabidopsis root confirms that position, not lineage, determines cell fate. Planta 211:191-199.

Kidner,C.A. and Martienssen,R.A. (2004) Spatially restricted microRNA directs leaf polarity through ARGONAUTE1. Nature 428:81-84.

Kim,G.T., Shoda,K., Tsuge,T., Cho,K.H., Uchimiya,H., Yokoyama,R., Nishitani,K., and Tsukaya,H. (2002) The ANGUSTIFOLIA gene of Arabidopsis, a plant CtBP gene, regulates leaf-cell expansion, the arrangement of cortical microtubules in leaf cells and expression of a gene involved in cell-wall formation. Embo Journal 21:1267-1279.

Kim,I., Kobayashi,K., Cho,E., and Zambryski,P.C. (2005) Subdomains for transport via plasmodesmata corresponding to the apical-basal axis are established during Arabidopsis embryogenesis. Proceedings of the National Academy of Sciences of the United States of America 102:11945-11950.

Kim,J.Y., Yuan,Z., and Jackson,D. (2003) Developmental regulation and significance of KNOX protein trafficking in Arabidopsis. Development 130:4351-4362.

Knoblauch,M. and van Bel,A.J.E. (1998) Sieve tubes in action. Plant Cell 10:35-50.

Kobayashi,K., Insoon,I., Cho,E., and Zambryski,P.C. (2005) Plasmadesmata and plant morphogenesis. In Plasmodesmata: Annual Plant Reviews, K.J.Oparka, ed (Oxford: Blackwell Publishing Ltd.).

Kobayashi,K., Otegui,M.S., Krishnakumar,S., Mindrinos,M., and Zambryski,P. (2007) Increased Size Exclusion Limit2 Encodes A Putative Devh Box Rna Helicase Involved in Plasmodesmata Function During Arabidopsis Embryogenesis. Plant Cell 19:1885-1897.

Kohler,P. and Carr,D.J. (2006) A somewhat obscure discoverere of plasmodesmata: Eduard Tangl (1848-1905). In The Global and the Local: The History of Science and the Cultural Integration of Europe. Proceedings of the 2nd ICESHS., M.Kokowski, ed (Cracow: European Society for the History of Science), pp. 208-211.

Kragler,F. (2005) Plasmodesmata: protein transport signals and receptors. PLASMODESMATA

Kronberg,K., Vogel,F., Rutten,T., Hajirezaei,M.R., Sonnewald,U., and Hofius,D. (2007) The silver lining of a viral agent: Increasing seed yield and harvest index in Arabidopsis by ectopic expression of the potato leaf roll virus movement protein. Plant Physiology 145:905-918.

Krull,R. (1960) Untersuchungen Uber den Bau und Die Entwicklung der Plasmodesmen Im Rindenparenchym Von Viscum-Album. Planta 55:598-629.

Laguna,M.F., Bohn,S., and Jagla,E.A. (2008) The role of elastic stresses on leaf venation morphogenesis. Plos Computational Biology 4.

Lee,J.Y. and Lu,H. (2011) Plasmodesmata: the battleground against intruders. Trends in Plant Science 16:201-210.

Lee,J.Y., Wang,X., Cui,W., Sager,R., Modla,S., Czymmek,K., Zybaliov,B., van Wijk,K., Zhang,C., Lu,H., and Lakshmanan,V. (2011) A Plasmodesmata-Localized Protein Mediates Crosstalk between Cell-to-Cell Communication and Innate Immunity in Arabidopsis. Plant Cell 23:3353-3373.

Lee,J.Y., Yoo,B.C., Rojas,M.R., Gomez-Ospina,N., Staehelin,L.A., and Lucas,W.J. (2003) Selective trafficking of non-cell-autonomous proteins mediated by NtNCAPP1. Science 299:392-396.

Lipavska,H. and Vreugdenhil,D. (1996) Uptake of mannitol from the media by in vitro grown plants. Plant Cell Tissue and Organ Culture 45:103-107.

Lovell,P.H., Barratt,E., and Moore,K.G. (1970) Rooted Excised Cotyledon As An Experimental System. New Phytologist 69:1185-&.

Lucas,W.J., Ding,B., and Vanderschoot,C. (1994) Plasmodesmata and the Supracellular Nature of Plants (Vol 125, Pg 435, 1993). New Phytologist 126:719.

Maizel,A., von Wangenheim,D., Federici,F., Haseloff,J., and Stelzer,E.H. (2011) High-resolution live imaging of plant growth in near physiological bright conditions using light sheet fluorescence microscopy. Plant Journal 68:377-385.

Marchant,A., Kargul,J., May,S.T., Muller,P., Delbarre,A., Perrot-Rechenmann,C., and Bennett,M.J. (1999) AUX1 regulates root gravitropism in Arabidopsis by facilitating auxin uptake within root apical tissues. Embo Journal 18:2066-2073.

Marcotrigiano,M. (2001) Genetic mosaics and the analysis of leaf development. International Journal of Plant Sciences 162:513-525.

Martens,H.J., Roberts,A.G., Oparka,K.J., and Schulz,A. (2006) Quantification of plasmodesmatal endoplasmic reticulum coupling between sieve elements and companion cells using fluorescence redistribution after photobleaching. Plant Physiology 142:471-480.

Massonnet,C., Vile,D., Fabre,J., Hannah,M.A., Caldana,C., Lisec,J., Beemster,G.T., Meyer,R.C., Messerli,G., Gronlund,J.T., Perkovic,J., Wigmore,E., May,S., Bevan,M.W., Meyer,C., Rubio-Diaz,S., Weigel,D., Micol,J.L., Buchanan-Wollaston,V., Fiorani,F., Walsh,S., Rinn,B., Gruissem,W., Hilson,P., Hennig,L., Willmitzer,L., and Granier,C. (2010) Probing the Reproducibility of Leaf Growth and Molecular Phenotypes: A Comparison of Three Arabidopsis Accessions Cultivated in Ten Laboratories. Plant Physiology 152:2142-2157.

Maule,A.J. (2008) Plasmodesmata: structure, function and biogenesis. Current Opinion in Plant Biology 11:680-686.

McDowell,J.M. and Dangl,J.L. (2000) Signal transduction in the plant immune response. Trends in Biochemical Sciences 25:79-82.

Melcher,U. (2000) The '30K' superfamily of viral movement proteins. Journal of General Virology 81:257-266.

Mita,S., Suzukifujii,K., and Nakamura,K. (1995) Sugar-Inducible Expression of A Gene for Beta-Amylase in Arabidopsis-Thaliana. Plant Physiology 107:895-904.

Mussig,C., Shin,G.H., and Altmann,T. (2003) Brassinosteroids promote root growth in Arabidopsis. Plant Physiology 133:1261-1271.

Nadeau,J.A. and Sack,F.D. (2002) Stomatal development in Arabidopsis. The Arabidopsis book / American Society of Plant Biologists 1:e0066.

Navarro,L., Zipfel,C., Rowland,O., Keller,I., Robatzek,S., Boller,T., and Jones,J.D.G. (2004) The transcriptional innate immune response to flg22. interplay and overlap with Avr gene-dependent defense responses and bacterial pathogenesis. Plant Physiology 135:1113-1128.

Northcote,D.H., Davey,R., and Lay,J. (1989) Use of Antisera to Localize Callose, Xylan and Arabinogalactan in the Cell-Plate, Primary and Secondary Walls of Plant-Cells. Planta 178:353-366.

Okada,Y. (1999) Historical overview of research on the tobacco mosaic virus genome: genome organization, infectivity and gene manipulation. Philosophical Transactions of the Royal Society of London Series B-Biological Sciences 354:569-582.

Oparka,K. and Boevink,P. (2005) Techniques for imaging intercellular transport. PLASMODESMATA. Annual Plant Reviews.

Oparka,K.J. (2004) Getting the message across: how do plant cells exchange macromolecular complexes? Trends in Plant Science 9:33-41.

Oparka,K.J., Roberts,A.G., Boevink,P., Santa Cruz,S., Roberts,L., Pradel,K.S., Imlau,A., Kotlizky,G., Sauer,N., and Epel,B. (1999) Simple, but not branched, plasmodesmata allow the nonspecific trafficking of proteins in developing tobacco leaves. Cell 97:743-754.

Ormenese,S., Bernier,G., and Perilleux,C. (2006) Cytokinin application to the shoot apical meristem of Sinapis alba enhances secondary plasmodesmata formation. Planta 224:1481-1484.

Ormenese,S., Havelange,A., Deltour,R., and Bernier,G. (2000) The frequency of plasmodesmata increases early in the whole shoot apical meristem of Sinapis alba L. during floral transition. Planta 211:370-375.

Overall,R.L. and Blackman,L.M. (1996) A model of the macromolecular structure of plasmodesmata. Trends in Plant Science 1:307-311.

Panteris,E. and Galatis,B. (2005) The morphogenesis of lobed plant cells in the mesophyll and epidermis: organization and distinct roles of cortical microtubules and actin filaments. New Phytologist 167:721-731.

Pepperkok,R. and Ellenberg,J. (2006) Innovation - High-throughput fluorescence microscopy for systems biology. Nature Reviews Molecular Cell Biology 7:690-696.

Perbal,M.C., Haughn,G., Saedler,H., and SchwarzSommer,Z. (1996) Non-cell-autonomous function of the Antirrhinum floral homeotic proteins DEFICIENS and GLOBOSA is exerted by their polar cell-to-cell trafficking. Development 122:3433-3441.

Pfluger,J. and Zambryski,P.C. (2001) Cell growth: The power of symplastic isolation. Current Biology 11:R436-R439.

Pina,A., Errea,P., Schulz,A., and Martens,H.J. (2009) Cell-to-cell transport through plasmodesmata in tree callus cultures. Tree Physiology 29:809-818.

Prusinkiewicz,P. and de Reuille,P.B. (2010) Constraints of space in plant development. Journal of Experimental Botany 61:2117-2129.

Qi,X.P., Zhou,J., Jia,Q.J., Shou,H.X., Chen,H.M., and Wu,P. (2005) A characterization of the response to auxin of the small GTPase, Rha1. Plant Science 169:1136-1145.

Reis,R., Jr., Lima,E.R., Vilela,E.F., and Barros,R.S. (2000) Method for maintenance of coffee leaves in vitro for mass rearing of Leucoptera coffeellum (Guerin-Meneville) (Lepidoptera: Lyonetiidae). Anais da Sociedade Entomologica do Brasil 29:849-854.

Rinne,P.L.H. and van der Schoot,C. (1998) Symplasmic fields in the tunica of the shoot apical meristem coordinate morphogenetic events. Development 125:1477-1485.

Rivas-San Vicente,M. and Plasencia,J. (2011) Salicylic acid beyond defence: its role in plant growth and development. Journal of Experimental Botany 62:3321-3338.

Robards,A.W. and Lucas,W.J. (1990) Plasmodesmata. Annual Review of Plant Physiology and Plant Molecular Biology 41:369-419.

Roberts,A.G. (2005) Plasmodesmal structure and development. PLASMODESMATA

Roberts,A.G. and Oparka,K.J. (2003) Plasmodesmata and the control of symplastic transport. Plant Cell and Environment 26:103-124.

Roberts,I.M., Boevink,P., Roberts,A.G., Sauer,N., Reichel,C., and Oparka,K.J. (2001) Dynamic changes in the frequency and architecture of plasmodesmata during the sink-source transition in tobacco leaves. Protoplasma 218:31-44.

Roy,S., Watada,A.E., and Wergin,W.P. (1997) Characterization of the cell wall microdomain surrounding plasmodesmata in apple fruit. Plant Physiology 114:539-547.

Royal Horticultural Society. Royal Horticultural Society: Leaf Cuttings. http://apps.rhs.org.uk/advicesearch/Profile.aspx?pid=427 . 2012.

Rustom,A. (2009) Hen or egg?: some thoughts on tunneling nanotubes. Annals Of The New York Academy Of Sciences 1178:129-136.

Ryals,J.A., Neuenschwander,U.H., Willits,M.G., Molina,A., Steiner,H.Y., and Hunt,M.D. (1996) Systemic acquired resistance. Plant Cell 8:1809-1819.

Sakr,S., Lemoine,R., Gaillard,C., and Delrot,S. (1993) Effect of Cutting on Solute Uptake by Plasma-Membrane Vesicles from Sugar-Beet (Beta-Vulgaris L) Leaves. Plant Physiology 103:49-58.

Salomon,S., Grunewald,D., Stueber,K., Schaaf,S., MacLean,D., Schulze-Lefert,P., and Robatzek,S. (2010) High-Throughput Confocal Imaging of Intact Live Tissue Enables Quantification of Membrane Trafficking in Arabidopsis. Plant Physiology 154:1096-1104.

Sauret-Güeto,S., Calder,G., and Harberd,N.P. (2011) Transient gibberellin application promotes Arabidopsis thaliana hypocotyl cell elongation without maintaining transverse orientation of microtubules on the outer tangential wall of epidermal cells. Plant Journal Epub ahead of print.

Sawchuk,M.G., Head,P., Donner,T.J., and Scarpella,E. (2007) Time-lapse imaging of Arabidopsis leaf development shows dynamic patterns of procambium formation. New Phytologist 176:560-571.

Scarpella,E., Barkoulas,M., and Tsiantis,M. (2010) Control of Leaf and Vein Development by Auxin. Cold Spring Harbor Perspectives in Biology 2.

Schellmann,S., Schnittger,A., Kirik,V., Wada,T., Okada,K., Beermann,A., Thumfahrt,J., Jurgens,G., and Hulskamp,M. (2002) TRIPTYCHON and CAPRICE mediate lateral inhibition during trichome and root hair patterning in Arabidopsis. Embo Journal 21:5036-5046.

Schermelleh,L., Carlton,P.M., Haase,S., Shao,L., Winoto,L., Kner,P., Burke,B., Cardoso,M., Agard,D.A., Gustafsson,M.G., Leonhardt,H., and Sedat,J.W. (2008) Subdiffraction multicolor imaging of the nuclear periphery with 3D structured illumination microscopy. Science 320:1332-1336.

Schluepmann,H., Pellny,T., van Dijken,A., Smeekens,S., and Paul,M. (2003) Trehalose 6-phosphate is indispensable for carbohydrate utilization and growth in Arabidopsis thaliana. Proceedings of the National Academy of Sciences of the United States of America 100:6849-6854.

Schnittger,A., Folkers,U., Schwab,B., Jurgens,G., and Hulskamp,M. (1999) Generation of a spacing pattern: The role of TRIPTYCHON in trichome patterning in Arabidopsis. Plant Cell 11:1105-1116.

Schulz,A. (1995) Plasmodesmal Widening Accompanies the Short-Term Increase in Symplasmic Phloem Unloading in Pea Root-Tips Under Osmotic-Stress. Protoplasma 188:22-37.

Schwarzlaender,M., Fricker,M., Mueller,C., Marty,L., Brach,T., Novak,J., Sweetlove,L., Hell,R., and Meyer,A. (2008) Confocal imaging of glutathione redox potential in living plant cells. Journal of Microscopy 231:299-316.

Simon,A.M. and Goodenough,D.A. (1998) Diverse functions of vertebrate gap junctions. Trends in Cell Biology 8:477-483.

Simpson,C., Thomas,C., Findlay,K., Bayer,E., and Maule,A.J. (2009) An Arabidopsis GPI-Anchor Plasmodesmal Neck Protein with Callose Binding Activity and Potential to Regulate Cell-to-Cell Trafficking. Plant Cell 21:581-594.

Skirycz,A., Claeys,H., De Bodt,S., Oikawa,A., Shinoda,S., Andriankaja,M., Maleux,K., Eloy,N.B., Coppens,F., Yoo,S.D., Saito,K., and Inze,D. (2011) Pause-and-Stop: The Effects of Osmotic Stress on Cell Proliferation during Early Leaf Development in Arabidopsis and a Role for Ethylene Signaling in Cell Cycle Arrest. Plant Cell 23:1876-1888.

Spoel,S.H. and Dong,X. (2012) How do plants achieve immunity? Defence without specialized immune cells. Nature Reviews Immunology 12:89-100.

Stadler,R., Wright,K.M., Lauterbach,C., Amon,G., Gahrtz,M., Feuerstein,A., Oparka,K.J., and Sauer,N. (2005) Expression of GFP-fusions in Arabidopsis companion cells reveals non-specific protein trafficking into sieve elements and identifies a novel post-phloem domain in roots. Plant Journal 41:319-331.

Staswick,P.E., Su,W.P., and Howell,S.H. (1992) Methyl Jasmonate Inhibition of Root-Growth and Induction of A Leaf Protein Are Decreased in An Arabidopsis-Thaliana Mutant. Proceedings of the National Academy of Sciences of the United States of America 89:6837-6840.

Stonebloom,S., Brunkard,J.O., Cheung,A.C., Jiang,K., Feldman,L., and Zambryski,P. (2012) Redox States of Plastids and Mitochondria Differentially Regulate Intercellular Transport via Plasmodesmata. Plant Physiology 158:190-199.

Stonebloom,S., Burch-Smith,T., Kim,I., Meinke,D., Mindrinos,M., and Zambryski,P. (2009) Loss of the plant DEAD-box protein ISE1 leads to defective mitochondria and increased cell-to-cell transport via plasmodesmata. Proceedings of the National Academy of Sciences of the United States of America 106:17229-17234.

Stoop,J.M.H., Williamson,J.D., and Pharr,D.M. (1996) Mannitol metabolism in plants: A method for coping with stress. Trends in Plant Science 1:139-144.

Sun,W.X., Dunning,F.M., Pfund,C., Weingarten,R., and Bent,A.F. (2006) Within-species flagellin polymorphism in Xanthomonas campestris pv campestris and its impact on elicitation of Arabidopsis FLAGELLIN SENSING2-dependent defenses. Plant Cell 18:764-779.

Sussex,I.M. (1951) Experiments on the Cause of Dorsiventrality in Leaves. Nature 167:651-652.

Tacke,E., Prufer,D., Schmitz,J., and Rohde,W. (1991) The Potato Leafroll Luteovirus 17K Protein Is A Single-Stranded Nucleic Acid-Binding Protein. Journal of General Virology 72:2035-2038.

Terry,B.R. and Robards,A.W. (1987) Hydrodynamic Radius Alone Governs the Mobility of Molecules Through Plasmodesmata. Planta 171:145-157.

Thomas,C.L., Bayer,E.M., Ritzenthaler,C., Fernandez-Calvino,L., and Maule,A.J. (2008) Specific targeting of a plasmodesmal protein affecting cell-to-cell communication. Plos Biology 6:180-190.

Tilsner,J., Amari,K., and Torrance,L. (2011) Plasmodesmata viewed as specialised membrane adhesion sites. Protoplasma 248:39-60.

Tirlapur,U.K. and Konig,K. (1999) Near-infrared femtosecond laser pulses as a novel non-invasive means for dye-permeation and 3D imaging of localised dye-coupling in the Arabidopsis root meristem. Plant Journal 20:363-370.

Tiryaki,I. and Staswick,P.E. (2002) An Arabidopsis mutant defective in jasmonate response is allelic to the auxin-signaling mutant axr1. Plant Physiology 130:887-894.

To,J.P.C., Haberer,G., Ferreira,F.J., Deruere,J., Mason,M.G., Schaller,G.E., Alonso,J.M., Ecker,J.R., and Kieber,J.J. (2004) Type-A Arabidopsis response regulators are partially redundant negative regulators of cytokinin signaling. Plant Cell 16:658-671.

Tomenius,K., Clapham,D., and Meshi,T. (1987) Localization by Immunogold Cytochemistry of the Virus-Coded 30K Protein in Plasmodesmata of Leaves Infected with Tobacco Mosaic-Virus. Virology 160:363-371.

Trip,P., Krotkov,G., and Nelson,C.D. (1964) Metabolism of Mannitol in Higher Plants. American Journal of Botany 51:828-&.

Truernit,E. and Sauer,N. (1995) The Promoter of the Arabidopsis-Thaliana Suc2 Sucrose-H+ Symporter Gene Directs Expression of Beta-Glucuronidase to the Phloem - Evidence for Phloem Loading and Unloading by Suc2. Planta 196:564-570.

Tsuge,T., Tsukaya,H., and Uchimiya,H. (1996) Two independent and polarized processes of cell elongation regulate leaf blade expansion in Arabidopsis thaliana (L) Heynh. Development 122:1589-1600.

Tucker,J.E., Mauzerall,D., and Tucker,E.B. (1989) Symplastic Transport of Carboxyfluorescein in Staminal Hairs of Setcreasea-Purpurea Is Diffusive and Includes Loss to the Vacuole. Plant Physiology 90:1143-1147.

Turgeon,R. (1989) The Sink-Source Transition in Leaves. Annual Review of Plant Physiology and Plant Molecular Biology 40:119-138.

Turgeon,R. (2006) Phloem loading: How leaves gain their independence. Bioscience 56:15-24.

Turgeon,R. and Webb,J.A. (1973) Leaf Development and Phloem Transport in Cucurbita-Pepo - Transition from Import to Export. Planta 113:179-191.

Van Steveninck,R.F.M. (1975) The Washing Or Aging Phenomenon in Plant Tissues. Briggs, Winslow R.(Ed.).Annual Review of Plant Physiology, Vol.26.531P.Illus.Annual Reviews Inc.: Palo Alto, Calif., U.S.A.Isbn 0-8243-0626-0:237-258.

Vogel,F., Hofius,D., and Sonnewald,U. (2007) Intracellular trafficking of Potato leafroll virus movement protein in Transgenic Arabidopsis. Traffic 8:1205-1214.

Waigmann,E. and Zambryski,P. (1995) Tobacco mosaic virus movement protein-mediated protein transport between trichome cells. Plant Cell 7:2069-2079.

Wang,C., Zhang,L.J., and Huang,R.D. (2011) Cytoskeleton and plant salt stress tolerance. Plant signaling & behavior 6:29-31.

White,R.G., Badelt,K., Overall,R.L., and Vesk,M. (1994) Actin Associated with Plasmodesmata. Protoplasma 180:169-184.

Willmer,C.M. and Sexton,R. (1979) Stomata and Plasmodesmata. Protoplasma 100:113-124.

Wright,K.M. and Oparka,K.J. (1989) Sucrose Uptake and Partitioning in Disks Derived from Source Versus Sink Potato-Tubers. Planta 177:237-244.

Zhu,T., Lucas,W.J., and Rost,T.L. (1998) Directional cell-to-cell communication in the Arabidopsis root apical meristem - I. An ultrastructural and functional analysis. Protoplasma 203:35-47.